R-10-66

Long Term Sorption Diffusion Experiment (LTDE-SD)

Supporting laboratory program – Sorption diffusion experiments and rock material characterisation

With supplement of adsorption studies on intact rock samples from the Forsmark and Laxemar site investigations

Henrik Widestrand, Johan Byegård, Eva Selnert,
Mats Skålberg, Susanne Höglund, Erik Gustafsson
Geosigma AB

December 2010

Svensk Kärnbränslehantering AB
Swedish Nuclear Fuel
and Waste Management Co

Box 250, SE-101 24 Stockholm
Phone +46 8 459 84 00

ISSN 1402-3091
SKB R-10-66

Long Term Sorption Diffusion Experiment (LTDE-SD)

Supporting laboratory program – Sorption diffusion experiments and rock material characterisation

With supplement of adsorption studies on intact rock samples from the Forsmark and Laxemar site investigations

Henrik Widestrand, Johan Byegård, Eva Selnert,
Mats Skålberg, Susanne Höglund, Erik Gustafsson
Geosigma AB

December 2010

Keywords: Crystalline rock, Matrix rock, Natural fracture, Diffusion, Sorption, Porosity, Radionuclides, Groundwater, Geological characterisation.

Abstract

The LTDE-SD experiment, (Long Term Sorption Diffusion Experiment) aims at increasing the scientific knowledge of sorption and diffusion under in situ conditions and to provide data for performance and safety assessment calculations.

In this report, performance and results of laboratory sorption and diffusion experiments and porosity investigations using site-specific crushed and intact rock materials are presented, including a geological and mineralogical characterization of the samples. A synthetic groundwater and a part of the radionuclide tracer cocktail that was used for the in situ experiment were used also in the laboratory experiments. 13 radionuclide tracers were analysed in the laboratory experiments. The method descriptions from SKB Site Investigations were applied in order to enable comparisons with Site Investigations data.

The water saturation porosity of 10 unaltered matrix rock samples from KA3065A02 and A03 is 0.26 ± 0.08% and two fracture material samples show porosities of 2.4% and 5.2% respectively. ^{14}C-methylmethacrylate impregnation (the PMMA-method) show that the unaltered rock matrix porosity is relatively homogeneous with grain boundary porosity, while the porosity of fracture samples is heterogeneous and have increased porosity up to more than 10% in some parts.

Through-diffusion experiments using tritiated water (H^3HO) give a matrix diffusivity in the range from $2.7 \cdot 10^{-14}$ to $6.5 \cdot 10^{-14}$ m^2/s in four samples from KA3065A02 and A03.

The results of the porosity and diffusion measurements are coherent in ranges with earlier LTDE-SD measurements and are also in line with the SKB Site Investigations results.

In the batch sorption experiments using crushed rock material, two matrix rock samples of Ävrö granodiorite, one red-stained altered Ävrö granodiorite sample and two chlorite-calcite dominated fracture samples were analysed for three different size fractions as a function of time up to 186 days contact time. The strongest sorption was observed in the fracture material samples. The two matrix rock samples and the altered sample showed nearly the same sorption properties. K_d values in the range from 1×10^{-3} to 1 m^3/kg could be detected with the method. The individual results for different tracers and species are interpreted in the report.

Sorption-diffusion on intact rock samples showed concentration losses that were basically in line to what could be expected from the outcome of the batch sorption experiments within the LTDE-SD and the Site Investigation program. Modelling of the diffusion process showed that the product of the sorption coefficient and the formation factor, $K_d \cdot F_f$, can only be resolved by analysis of the tracer concentration profiles in the rock.

Sammanfattning

Syftet med LTDE-SD experimentet är att öka den vetenskapliga kunskapen angående sorption och diffusion under in situ förhållanden och att tillhandahålla data för säkerhetsanalys.

I denna rapport presenteras resultat och genomförande av sorptions- och diffusionsexperiment utförda på laboratorium och porositetsunderökningar på platsspecifikt krossat och intakt bergmaterial. Rapporten omfattar även en geologisk och mineralogisk karakterisering av proverna. I laboratorieexperimenten användes ett syntetiskt grundvatten och en fraktion av den spårämnescocktail som användes i in situ-experimentet. 13 stycken radioaktiva spårämnen analyserades i laboratorieexperimenten. Metodbeskrivningar från SKB:s platsundersökningar tillämpades för att möjliggöra jämförelse med platsundersökningsdata.

Vattenmättnadsporositeten hos 10 stycken ej omvandlade bergmatrisprover från KA3065A02 och A03 är 0.26 ± 0.08 % och två sprickmineralsprover visar en porositet på 2.4 % respektive 5.2 %. ^{14}C-metylmetakrylat impregnering (PMMA-metoden) visar att porositeten hos den opåverkade bergmatrisen är relativt homogen med korngränsporositet medan porositeten hos sprickproverna är heterogen, med upp till mer än 10% porositet i vissa delar.

Genomdiffusionsexperiment med tritierat vatten (H^3HO) utfört på fyra prover från KA3065A02 och A03 ger en matrisdiffusion i intervallet $2.7 \cdot 10^{-14}$ till $6.5 \cdot 10^{-14}$ m^2/s.

Resultaten från porositets- och diffusionsmätningarna är samstämmiga med tidigare LTDE-SD undersökningar och är också i linje med SKB:s platsundersökningsresultat.

I sorptionsförsöken användes prover av krossat bergmaterial; matrisberg från Ävrö granodiorit (två st.), ett rödfläckigt omvandlat Ävrö granodioritprov samt två klorit-kalcitdominerade sprickmineralprover. Tre olika storleksfraktioner användes i försöken och proverna analyserades upp till en kontakttid av 186 dagar.

Sorption-diffusionsexperiment på intakta bergprover visade koncentrationsförluster som huvudsakligen var i linje med vad som kunde förväntas från sorptionsexperiment med krossat material inom LTDE-SD- och platsundersökningsprogrammet. Modellering av diffusionsprocessen visade att produkten av sorptionskoefficienten och formationsfaktorn, $K_d \cdot F_f$, endast kan bestämmas genom analys av spårämnenas koncentrationsprofiler i bergmaterialet.

Acknowledgement

The experimental work with sorption-diffusion experiments was performed by Prof. Gunnar Skarnemark and Ph.D Stellan Holgersson at Nuclear Chemistry Group, Department of Chemistry, Chalmers University of Technology. The good cooperation and skilful experimental work is gratefully acknowledged.

We also appreciate the cooperation, engagement and skilful ^{14}C-PMMA work performed by Prof. Marjja Siitari-Kauppi, Laboratory of Radiochemistry, University of Helsinki.

Finally, we are very grateful for the in depth and constructive review that was provided by Peter Vilks, Atomic Energy of Canada Limited (AECL), and Bill Wallin, Geokema AB.

Contents

1 Introduction

The Long Term Sorption Diffusion Experiment (LTDE-SD) is one of the experiments within the Natural Barriers research programme at the SKB Äspö Hard Rock Laboratory (HRL) the goal of which is to increase the scientific knowledge of the safety margins of the final repository for spent nuclear fuel and to provide data for performance and safety assessment calculations.

Transport of radionuclides in water-conducting rock fractures over 5–50 m distances is studied within the Tracer Retention and Understanding Experiments (TRUE) experimental programme since the late 90's /Winberg et al. 2000, Andersson et al. 2002/. Advection, dispersion, sorption and diffusive mass transfer are relevant processes of which dispersion and diffusive mass transfer can be difficult to distinguish by modelling alone of concentration-time curves.

Because the evaluation of the results of the TRUE experiment /Winberg et al. 2003a/ identified diffusion processes as an important retention mechanism, a demand for extended knowledge of diffusion and sorption processes over longer time scales in a controlled rock volume was identified. A sorption-diffusion experiment without advection and dispersion effects, LTDE-SD, was consequently set up. The LTDE-SD experiment aims at increasing knowledge of sorption and diffusion under in situ conditions and to provide data for performance and safety assessment calculations, i.e.:

- To obtain data on sorption properties and processes of individual radionuclides on natural fracture surfaces and inner surfaces in the rock matrix.
- To investigate the magnitude and extent of diffusion into matrix rock from a natural fracture in situ under natural rock stress conditions and hydraulic pressure and groundwater chemical conditions.
- To compare laboratory derived diffusion constants and sorption coefficients for the investigated rock fracture system with the sorption behaviour observed in situ at natural conditions, and to evaluate if laboratory scale sorption results are representative also for in situ conditions.

The main in situ experiment was performed from September 2006 through April 2007. During this time period of ~7 months, radionuclide tracers were circulated, sampled and monitored in the test section of borehole KA3065A03 (see Section 1.3). Following the termination of the in situ experiment, the target rock volume was over-cored by drilling of a 300 mm diameter borehole which was subsequently sampled, geologically characterized and analysed for trace element concentration profiles within the rock.

A laboratory program was performed in parallel to the in situ experiment and the subsequent analysis of the in rock material. The aim of the laboratory experiments was to produce site-specific laboratory derived retention parameters (e.g. diffusivity and sorption distribution coefficients) for which the applicability to the actual in situ experiment results later can be tested. The laboratory experiments were performed with material from the exploration borehole KA3065A02, the core of the 36 mm extension borehole and fracture material from the opposite side of the stub surface in KA3065A03. A common tracer solution was prepared and divided for use in situ and in the laboratory experiments.

1.1 Scope

One task of the LTDE-SD program was thus to produce site-specific laboratory derived retention parameters (e.g. diffusivity and sorption distribution coefficients) for which the applicability in the actual in situ experiment is tested.

This report is focused on data and results from the LTDE-SD laboratory investigations and the experiments presented in this report mainly follow the methods used in the laboratory measurements programme for the SKB site investigations at Forsmark and Laxemar /Widestrand et al. 2003, Byegård et al. 2008, Selnert et al. 2009b/. Consequently, a link is established between LTDE-SD data and Site Investigation data and the data are comparable. The analysis of rock material penetration profiles and a comparison of laboratory and in situ data is reported in /Nilsson et al. 2010/.

A part of the laboratory program included in this report is the sorption on intact drill cores, in which an attempt of addressing batch sorption determined K_d and diffusivities in the total interaction of the tracer with the rock is done. In addition to the LTDE-SD data for such experiments, this report also contains an evaluation of similar studies on intact rock samples performed to support laboratory data produced within the Laxemar and Forsmark site investigations /Byegård et al. 2008, Selnert et al. 2009b/. These samples link the LTDE-SD and the site investigation materials together by using the same laboratory methods and tracers.

1.2 LTDE-SD-reports

This particular report, R-10-66, constitutes one in a suit of three SKB R-reports presenting the performance, results and conclusions of the LTDE-SD laboratory and in situ experiment.

- R-10-66, i.e. this report, covers the performance and results of laboratory sorption and diffusion experiments and porosity investigations, using geologically and mineralogical characterised site-specific crushed and intact rock materials.
- R-10-67 /Widestrand et al. 2010/. The report covers the performance of the main in situ experiment and results from water phase measurements. Sorption coefficients were determined from tracer declining concentration time curves by applying a surface sorption model and a one-dimensional diffusion-sorption model.
- R-10-68 /Nilsson et al. 2010/. The report covers the performance and results of over-core drilling of the in situ experiment target rock volume, subsequent sampling, geological characterisation and analysis of radionuclide penetration and distribution in the rock. The report is focused on evaluation and modelling of the penetration profiles as well as the distribution of the radionuclides between fracture minerals and matrix rock. Results are compared to sorption and diffusion coefficients determined in the supporting laboratory experiments (R-10-66) and from the water phase measurements (R-10-67) of the in situ experiment.

The preparations for the LTDE-SD experiments included geological and hydrogeological characterisation of the site at Äspö HRL, as well as supporting laboratory tests and a functionality test with short lived radionuclides. These preparatory activities are presented in a set of reports.

/Winberg et al. 2003b/ describes in detail the geologic features of the rock matrix in the vicinity of the test area. Borehole imaging by BIPS (Borehole Image Processing System) and core logging in the two boreholes were used to correlate fractures in the two holes. The correlation was substantiated by mineralogical and geochemical studies including stable isotopes.

Within the framework of collaboration between SKB and Ontario Power Generation's (OPG) Nuclear Waste Management Division, supporting laboratory experiments on core samples from the LTDE-SD borehole KA3065A03 were performed by /Vilks et al. 2005/. The experimental programme consisted of porosity measurements, diffusion cell experiments, radial diffusion experiments and permeability measurements.

During 2004, in situ pre-tests including hydraulic testing (flow logging, interference and pressure build-up tests) and non radioactive tracer tests (dilution test and leakage testing) were performed by /Wass 2005/.

Installation and installation tests of the experimental set up at LTDE-SD were finalized during 2005.

During September to October 2005 a functionality test with short lived radionuclides was conducted in the experimental borehole KA3065A03 /Widestrand et al. 2006/. The functionality test was the final preparation for the main experiment and it showed that concentration-time curves based on sampling and on-line measurements of the radioactivity in the test section could be produced with the experimental set-up used. The successively decreasing concentrations with time for the sorbing tracers showed that sorption processes in the test section could be studied at the LTDE-SD site. Only minor sorption on tubings could be measured for the most strongly sorbing tracers, which indicated that the sorption mainly occurred on the stub and 36 mm section rock surfaces. It was concluded that sampling and on-line measurements complement each other and that both should be used in the main experiment.

1.3 Overview of the LTDE-SD in situ experiment

A brief overview of the LTDE-SD site, experiment and sample locations for the supporting laboratory tests is given in this section. For details, see /Widestrand et al. 2010/ and /Nilsson et al. 2010/.

The site is located in the niche at tunnel Section 3,065 m at a depth of approximately –410 m.a.s.l. in the Äspö HRL. KA3065A03 is the experimental borehole and KA3065A02 has served as exploration pilot borehole to find a suitable target structure on which to perform the experiment, see Figure 1-1.

The telescoped large diameter (300/197 mm) experimental borehole KA3065A03 had a natural fracture on the surface of the stub of the 197 mm borehole. This fracture was sealed off with a polyurethane cylinder and a peek lid, which constituted a “cup-like” packer. A small diameter (36 mm) extension at the end of KA3065A03 was packed off using a double packer system leaving a 300 mm long section. Further, the borehole outside the stub was packed off with a system of one mechanical and two inflatable packers. The system of packers and an advanced pressure regulating system was used to eliminate the hydraulic gradient along the borehole, during the in situ tests.

The in situ experiment comprised of injection and seven months monitoring and sampling of 22 trace elements representing a variety of chemical species and sorption behaviour. A borehole section consisting of the natural fracture surface in the 197 mm diameter borehole and the matrix rock surface in the 36 mm diameter borehole was used. The in situ experiment phase is reported in /Widestrand et al. 2010/.

Following the in situ experiment, the experiment section was emptied from trace elements and injected by an epoxy resin in order to increase the mechanical strength prior to over-coring. The target rock volume was over-cored by drilling of a 300 mm diameter borehole which was subsequently sampled and analysed for trace element concentration profiles within the rock. The analysis of the rock material is reported in /Nilsson et al. 2010/.

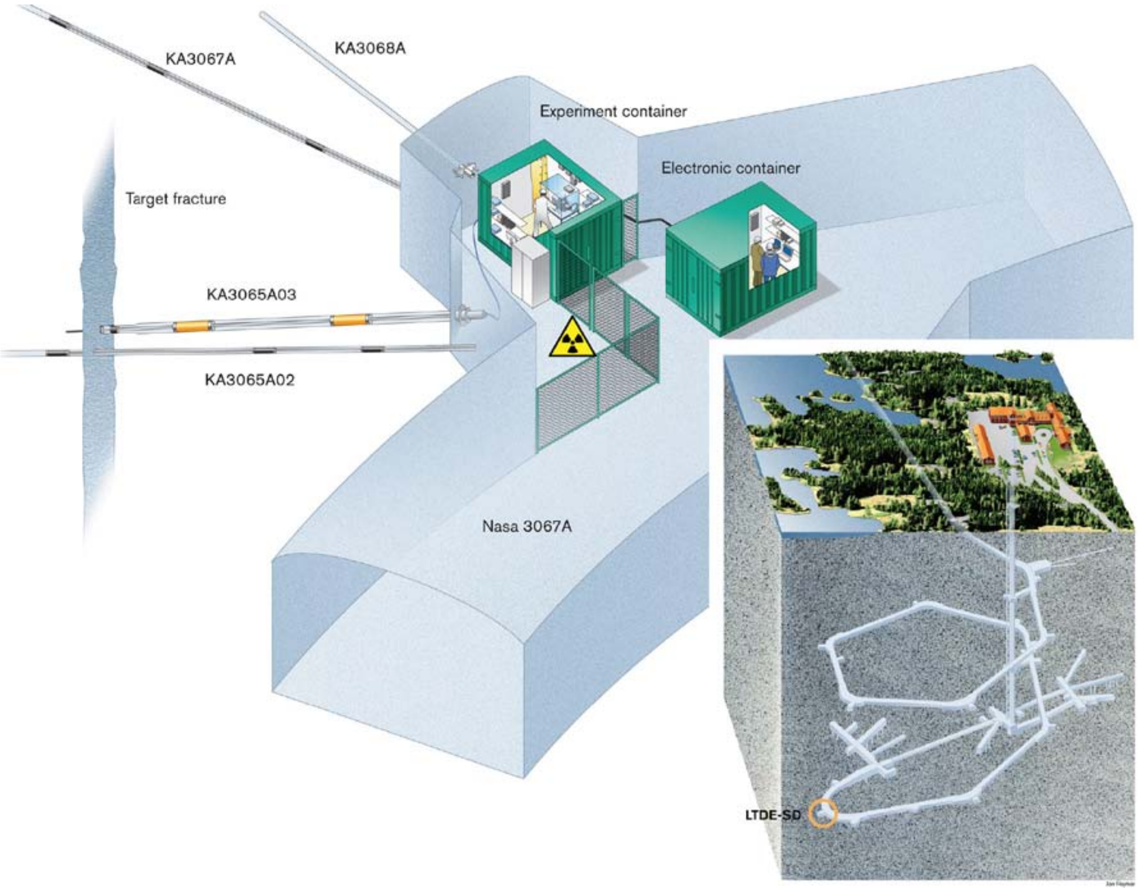

Figure 1-1. *LTDE-SD experimental site and borehole layout at NASA 3067A in Äspö HRL. The experimental borehole KA3065A03 is shown beside the pilot borehole KA3065A02.*

1.4 Overview of this work

In this work the focus is on investigating the sorption properties of the different materials relevant for the in situ test. Both "batch" sorption technique using crushed rock material and sorption-diffusion experiments on intact drill core samples were conducted for the determination of sorption distribution coefficients (K_d). In addition, a few through-diffusion experiments using H^3HO of samples from the 36 mm borehole (KA3065A03) and the exploration borehole (KA3065A02) are included in this study to determine matrix diffusivity (D_e).

Samples from the following borehole positions were used (see Figure 1-1):

- Samples from the mate of the stub in the 197 mm borehole of KA3065A03.
- Core samples from the 36 mm extension of KA3065A03.
- Core samples from the exploration borehole KA3065A02.

The samples are described further in Section 2.

In this report data and results of the laboratory experiments are presented. The results will further be used to evaluate to what extent laboratory sorption results determined on small rock samples are representative for the in situ conditions; e.g. if factors as stress release and/or atmospheric exposure of sampled rock has a considerable impact.

1.5 Previous laboratory experiments at AECL

Laboratory experiments on core samples from the 300 mm section of the LTDE-SD borehole KA3065A03 was carried out at AECL´s Whiteshell Research Laboratories, as part of the framework of collaboration between SKB and OPG´s Nuclear Waste Management Division /Vilks et al. 2005/. The experimental programme reported by Vilks et al. consisted of porosity measurements, diffusion cell experiments and permeability measurements on 22 mm diameter core samples extracted from the large diameter core (270 mm). Tritiated water (H^3HO) and non-radioactive weakly-sorbing and conservative tracers was used. A radial diffusion experiment was also carried out in a 150 mm long specimen of the large diameter core, where a 36 mm bore was drilled in the middle of the core parallel to the core axis. Some of the main findings from the experiments performed by Vilks are:

- Although there was a factor 1.6 in difference between high and low porosity values, both iodide and tritiated water diffusivity values ranged over 3 orders of magnitude. This indicates that variation in diffusivity is attributed mainly to differences in pore geometry and not to the total porosity.
- Diffusivity appeared to be the same in all directions (isotropic), whether parallel or perpendicular to the core axis.
- Since diffusivity was the same near the core edge as towards the core centre, drilling does not seem to have damaged the edges of the core. Actually the generally low diffusivity values observed in the diffusion cell experiments suggests that samples have not been significantly altered by drilling.
- The diffusivity of iodide within the alteration zone was not significantly lower than that in the rest of the core. This suggests that, except for sorption processes on alteration minerals, the alteration around fracture surfaces is not an additional barrier to diffusion into the rock matrix and one could treat diffusion near the fracture with the same diffusion coefficients as applied to the bulk rock.

Iodide D_e values estimated from the radial diffusion experiment by the diffusive flux, $(1.58 \pm 0.22)\cdot10–13$ m^2/s, and from modelling of diffusion profiles, of $1.4\cdot10–13$ m^2/s, were similar to the geometric mean of D_e values estimated from diffusion cell experiments ($1.7\cdot10–13$ m^2/s). Thus, the De values estimated from a large sample approximated the geometric mean of values estimated from a number of smaller samples.

2 Materials

2.1 General

The main purpose with the laboratory program has been to investigate the properties of the intact as well as the altered bedrock, in addition to the fracture material at the target structure (i.e. the mature of the stub) in the LTDE-SD project. The geological description of the available rock material for this laboratory work is presented in Section 2.2 and Appendices 1, 2 and 13, and an overview of the selected rock samples is presented in Section 2.3.

2.2 Geological description of the small diameter core, pilot borehole and replica

The Äspö tunnel is according to /Rhén et al. 1997/ dominated by four major rock types; fine-grained greenstone, Äspö diorite, Småland (Ävrö) granite and fine-grained granite. The nomenclature of these rock types have previously been updated (Hultgren P (SKB), pers. comm.) in order to get correspondence between the Äspö rock types and the Site investigations rock types. The Småland (Ävrö) granite has been updated to Ävrö granodiorite, the Äspö diorite to Ävrö granodiorite or Ävrö quartzmonzodiorite when mineralogical, chemical or density data is available. The investigated unaltered matrix rock in the current report (i.e. rock samples from KA306502 and KA3065A03), as well as corresponding LTDE-SD reports (e.g. /Vilks et al. 2005/), is interpreted to be Ävrö granodiorite based on mineralogical observations and density data (average density is 2,66 g/cm^3 in samples measured with water saturation method).

As mentioned in Section 1.1, the available materials for laboratory measurements are from a small diameter core (22 mm, KA3065A03), a large diameter core (44 mm, KA3065A02) and from the replica of the fracture surface of structure #10 (i.e. the remaining/opposite fracture mineralization on the 300 mm section of the KA3065A03 drill core). Both rock cores, and consequently the associated rock samples, are of the porphyritic Ävrö granodiorite rock type; i.e. with a major mineralogical composition of plagioclase, k-feldspar, quartz, biotite and chlorite (cf. Table 2-1). Each rock sample included in the laboratory measurements was characterized and documented with stereomicroscope with respect to the mineralogy, fractures/micro fractures and alteration. A sample overview is presented in Figures 2-2 to 2-4 and a detailed description in Appendix 13.

The target structure in the main sorption diffusion experiment, i.e. structure #10 in /Winberg et al. 2003b/ can be described as two parallel open fractures (10a and 10b) with a lens of 5 to 17 mm thickness in between. This lens constitutes of mylonite/cataclasite with a matrix that mainly consists of epidote and chlorite, in addition to strongly altered (red-stained and fractured) Ävrö granodiorite. The latter is red-stained due to small hematite grains and has secondary mineralizations as chlorite and saussurite.The fracture coating in fracture 10a (the opposite side of the LTDE-SD fracture surface) consist of calcite and quartz together with minor amounts of chalcopyrite and small crystals of barite and fluorite. Epidote, chlorite and calcite dominate in the fracture coating of fracture 10b. The fracture coatings of epidote, chlorite and calcite are difficult to distinguish and separate from the cataclasite matrix due to similar mineralogy, however the latter is supposed to have a larger amount of epidote.

2.2.1 Thin sections analysis

The mineral distribution in three thin sections, representative for the rock type and altered variants at the LTDE experiment, has been determined using transmissive light microscope (so-called point counting). The work was performed by Isochrone Geoconsulting AB and the results are presented in Table 2-1.

The first thin section, A02, represents an unaltered Ävrö granodioritic rock; i.e. a rock sample without any visible red-staining. Nevertheless, the microscopic examination showed that the plagioclase to a great extent has undergone saussuritization. The result from the point counting of this sample is in accordance with previous results of the same rock type from the Oskarshamn Site Investigations.

The second thin section, A03#10, represents the mylonitic/cataclasitic lens with strongly altered bedrock (Ävrö granodiorite), between the two fractures (#10a and #10b). Sealed fractures (see Figure 2-1) filled with mainly epidote and adularia are visible. The small amounts of calcite are supposed to be part of the fracture surface at #10a, i.e. the fracture which constitutes the surface of the stub.

The A03#14 thin section represents the rock close to and at the fracture #14. However, the examined area does not include the fracture surface but stands for a relatively unaltered greyish Ävrö granodiorite, although slightly red coloured in the last cm before the fracture surface area.

In addition to the geological characterization above, chemical analyses have been performed on two rock samples; A02:6 and A03:1 Batch 1 (see Table 2-2), in order to verify content of major and trace elements. The results from these analyses, presented in Appendix 1, is in accordance with e.g. results within the Transport laboratory program /Selnert et al. 2009a/ and these samples are consequently supposed to represent an ordinary Ävrö granodiorite.

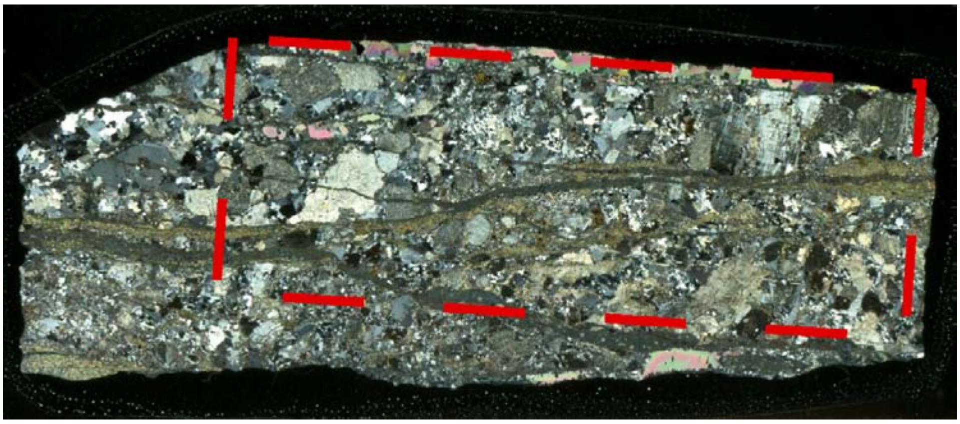

Figure 2-1. Scanned thin section with crossed polars, KA3065A03 #10. The red mark shows the area which is point counted. The thin section was sampled from a rock piece similar to sample A03:10 (see Table 2.3). The base of the figure is approximately 41 mm.

Table 2-1. Mineralogical composition and distribution of three thin sections, representing rock samples from KA3065A02 and KA3065A03, determined by thin section analysis (so-called point counting). Mean value of Ävrö granodiorites included in the Transport laboratory programme (SKB Site Investigation) is given as a comparison.

	A02, Unaltered rock sample of Ävrö granodiorite (adjacent to rock sample A02:5)	A03 #10, strongly altered rock (Ävrö granodiorite), mylonitic/cataclasitic rock and fracture coating	A03 #14, slightly red-stained Ävrö granodiorite	Ävrö granodiorite within the Transport laboratory programme*
Mineral	vol.%	vol.%	vol.%	vol.%
Quartz	30.6	33.2	35.2	30.4
Plagioclase	3.0		13.0	33.2***
Sauss. Plag.	27.6		13.2	
Sericitised Plag*		16.3		
K-feldspar	28.6	30.8	31.8	25.8
Biotite	5.8		3.0	2.2
Chlorite	1.8	3.6	2.0	3.6
Titanite	1.0		0.4	0.4
Epidote	0.6	13.1	0.6	2.8
Opaque	1.0		0.6	0.4
Hornblende				0.6
Apatite	– **	0.2	0.2	
Calcite		2.6		
Allanite		0.2		

* Data from rock sample KLX02 753.80 (Oskarshamn Site Investigation).
** less than 0.2 percent.
*** The plagioclase is to some extent saussuritized, although not determined in percentage.

2.3 Overview of the selected samples

As mentioned in Section 2.1, the main purpose during the laboratory program was to investigate three different states of rock material; intact bedrock, altered bedrock and fracture material. Consequently, three groups of rock samples were selected and are presented in Table 2-2, 2-3 and 2-4. A more detailed sample description is given in Appendix 13.

Table 2-2. Rock samples representing the intact rock.

Rock sample ID/ Alias	Method/Parameter achieved	Photograph
A02:4	Through-diffusion, porosity /D_e, ε	
A02:5	Electrical resistivity, porosity/ F_f, ε	
A02:6	BET + Batch sorption /specific surface area and K_d, Geochemical analysis	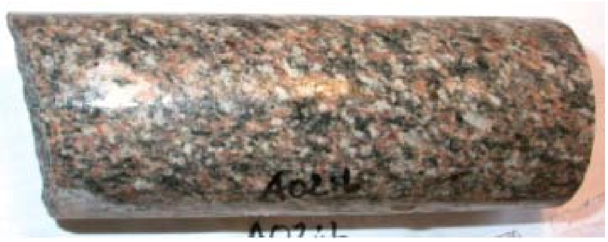
A02:7	Electrical resistivity, porosity /F_f , ε	

Table 2-2. Continued.

Rock sample ID/ Alias	Method/Parameter achieved	Photograph
A02:8	Through-diffusion, porosity /D_e, ε	
A03:1/ Batch 1	BET + Batch sorption /specific surface area and $K_{d,}$. Geochemical analysis.	
A03:4/ Diff II	Sorption/diffusion, through-diffusion, porosity/ $D_{e,}$ K_d, ε	
A03:5/ Diff III	Sorption/diffusion, through-diffusion, porosity/ $D_{e,}$ $K_{d,}$ ε	

Table 2-2. Continued.

Rock sample ID/ Alias	Method/Parameter achieved	Photograph
A03:6/ Diff IV	Sorption/diffusion, through-diffusion porosity/ D_e, K_d, ε	
A03:7/ PMMA 1	Porosity with water saturation and PMMA, ε	
A03:8/ PMMA 2	Porosity with water saturation and PMMA, ε	

Table 2-2. Continued.

Rock sample ID/ Alias	Method/Parameter achieved	Photograph
A03:3/ Diff I	Sorption/diffusion, through-diffusion, porosity/ D_e, K_d, ε	 
A19	PMMA, ε	 

Table 2-3. Rock samples representing the altered, red-stained rock.

Rock sample ID/Alias	Method/Parameter achieved	Photograph
A02:1	BET + Batch sorption /specific surface area and K_d	
A03:2/ Batch 2	BET /specific surface area	

Table 2-4. Rock samples representing the fracture material.

Rock sample ID/Alias	Method/Parameter achieved	Photograph
A02:2	BET + Batch sorption /specific surface area and K_d	
A03:9/ Feature #10 "liten sten"	BET + Batch sorption /specific surface area and $K_{d,}$	
A03:10/ Feature#10, "stor sten	Porosity with water saturation and PMMA, ε. Thin section	
A03:11/Feature#10	Porosity with water saturation and PMMA, ε	

2.4 Rock samples from the Site Investigations

Ten rock samples, measured during the SKB Site Investigations at Forsmark and Oskarshamn are included in the current report as they were not completely evaluated and reported during that phase. Six of the rock samples have also been involved in previous through-diffusion measurements during the Site Investigations. Further on, the rock core samples represent three major rock types at Forsmark and Oskarshamn respectively, in addition to one minor rock type and one extremely altered rock type from Forsmark. Nine of the rock samples are estimated as fresh and unaltered. The major rock types can briefly be described as granitic to quartz monzodioritic with a mineralogical content similar to that of the LTDE-SD rock samples although the percentage distribution of the minerals as well as the texture is varying. The Ävrö granodiorite in LTDE-SD corresponds to the Ävrö granodiorite sample in Table 2-5 (SKB Rock code 501056). It can be noted that only very small mineralogical differences exists between the Ävrö granodiorite sample and the two Ävrö quartz monzodiorite samples included in this work.

The rock samples are 50 mm in diameter and of 30 mm length. An overview of the rock samples (e.g. sample-ID, rock type and comments) is presented in Table 2-5, the complete descriptions of the rock types are found in /Stephens et al. 2007, Wahlgren et al. 2005, 2008/. A more detailed rock sample description is given in Appendix 13.

Table 2-5. Rock samples from the Site Investigations at Forsmark and Oskarshamn.

Sample-ID	Rock type (SKB rock code)	Method/parameter	Photograph
KFM02A 276.06	Altered variety of 101057, "Episyenite"	Sorption/diffusion, porosity/ D_e, K_d, ε	 *
KFM03A 242,43	101054	Sorption/diffusion, porosity/ D_e, K_d, ε	
KFM07A 608,75	101057	Sorption/diffusion, porosity/ D_e, K_d, ε	
KFM09A 713,67	101057	Sorption/diffusion, porosity/ D_e, K_d, ε	

Table 2-5 Continued.

Sample-ID	Rock type (SKB rock code)	Method/parameter	Photograph
KSH01 891,91	501046	Sorption/diffusion, porosity/ $D_{e,}$ $K_{d,}$ ε	
KSH01 981,43	501036	Sorption/diffusion, porosity/ $D_{e,}$ $K_{d,}$ ε	
KLX02 235,08	501056	Sorption/diffusion, porosity/ $D_{e,}$ $K_{d,}$ ε	
KLX04 726,07	501036	Sorption/diffusion, porosity/ $D_{e,}$ $K_{d,}$ ε	No picture

Table 2-5 Continued.

Sample-ID	Rock type (SKB rock code)	Method/parameter	Photograph
KLX08 417,05	501046	Sorption/diffusion, porosity/ D_e, K_d, ε	
KLX10 995,79	501036	Sorption/diffusion, porosity/ D_e, K_d, ε	

* The picture is from an adjacent rock sample; i.e. KFM02A 275.45.

2.5 Synthethic groundwater

A synthetic groundwater was used in all laboratory experiments with a composition resembling groundwater that was sampled from the LTDE-SD site 2006-06-20 (KA3065A03:1-2, SICADA# 1066076). The synthetic groundwater composition is presented in Table 2-6.

Table 2-6. Chemical composition of the synthetic groundwater used in the experiments. Concentrations are given in mg/L.

	Synthetic groundwater
F^-	1.43E+0
Cl^-	5.88E+3
Br^-	3.18E+1
$SO4^{2-}$	3.59E+2
Si(tot)	6.66E+0
HCO_3^-	3.61E+1
S^{2-}	1.01E-1
Li^+	1.23E+0
Na^+	1.92E+3
K^+	1.15E+1
Mg^{2+}	6.09E+1
Ca^{2+}	1.70E+3
Sr^{2+}	3.07E+1
Rb^+	3.37E-2
Cs^+	2.70E-3
Ba^{2+}	8.59E-2
NH_4^+	7.30E-2
Fe^{2+}	6.79E-1
Mn^{2+}	3.59E-1
pH	7.34*
Ionic strength	2.23E-1

*pH prepared in the original synthetic groundwater. During the experiments this pH may change due to e.g. degassing of of CO_2 from the samples to the N_2-atmosphere used in the glove boxes and/or due to different mineral reactions.

2.6 Radionuclide tracers and analysis

The LTDE-SD tracer cocktail was originally produced for the in situ experiment and its composition and production is described in /Widestrand et al. 2010/. A part of the cocktail was used for the laboratory experiments. The tracers that were selected for evaluation in the laboratory program are noted in Table 2-7 as well as the full tracer list with comments of tracers not evaluated in the laboratory program. A deeper motivation for the selection of tracers is given in Appendix 14. Tritiated water, H^3HO, was used as additional tracer for the through-diffusion experiments. Chemical separation methods with subsequent liquid scintillation analysis were applied for Ni-63 and Cl-36 at Baslab, CLAB. All other radionuclide analyses were done at Chalmers Technical University, Nuclear Chemistry Group.

Table 2-7. List of tracers in the LTDE-SD trace element cocktail and evaluated tracers in the laboratory experiments using LTDE-SD materials. LSC = Liquid Scintillation Counting, ICP-MS = Ionic Coupled Plasma-Mass Spectrometry.

Nuclides Field experiment (Reference date 2006-09-28)	Half-lives	Tracer group*	Nuclides evaluated in laboratory experiment (Reference date 2008-05-23)	Analysis method in laboratory experiment	Comments
Ag-110 m	249.9 d	B2	(Ag-110 m)	γ-spectrometry	Low activity in the laboratory experiment.
Ba-133	10.51 y	B1	Ba-133	γ-spectrometry	
Cd-109	462,6 d	B2	Cd-109	γ-spectrometry	
Cl-36	3.01E5 y	A	Cl-36	Chemical-separation+LSC	
Co-57	271.8 d	B2	Co-57	γ-spectrometry	
Cs-137	30.07 y	B1	Cs-137	γ-spectrometry	
Gd-153	240.4 d	B2	(Gd-153)**	γ-spectrometry	Not evaluated due to strong sorption (no activity left in the aqueous phase).
–	12.33 y	A	H^3HO	LSC	Not used in situ.
Hf-175	70 d	B2	–**		Short half life.
Na-22	2.602 y	B1	Na-22	γ-spectrometry	
Ni-63	100.1 y	B2	Ni-63	Chemical-separation+LSC	
Nb-95	34.98 d	B2	–		Short half life.
Np-237	2.144E6 y	B3	Np-237	ICP-MS	
Pd-102	Stable	B2	–		Interferences from SrO.
Ra-226	1,600 y	B1	Ra-226	ICP-MS	
S-35	87.5 d	A	–		Short half life.
Se-75	119.8 d	?	Se-75	γ-spectrometry	
Sn-113	115.1 d	B2	–**		Short half life.
Sr-85	64.9 d	B1	–**		Short half life.
Tc-99	2.111E5 y	B3	Tc-99	ICP-MS	
U-236	2.341E7 y	B3	U-236	ICP-MS	
Pa-233	27 d	B2	–		Short half life, interference with ingrowth from ^{237}Np.
Zr-95	64 d	B2	–		Short half life.

*Tracer group: A = non-sorbing, B1 = ion exchange, B2 = mainly surface complexation, B3 = electrochemical reduction dependent.

**This nuclide was evaluated (not yet decayed) in the sorption studies of intact site investigations samples which was performed earlier than the studies on LTDE-SD samples.

3 Methods

3.1 Porosity

Porosity measurements on rock samples have been performed in order to give information about available transport pathways of fluids in the rock and consequently, the measured porosity in this investigation refers to connected porosity, which hereafter simply is referred to as porosity, ε (vol.%). However, the pores available for water to soak into a core sample may deviate significantly from the pores available under e.g. diffusion measurements as well as under *in situ* conditions.

Among several different ways to measure the porosity of a rock sample, two different methods have been used (described below) during this investigation; water saturation measurements and ^{14}C-PMMA measurements.

3.1.1 Water saturation

The most common method for measuring the porosity of a rock sample is the water saturation technique. In the present laboratory investigations the porosity has been determined according to standard method, /SS-EN 1936/. Briefly summarized, this method consists of two steps; drying of the rock samples at 70º C until constant mass is reached, and thereafter water saturation in vacuum.

SS-EN 1936 is considered to be a rather non-destructive method and differs slightly from e.g. ISRM 1979 (previously used for porosity measurements by the Geology program within the Site investigations) primarily with respect to the drying temperature. Several of the measured rock samples have been further investigated in diffusion or resistivity measurements. Therefore, a low drying temperature has been supposed to be of importance in order to avoid any extra chemical and mechanical degradation of the samples that possibly could result from the higher temperature (105° C) used in other methods.

The measured core samples from KA3065A02 have a diameter of approximately 44 mm whereas the samples from KA3065A03 are 22 mm in diameter. The majority of the rock core samples have a thickness of 3 cm but single samples represent greater thickness as well as irregular rock samples from the replica (see Appendix 13). Porosity measurements with water saturation technique were performed at the Swedish Cement and Concrete Research Institute, CBI, (former SP Technical Research Institute of Sweden).

3.1.2 PMMA

The ^{14}C-PMMA method can be used to measure the two-dimensional distribution of the porosity, to evaluate porosity gradients in e.g. altered and fractured rock materials as well as to study micro fracturing. The method entails drying slices of drill cores and impregnating them with a ^{14}C-tagged polymethylmethacrylate monomer, irradiation polymerization (with ^{60}Co-source), autoradiography and optical densitometry using digital image-processing techniques whereby both the porosity and its spatial distribution in the rock matrix are determined.

According to /Siitari-Kauppi 2002/, the most valuable results obtainable by the PMMA method are spatial porosity distributions; absolute bulk porosities are better determined by conventional methods. Further and more detailed descriptions of the method are presented in e.g. /Siitari-Kauppi 2002, Penttinen et al. 2006/.

The porosity investigations using the ^{14}C-PMMA technique were performed at the Laboratory of Radiochemistry, University of Helsinki (HYRL).

3.2 Diffusion

Diffusion experiments are aimed to quantify the rock formation factor F_f (–) or the matrix diffusivity, D_e (m^2/s), i.e. the ability for a solute to diffuse in porous rock.

The effective diffusivity is related to the water diffusivity, D_w, through the rock formation factor as:

$$D_e = F_f \cdot D_w \tag{3-1}$$

The rock formation factor depends only on the properties of the rock and not on the tracer or solute properties. In this work, a water diffusivity of $2.1 \cdot 10^{-9}$ m^2/s has been used for calculation of the formation factor, which is based on the /Mills and Lobo 1989/ using a temperature compensation for the somewhat elevated temperatures obtained in the glove box in which the through-diffusion experiments have been performed.

3.2.1 Through-diffusion

Through-diffusion experiments are aimed to quantify the matrix diffusivity, also often referred to as the effective diffusivity, D_e (m^2/s), i.e. the ability for a solute to diffuse through a rock disc. Beside that, the rock capacity factor α(%) is also determined. In theory, the rock capacity factor is equivalent to the porosity, ε (%), for a non-sorbing tracer such as H^3HO.

Matrix diffusivity measurements are carried out by measuring how quickly an added substance diffuses through a piece of a drill core, so-called through-diffusion measurements /Ohlsson and Neretnieks 1995, Byegård et al. 1998/. Matrix diffusivity and rock capacity factor are the primary parameters obtained in the evaluation procedure. A general description of the measurement procedure and evaluation follows below:

The cut and plane-parallel ground rock core samples are cast to obtain an epoxy resin mantling, plane grounded again and are thereafter evacuated in a vacuum chamber and equilibrated with synthetic groundwater for a minimum time of three weeks. Next, the samples are mounted in a measurement cell (Figure 3-1). Both sides of the core piece are in contact with synthetic groundwater and the radionuclide to be studied (in this case tritiated water, H^3HO) is injected to the volume on one side. Samples are then taken on the other (target) side, and the effective diffusion coefficients, D_e, for the rock matrix are calculated based on the concentration increase on the target side.

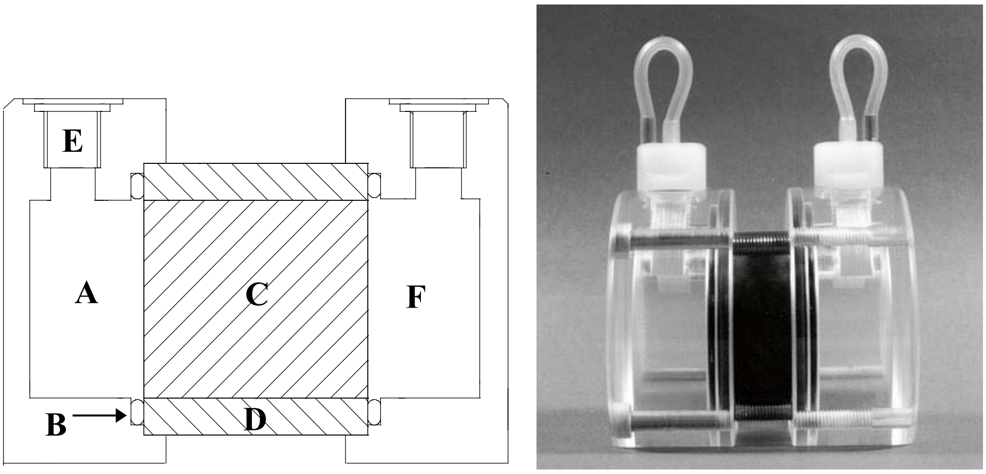

***Figure 3-1.** Schematic drawing and photograph of a rock sample assembled in a diffusion cell. A injection container, B o-ring, C rock cylinder, D epoxy resin, E sampling hole, F measurement container.*

Diffusion model

For a homogeneous, porous media, the accumulated scaled ratio of concentration, C_r (–), of the diffusing species which has passed through the rock disc (initially at zero concentration at time t) can be obtained by solving the diffusion equation for the boundary conditions: constant inlet concentration C_1 from $t = 0$ and outlet concentration C_2 ($C_2 \ll C_1$) at a distance l /Crank 1975/. The result is:

$$C_r = \frac{C_2 V_2}{C_1 A l} = \frac{D_e t}{l^2} - \frac{\alpha}{6} - \frac{2\alpha}{\pi^2} \sum_{n=1}^{\infty} \frac{(-1)^n}{n^2} \exp\left\{ -\frac{D_e n^2 \pi^2 t}{l^2 \alpha} \right\} \qquad (3\text{-}2)$$

where t is the experimental time after injection of tracer, l is the length of the rock sample, n is the summation factor, V_2 is the volume of the outlet container and A is the geometrical surface area. The capacity factor is defined as

$$\alpha = \varepsilon + K_d \rho \qquad (3\text{-}3)$$

where ρ (kg/m^3) is the rock bulk density and K_d (m^3/kg) is the sorption coefficient. Consequently, for a truly non-sorbing tracer ($K_d = 0$) the matrix porosity is in theory equivalent to the rock capacity factor ($\alpha = \varepsilon$).

The effective diffusivity D_e and the rock capacity factor α were fitted to the experimental data (time history of C_r (–)) using Equation 3-2.

The latter part of the experimental data was also fitted to a simplified linear form of Equation 3-2, *i.e.*

$$C_r = \frac{D_e t}{l^2} - \frac{\alpha}{6} \qquad (3\text{-}4)$$

Equation 3-4 was used for control of the results obtained in Equation 3-2 and also for estimation of the individual errors in D_e and α for a particular sample.

Experimental conditions

The through-diffusion experiments were carried out at the Nuclear Chemistry Group at Chalmers University of Technology (CTH) according to SKB MD 540.001 (SKB internal document). 6 rock core pieces, sawn out from the KA3065A02 and KA3065A03, were included (see Table 2-2).

The synthetic groundwater described in Section 2.5 was used and tritiated water, H^3HO, was used as a tracer. The experiments were performed at room temperature (20–25°C) under inert gas atmosphere.

For all diffusion cells the following applies: V_2 = 3.5E-5 m^3 and A = 1.52E-3 m^2 (44 mm core diameter) or 3.8E-4 m^2 (22 mm core diameter). Relative measurements were applied for C_1 and C_2 and consequently no absolute calibration of H^3HO radioactivity concentration was required. The inlet concentration C_1 of H^3HO was 4E12 CPM/m^3 (CPM = counts per minute in the radiation measurement of H^3HO).

3.2.2 Electrical resistivity

Resistivity is a measure of the disability to conduct electric current in the form of ions in the pore space of a rock sample. Low resistivity will thus correspond to a high ability of conduction and vice versa. The resistivity of the water that the sample has been soaked in is often normalized with the resistivity of the sample. The resulting ratio is then referred to as the formation factor, F_f, which in turn is related to the effective diffusivity, D_e (see Equation 3-1).

Resistivity measurements for obtaining the formation factor were performed by GeoVista AB, according to /Löfgren and Neretnieks 2005/, on 3 cm long rock core samples with plane-parallel end surfaces. Resistivity along the sample axis was measured with an in-house two-electrode equipment at the frequencies of 0.1, 0.6 and 4.0 Hz, after saturation of the rock core samples in 1.0 M NaCl-solution for approximately ten weeks. The formation factor was then calculated as the ratio between the resistivity of the soaking water and the resistivity of the samples at 0.1 Hz:

$$F_f = \frac{\rho_{water}}{\rho_{sample}} \qquad (3\text{-}5)$$

3.3 Sorption

The measurements performed within this activity, are aimed to quantify the adsorptive properties of the rock material, i.e. the ability for the different radionuclides to adsorb on the rock surfaces. Two different methods have been used and are described in the sections below:

- Specific surface area measurements of the rock material, BET.
- Actual measurements of the distribution of a radionuclide between the rock/groundwater phases, i.e. Batch sorption experiments.

3.3.1 BET surface area

BET surface area measurement (Brunauer, Emmet, Teller, cf. /Brunauer et al. 1938/) is a method for measuring the specific surface area of a solid material by use of gas adsorption. The BET surface area is a good diagnostic parameter in order to give rough qualitative estimations of the sorption capacity of different geologic materials, but it does not produce parameters that are used for determining the retardation of radionuclides due to adsorption onto mineral surfaces.

The BET measurements have been performed according to the ISO 9277 standard method on totally six rock samples from KA3065A02 and KA3065A03 at the CBI, Swedish Cement and Concrete Research Institute (former SP Technical Research Institute of Sweden). Generally, BET surface areas in the current investigation have been measured on double samples from crushed and sieved rock samples in the fractions 0.063–0.125 mm and 2–4 mm. However, for a few samples there was a lack of material and therefore only single samples were measured. In addition, one rock sample representing the fracture coating at the "mate of the stub", has been measured on single samples of < 0.125 mm fraction.

3.3.2 Batch sorption

In batch sorption measurements, crushed rock is contacted with a synthetic groundwater with addition of radionuclides. The distribution of the radionuclides between the aqueous and the solid phase is measured according to the method applied within the SKB Site Investigations (cf. e.g. /Byegård et al. 1998, Selnert et al. 2009a/). The batch sorption measurements were performed at Chalmers University of Technology (CTH). Rock samples of material from both KA3065A02 and KA3065A03 were crushed and sieved into different size fractions. A general description of the geological material can be found in Section 2.2. It may be worth noticed that the names KA3065A03_Batch 1 and KA3065A03_Replica often are used in this report for A03:1 and A03:9, respectively. It may also be worth noticed that the full name is used in the result for experiment carried out with material from KA3065A02, e.g. KA3065A02:2 is used for A02:2.

Size fractions of 0.063–0.125 mm, 0.25–0.5 mm and the 1–2 mm were used. These are the same sizes as were used in the Site Investigations and it enables comparisons between LTDE-SD and the Site Investigations results. The distribution ratio, $R_{d,}$ for each radionuclide was measured for these size fractions. In total five different rock samples were studied, represented by three from KA3065A02 and two from KA3065A03. With three different size fractions for each rock sample it ends up with a total of 15 samples. With two parallel experiments for each rock sample, a total of 30 separate batch experiments were conducted.

R_d is simply a distribution factor where the measured concentration in the solid phase is divided by the concentration in the water phase and will hence have the unit (m^3/kg). Due to practical reasons it can be difficult to measure the concentration in the solid phase. Instead, the concentration in the solid phase is calculated from the measured difference in concentration in the liquid phase which is subtracted by the concentration in the blank sample. The blank sample is taken as a mean value of measured concentrations in three blank samples, which only contain the water phase, without any solid phase.

Since it can be expected that the R_d due to slow diffusion into the particles should be influenced by the contact time, sampling was performed at different contact times, after approximately 1, 7, 30, 90 and 180 days. A solid to liquid ratio of 1 g solid phase to 4 ml water phase was applied in most of the experiments. In some cases with only a limited amount of solid phase available, only 0.5 g solid and 2 ml aqueous was used. The solid to liquid ratio of 1/4 (g/ml) was allowed to change at a total of < 10% due to the sampling during the experiment period.

The batch sorption experiments were performed in glove-boxes with continuous nitrogen flow attempting to minimize the influence of oxygen during the experiments. Synthetically produced groundwater (i.e. addition of salts to distilled water) having the same chemical composition as sampled groundwater at the LTDE-SD site was used in the experiments (cf. Section 2.5). The addition of redox-sensitive chemicals (e.g. salts of Fe(II), Mn(II) and S(-II)) together with potentially volatile chemicals (salts of HCO_3^-) were added inside the glove-box, after a thorough bubbling of water had been performed). The composition of the groundwater can be found in Table 2-6 and the radionuclides studied are found in Table 2-7.

Evaluation of K_d

In some earlier SKB Site Investigations work (e.g. /Selnert et al. 2008, 2009a/) K_d (m^3/kg) values were evaluated from the measured R_d values. With the assumption that the solid phase consists of spherical particles, an evaluation of a plot of R_d as a function of the inverted particle diameter (m^{-1}) gives ideally a straight line. The intercept with the y-axis corresponds to the K_d-value (sorption on inner particle surfaces) and the slope corresponds to $6K_a/\rho$, where ρ is the rock density (kg/m^3) and K_a (m) is the surface sorption coefficient (sorption on outer particle surfaces). Both K_d and K_a could thus be estimated from the measured R_d.

Practical experiences of evaluation of K_d-values according to the method described above, show that it is often connected with problems, such as the difficulty to fit a straight line. Based on the difficulties encountered, the method of evaluation of K_d was changed in the final reports of the retardation models in SKB Site Investigations /Byegård et al. 2008, Selnert et al. 2009a/. In this work, the same concept was adopted as finally applied by Byegård et al. and Selnert et al. Consequently, the R_d-value for the largest particles (1–2 mm) in the batch sorption experiments, after a contact time of about 180 days (186 days), was is in this work defined and used as a K_d-value; i.e. the same method was applied as in the SKB Site Investigations. The arguments presented by Byegård et al. and Selnert et al. for using the 1–2 mm fraction data are e.g. that the surfaces for this fraction is representative for those of intact rock (polymineralic grains less disturbed by crushing than smaller size fractions) and it has a BET-surface close to that of intact rock.

3.4 Sorption-diffusion experiments on intact drill cores

The sorption data obtained using batch sorption technique and crushed rock material can be criticized due to the fact that the major mechanisms for radionuclide retardation (i.e. diffusion into the rock matrix and sorption) are not studied interactively and are mainly addressed using disturbed rock material. At least for confirmation purposes, it would be advantageous to check if the sorption parameters determined on a very small scale can be used to correctly predict radionuclide retardation on a larger scale (intact samples). Such an experiment would also mimic the in situ experiment methodology but in a laboratory scale with intact core, however possibly disturbed by the drilling and pressure release.

In these experiments the diffusion cells used for the through-diffusion experiments were spiked with the LTDE-SD radionuclide cocktail on one side of the cell. The loss of tracer in the injection cell of the diffusion cell was thereafter studied as a function of time. According to the sorption concept used, the rate of losses should be dependent on the diffusivity as well as the sorption coefficient.

A prediction (for confirmatory purposes, see 3.4.1) of the expected rate of loss of tracer in the injection cell was made based on the analytical solution for diffusion in a sheet /Crank 1975/. The model for diffusion in a sheet has been presented earlier in /Widestrand et al. 2006/ and is included in Appendix 12. In addition to the predictions, evaluations with estimation of K_d, D_e or both parameters were performed for some selected tracers (further described in 3.4.2).

The sorption-diffusion experiments on intact drill core samples were performed for the SKB Site Investigations samples from Oskarshamn and Forsmark (cf. Table 2-5) and for four samples from the small-diameter section in KA3065A03 at LTDE-SD (cf. Table 2-2). Six of the rock samples had undergone previous through-diffusion measurements to determine the diffusivity in the laboratory experiments during the Site Investigation. It should be noted that the surface area to volume ratio, differs somewhat due to varying core diameters since the volume was constant (~35 ml). For the small-diameter (~22 mm) LTDE-SD samples the surface to volume ratio was 0.11 cm^2/ml while it was 0.56 cm^2/ml for the Site Investigations samples (~50 mm core diameter) which is comparable to that of the LTDE-SD in situ experiment of 0.51 cm^2/ml. Consequently, a slightly weaker concentration decrease was expected for the LTDE-SD samples relative to that of the Site Investigations samples for comparable rock types.

The sorption measurements were performed according to the procedure described below, which is a modification/combination of the methods used in through-diffusion (cf. Section 3.2.1) and batch sorption experiments on crushed rock material (Section 3.3.2):

1. The samples were placed in a diffusion cell according to the description in Section 3.2.1 and LTDE-SD tracer solution was injected at the start of the experiment. For those rock core samples that had not undergone previous through-diffusion measurements, tritiated water (H^3HO) was added to the tracer solution.
2. Sampling of the water phase at the high concentration side of the diffusion cell was performed with the same frequency as during batch sorption measurements (cf. Section 3.3.2) for all samples.
3. Sampling at the low-concentration side was performed for those samples that had H^3HO in the tracer solution.
4. Analysis of nuclide concentrations were thereafter performed with analysis methods as specified in Table 2-7.
5. Evaluations were done by fitting K_d, F_f or both to the model using a least square minimization method.

All sampling was done by using an automatic pipette. H^3HO was injected in such amounts that the detection limit (roughly 1 Bq/ml) gave a dynamic measurement range of about five orders of magnitude relative to the injected concentration. The LTDE-SD synthetic groundwater described in 3.3.2 above was used for both LTDE-SD and Site Investigations samples. The sorption-diffusion experiments on intact rock samples were carried out at the Nuclear Chemistry Group at Chalmers University of Technology (CTH).

3.4.1 Predicted loss of tracer in the aqueous phase

A "prediction", here defined as a calculation using fixed ε, K_d and D_e data, of the rate of loss of tracer in the aqueous phase and the final penetration profile in the rock as a function of depth, was made for confirmatory purposes. The prediction was calculated using the analytical solution for diffusion in a sheet presented in Appendix 12. The predictions were based on:

- Tracer-specific diffusivities (or formation factor) determined by through-diffusion of H^3HO for that particular sample, combined with the tabulated water diffusivity of the tracer.
- K_d values determined for the particular rock type in batch sorption experiments using crushed rock material (1–2 mm size fraction, 186 d of contact time; according to the selections presented and motivated in /Byegård et al. 2008, Selnert et al. 2009b/.
- Water saturation porosity from the particular sample.

3.4.2 Parameter estimations of K_d and/or F_f

Estimation of K_d, F_f (related to D_e according to Equation 3-1) or both parameters were performed for some selected tracers. In the estimations, K_d, F_f or both parameters were estimated by curve fitting to the experimental data using a least squares minimization method. A corresponding penetration profile was calculated for each estimation. In all cases the water saturation porosity of each individual sample was used and it was held constant. The different cases estimated were:

- **Estimation of K_d** with fixed F_f from H^3HO through-diffusion experiment of the specific sample.
- **Estimation of F_f** with K_d values fixed from the results of batch sorption experiments determined for the particular rock type using crushed rock material (1–2 mm size fraction, 186 d of contact time).
- **Estimation of K_d and F_f** simultaneously.

3.5 Summary of the rock samples and methods

A single rock sample used in the present laboratory investigation might be involved in one or several measurements. Table 3-1 present the method/methods applied for each rock sample.

Table 3-1. Overview of the rock samples versus the different methods. The samples have been divided into three general types: 1, matrix rock; 2, matrix rock with fracture surface; 3, mainly fracture mineralizations, in addition to mylonitic/cataclasitic rock matrix; 4, strongly altered bedrock.

Sample ID	Type of sample	Porosity. water saturation	PMMA porosity	Electrical resistivity	Through-diffusion	Sorption/ diffusion	BET, specific surface area	Batch sorption, crushed rock
LTDE-SD rock samples:								
A02:1	2						X	X
A02:2	2–3						X	X
A02:4	1	X			X			
A02:5	1	X		X				
A02:6	1						X	X
A02:7	1	X		X				
A02:8	1	X			X			
A03:1	1						X	X
A03:2	1						X	X
A03:3	2	X			X	X		
A03:4	1	X			X	X		
A03:5	1	X			X	X		
A03:6	1	X			X	X		
A03:7	1	X	X					
A03:8	1	X	X					
A03:9	3						X	X
A03:10	3/4	X	X					
A03:11	3	X	X					
A19	2		X					
Site investigation rock samples:								
Forsmark site investigation samples /Selnert et al. 2008/:								
KFM02A 276.06	4	X	(X)**		(X)*	X		
KFM03A 242,43	1	X	(X)**		(X)*	X		
KFM07A 608,75	1	X	(X)**		(X)*	X		
KFM09A 713,67	1	X				X		
Oskarshamn site investigation samples /Selnert et al. 2009a/:								
KSH01 891,91	1	X			(X)*	X		
KSH01 981,43	1	X			(X)*	X		
KLX02 235,08	1	X			(X)*	X		
KLX04 726,07	1	X				X		
KLX08 417,05	1	X				X		
KLX10 995,79	1	X						

*Result used in evaluation of sorption-diffusion on intact rock but not presented in this report.

**Measured on adjacent rock sample.

4 Experimental results and interpretation

4.1 Porosity measurements

Porosity has been investigated for 12 rock samples, primarily with water saturation technique although a few samples have undergone measurements with the ^{14}C-PMMA technique.

4.1.1 Water saturation

The porosity results are presented in Table 4-1 and Figure 4-1. See also Appendix 2 for the sample positions in the cores. The average porosity value and sample standard deviation for all A02 and A03 rock core samples are 0.26 ± 0.08%, which is consistent with the porosity results for Ävrö granodiorite obtained during the Site Investigations (0.32 ± 0.15% for samples located outside deformation zones /Selnert et al. 2009a/). When the samples are divided into groups of 22 mm and 44 mm rock cores respectively, the 44 mm rock cores seem to have a somewhat more homogenous distribution than the 22 mm samples. A plausible explanation for that could be that there is a higher frequency of microfractures in the 22 mm core samples.

An important observation is made for the two fracture material samples (A03:10 and 11), which have porosities of 2.35% and 5.16%, i.e. a factor of 10 to 20 times higher than the porosity of the matrix rock. The first sample consists of both altered (red-stained) bedrock, mylonitic/cataclasitic rock and fracture coatings, while the latter sample nearly entirely consist of fracture minerals and cataclasite with a matrix dominated by chlorite and epidote.

Most variations of porosity observed for the samples A02:4-8 and A03:3-8 are close to or within the measurement uncertainty intervals (± 0.1% for 2σ in the water saturation method). The weakly oxidized 36 mm borehole samples A03:7-8 indicate a slightly increased porosity compared to the less oxidized samples A03:3-6. The PMMA porosity of these samples is higher than the water saturation porosity, normally the opposite result apply /Siitari-Kauppi 2002/. A possible explanation may be that the drying temperature is 70°C in the method applied in this work, whereas higher drying temperatures were applied in the comparison by Siitari-Kauppi. It should however also be acknowledged that no well-defined measure of the uncertainty in an individual measurement with the PMMA method is available.

The Site Investigation samples represent different rock types from the Laxemar and Forsmark areas and thus a slightly broader range in porosities, which is further described in /Selnert et al. 2009b, Byegård et al. 2008/.

Table 4-1. Summary of the results from measurements of porosity, ε, in rock material from KA3065A02, KA3065A03 as well as the rock samples from the Site investigation included in the sorption/diffusion experiments on intact cores. The porosity is expressed in vol.%. The measurement uncertainty of a single porosity value determined by the water saturation method is 0.05 vol.%, given with 1σ confidence. The samples have been divided into four general types: 1, matrix rock; 2, matrix rock with fracture surface on one side; 3, mainly fracture mineralizations and cataclasitic rock matrix; 4, strongly altered bedrock.

Rock sample ID	Type of sample	Water saturation measurements (vol.%)				^{14}C-PMMA measurements (vol.%)	
		22 mm core diameter	44 mm core diameter	50 mm core diameter	irregular rock samples	22 mm core diameter	irregular rock samples
LTDE-SD samples							
A02:4	1		0.23				
A02:5	1		0.28				
A02:7	1		0.23				
A02:8	1		0.17				
A03:3/Diff I	2	0.33					
A03:4/Diff II	1	0.16					
A03:5/Diff III	1	0.19					
A03:6/Diff IV	1	0.27					
A03:7	1	0.36				0.51	
A03:8	1	0.40				0.61	
A03:10	3/4				2.35		2.4/11*
A03:11	3				5.16		2.0/11*
Forsmark site investigation samples /Selnert et al. 2008/							
KFM02A 276.06	4			18.4			
KFM03A 242,43	1			0.19			
KFM07A 608,75	1			0.29			
KFM09A 713,67	1			0.24			
Oskarshamn site investigation samples /Selnert et al. 2009a/							
KSH01 891,91	1			0.46			
KSH01 981,43	1			0.29			
KLX02 235,08	1			0.39			
KLX04 726,07	1			0.08			
KLX08 417,05	1			0.45			
KLX10 995,79	1			0.06			

*Concerning the PMMA; mean values for the strongly altered bedrock are given to the left and for the cataclasite to the right.

4.1.2 ^{14}C-PMMA

In this section the results of the ^{14}C-PMMA- measurements are summarized. A more detailed description with all PMMA-results is given in Appendix 3.

Matrix rock

The porosity distribution in the matrix rock is relatively homogeneous which is exemplified in Figure 4-2 and Figure 4-3, where two subsamples representing two different surface areas of the rock sample A03:7 are shown. The autoradiograph reveals grain boundary pores which are visible around feldspar and quartz grains. In addition dark minerals show high porosities, so the sorption properties of the dark minerals might dominate during diffusive transport. Furthermore, dark minerals contain more Fe, required to reduce U, Np and possibly Tc. Similar results were obtained for sample A03:8 and in the deeper parts of sample A19 (which is also a KA3065A03 sample, see Table 2-3).

Based on the water saturation and PMMA-results, this type of relatively homogeneous porosity distribution can be expected for the matrix rock in the 36 mm extension borehole of KA3065A03 and in the deeper parts of the stub (behind the altered part of the fracture surface).

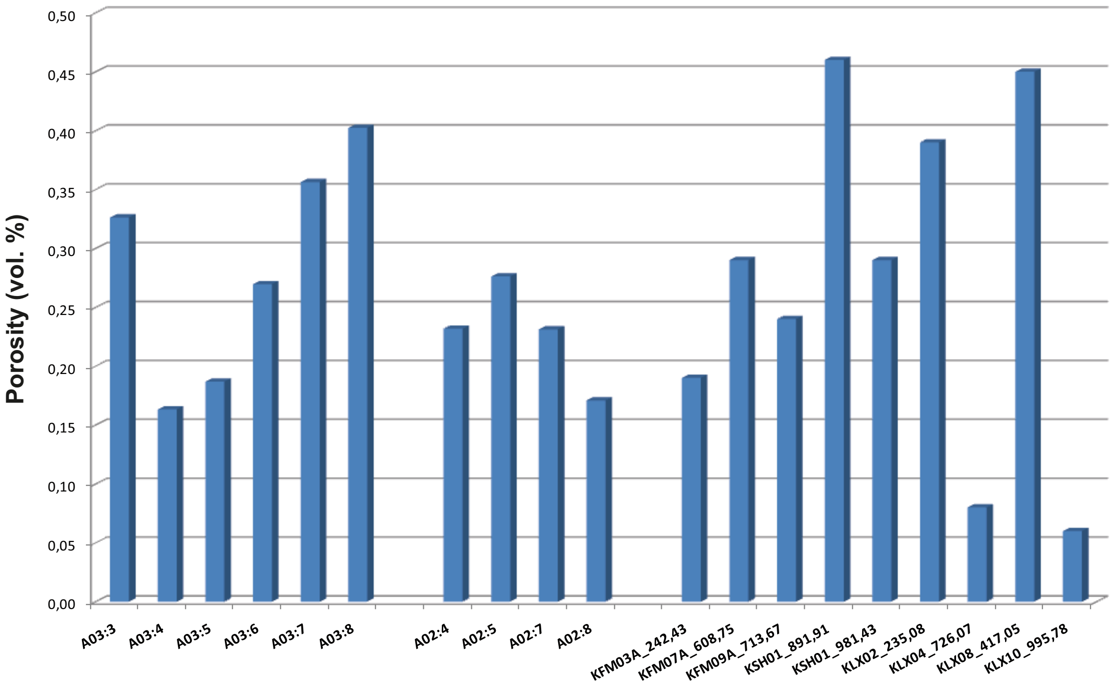

Figure 4-1. *Porosities, measured with water saturation technique, for rock core samples from KA3065A03 (22 mm in diameter) to the left in the figure, KA6035A02 (44 mm in diameter) in the middle of the figure and rock core samples from the Site Investigation at Forsmark and Oskarshamn to the right in the figure. The current rock samples represent the fresh to medium altered bedrock. For rock type descriptions, see Table 2-2 and Table 2-5. One rock sample from the Site Investigation is excluded due to extremely high porosity (i.e. KFM02A 276.06, 18.4% porosity).*

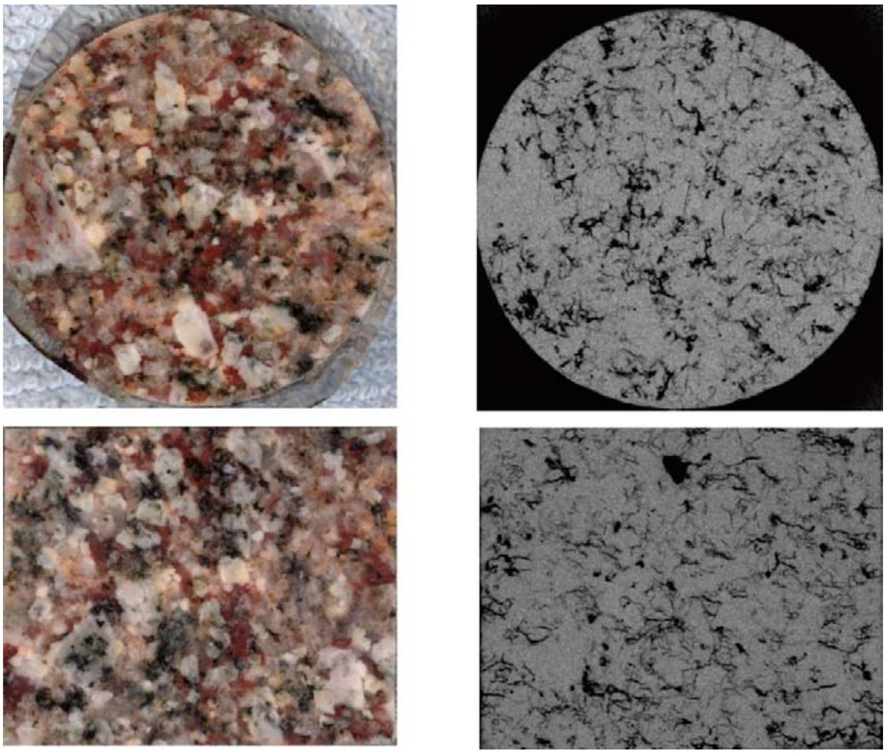

Figure 4-2. *Photo image of; sample A03:7A (upper left) and the corresponding autoradiograph (upper right) with a diameter of 22 mm, sample A03:7B (lower left) and the corresponding autoradiograph (lower right). The width of the sample A03:7B is 23 mm.*

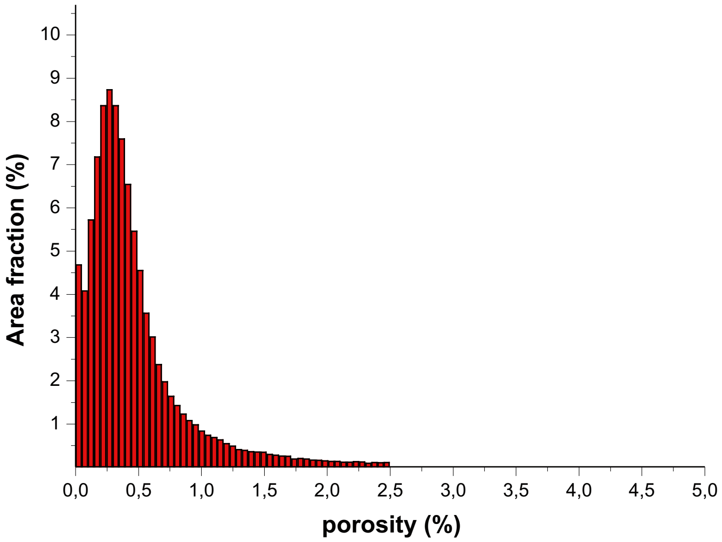

Figure 4-3. *Porosity histogram obtained for sample A03:7 measured using the PMMA technique. The mean value of porosity in this measurement is 0.51% which can be compared to the porosity determined by the water saturation technique, i.e. 0.36%.*

Fracture mineralizations and altered rock

The two fracture samples that were analyzed, A03:10 and 11, both show a strongly heterogeneous porosity distribution. A03:11 is presented as an example in Figure 4-4 and Figure 4-5. The main observations are:

- Increased porosities in the range from 1% to 3% are found in parts with altered bedrock (i.e. red stained and fractured Ävrö granodiorite).
- Fracture coatings and cataclasitic rock matrix with minerals as chlorite and epidote are generally, i.e. to the largest parts of the areas observed, clearly more porous than the adjacent altered bedrock. Average porosities of ~11% in these mineralizations are found in both samples.
- A minor part of the sample indicates poor penetration and thus a dense matrix, possibly caused by mylonitization. Such observations were e.g. done in TRUE-1 materials /Widestrand et al. 2007/ where light green, highly chloritized layers were not fully impregnated and were classified nonporous with the PMMA method (< 0.05% porosity).
- Porosity profiles are observed in the fracture mineralizations, with increasing porosity towards the fracture surface (see A03:10C in Appendix 3).

The A19 sample, which was drilled from the fracture close to the stub surface (see Appendix 3) and analysed by PMMA, show a relatively low porosity also near the fracture surface. Consequently, variations in the porosity of the fracture surface area can be expected from even denser matrix than in the typical matrix rock to strongly increased porosity.

The actual amounts of fracture mineralizations, cataclasitic rock matrix and strongly altered rock found after excavation and analysis of the rock /Nilsson et al. 2010/ show only relatively thin layers of fracture coatings (< 2 mm) and altered rock to about 1 cm. Nevertheless, based on the water saturation and PMMA-results, we expect the following general features of the stub materials relevant for the in situ tracer test (without respect to the actually existing amounts):

- *Fracture mineralizations and cataclasitic rock matrix*: a strongly increased porosity compared to that of matrix rock is expected, with a heterogeneous distribution and a decreasing gradient inwards.
- *Rock with different degrees of alteration close to the fracture surface:* porosity from 0.2 to a few % with a more heterogeneous distribution than in the matrix rock is expected near the fracture surface. This applies to a major part of the stub area.
- *Mylonitized parts close to the fracture surface:* in these areas, that are estimated to apply for a minor part of the stub area, a low porosity that may even be decreased compared to the porosity of matrix rock is expected. The quantity of mylonite seems to be confined to minor areas in the rock samples examined; it should be acknowledged though that only a few samples are studied and that this quantification is uncertain.
- *Matrix rock:* a relatively homogeneous distribution is expected.

***Figure 4-4**. Photo image of sample A03:11 (left) and corresponding autoradiograph (right). The width of the sample is 23 mm. The porosity of the white calcite coating is 1.7% and the porosity of the fracture coating and cataclasitic rock matrix is 11%. The thin bedrock material close to the calcite coating is of low porosity compared to the other materials. The sample was in contact with open fractures on both sides (left and right).*

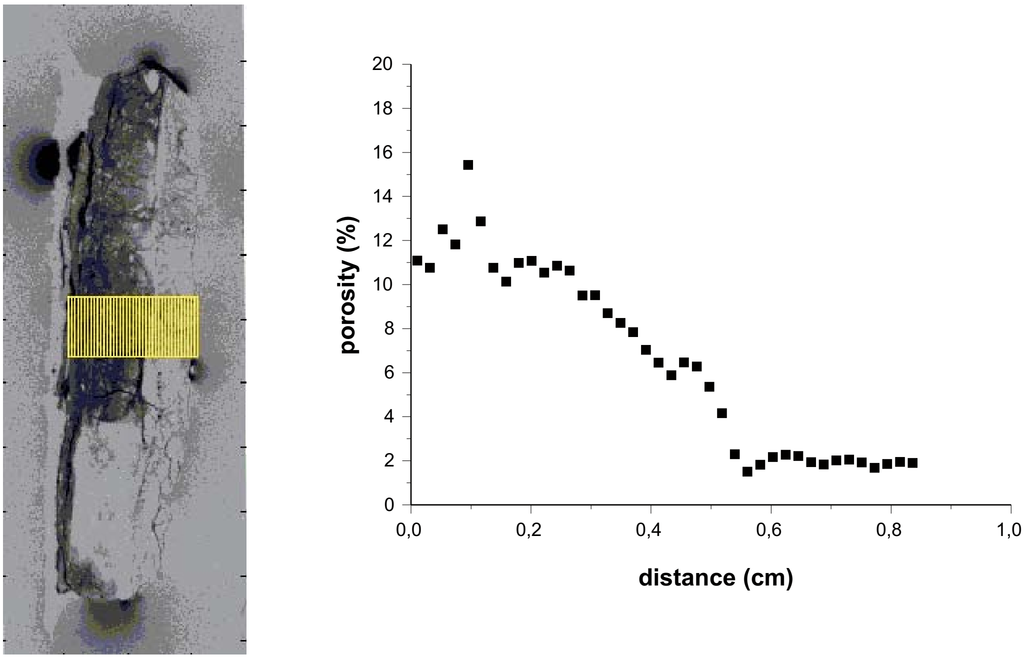

***Figure 4-5**. Porosity profile of the yellow-marked area on rock sample A03:11. The sample was in contact with open fractures on both sides (left and right) at position 0.0 and ~0.85 cm respectively.*

4.2 Through-diffusion and electrical resistivity experiments

Results from the through-diffusion experiments are presented in the form of examples of concentration-time curves including model fit in Figure 4-6 to Figure 4-8 and in Table 4-2 where the results are summarized. The full result presentation can be found in Appendix 4. The qualitatively best results were obtained for the two A02 samples for which the concentration slowly increases and a steady state is reached and the overall fit to the model is excellent. The A03-samples all indicate an initial contamination of the target cell which affects the α-value. Consequently, only D_e was evaluated for the A03 samples. Sample A03:3 gave no verified breakthrough due to its comparably large thickness (70 mm) relative to the monitored time range. Sample A03:2 had a leakage and had to be interrupted.

The diffusivities obtained in A02 and A03 samples are all in the relatively narrow range from $2.7 \cdot 10^{-14}$ to $6.5 \cdot 10^{-14}$ m^2/s, a result which is coherent with the fact that the sampled borehole sections are close to each other (< 1 m) and of the same rock type and also being sampled as homogeneous and relatively undisturbed specimens. Estimation of D_e with fixed porosity (=water saturation porosity) give nearly the same result as for estimated α values for the A02 samples. Thus, the homogeneous porosity model seems to be a good approximation for the pore system of the A02 samples. The homogeneous structure of the porosity in the samples from the 36 mm extension borehole of KA3065A03 is verified by the PMMA results, see Figure 4-2.

^{36}Cl was detected in the target cell of A03:5 in the last four samples during the experiment, see Figure 4-8. The reason for the late detection is that a much lower activity concentration was used than that of H^3HO, which was added separately in addition to the LTDE-SD cocktail that included the ^{36}Cl. No difference in diffusivity can be observed between ^{36}Cl and H^3HO in this sample, which on one hand can be interpreted as absence of anion exclusion in the sample. On the other hand, ^{36}Cl was not detected in A03:6 within 513 days, although A03:5 and A03:6 had nearly equal H^3H O diffusivities. Based on the minimum detectable activity in the measurements, a maximum diffusivity of about $2 \cdot 10^{-15}$ m^2/s could be estimated for A03:6, which could be interpreted as an anion exclusion effect in this sample. The results of the ^{36}Cl diffusion in these two samples are contradictory and difficult to explain and a larger sample quantity would be needed for future studies of anion exclusion.

The formation factors obtained from electrical resistivity measurement of samples A02:5 and 7 are slightly higher relative to those obtained by through-diffusion (see Appendix 4). Earlier comparisons between the two methods have shown that somewhat higher formation factor values generally are obtained by the resistivity method /Byegård et al. 2008, Selnert et al. 2009b/. In that view, the A02 samples do not differ significantly.

The diffusivities and porosities of the Forsmark and Laxemar samples are included for comparative purposes in Table 4-2. The full experiment evaluation of these samples is presented earlier in /Selnert et al. 2008, 2009a/.

Table 4-2. Summarized results from the through-diffusion and electrical resistivity experiments of the LTDE-SD samples. The errors given represent individual uncertainty (2 σ) in the estimation procedure for each through-diffusion sample. The Forsmark and Laxemar Site Investigations samples results are included for comparison. All data are presented in Appendix 4 Through-diffusion results.

Sample	ε (vol.%) (water saturation)	$F_{f,\text{ electrical resistivity}}$ (–)	$D_{e,H3HO}$ (m^2/s) (D_e and α fitted)	$D_{e,H3HO}$ (m^2/s) (D_e fitted, α=ε)	$D_{e,Cl\text{-}36}$ (m^2/s) (D_e and α fitted)	Comments
A02:5	0.28	$5.7\cdot10^{-5}$	–	–	–	Repeated measurements gave a variation of about ± 1%
A02:7	0.23	$3.9\cdot10^{-5}$	–	–	–	Repeated measurements gave a variation of about ± 1%
A02:4	0.23	–	$(6.5 \pm 0.4)\cdot10^{-14}$	$6.1\cdot10^{-14}$	Not used	
A02:8	0.17	–	$(3.0 \pm 0.2)\cdot10^{-14}$	$2.7\cdot10^{-14}$	Not used	
A03:3	0.33	–	No breakthrough	No breakthrough	No breakthrough	No verified breakthrough observed during exp.time.
A03:4	0.16	–	–	–	–	Disrupted due to mechanical failure.
A03:5	0.19	–	$(4.5 \pm 0.1)\cdot10^{-14}$	$5.2\cdot10^{-14}$	$(5 \pm 2)\cdot10^{-14}$	α could not be evaluated due to disturbance of initial contamination. Cl-36 detected after 316 days, evaluated on 4 data points.
A03:6	0.27	–	$(4.3 \pm 0.4)\cdot10^{-14}$	$5.8\cdot10^{-14}$	Not detected	α could not be evaluated due to disturbance of initial contamination. Cl-36 was not detected within 513 days. Note that detection limits are different between H^{3}HO and Cl-36.
KFM02A 276.06	18.4		$3.4\cdot10^{-11}$			
KFM03A 242,43	0.19		$1.8\cdot10^{-13}$			
KFM07A 608,75	0.29		$1.4\cdot10^{-12}$			
KFM09A 713,67	0.24		$(2.5\cdot10^{-13})$*			
KSH01 891,91	0.46		$1.1\cdot10^{-12}$			
KSH01 981,43	0.29		$4.8\cdot10^{-13}$			
KLX02 235,08	0.39		$6.8\cdot10^{-13}$			
KLX04 726,07	0.08		$(2.4\cdot10^{-13})$*			
KLX08 417,05	0.45		$(9.8\cdot10^{-13})$*			
KLX10 995,79	0.06		$(4.8\cdot10^{-13})$*			

*Rock type mean value, the specific sample was not measured.

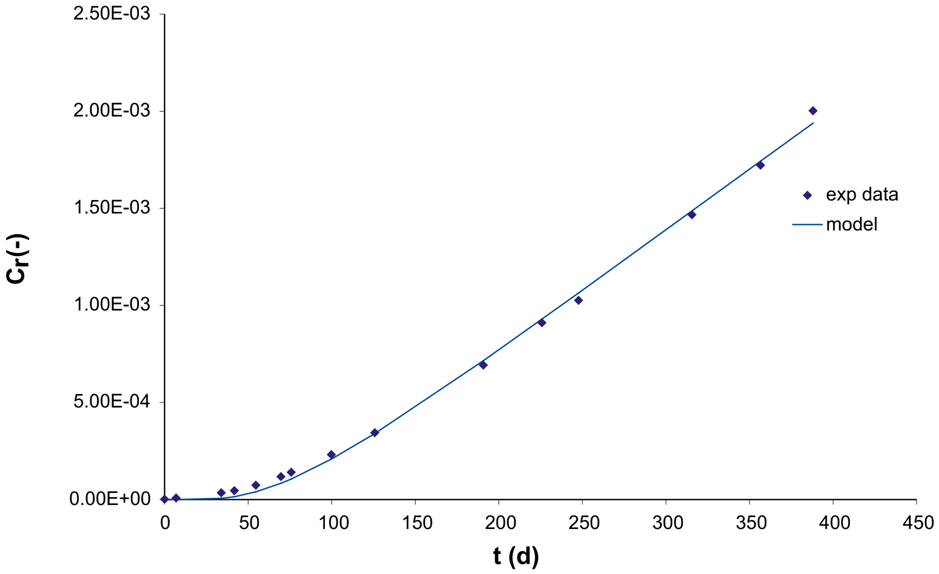

Figure 4-6. *Results of the through-diffusion experiment for the A02:4 sample, using H^3HO as tracer. The reduced concentration, C_r, (Cf. Equation 3-2) is presented as a function of the experimental time, t.*

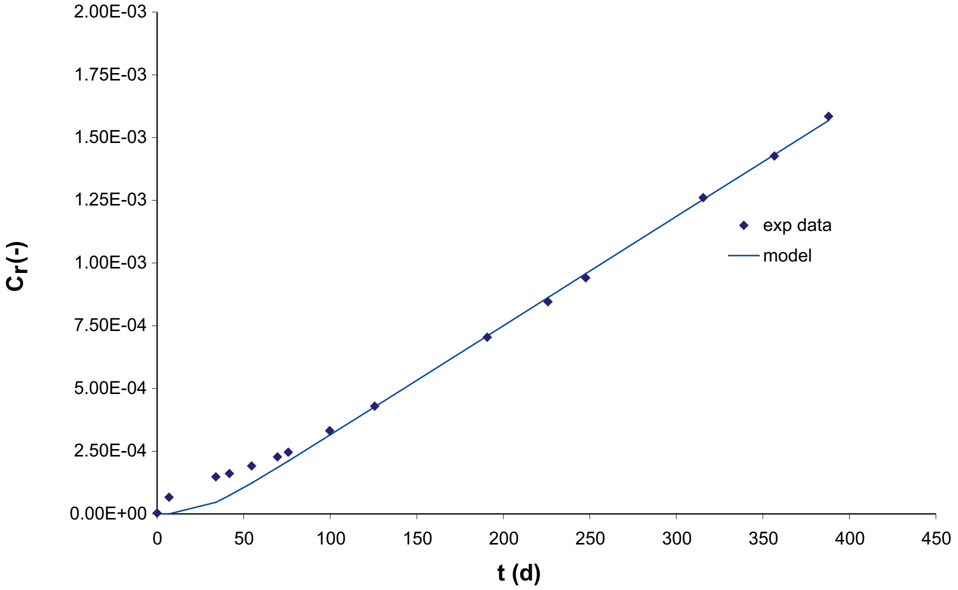

Figure 4-7. *Results of the through-diffusion experiment for the A03:5 sample, using H^3HO as tracer. The reduced concentration, C_r, (Cf. Equation 3-2) is presented as a function of the experimental time, t.*

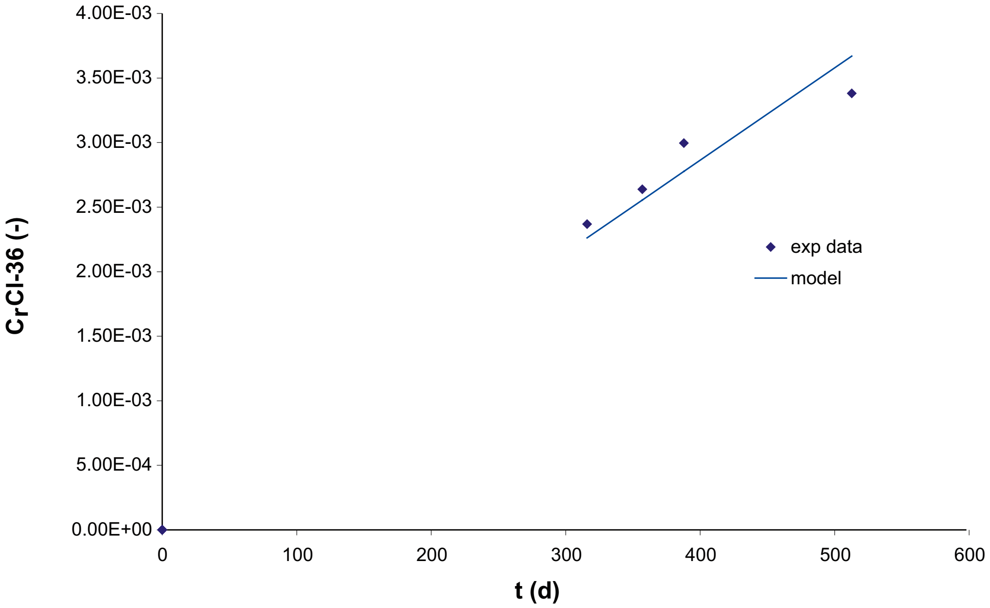

Figure 4-8. *Results of the through-diffusion experiment for the A03:5 sample, using Cl-36 as tracer. The reduced concentration,* C_r*, (Cf. Equation 3-2) is presented as a function of the experimental time, t.*

4.3 Sorption-diffusion experiments on intact drill cores

4.3.1 Results for LTDE-SD samples

All four concentration-time curves for the LTDE-SD sorption-diffusion samples of intact drill cores are shown in Appendix 5 and an example from A03:3/Diff I is presented in Figure 4-9. The strongest sorption is generally observed for $^{110\,m}$Ag which only could be detected in the first one or two samples. ^{63}Ni, ^{57}Co, ^{109}Cd and ^{236}U show a relatively strong sorption; ^{137}Cs and ^{75}Se show intermediate sorption and ^{22}Na, ^{36}Cl, ^{133}Ba, ^{237}Np and ^{226}Ra show only weak or no sorption at all. The results are mainly in line with what could be expected from the outcome of the batch sorption experiments with a few exceptions. The Ra sorption is weaker than expected, but the C/C0 reaches almost 1.4 for Ra and Np, which, in combination with the rather large error bars, indicate difficulties in the ICP-MS detection of these radionuclides. The sorption of U is relatively strong in all four samples, which possibly is a result of reduction from the hexavalent state to its very insoluble and strongly sorbing tetravalent state. No analysis results were obtained for Tc due to ICP-MS equipment failure.

Sorption was also studied on an epoxy resin disc, and the only tracer that indicate sorption (although observed for two samples only) was $^{110\,m}$Ag (see the last figure in Appendix 5).

Table 4-3. D_e and K_d values and selection basis for predictions of loss of tracer in the aqueous phase for Ni-63 and Cs-137. Average values for the 1–2 mm fraction at 186 d were used for the K_d values. Porosities were used for each sample according to water saturation data in Table 4-1.

	A03:3/Diff I	A03:4/Diff II	A03:5/Diff III	A03:6/Diff IV
ε	0.33 (vol.%)	0.16 (vol.%)	0.19 (vol.%)	0.27 (vol.%)
K_d	Replica material/ A03:9	KA3065A03_Batch 1_C/ A03:1 (matrix rock)		
Ni-63	2.7E-01 m³/kg	No data	8.2E-03 m³/kg	8.2E-03 m³/kg
Cs-137	8.6E-01 m³/kg	2.2E-02 m³/kg	2.2E-02 m³/kg	2.2E-02 m³/kg
$D_{e(H3HO)}$	Average of Diff III and IV	Average of Diff III and IV	Diff III	Diff IV
	4.4E-14 m²/s	4.4E-14 m²/s	4.5E-14 m²/s	4.3E-14 m²/s

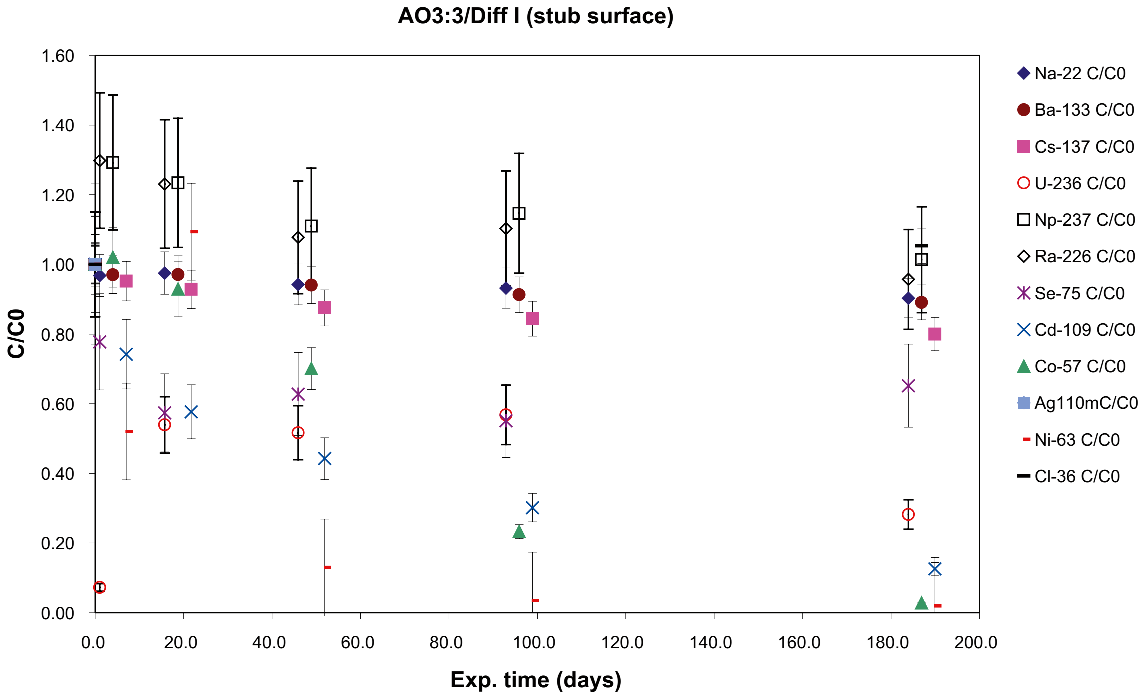

Figure 4-9. *Results of the sorption experiment on entire drill core, i.e. the relative concentration, C/C_0, in the start cell as a function of the experimental time, data presented for sample A03:3.*

4.3.2 Predictions of loss of tracer in the aqueous phase for LTDE-SD sorption-diffusion intact rock samples

Predictions of concentration-time curves based on laboratory determined diffusivity and sorption coefficient were performed for the ^{137}Cs and ^{63}Ni tracers; two of the tracers that have been extensively used in the site batch laboratory experiments within the site investigation program /Byegård et al. 2008, Selnert et al. 2009b/. The calculated results are shown in Figure 4-10 (delta 1 and delta 2 represents the prediction when calculated with the upper and lower uncertainty in the batch K_d values) given in comparison to the measured experimental data. Besides that, the theoretical penetration profiles for diffusion in to the rock obtained using the same retention data is given in Figure 4-11. The diffusivities and batch K_d values selected for the calculations are shown in Table 4-3. For A03:3 the K_d is based on the replica material data, since it is assumed that this best reflects the properties of the stub surface, whereas 36 mm borehole data for matrix rock is used for the other samples. All results are included in Appendix 7.

The concentration loss of ^{137}Cs in two of the samples (Diff II and III) is underpredicted relative to the measurement data (i.e. the calculated concentrations are higher than the measurement uncertainty range for a majority of the samples), one is within the measurement uncertainties (Diff IV) and one is slightly overpredicted (Diff I). The concentration losses for all three ^{63}Ni evaluations were underpredicted. Apparently, Ni sorbs stronger in the intact rock sample than what is predicted based on the batch sorption measurement. One may speculate that the poor prediction for Ni is related to increased surface complexation possibilities in the intact rock compared to the crushed rock material but no such conclusions can be made based on the available data. It can also be noted that Äspö quartz monzodiorite and Quartz monzodiorite in the Laxemar Site Investigations /Selnert et al. 2009b/ had about two to three times larger K_d for Ni compared to Cs for brackish to saline water. For the Ävrö granodiorite in this work the opposite relation is observed. ^{63}Ni was not analysed in the Site Investigation studies of sorption on intact rock samples so for the LTDE-SD result no such comparison can be made for Ni.

The predicted penetration depths are on the order of a few tenths of a mm up to one mm for all predictions of ^{137}Cs and ^{63}Ni, which is exemplified for A03:3/Diff I in Figure 4-11.

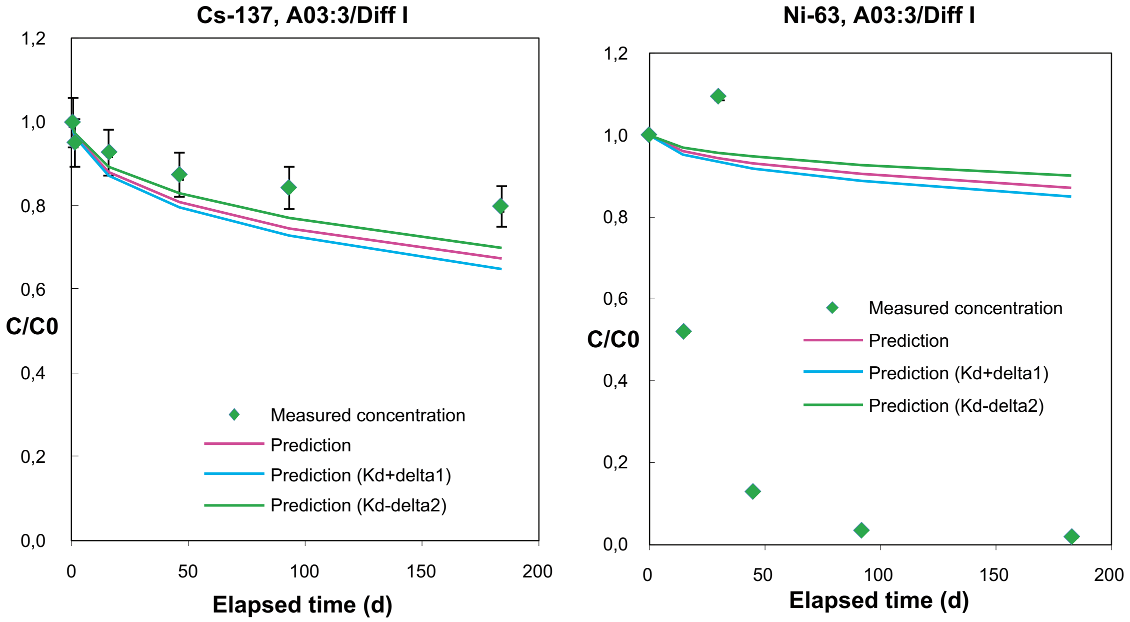

Figure 4-10. Predictions of the sorption of ^{137}*Cs (left) and of* ^{63}*Ni (right) in an experiment comprising sorption on an entire drill core sample, in this case the A03:3/Diff I sample. The experimentally measured data are presented as a comparison.*

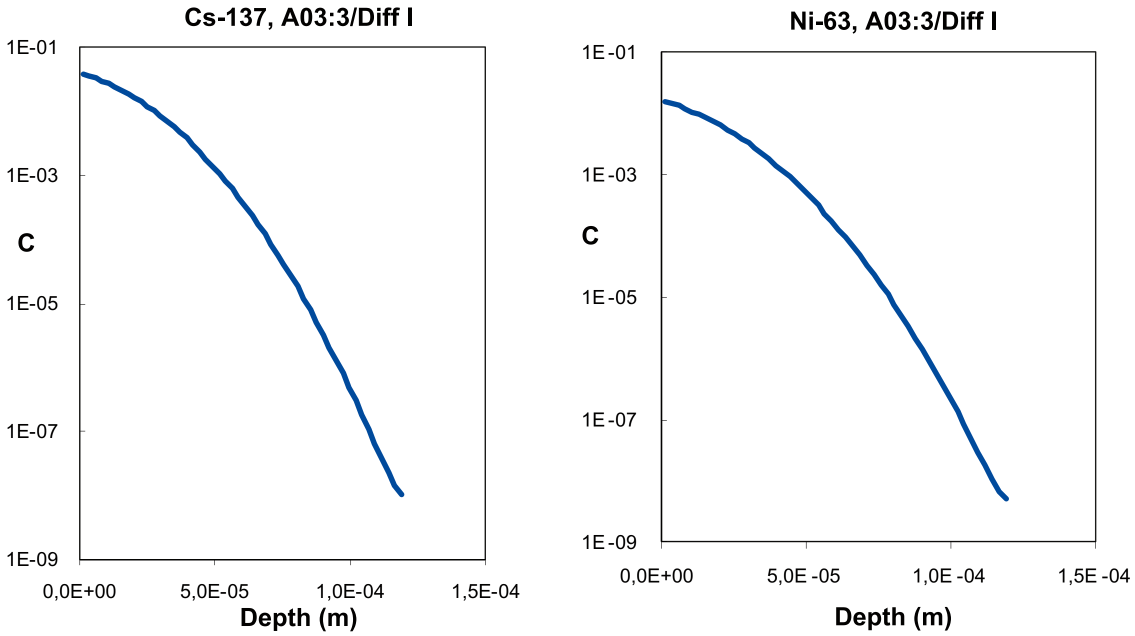

Figure 4-11. Examples of predicted penetration depths for A03:3/Diff I, ^{137}*Cs (left) and* ^{63}*Ni (right) using laboratory data for the retention parameters (batch sorption experiment for* K_d *and through diffusion experiment for* F_f*).The C parameter on the Y-axis refers to the part of the total added tracer that is present at the depth given by the projection to the X-axis.*

4.3.3 Parameter estimations of K_d and/or F_f for LTDE-SD sorption-diffusion intact rock samples

After the pure predictive exercise had been performed, attempts were made to vary the retention parameters in order to obtain a better agreement with the measured laboratory data. Calculations were performed by varying K_d together with a F_f from laboratory data and vice versa by varying F_f and using a laboratory determined K_d according to the procedure described in Section 3.4.2.

It was soon realised that the rate of the loss of tracer in the aqueous phase is solely determined by the combined product of $K_d\,F_f$. This assumption is valid as long as the porosity, ε, is negligible compared to the $K_d\,\rho$; under normal crystalline rock conditions this is fulfilled as long as the $K_d > 1\cdot10^{-4}$ m^3/kg. However, as explained in Figure 4-12, the present experimental technique (studies of losses of tracer in the aqueous phase) can only produce a unique $K_d{\cdot}F_f$– value for a given dataset and can not evaluate the individual values in this product. To do so, one need to obtain and analyse the data for the penetration profile in the rock; an experimental technique that was not addressed within this part of the project but will be dealt with in the analyses of the rock material in the in situ experiment /Nilsson et al. 2010/.

The results of the parameter estimation is given in Table 4-4 where the lumped parameter $K_d{\cdot}F_f$ that gives the best fit to the experimental data, is presented. Furthermore, attempts are made to use this lumped parameter to calculate a K_d using the F_f determined in laboratory through diffusion experiment. Additionally, a reversed attempt is made to calculate a F_f by inserting the batch sorption K_d in the lumped parameter. The resulting values are presented and compared to the corresponding batch sorption/through diffusion data in Figure 4-13 and a comparison of the $K_d{\cdot}F_f$ estimated values with the $K_d{\cdot}F_f$ determined from laboratory data is also presented in the bar charts in Figure 4-14 and in Table 4-5. All resulting concentration-time curves and associated penetration depth curves are shown in Appendix 9.

The results presented in Figure 4-13 indicate that one, for the majority of tracers, has to apply a very high K_d (or significantly increased F_f) to explain the observed rate of losses in the aqueous phase. For e.g. ^{63}Ni, one has to include a K_d 2–3 orders of magnitudes higher than the corresponding K_d determined in the laboratory sorption experiment. The only exception to this trend is the ^{137}Cs tracer in the A03:3 sample where the estimated K_d is slightly lower than the batch sorption K_d. A possible explanation to this might be that the diffusion rate in the first pore layer closest to the rock water boundary is higher than the diffusivity determined for a large piece of drill core, i.e. that the formation factor used in the calculation is non-representative for the extremely short penetration depth where the sorption interaction is assumed to take place. An alternative explanation is increased porosity at the interface as a result of material preparation.

Concerning the ^{22}Na tracer, one would from results in literature (e.g. /Byegård et al. 1998/) expect more or less no sorption in the present experiment. However, the experimental results (Appendix 9) that there is a trend of small concentration decrease, is nevertheless one that still can be statistically verified. The last value at a contact time indicate a ~10% decrease of the tracer which, given the low diffusivity measured for the sample, still is enough to give a K_d of ~0.1 m^3/kg in the estimation. The prediction of the penetration profile show that no tracer should have diffused longer than 0.3 mm into the matrix. Based on earlier experiments with just a very minor retardation of ^{22}Na in through-diffusion experiment (e.g. /Byegård et al. 1998/) these results seem unrealistic. It is possible that the 10% loss in the aqueous phase represents a general limit of sensitivity of this type of experiment and the results, especially for ^{22}Na, should be regarded as doubtful.

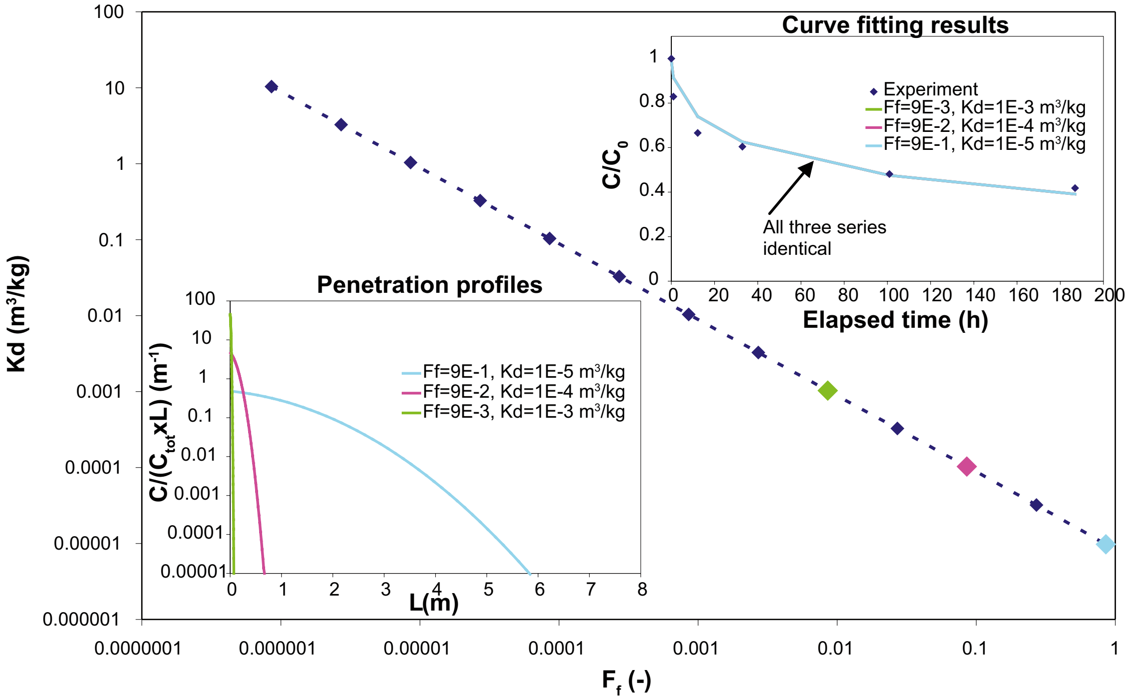

__Figure 4-12.__ Illustration of the dependence of the formation factor (F_f) and the K_d-value in the curve fitting procedure for the sorption loss of Cs tracer in the sorption on intact rock experiment. The major figure show that, within at least a range of 6 orders of magnitudes, the best fitting can be obtained independently of the individually used F_f and K_d, as long as the their product is constant (in this particular case $F_f{\cdot}K_d$=9E-6). However, as expected the penetration profiles differ strongly between the different cases which illustrates that penetration profile measurements are necessary in order to identify the individual values of F_f and K_d, respectively.

Table 4-4. Estimation results for the LTDE-SD sorption-diffusion using intact drill core samples. The estimation results of ($K_d{\cdot}F_f$) combined with the laboratory retention parameters $K_{d(batch)}$ and $F_{f(lab)}$ (values given in italics) were used to calculate individual values of K_d and F_f, respectively. K_d +Δ⁺, K_d –Δ⁻, F_f+Δ⁺ and F_f–Δ⁻ represent the uncertainty range in the parameter estimation.

				K_d calculated using through diffusion formation factor, i.e. =(K_d F_f)/$F_{f(lab)}$				F_f calculated using batch experiment. K_d value i.e. =($K_d{\cdot}F_f$)/$K_{d(batch)}$		
Nuclide	*ε*)* *(vol%)*	($K_d{\cdot}F_f$) (m³/kg)	$F_{f(lab)}$**)	K_d (m³/kg)	Δ⁺	Δ⁻	$K_{d(batch)}$ *(m³/kg)*	F_f	Δ⁺	Δ⁻
Co-57										
Diff I (A03:3)	*0.33*	7.4E-4	*2.1E-5*	3.5E+1	7.0E+1	2.4E+1	*5.3E-1*	1.4E-3	2.8E-3	9.6E-4
Diff III (A03:5)	*0.19*	2.9E-5	*2.1E-5*	1.4E+0	1.0E+0	6.7E-1	*3.5E-2*	8.3E-4	5.9E-4	4.0E-4
Cs-137										
Diff I (A03:3)	*0.33*	5.7E-6	*2.1E-5*	2.7E-1	1.4E-1	1.4E-1	*8.6E-1*	6.5E-6	3.4E-6	3.3E-6
Diff III (A03:5)	*0.19*	7.4E-6	*2.1E-5*	3.5E-1	2.7E-1	1.8E-1	*2.2E-2*	3.4E-4	2.6E-4	1.7E-4
Na-22										
Diff I (A03:3)	*0.33*	1.6E-6	*2.1E-5*	7.6E-2	1.3E-1	6.4E-2	< *3.7E-4*	> 4.3E-3		
Diff III (A03:5)	*0.19*	2.1E-6	*2.1E-5*	1.0E-1	1.2E-1	7.3E-2	< *9.7E-4*	> 2.2E-3		
Ni-63										
Diff I (A03:3)	*0.33*	1.8E-3	*2.1E-5*	8.8E+1	5.4E+2	7.1E+1	*2.7E-1*	6.7E-3	4.1E-2	5.4E-3
Diff III (A03:5)	*0.19*	1.4E-4	*2.1E-5*	6.6E+0	4.3E+0	2.8E+0	*8.2E-3*	1.7E-2	1.1E-2	7.3E-3
Ba-133										
Diff I (A03:3)	*0.33*	3.4E-6	*2.1E-5*	1.6E-1	1.9E-1	1.2E-1	*1.5E-2*	2.3E-4	2.7E-4	1.7E-4
Diff III (A03:5)	*0.19*	9.2E-6	*2.1E-5*	4.4E-1	7.2E+0	4.4E-1	*2.0E-3*	4.6E-3	7.5E-2	4.6E-3
Cd-109										
Diff I (A03:3)	*0.33*	2.7E-5	*2.1E-5*	1.3E+0	1.3E+0	7.6E-1	*9.2E-2*	2.9E-4	2.9E-4	1.7E-4
Diff III (A03:5)	*0.19*	3.4E-3	*2.1E-5*	1.6E+2	9.9E+1	5.5E+1	*4.0E-3*	8.5E-1	5.3E-1	2.9E-1

*) From Table 4-3.

**) For Diff I (A03:3): F_f is based on the average diffusivity of $D_{e(H3HO)}$_Diff III (m²/s) and $D_{e(H3HO)}$_Diff IV (m²/s), see Table 4-3. For Diff III (A03:5): F_f is taken from Table 4-3.

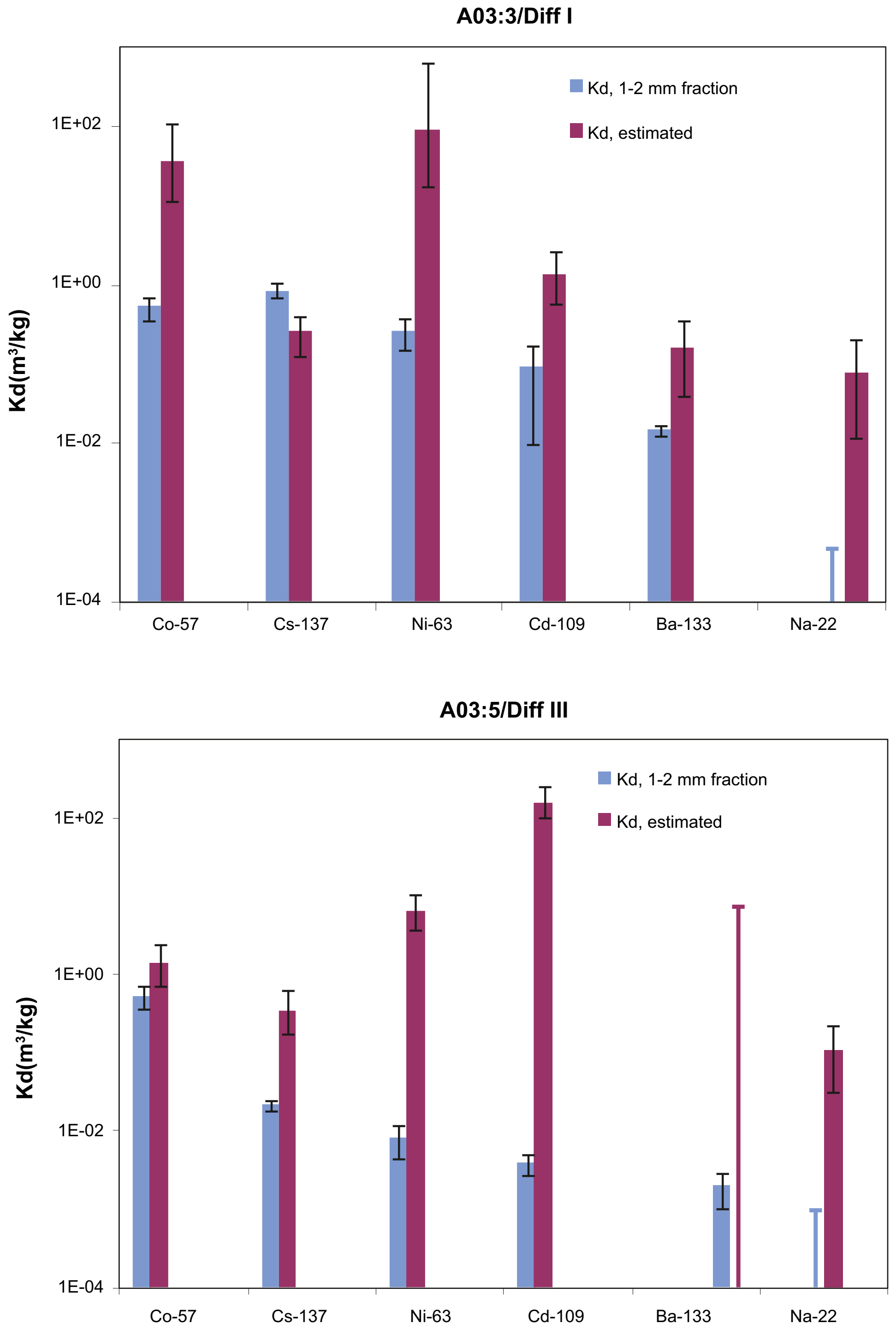

Figure 4-13. *Comparison of estimated K_d values (m^3/kg) with batch sorption data for A03:3/Diff I, matrix rock with fracture surface (top) and A03:5/Diff III, matrix rock (bottom).*

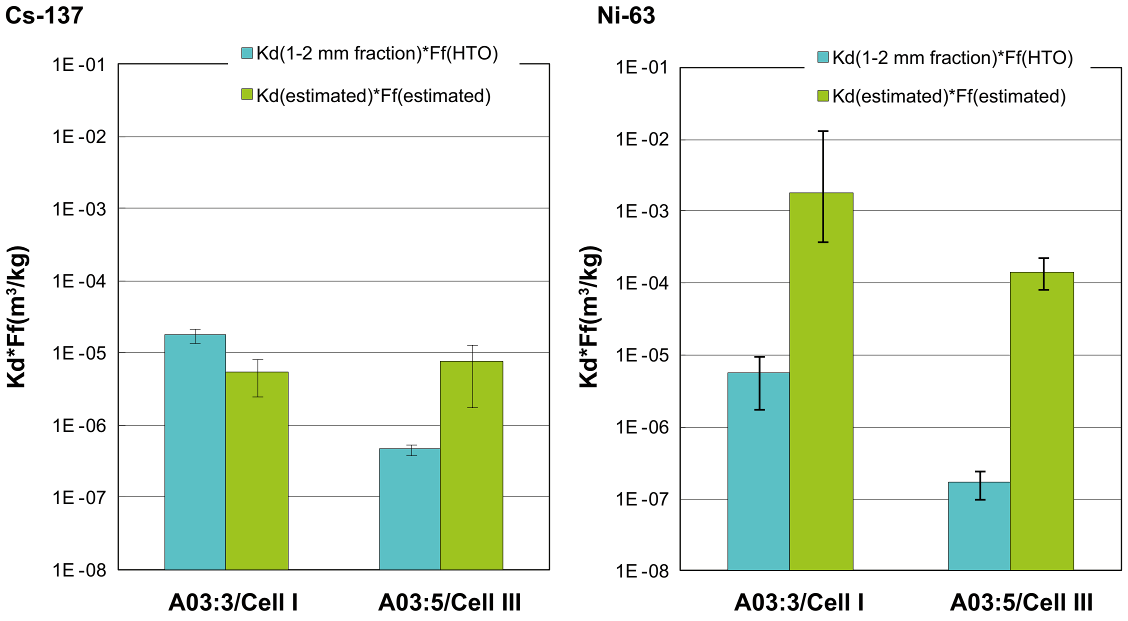

Figure 4-14. *Comparison of estimated $K_d \cdot F_f$ values (in green) for sorption-diffusion on intact drill cores with the product $K_d \cdot F_f$, where K_d is a mean value determined from batch sorption laboratory data (for 1–2 mm fraction, t=186 d) and F_f is determined from through diffusion experiments of H^3HO (see Table 4-3).*

Table 4-5. Summary of the $K_d \cdot F_f$ (m^3/kg) values for Ni and Cs shown in Fig. 4-14.

	Cs-137		Ni-63	
Core	Estimated $K_d \cdot F_f$ (m^3/kg)	Sample specific $K_d \cdot F_f$	Estimated $K_d \cdot F_f$ (m^3/kg)	Sample specific $K_d \cdot F_f$
A03:3/ Diff I	5,7E-06	1,8E-05	1,8E-03	5,7E-06
A03:5/ Diff III	7,4E-06	4,7E-07	1,4E-04	1,8E-07

4.3.4 Results for Forsmark and Laxemar sorption-diffusion intact rock samples

The concentration-time curves are shown in Appendix 6. As an example, the concentration-time curve for Ävrö granodiorite sampled at KLX02 235.08 m is given in Figure 4-15. The Ävrö granodiorite is the rock type also present at the LTDE-SD experiment site at Äspö HRL The results presented in Figure 4-14 are basically in line to what can be expected from the outcome of the batch sorption experiments within the LTDE-SD and Site investigation program; e.g. very low (if any) losses of Sr, moderate losses of Cs and a complete sorption of the trivalent lanthanide Gd. Rather strong sorption of the U-236 isotope is observed which is not expected from the batch sorption results using the 1–2 mm size fraction. However, indication of strong sorption of U (possibly as a result of reduction to its tetravalent state) was indicated for the smaller size fractions which could be an indication that the surface of the drill core sample could be better approximated by crushed rock material of smaller size than the 1–2 mm size fraction.

However, the non-sorption for Tc (and very low sorption for Np) contradicts the hypothesis of reducing conditions in the interface of the water and the drill core sample surface. The C/C0 going up to almost 1.4 for Tc in combination with the rather large error bars, indicate difficulties in the ICP-MS detection of this radionuclide.

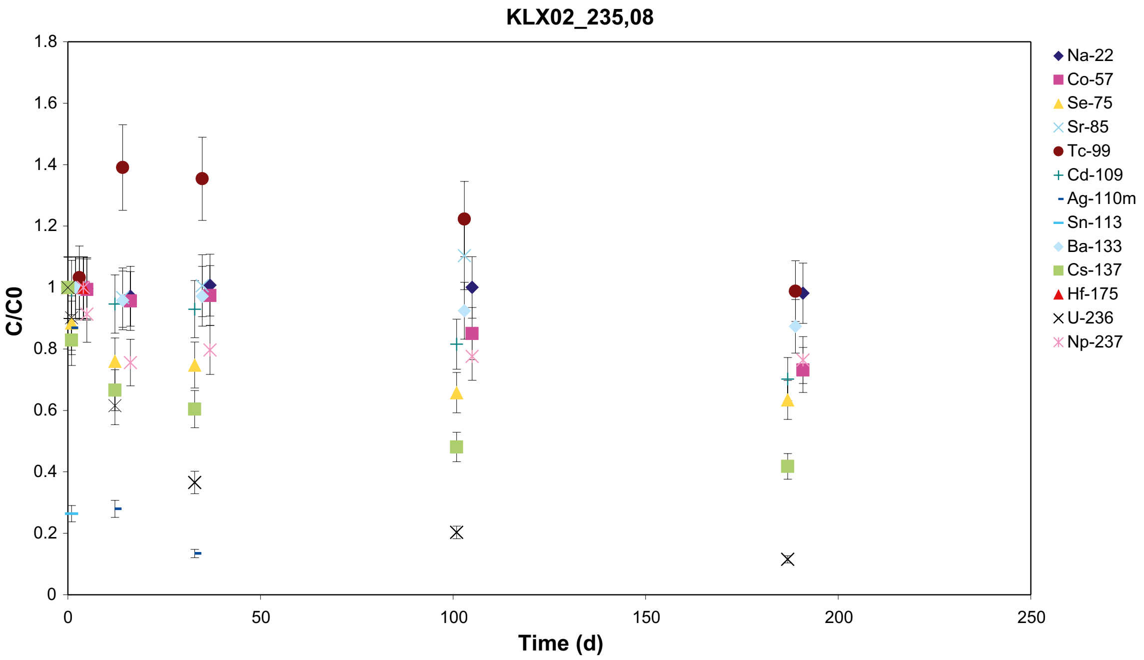

Figure 4-15. *Concentration time curve for the sorption experiment using intact rock, in this case Ävrö granodiorite (501056) sampled in KLX02A at 235.08 m (within the site investigation program).*

4.3.5 Predictions of the loss of tracer in the aqueous phase for Forsmark and Laxemar sorption-diffusion intact rock samples

Predictions (see definition in Section 3.4.1) were done for a selection of combinations of tracers and sample specific or rock type specific sorption and diffusion data according to the summary in Table 4-6. In the predictions the following two sources for data has been applied:

- Sample specific, means that the values of the diffusion parameters (i.e. the formation factor and the porosity) had been determined for the particular drill core sample used in the experiment, i.e. by applying through diffusion experiment and water saturation porosity measurement data as presented in Table 4-2. With respect to sorption parameters, the term sample specific refers to batch sorption experiments (1–2 mm fraction at 186 days) done using rock material in the absolute vicinity of the sample position of the particular drill core used in the experiment. The sample specific sorption data is presented in Table 4-7 below.
- Rock type specific, means that the values used for K_d, F_f and/or ε had been determined in the site investigations as values representative for the entire rock type, i.e. average values for a large number of determinations done on the rock type present in the particular drill core sample. The rock type specific data is presented in Table 4-7 below.

A slight exception to the outline described was the Ävrö granodiorite sampled at KLX02A 235.08 m where the used sample specific data for adsorption was the LTDE-SD batch sorption database (cf. Section 4.4, Table 4-11). This selection was motivated by the fact that these samples represent the same rock type and that, by this strategy, a good connection from the LTDE-SD data to the Site investigation program, was obtained.

The resulting concentration-time curves together with the corresponding measured values are shown in Appendix 8. For comparative purpose the corresponding predicted penetration depth curves are also presented, given as an indication of the predicted depth of interaction between the tracer and the rock sample.

A summary of the number of well-predicted, over-predicted and under-predicted sorption-diffusion intact rock samples for Cs-137 obtained by this method is given in Table 4-8. Examples of predictions using sample specific data for Ävrö granodiorite sample KLX02A 235.08 for Cs (well predicted), Ba (over-predicted) and U (under-predicted) are presented in Figure 4-16. The predictions for ion exchange sorbing tracers with a relatively simple sorption mechanism seem to work quite well while that of the redox sensitive U is poor. The redox sensitive elements are further discussed in Section 4.3.6.

Table 4-6. Summary of predictions #1 to #6 for the Forsmark and Laxemar sorption-diffusion intact rock samples. X=prediction was performed.

	#1. Sample specific data KLX02 235.08 (Ävrö granodiorite), sorption parameters from the LTDE laboratory experiment, (Table 4-11, KA3065A03 Batch 1 Matrix rock)	#2. Rock type mean values K_d and F_f KLX02 235.08 (Ävrö granodiorite, PLU lab program)	#3. Sample specific data KSH01 981,43 KFM02A 276.06 KFM03A 242,43	#4. Rock type mean values K_d and F_f KSH01 891,91, KSH01 981,43, KLX02 235,08, KLX04 726,07, KLX08 417,05, KLX10 995,78, KFM02A 276.06, KFM03A 242,43, KFM07A 608,75, KFM09A 713,67	#5. Rock type mean value K_d, sample specific F_f KSH01 891,91 KSH01 981,43 KLX02 235,08 KLX08 417,05 KLX10 995,78 KFM02A 276.06 KFM03A 242,43 KFM07A 608,75	#6. Sample specific K_d, rock type mean value F_f KFM02A 276.06 KFM03A 242,43 KSH01 891,91
Na-22	X	–	–	–	–	–
Co-57	X	–	–	–	–	–
Se-75	X	–	–	–	–	–
Sr-85	–	X	–	–	–	–
Tc-99	X	–	–	–	–	–
Cd-109	X	–	–	–	–	–
Ba-133	X	–	–	–	–	–
Cs-137	X	X	X	X	X	X
U-236	X	–	–	–	–	–
Np-237	X	–	–	–	–	–

Table 4-7. Summary of sample specific and rock type mean value data imported from the site investigations programme used in predictions #1 to #6 as presented in Table 4-6.

Sample	Rock type mean value K_d(m^3/kg) for Cs-137	Sample specific K_d(m^3/kg) for Cs-137	Rock type mean value K_d(m^3/kg) for Sr-85	Rock type mean value F_f*	Rock type mean value ε*
KSH01 891,91	2.9E-02	–	–	4.1E-04	3.5E-03
KSH01 981,43	2.4E-02	1.6E-02	–	1.1E-04	1.9E-03
KLX02 235,08	5.5E-03	2.2E-02	3.9E-04	1.5E-04	3.2E-03
KLX04 726,07	2.4E-02	–	–	1.1E-04	1.9E-03
KLX08 417,05	2.9E-02	–	–	4.1E-04	3.5E-03
KLX10 995,79	2.4E-02	–	–	1.1E-04	1.9E-03
KFM02A 276.06	2.0E-03	2.0E-03	–	1.2E-02	1.3E-01
KFM03A 242,43	8.4E-03	8.4E-03	–	7.8E-05	1.6E-03
KFM07A 608,75	4.0E-03	–	–	1.6E-04	1.0E-02
KFM09A 713,67	4.0E-03	–	–	1.6E-04	1.0E-02

*Sample specific F_f and ε are given in Table 4-2/Appendix 4.

Table 4-8. Summary of well-, under- and over-predicted cases for all ^{137}Cs predictions (regarding the predicted concentration loss). Under-predicted concentration loss is defined as the calculated concentrations being higher than the maximum uncertainty range for a majority of the measurements, and vice versa for over-predicted concentration loss. Well-predicted means that the calculated concentration is within the uncertainty range for the majority of the measurements.

		# of under-predicted samples	# of well-predicted samples	# of over-predicted samples
#1	Sample specific data KLX02 235.08 (Ävrö granodiorite), LTDE-SD data		1	
#2	Rock type mean values KLX02 235.08 (Ävrö granodiorite, PLU lab program)	1		
#3	Sample specific data	3		
#4	Rock type mean values	8	2	
#5	Rock type mean value K_d, sample specific F_f	*4*	*2*	
#6	Sample specific K_d, rock type mean value F_f			3
	TOTAL:	*16*	*5*	*3*

4.3.6 Estimations of K_d and/or D_e for Forsmark and Laxemar sorption-diffusion intact rock samples

The numerical results are presented in tables in Appendix 10. In this Section, bar charts are given for comparison of laboratory batch sorption experiment determined K_d-values to the values obtained from the best fit of the estimated results to the experimental data of the intact rock sorption experiments.

In Figure 4-17, the results for the sorption on the KLX02 235.08 m Ävrö granodiorite samples are presented; K_d was used as the fitting parameter with ε and F_f fixed to the experimentally determined values. Cases for using both the average values for the Ävrö granodiorite rock (F_f, ε*)* and the sample specific values (F_f, ε) were applied. The results show that no significant difference is obtained between the two cases, which is expected given the relatively slight difference between them.

Regarding the different tracers, it is obvious that for the moderately sorbing cation tracers (e.g. Co, Cd, Ba and Cs) the laboratory measured K_d of the 1–2 mm fraction is in good agreement with the K_d obtained from estimations (curve fitting). One does not have to adjust any of them more than one order of magnitude, which must be considered as fairly good during these circumstances. For the very slightly sorbing tracers (e.g. Na, Sr and Tc) the sorption is so low that only "lower than"-values for the K_d can be produced from the estimations; however, all of them agree fairly well with the experimental values.

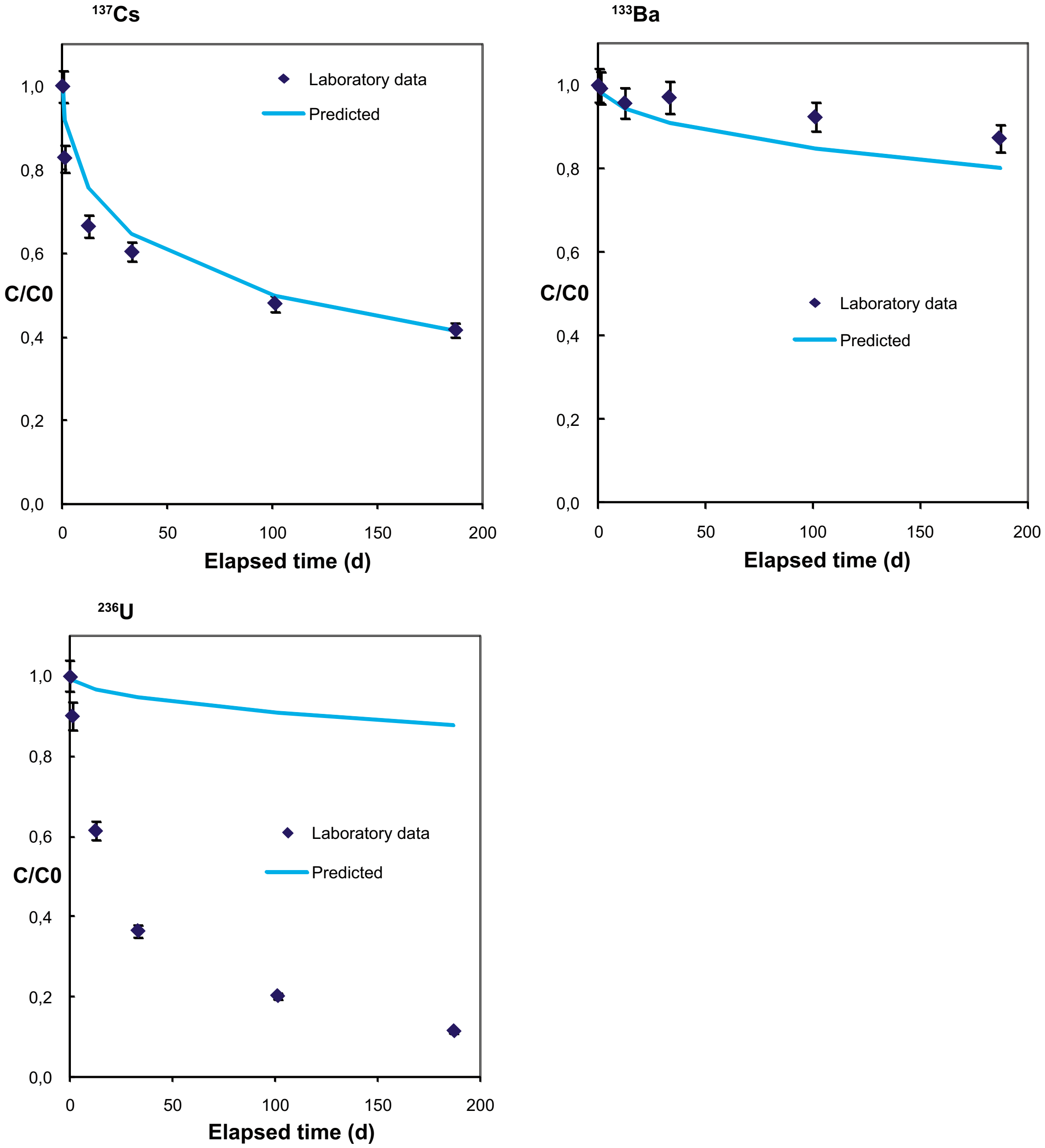

Figure 4-16. *Sample specific predictions of the sorption on Ävrö granodiorite (KLX02 235.08 m) together with the corresponding laboratory results. Examples of well–predicted (Cs, top, left), over-predicted (Ba, top, right) and under-predicted (U, bottom, right) sorption are given.*

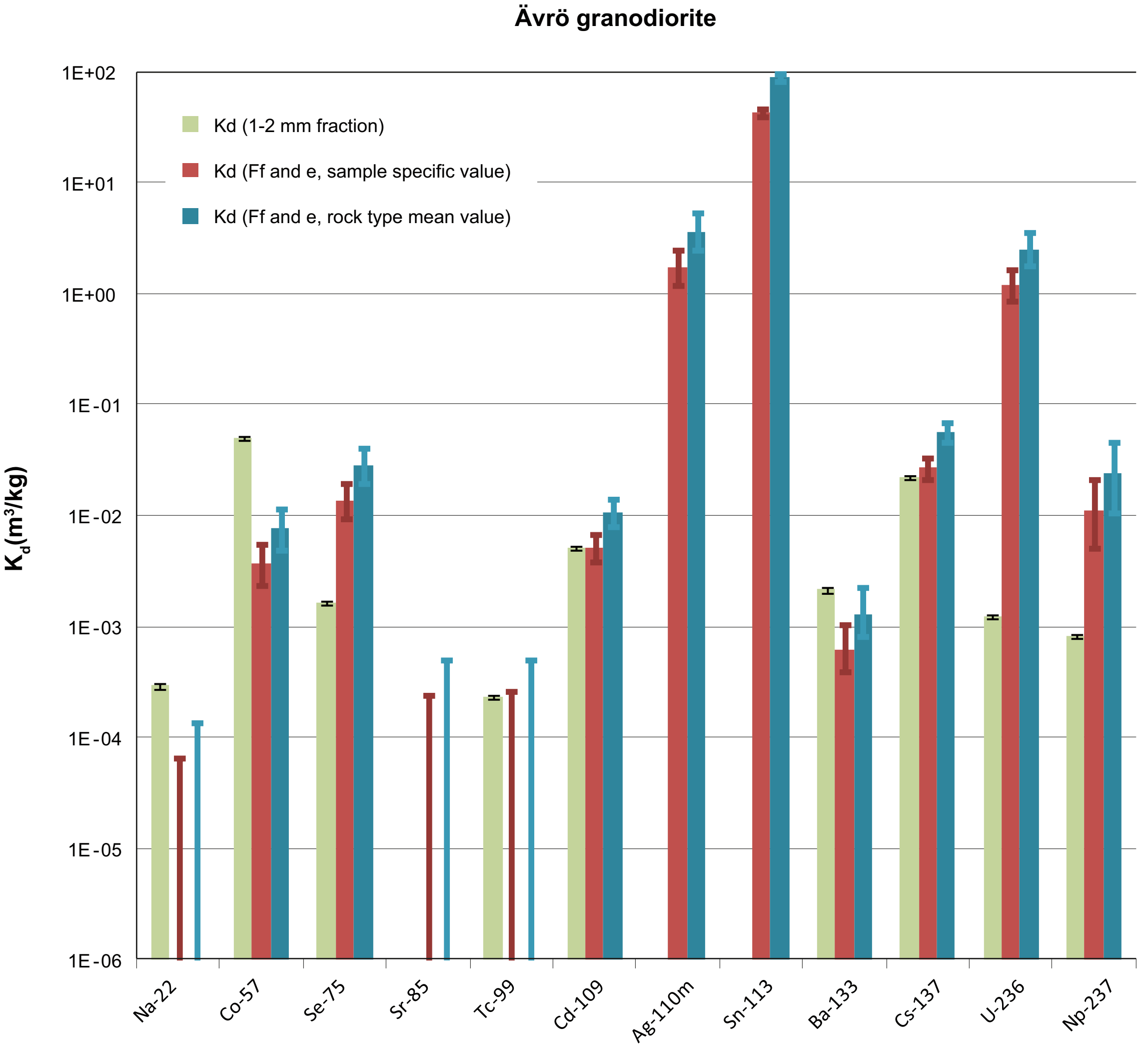

Figure 4-17. *K_d values (m^3/kg) obtained from the estimation (curve fitting) procedure using the K_d value as the fitting parameter together with ε and F_f fixed to the measured values (see text for details). Comparisons are made to K_d values determined in laboratory batch experiments (1–2 mm size crushed rock, 186 d of contact time).*

However, strong deviations can be observed for the redox sensitive U and Np; in the case of U one has to increase the batch sorption determined K_d with three orders of magnitudes in order to obtain a reasonable fit. It was speculated in Section 4.3.4 that this could be a result of different redox conditions in the water-drill core interface than what is found in the surface of the relatively large crushed rock particles (1–2 mm) used in batch experiments.

In Figures 4-18,19, 21, 23 and 24, K_d-values estimated by curve fitting from sorption on entire drill cores for different tracers and various rock samples are shown in staple-bar diagrams. The estimated K_d-values are obtained from a curve fitting procedure together with ε and F_f fixed to measured values, sample specific or rock type mean values. In the diagrams comparisons are also made to K_d values determined in laboratory batch experiments (crushed rock, size fraction: 1–2 mm and a contact time of 186 d).

For cobalt, presented in Fig. 4-18, a comparison of K_d measured by batch sorption technique and obtained from experiments on entire drill core is only possible for the Ävrö granodiorite rock sample. It can be seen that the K_d-values obtained from measurements on entire drill core is at least one order of magnitude lower than the corresponding values obtained by batch sorption measurement. There is also a very varying sorption of Co observed in the different intact rock sorption experiments. For example, for the Äspö quartz monzodiorite sampled at KSH01 at 891.91 m, one need K_d over 10 m^3/kg to explain the sorption; which can be compared to the same rock type sampled at KLX10 at 995.78 m

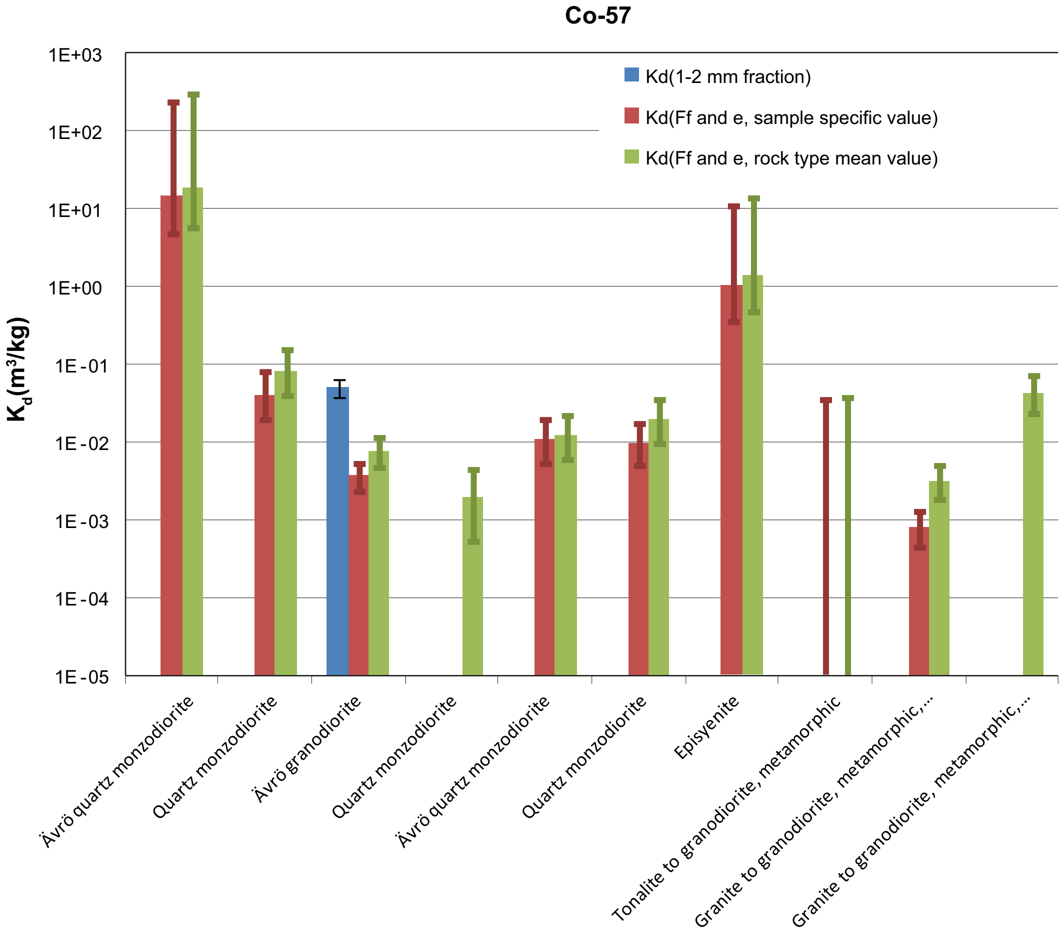

Figure 4-18. *K_d values for ^{57}Co obtained from the estimation (curve fitting) procedure using the K_d value as the fitting parameter together with ε and F_f fixed to the measured values (see text for details). Comparisons are made to K_d values determined in laboratory batch experiment (1–2 mm size crushed rock, 186 d of contact time).*

where a K_d of 0.01 m^3/kg is sufficient for explaining the sorption. This variation within three orders of magnitudes for a single rock type is unsatisfactory and may call for a more elaborate investigation of the explanation for this variation.

Except for this, the agreement of the fitted K_d are generally quite good to the only available laboratory batch sorption experiment value. However, the high sorption of Co on the strongly altered and highly porous episyentic sample is probably in agreement with the increased BET surface area of that rock type, i.e. favouring surface complexation binding of cobalt.

The ^{137}Cs is by far the tracer for which the basis for comparison to batch sorption determined K_d is best. The results are illustrated in Figure 4-19. One can observe a general trend that the batch laboratory determined K_d-values (average for the rock types in the SKB site investigations) underestimate the sorption obtained in the intact drill core experiment; for obtaining a good fit one generally have to increase the K_d < 1 order of magnitude. However, exceptions to this are the two Ävrö quartz monzodiorite samples included, where a fairly good agreement is obtained. One can speculate of existence of larger amount of surfaces and microfractures or available porosity in the near vicinity closest to the water interface of the rock; increasing the F_f or the K_d in the sub-mm thick depth of the rock in which almost all interaction (according to the corresponding penetration profile calculations) of the tracer takes place.

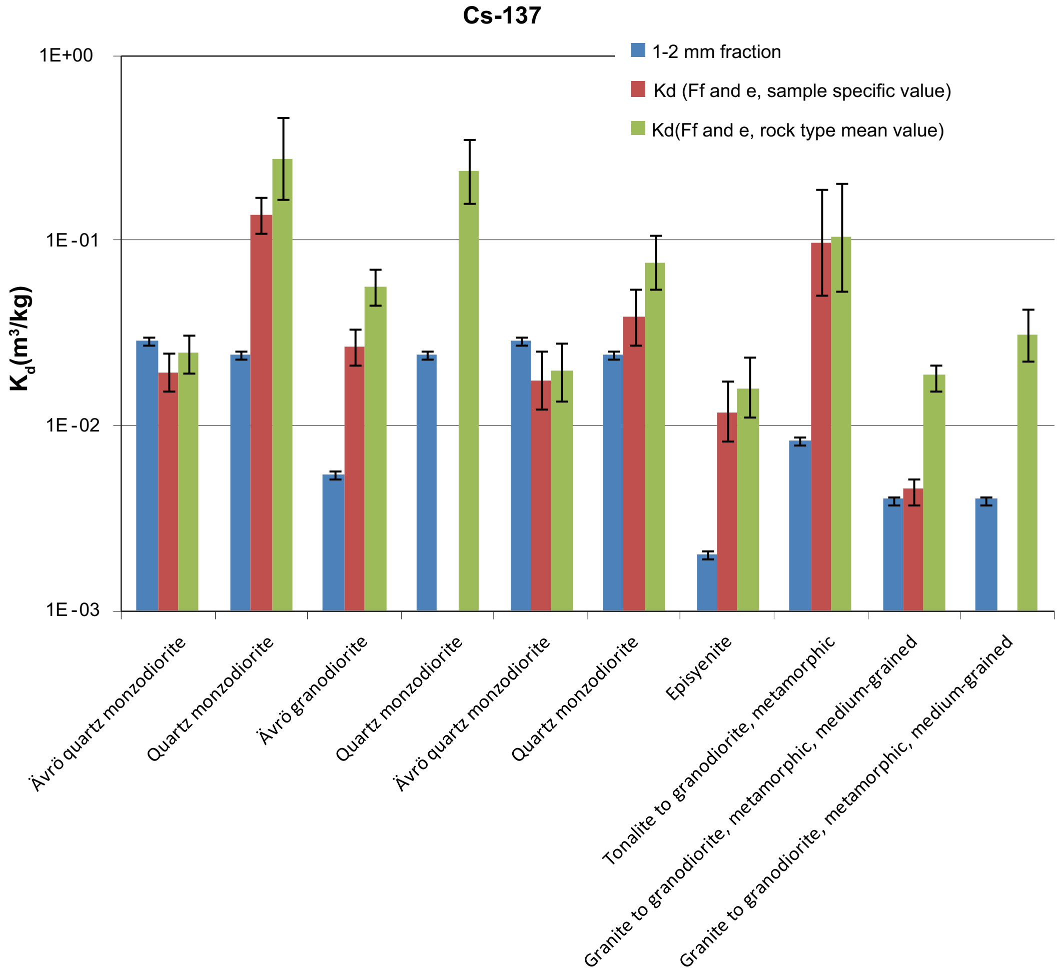

Figure 4-19. *K_d values for ^{137}Cs obtained from the estimation (curve fitting) procedure using the K_d value as the fitting parameter together with ε and F_f fixed to the measured values (see text for details). Comparisons are made to K_d values determined in laboratory batch experiment (1–2 mm size crushed rock, 186 d of contact time).*

As was illustrated in Section 4.3.3, the rate of the loss of tracer in the aqueous phase is sensitive to the product of $K_d{\cdot}F_f$. If no consideration of the penetration profile is made, individual values of the lumped parameter $K_d{\cdot}F_f$ can not be identified. Hence, the deviation in K_d discussed above may as well be explained by a similar deviation of the real diffusivity (formation factor) compared to the value of the diffusivity used in the modelling (through diffusion experiment results). It may therefore seem convenient to present the lumped retention factor $K_d{\cdot}F_f$ obtained from the evaluation of the sorption on intact drill core in comparison to the same lumped parameter based on the product of the batch sorption experiment determined K_d and through diffusion experiment determined F_f. Such a comparison gives a general validation of how well the smaller scale laboratory determined retention parameters can explain the results of the expanded scale experiment, i.e. the results of sorption on intact rock.

The results for ^{137}Cs (Figure 4-20) show that 8 of the 10 intact drill core samples give increased $K_d{\cdot}F_f$ of 0.5–1 order of magnitude compared to what is produced from the corresponding $K_d{\cdot}F_f$ obtained from batch sorption/through diffusion experiments. However, for the two Ävrö quartz monzodiorite samples included in the investigation, the agreement of the two methods is quite good, although the intact rock experiments indicate slightly lower retention properties.

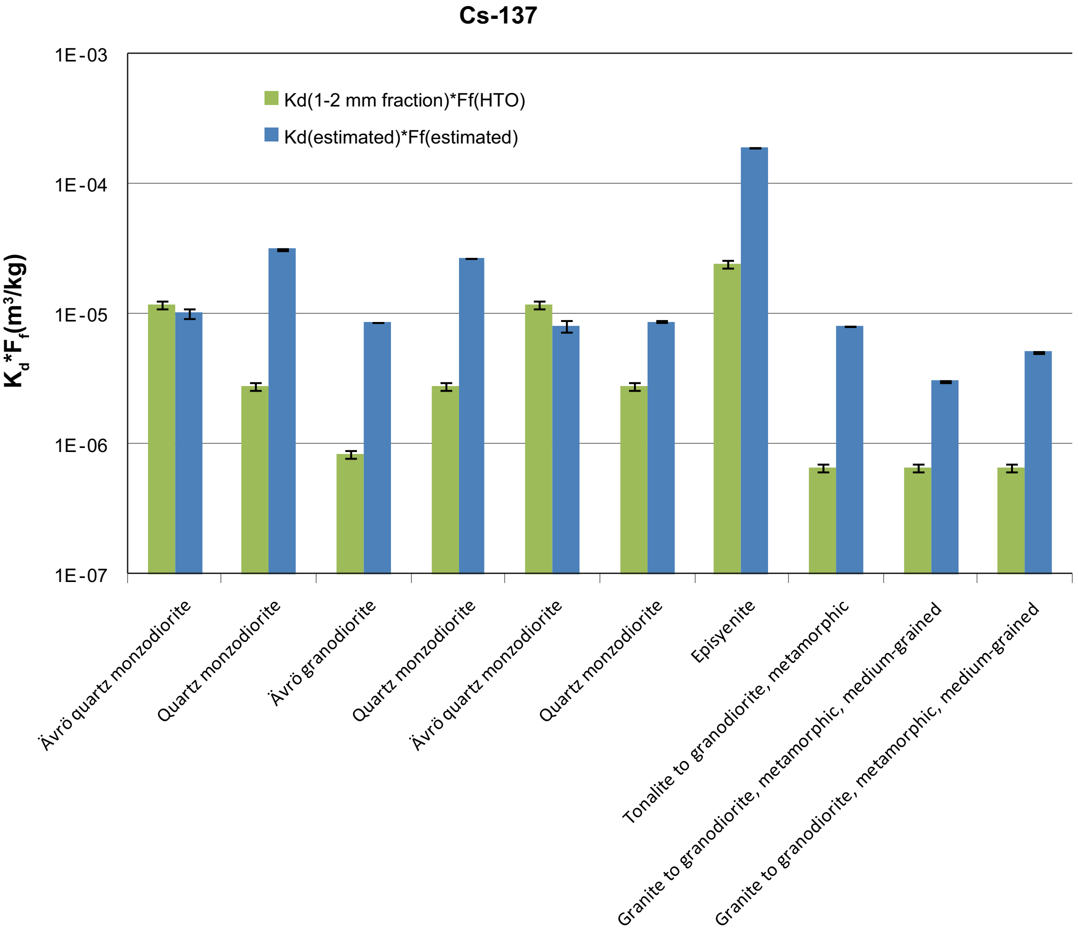

Figure 4-20. *Comparison of estimated $K_d{\cdot}F_f$ values (in blue) for ^{137}Cs for sorption-diffusion on intact drill cores with the product $K_d{\cdot}F_f$, where K_d is a mean value determined from batch sorption laboratory data (for 1–2 mm fraction, t=186 d) and F_f is determined from through diffusion experiments of H^3HO (see Table 4-3).*

In Figure 4-21, a summary is presented for the $K_d{\cdot}F_f$ results in the Ävrö granodiorite sample for all tracers analysed. In general, the method agreement is best for ion exchange and surface complexation sorbing tracers, while larger deviation between experiments on crushed and intact rock material is indicated for redox sensitive tracers. The redox issue is discussed further below for U.

The most striking observation for the uranium sorption results (Figure 4-22) is the strong sorption in the experiment using intact drill cores (K_d in the range of 0.1–100 m^3/kg) which can not be observed for the batch sorption experiment results (K_d in the range of 0.001–0.01 m^3/kg). The result is an indication that reduction is taking place of uranium from its hexavalent less sorbing species to the tetravalent strongly sorbing species. This is interesting to compare to the detailed results in the Oskarshamn/Forsmark site investigation /Byegård et al. 2008, Selnert et al. 2009b/ where a strong adsorption of uranium was shown in the smallest size fraction used (0.063–0.125 mm) contrary to the larger fractions where very low sorption was obtained. This could be an indication that the part of the rock materials causing reduction of uranium is enriched in the smaller size fraction and that the presently applied concept of addressing the 1–2 mm size fraction as the most representative size fraction /Byegård et al. 2008, Selnert et al. 2009b/ may underestimate the retention of redox-sensitive elements, such as uranium.

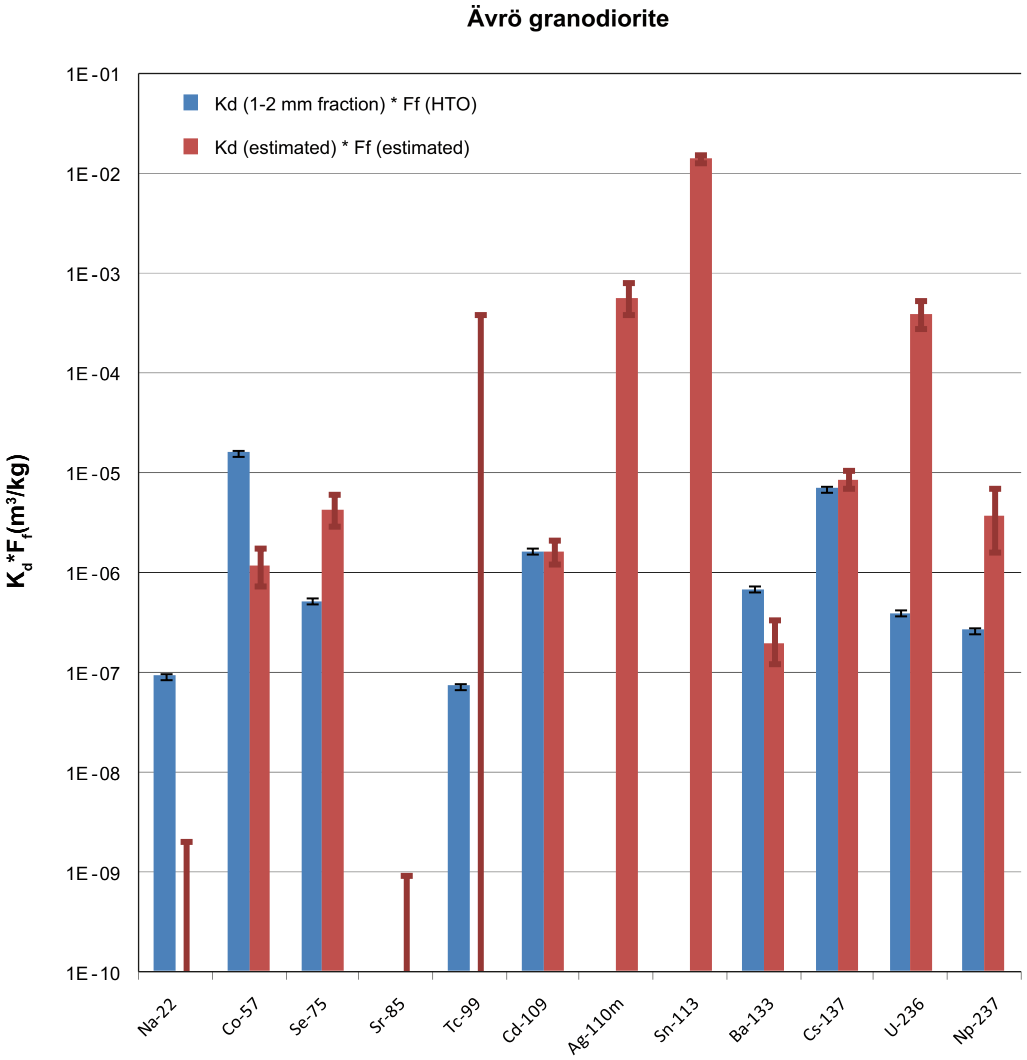

Figure 4-21. *Comparison of estimated $K_d{\cdot}F_f$ values (in red) for sorption-diffusion on intact Ävrö granodiorite drill core with the product $K_d{\cdot}F_f$ (in blue)., where K_d is a mean value determined from batch sorption laboratory data (for 1–2 mm fraction, t=186 d) and F_f is determined from through diffusion experiments of H^3HO (see Table 4-3).*

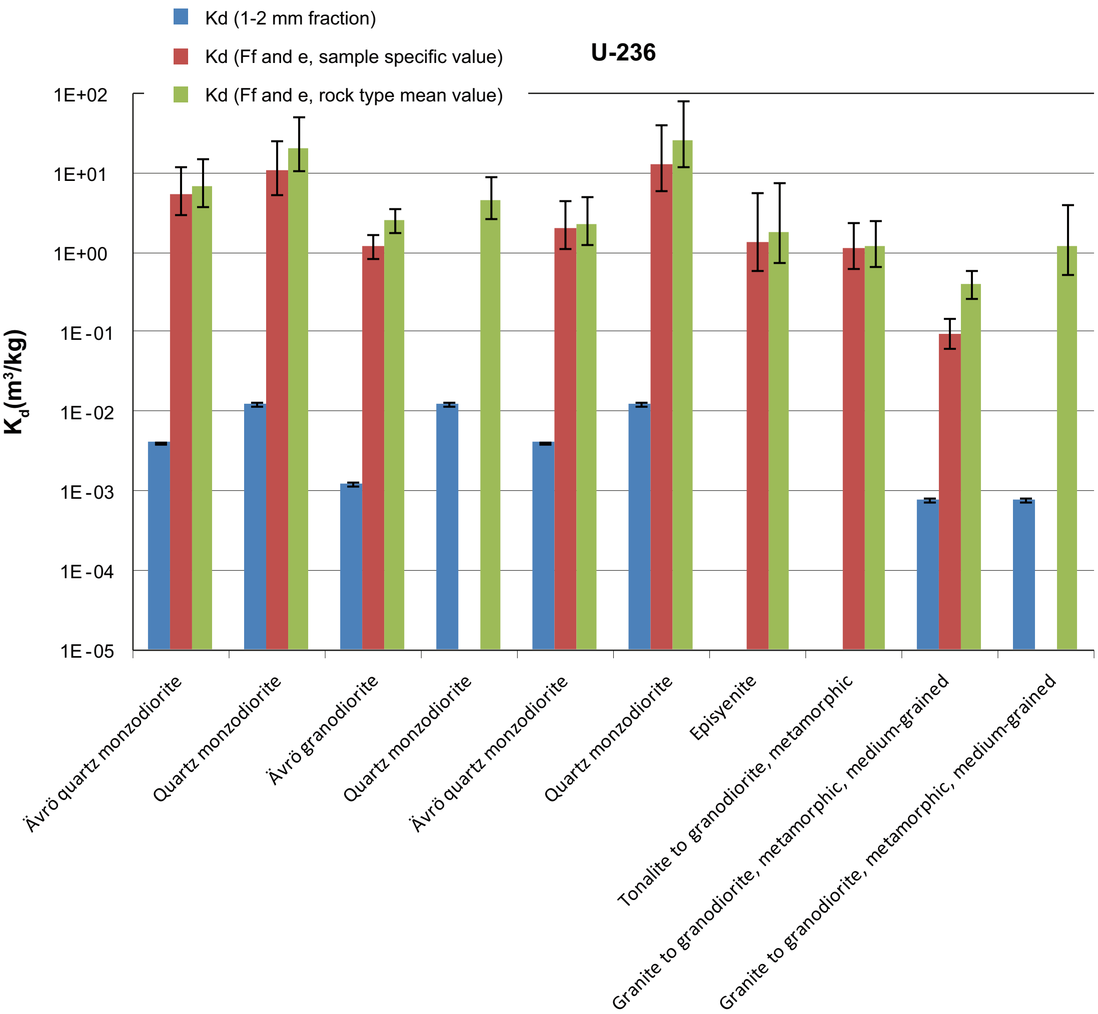

Figure 4-22. *K_d values for ^{236}U obtained from the estimation (curve fitting) procedure using the K_d value as the fitting parameter together with ε and F_f fixed to the measured values (see text for details). Comparisons are made to K_d values determined in laboratory batch experiment (1–2 mm size crushed rock, 186 d of contact time).*

Making a comparison of the lumped retardation factor $K_d{\cdot}F_f$ from sorption on intact rock to the values obtained in batch sorption experiment and through diffusion experiments (Figure 4-23) show higher values for the intact rock, in the range of 0.5–2.5 orders of magnitudes. It seems likely that the reduction of hexavalent uranium (see paragraph above) is the cause for this strong difference.

For the ^{133}Ba tracer the only comparison that can be made between batch sorption data and studies of sorption on entire drill core is for the Ävrö Granodiorite. The results (Figure 4-24) give a rather good agreement (given the uncertainty ranges) of the two different techniques. However, a general observation of the results for ^{133}Ba is that the materials from the Forsmark site investigation show much higher sorption than the samples from the Oskarshamn site investigation. This observation is difficult to explain, especially since no similar trend can be indicated for the other tracers studied. A deeper mineralogical analysis and comparison between the sites would be needed in order to give further information on this issue.

For the ^{109}Cd tracer, as described also for ^{57}Co and ^{133}Ba above, comparison of batch sorption data and sorption on entire drill core can only be made for the Ävrö granodiorite samples. A good agreement is obtained as can be seen in Figure 4-25. For the other rock materials, the investigation gives K_d in the range of 10^{-3}–10^{-1} m³/kg. For the Tonalite to Granodiorite, Metamorphic sample, only a “lower than value” can be reported; this since the experimental values show a large spreading and a mismatch to an expected curve of the presumed diffusion/sorption model.

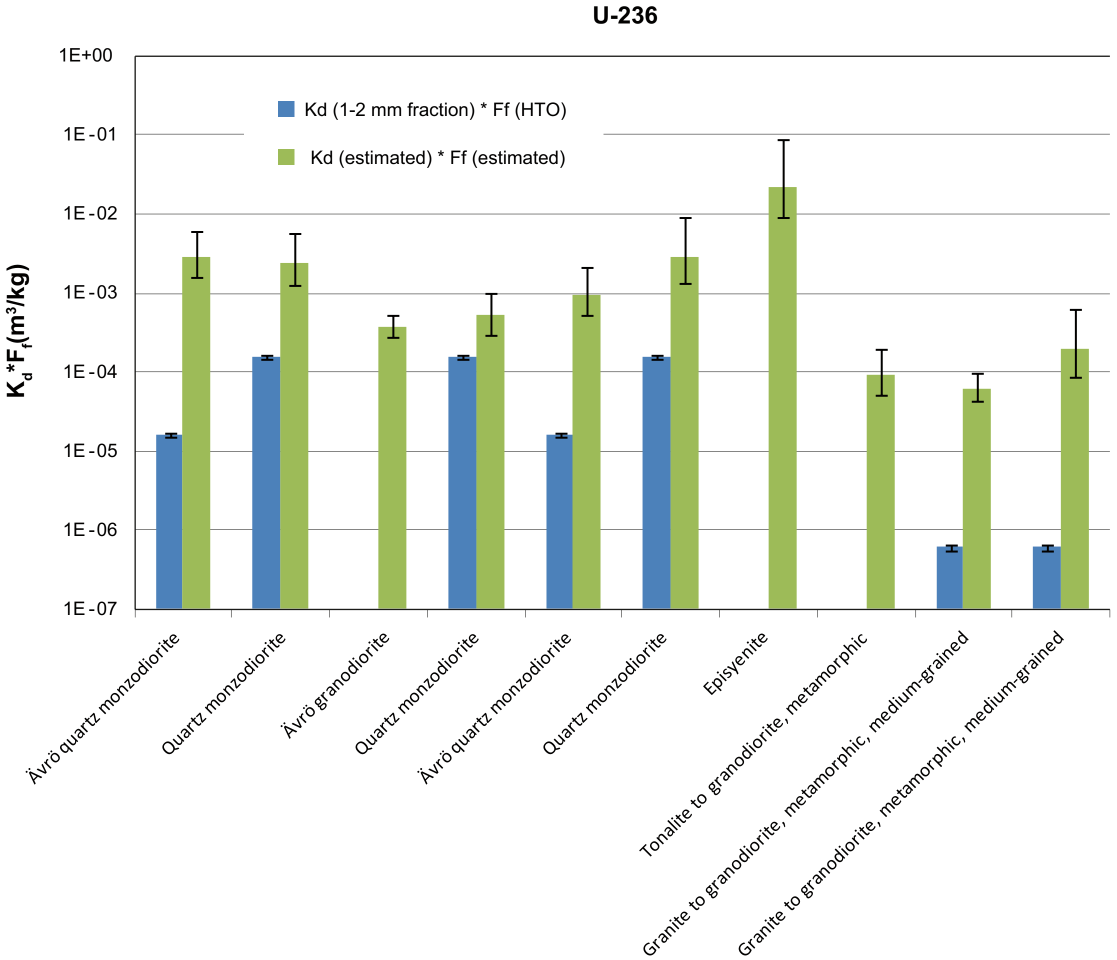

Figure 4-23. *Comparison of estimated $K_d \cdot F_f$ values (in blue) for ^{236}U for sorption-diffusion on intact drill cores with the product $K_d \cdot F_f$, where K_d is a mean value determined from batch sorption laboratory data (for 1–2 mm fraction, t=186 d) and F_f is determined from through diffusion experiments of H^3HO (see Table 4-3). A correlation analysis with Fe content could be of interest to perform since there is a range in Fe_2O_3 content from about 2 to 11% in the samples (from raw analysis data without respect to oxidation state in the mineral, used by Selnert et al. 2008 and 2009a/ to calculate mineral distribution). Ävrö granodiorite and Granite to granodiorite, metamorphic, medium-grained, have about 2–3% Fe_2O_3, Quartz monzodiorite about 8–10% and Episyenite varies between different size fractions from ~7% in small size fractions to ~2% in large size fractions. It is notable that Fe inclusions are found on the surface of the cavities in the Episyenite, i.e. in good contact with the aqueous phase.*

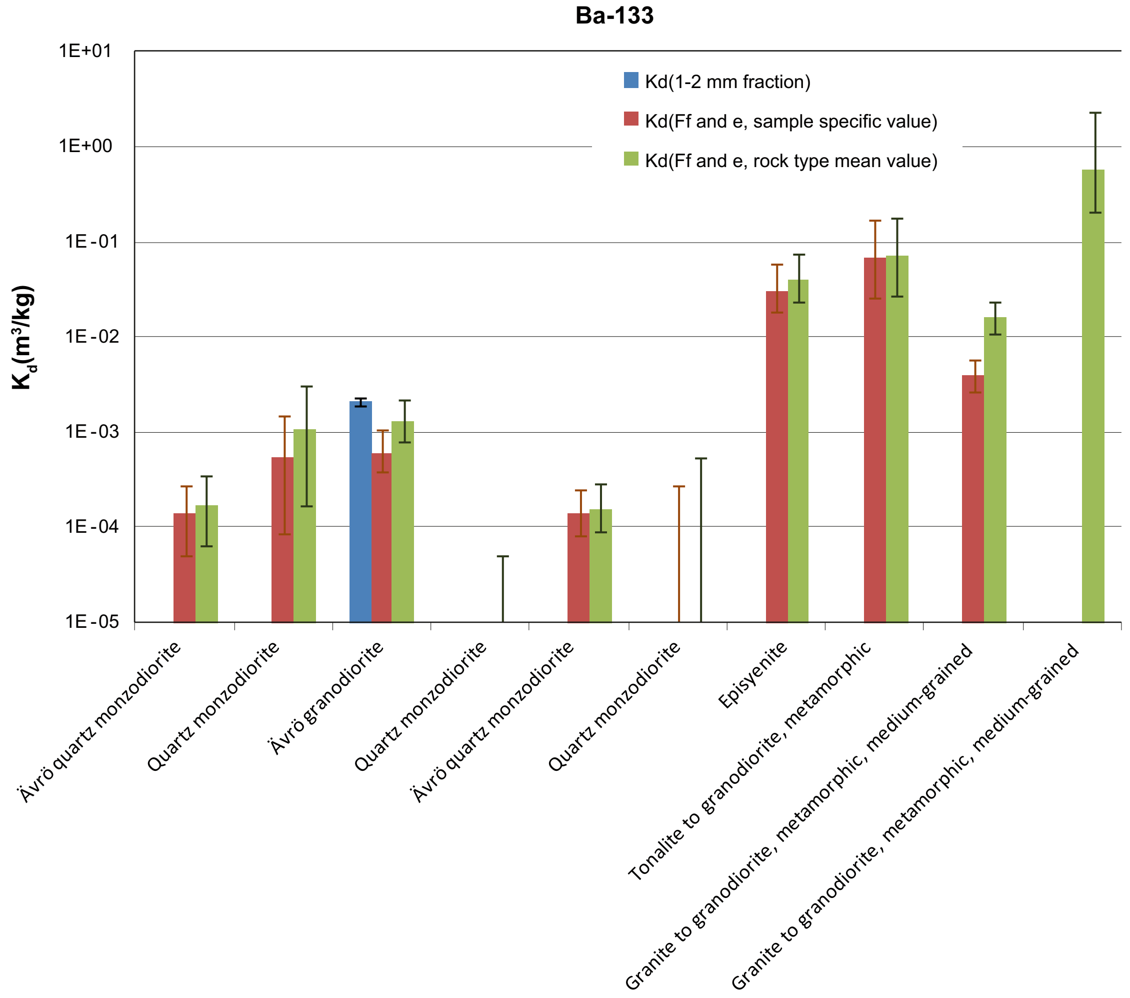

Figure 4-24. *K_d values for ^{133}Ba obtained from the estimation (curve fitting) procedure using the K_d value as the fitting parameter together with ε and F_f fixed to the measured values (see text for details). Comparisons are made to K_d values determined in laboratory batch experiment (1–2 mm size crushed rock, 186 d of contact time).*

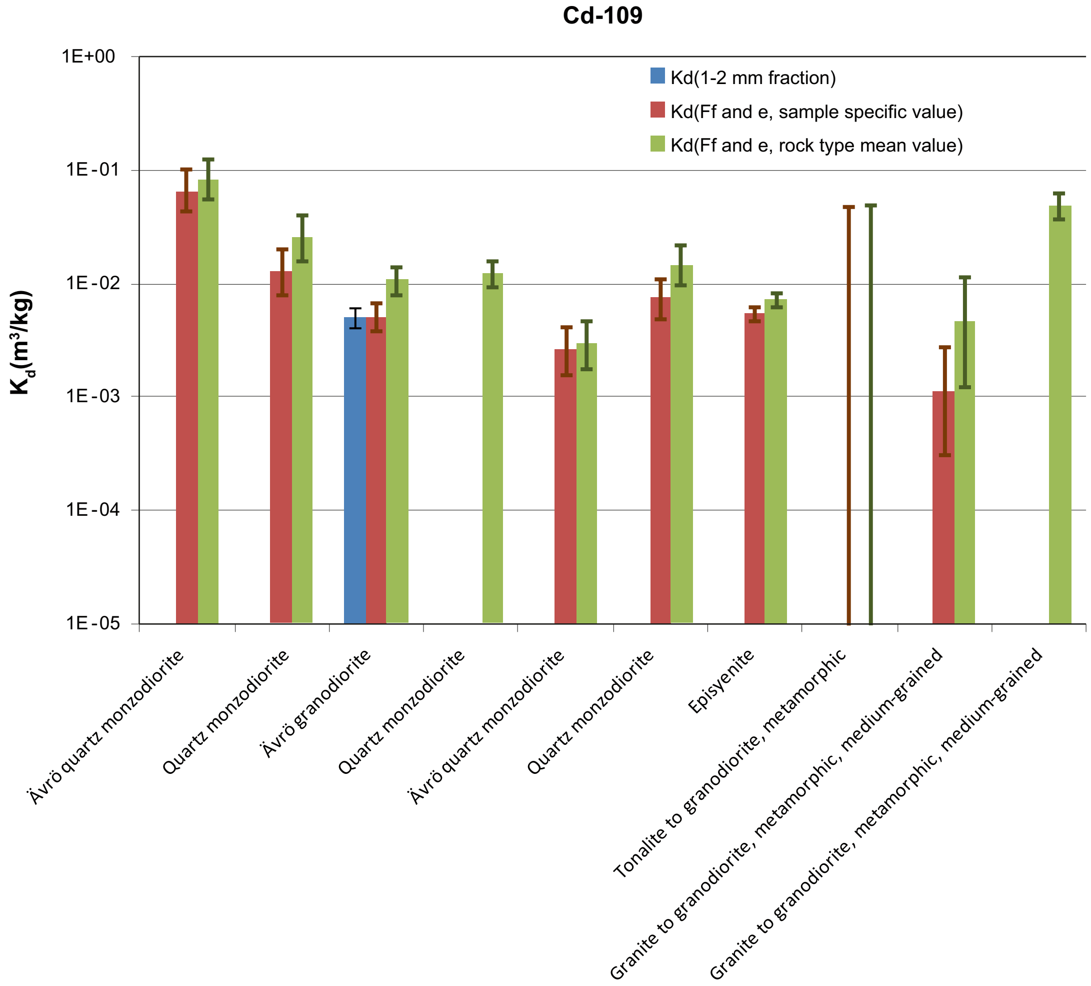

Figure 4-25. *K_d values for ^{109}Cd obtained from the estimation (curve fitting) procedure using the K_d value as the fitting parameter together with ε and F_f fixed to the measured values (see text for details). Comparisons are made to K_d values determined in laboratory batch experiment (1–2 mm size crushed rock, 186 d of contact time).*

4.4 Batch sorption experiments

The sorption behaviour of several of the radionuclides used in the *in situ* experiment was studied in laboratory batch sorption experiments. In the laboratory experiments the same stock solution, with a mixture of 22 radionuclides, as used in the in situ experiment was used, see Table 2-7. However, the laboratory experiments were performed almost two years after the *in situ* experiment, which limits the number of radionuclides that could be studied, due to the short half-lives. In the laboratory experiments the sorption of 12 radionuclides, as listed in Table 2-7, were studied.

In order to have representative rock samples for the laboratory program an extensive investigation of the geology was performed for samples collected close to the target rock mass intended for the *in situ* experiment. Representative rock samples that could be obtained close to the experimental site were selected, i.e. different samples from the drill cores of KA3065A02 and KA3065A03. The samples were divided in three groups according to the descriptions in Sections 2.1 to 2.3, i.e. the matrix rock consisting of Ävrö granodiorite, altered and red-stained rock and the fracture minerals dominated by chlorite and calcite. In the laboratory experiment one has, thus, to deal with these three types of rock materials.

In this chapter it may be somewhat confusing that the sample name describes the borehole and position number of each sample. However, this was chosen to be maintained since all data from the in situ experiment as well as the laboratory data will be transferred to the SICADA data base, where all data are correlated to the exact borehole position.

A sample description concerning the geology of the studied rock samples, used in the laboratory experiments, is summarized in Table 4-9.

Table 4-9. Rock material used in the batch laboratory experiments.

Name	Full name – Geological description
	Matrix rock samples = Ävrö granodiorite:
A02:6	**KA3065A02:6** – Matrix rock in the pilot bore hole. Dominated by quartz and feldspars
A03:1	**KA3065A03_Batch 1** – Matrix rock in the experimental bore hole. Dominated by quartz and feldspars
	Altered, red-stained rock sample:
A02:1	**KA3065A02:1** – Matrix rock in the pilot bore hole, red-stained but still dominated by quartz and feldspars.
	Fracture samples = dominated by chlorite and calcite:
A02:2	**KA3065A02:2** – Fracture minerals in the pilot bore hole. Dominated by chlorite and calcite
A03:9	**KA3065A03_Replica** – Fracture minerals in the experimental bore hole. Dominated by chlorite and calcite

The sample names are completed with letters that describe what particle size that have been studied and a number giving the order of sample studied, see Table 4-10. This gives the full name, such as KA3065A03_Batch_1_B_2(2).

Table 4-10. Naming of the rock material used in the laboratory experiments.

Name	Naming of samples used for the sorption results in this report
A	Particle size fraction 0,063–0,125 mm
B	Particle size fraction 0,25–0,5 mm
C	Particle size fraction 1–2 mm
D	Particle size fraction 2–4 mm (Used for BET measurements)
1_(1)	One single sample studied
1_(2)	One out of two samples studied
2_(2)	Two out of two samples studied

The objective with the reporting of the batch experiments is a presentation of the laboratory results, regarding the different geological samples, transport parameters and sorption properties. The results presented will later be subject for further evaluations of the LTDE-SD experiment as well as a source for performance assessments and safety analysis (PA/SA). Hence, the results presented are only examples of the results obtained and should not be regarded as a complete presentation of the results. All additional data from the batch experiments contains information that may be evaluated with regard to e.g. kinetics, red-ox conditions, sorption mechanisms and mineralogical composition which is only briefly discussed in this report.

4.4.1 K_d

The K_d values are evaluated according to Section 3.3.2, paragraph "*Evaluation of K_d*".

The results are presented in Figures 4-26 and 4-27. The K_d values presented are from two separate samples analyzed, except for ^{36}Cl and ^{63}Ni for which only single samples were analyzed. The mean K_d values, from the two separate samples analyzed, are summarised in Table 4-11. R_d (m^3/kg) values for the various contact times are given in Table "R_d (m^3/kg) results from the batch sorption experiments" in Appendix 11.

The error bars presented in Figures 4-26 and 4-27 refer to uncertainties based on error propagations for the individual samples. There are coloured staples representing the tracers ^{36}Cl, ^{22}Na, ^{99}Tc and ^{75}Se in the diagram of Figures 4-26 and 4-27 where no error bars are given. These coloured staples represent in each case an obtained maximum value of K_d. It was not possible to statistically verify any decrease of tracer concentration in the aqueous phase for these tracers. Hence, a value of K_d could not be calculated as the counting statistics were below the detection limit.

As can be seen in Table 4-11 below the K_d values vary in the order of three orders of magnitude (~0.001–1 m^3/kg). The highest values are obtained for the materials KA3065A02:2 and KA3065A03_Replica, with the A03 sample being the highest of all. Both these geological materials represent fracture minerals. Hence, they exhibit more mineral surfaces avaiable for sorption, that may explain the higher K_d values. The altered red-stained rock, KA3065A02:1, show similar values as the matrix rock, KA3065A02:6. An exception is ^{137}Cs, for which half an order of magnitude higher K_d is observed in the matrix rock. An integrated interpretation of the sorption results for different tracers and methods applied in this work is presented in Section 5.3.

4.4.2 BET area

The surface area of the two size fractions A and D from each geological material has been investigated by BET-measurements. The results are presented in Table 4-12. The results for matrix rock from both boreholes and red-stained rock show similar BET areas. 5 to 10 times higher BET areas are found in the fracture samples. The difference in BET area between the two analysed size fractions is smaller for the fracture samples than for the matrix rock. This can be explained by the smaller grain-size in the fracture minerals, which does not lead to such a large area increase in the crushing process as for the larger grain size of the matrix rock.

The geological material used in this project, can be compared with previous investigations within the SKB-Site investigation program (PLU), Most of the general geological description from the site investigation program, described in /Byegård et al. 2008, Selnert et al. 2009b/ can also be applied for the LTDE-SD geology, e.g. mineralogical distribution observed for the different size fractions etc. A sample specific description of the geological material used is presented in Appendix 13: Rock sample descriptions.

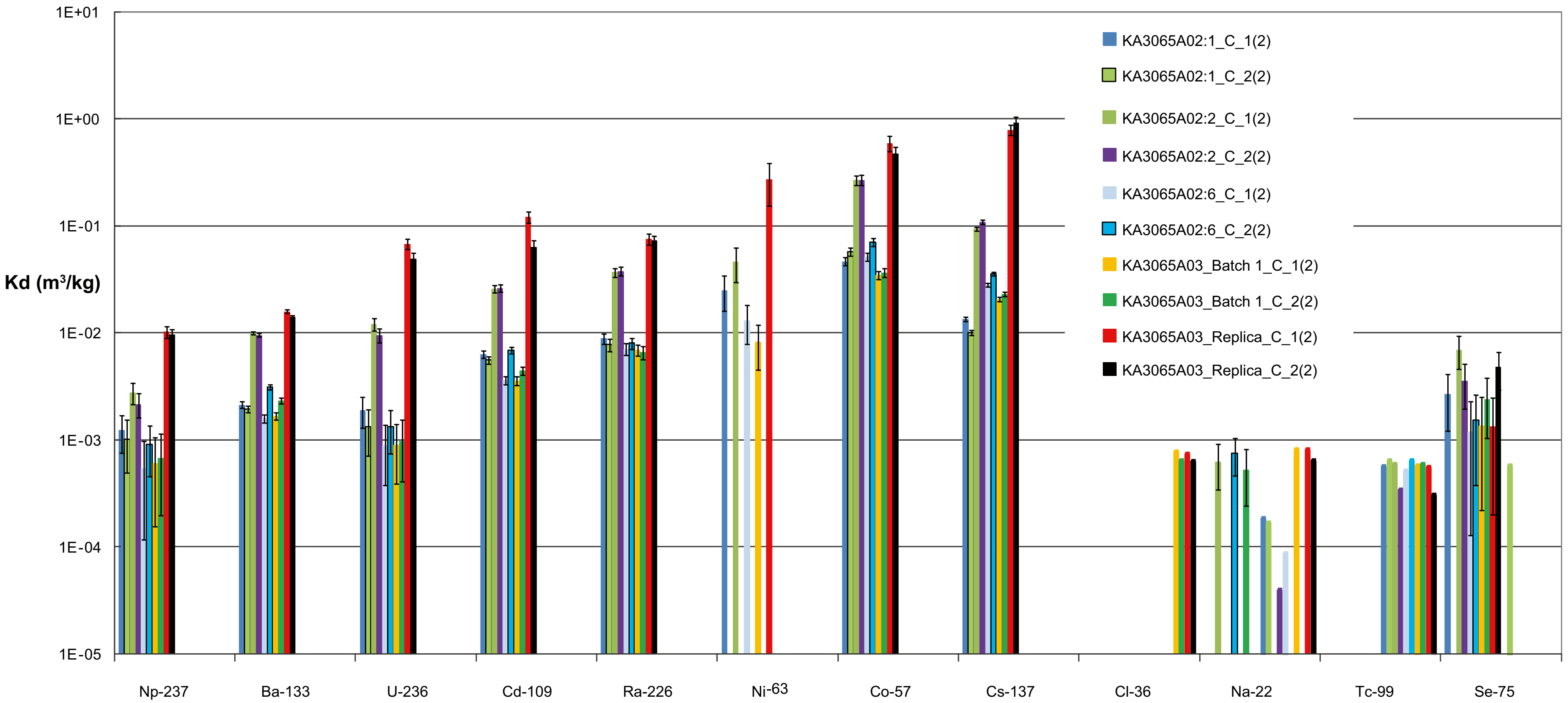

Figure 4-26. *K_d values (m^3/kg) obtained from the batch sorption experiments. Contact time: 186 days. Particle size fraction:1–2 mm. Note: The order of the staples for ^{22}Na and ^{75}Se differs from the order of the legends. The coloured staples without error bars for the tracers ^{36}Cl, ^{22}Na, ^{99}Tc and ^{75}Se represent in each case an obtained maximum value of K_d. It was not possible to statistically verify any decrease of tracer concentration in the aqueous phase for these tracers.*

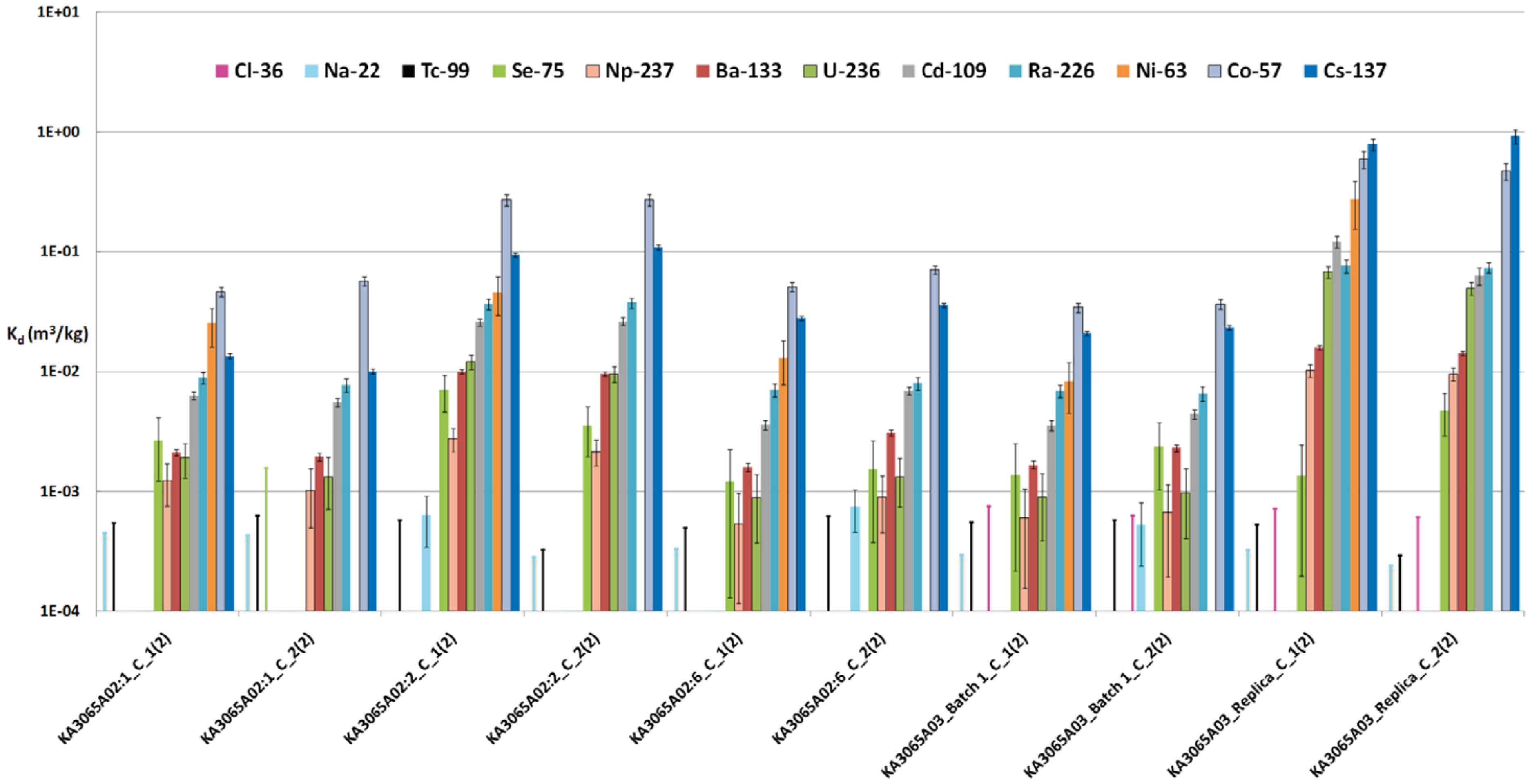

Figure 4-27. *K_d values (m^3/kg) obtained from the batch sorption experiments. Contact time: 186 days. Particle size fraction: 1–2 mm. Note: The order of the staples for ^{36}Cl, ^{22}Na and ^{99}Tc differs from the order of the legends.*

Table 4-11. Results from the batch sorption experiments. The presented K_d values are mean values of two individual measured samples. Contact time: 186 days. Particle size fraction: 1–2 mm.

	KA3065A02:1 **Red-stained matrix rock**		**KA3065A02:2** **Fracture minerals**		**KA3065A02:6** **Matrix rock**		**KA3065A03_Batch 1** **Matrix rock**		**KA3065A03_Replica** **Fracture minerals**	
Radionuclide	**K_d (m^3/kg)**	**+/–**	**K_d (m^3/kg)**	**+/–**	**K_d (m^3/kg)**	**+/–**	**K_d (m^3/kg)**	**+/–**	**K_d (m^3/kg)**	**+/–**
Cl-36 [1]							< 1.1E-03		< 8.8E-04	
Na-22	1.7E-04	2.2E-05	3.3E-04	8.3E-04	4.2E-04	9.4E-04	2.8E-04	6.9E-04	–9.6E-05	4.7E-04
Tc-99	2.5E-04	9.8E-05	1.3E-04	3.1E-04	2.3E-04	1.8E-04	2.1E-04	4.6E-05	3.0E-06	5.3E-04
Se-75	1.6E-03	3.0E-03	5.3E-03	4.8E-03	1.4E-03	4.5E-04	1.9E-03	1.5E-03	3.1E-03	4.9E-03
Np-237	1.1E-03	3.0E-04	2.5E-03	8.6E-04	7.2E-04	5.1E-04	6.4E-04	9.4E-05	9.9E-03	9.4E-04
Ba-133	2.0E-03	2.6E-04	9.8E-03	5.8E-04	2.3E-03	2.2E-03	2.0E-03	9.4E-04	1.5E-02	2.5E-03
U-236	1.6E-03	8.3E-04	1.1E-02	3.5E-03	1.1E-03	6.3E-04	9.3E-04	1.1E-04	5.9E-02	2.6E-02
Cd-109	5.9E-03	1.0E-03	2.6E-02	6.7E-04	5.3E-03	4.7E-03	4.0E-03	1.2E-03	9.2E-02	8.2E-02
Ra-226	8.3E-03	1.6E-03	3.7E-02	1.4E-03	7.5E-03	1.4E-03	6.7E-03	5.0E-04	7.5E-02	3.3E-03
Ni-63 [1]	2.5E-02	9.1E-03	4.6E-02	1.6E-02	1.3E-02	5.1E-03	8.2E-03	3.7E-03	2.7E-01	1.2E-01
Co-57	5.2E-02	1.5E-02	2.7E-01	2.4E-03	6.1E-02	2.8E-02	3.6E-02	2.9E-03	5.3E-01	1.7E-01
Cs-137	1.2E-02	4.8E-03	1.0E-01	2.1E-02	3.2E-02	1.1E-02	2.2E-02	3.4E-03	8.6E-01	1.8E-01
Ag-110 m	> 1E-02		> 1E-02		> 1E-02		> 1E-02		> 1E-02	
Gd-153	> 4E-01		> 4E-01		> 4E-01		> 4E-01		> 4E-01	

[1] Based on single samples measured.

Table 4-12. Surface area determined by BET measurement on the different geological materials.

Sample ID	Particle size (mm) Low	High	BET-area m²/g	BET-area (m²/g) Mean value	+/–
KA3065A02:1 (Red-stained matrix rock)					
KA3065A02:1_A_1(2)	0,063	0,125	0,34	0,36	0,02
KA3065A02:1_A_2(2)	0,063	0,125	0,37		
KA3065A02:1_D_1(2)	2	4	0,04	0,04	0,01
KA3065A02:1_D_2(2)	2	4	0,05		
KA3065A02:2 (Fracture minerals)					
KA3065A02:2_A_1(2)	0,063	0,125	1,94	1,94	
KA3065A02:2_D_1(2)	2	4	0,76	0,81	0,07
KA3065A02:2_D_2(2)	2	4	0,86		
KA3065A02:6 (Matrix rock)					
KA3065A02:6_A_1(2)	0,063	0,125	0,29	0,32	0,04
KA3065A02:6_A_2(2)	0,063	0,125	0,35		
KA3065A02:6_D_1(2)	2	4	0,04	0,04	
KA3065A03 (Matrix rock)					
KA3065A03_Batch 1_A_1(2)	0,063	0,125	0,24	0,24	0,01
KA3065A03_Batch 1_A_2(2)	0,063	0,125	0,25		
KA3065A03_Batch 1_D_1(2)	2	4	0,05	0,05	0,01
KA3065A03_Batch 1_D_2(2)	2	4	0,05		
KA3065A03_Replica (Fracture minerals)					
KA3065A03_Replica_A_1(2)	0	0,125	4,94	4,94	
KA3065A03_Replica_D_1	2	4	3,96	3,96	

4.4.3 The sorption properties of different size fractions

The influence of different size fractions on the sorption behaviour is often observed for the three different size fractions studied, as shown in Figure 4-28. The results clearly show the importance of surface area in this figure (increased R_d for the smaller size fractions). The BET surface area for the 2–4 mm fraction is roughly five times lower than that of the smallest fraction (see Table 4-12 above). It is expected that the factor for the 1–2 mm fraction would be less than five since it supposedly has somewhat larger area than the 2–4 mm fraction. The R_d values differ by a factor of ~3 between the smallest and largest size fractions analysed, so a normalization of the R_d values by BET surface area would decrease the differences between the size fractions. It should be acknowledged that mineralogical differences between the size fractions, such as increased biotite content in smaller size fractions, may also affect the results. However, in the Site Investigation laboratory studies /Selnert et al. 2008, 2009a/, mineralogical differences between size fractions were generally not observed.

As observed in the figure it is indicated that the sorption has reached steady state for the finest particle size fraction, whereas the larger mineral fractions can be interpreted to have a small increase after 186 days. As discussed in Section 3.3.2 the basis for evaluation of K_d is that R_d has reached a plateau after 186 days for the 1–2 mm size fraction. This is not always the case for the batch tests performed as will be shown in subsequent figures.

Example of a plot of R_d for ^{137}Cs as a function of time is shown for KA3065A03_Replica in Figure 4-29. The geological material consists of fracture rock minerals. The different size fractions show almost the same sorption behaviour, independent of the rock size fraction studied. This is in agreement with the small difference in the measured BET-surface areas between the smallest and the largest fraction measured, see Table 4-12.

The geology of KA3065A02:2 consist of fracture minerals dominated of chlorite and calcite. A plot of R_d for ^{137}Cs, as a function of time, for the fracture minerals in the pilot bore hole is shown in Figure 4-30. A peculiar behaviour is observed for size fractions A and B, where the sorption decreases significantly after 90 days. One might speculate if this has something to do with e.g. chemical weathering of the fracture minerals causing the drastic decrease in sorption at 186 days. Such a behaviour was not observed for Cs sorption in any material in the Oskarshamn Site Investigation /Selnert et al. 2009a/ and the result should therefore be regarded with doubtfulness.

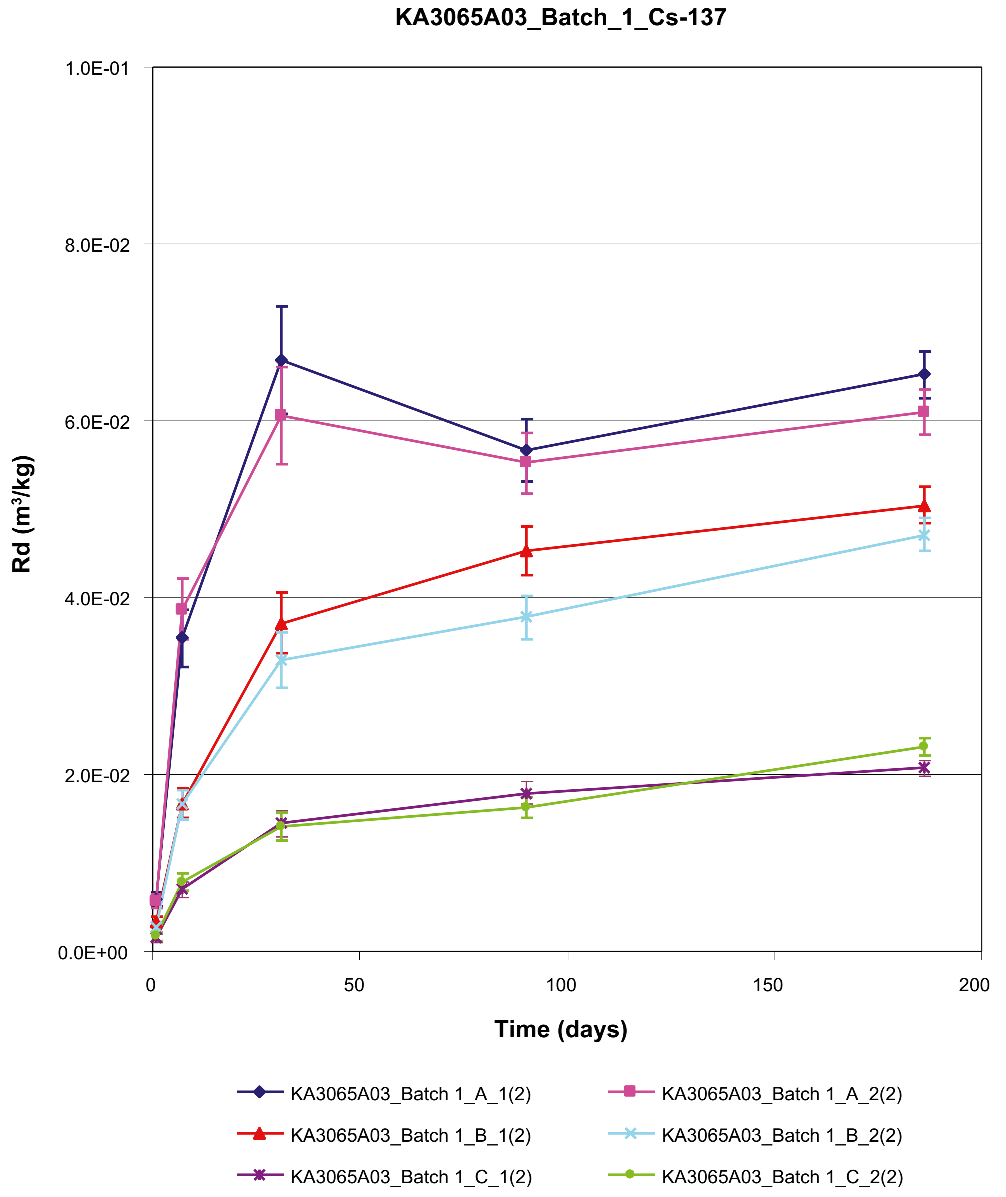

Figure 4-28. *The sorption behaviour of* ^{137}*Cs on different size fractions from KA3065A03_Batch_1 (matrix rock) as a function of contact time. Size fraction A=0.063–0.125 mm, B=0.25–0.5 mm and C=1–2 mm.*

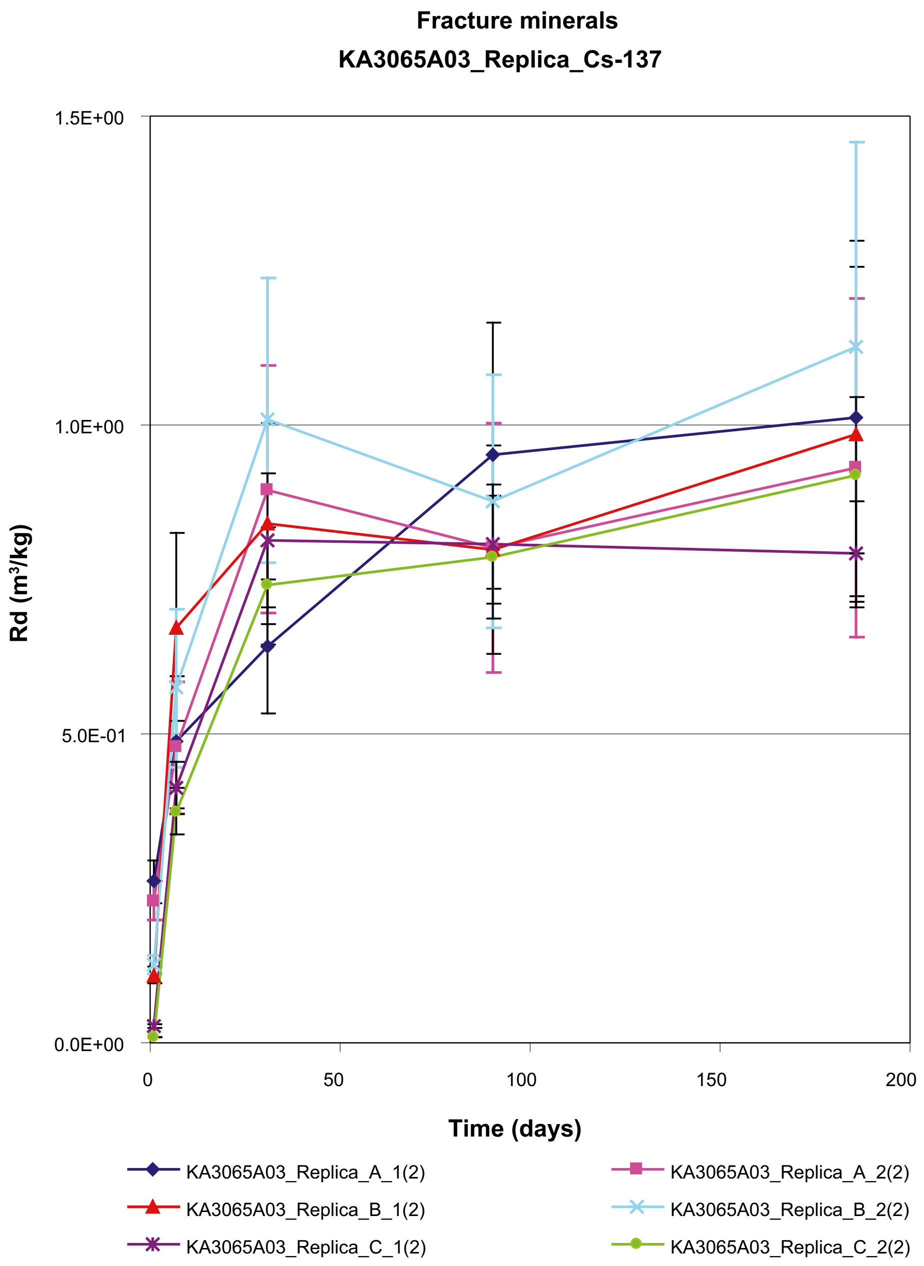

Figure 4-29. *The sorption behaviour of* ^{137}*Cs on different size fractions of KA3065A03_Replica_1 (fracture minerals) as a function of contact time. Size fraction A=0.063–0.125 mm, B=0.25–0.5 mm and C=1–2 mm.*

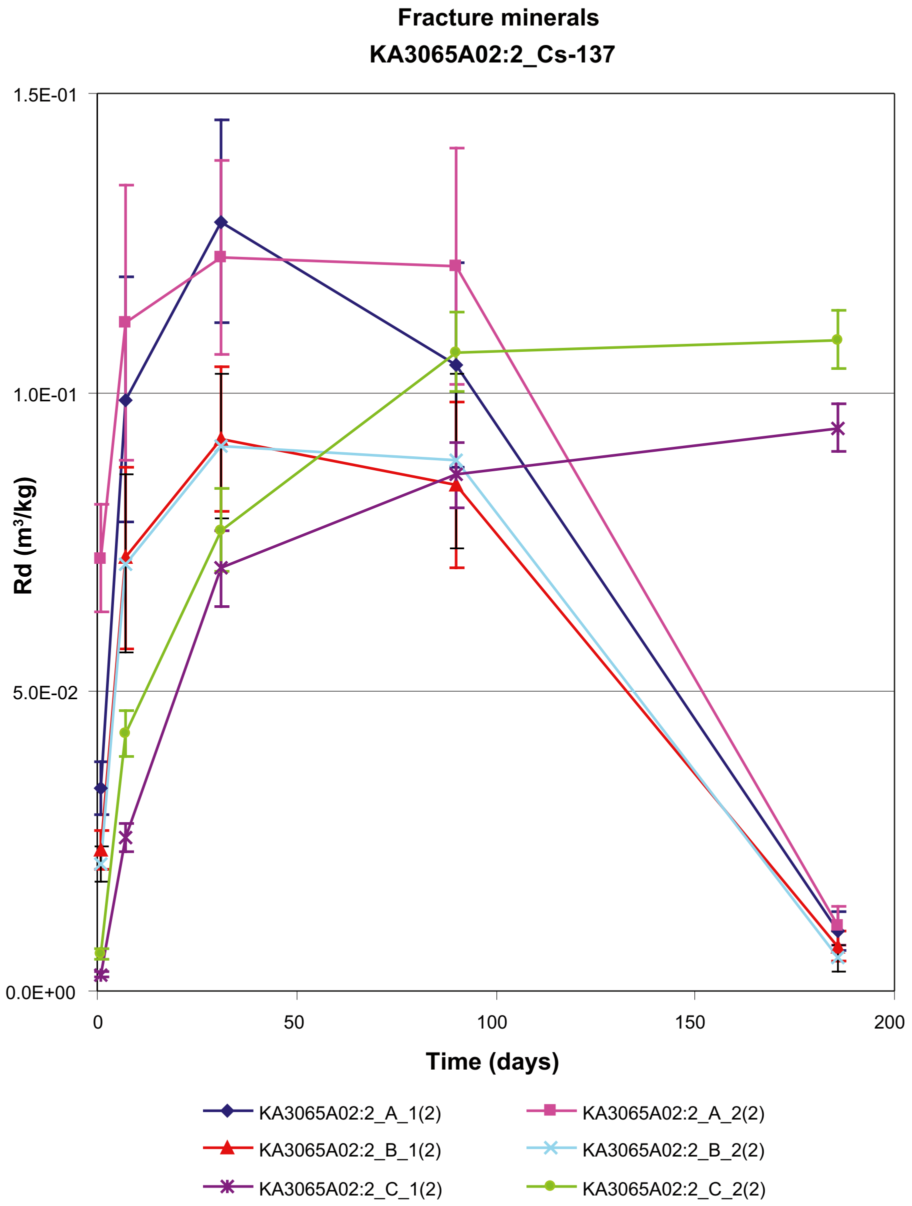

Figure 4-30. *The sorption behaviour of* ^{137}*Cs on different size fraction of KA3065A02:2 (fracture minerals) as a function of contact time. Size fraction A=0.063–0.125 mm, B=0.25–0.5 mm and C=1–2 mm.*

4.4.4 Sorption rate

The sorption behaviour as a function of time varies between the different radionuclides studied. Some of the radionuclides reach almost steady state after 186 days, whereas other seems to be still increasing after 186 days. As can be observed for ^{57}Co in Figure 4-31, the sorption has not reached steady state after 186 days.

The sorption increase of ^{57}Co is almost linear as a function of time. Another example of increasing sorption with time is observed for the sorption of ^{236}U on KA3065A03_Replica as shown in Figure 4-32. As can be observed there is no correlation between particle sizes and R_d. Furthermore, the sorption increases almost linearly with time.

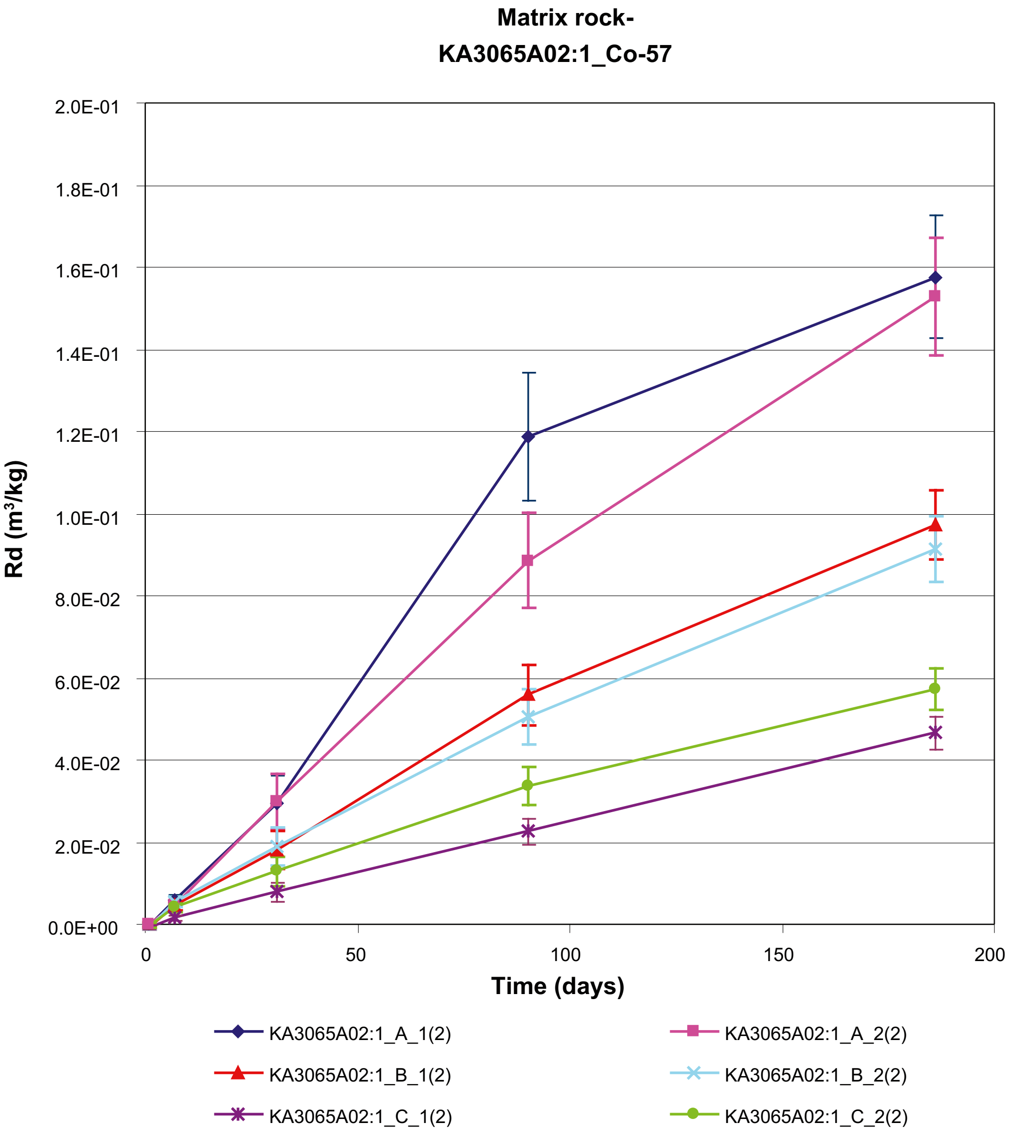

Figure 4-31. *Sorption behaviour of ^{57}Co on different size fractions of KA3065A02:1(matrix rock) as a function of time. Size fraction A=0.063–0.125 mm, B=0.25–0.5 mm and C=1–2 mm.*

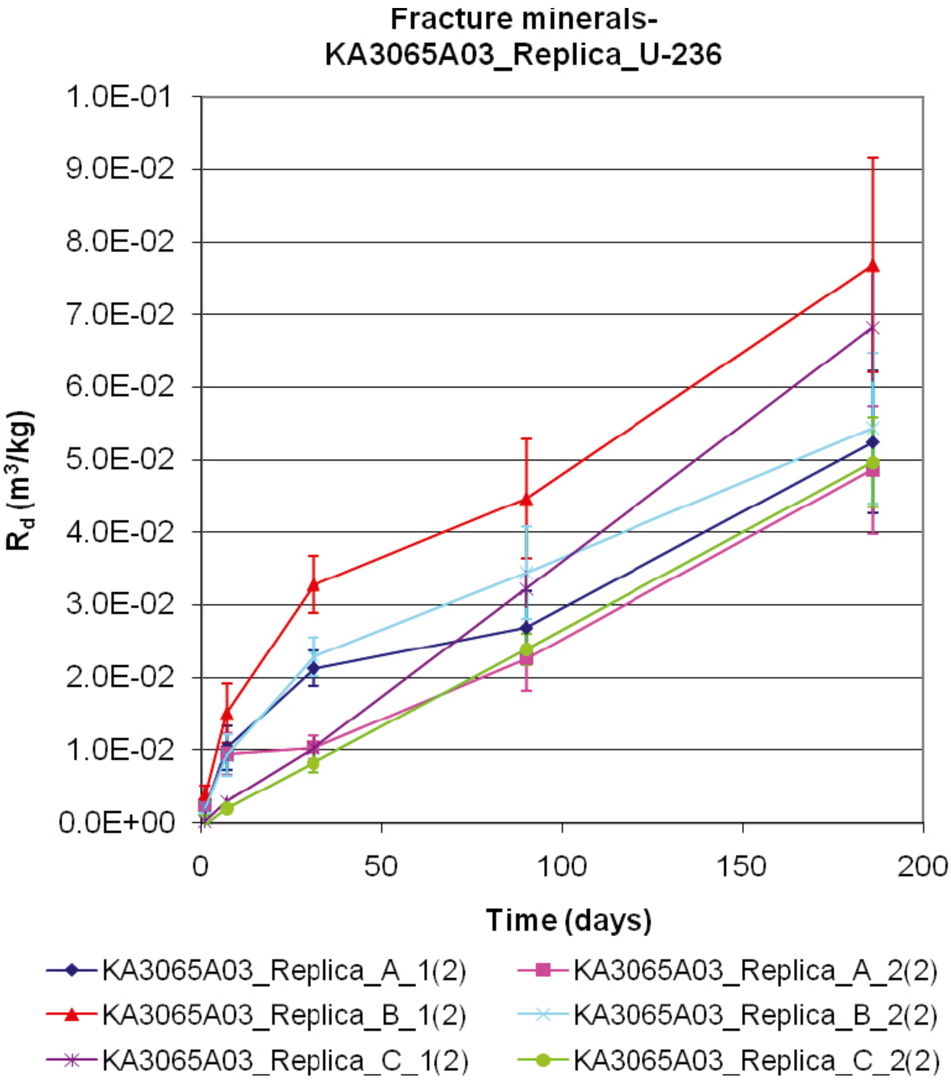

Figure 4-32. *Sorption behaviour of ^{236}U on different size fractions of KA3065A03_Replica (fracture minerals) as a function of time. Size fraction A=0.063–0.125 mm, B=0.25–0.5 mm and C=1–2 mm.*

In the reports of the laboratory measurements within the Site Investigations at Forsmark and Laxemar /Selnert et al. 2008, 2009a/, it was acknowledged that diffusive equilibrium may not have been reached for more strongly sorbing tracers under similar experimental conditions as in this work. It was also concluded that sorption coefficients should be regarded from a comparative perspective and that limitations in laboratory experiments should be regarded when using such data in e.g. performance assessment calculations. Longer experimental times would lead to increased degradation and weathering of the rock material, which also may give erroneous sorption coefficients.

Steadily increasing sorption with time was also obtained in the laboratory experiments in the TRUE-1 project /Byegård et al. 1998/ for similar Äspö materials. Byegård et al. mentioned slow sorption kinetics as an alternative explanation to diffusive in-equilibrium or weathering effects. Consequently, the former conclusion from the Site Investigations of using sorption coefficients in a comparative perspective with regard of limitations should be maintained.

4.4.5 Redox conditions

The batch sorption experiments described in this work are performed in such a way that reducing conditions can be expected, however; earlier experiences (e.g. /Byegård et al. 2008, Selnert et al. 2009b/) have indicated difficulties in maintaining true reducing conditions in such experimental conditions. The expected redox sensitive species in this study are $^{99}TcO_4^-$, $^{236}UO_2^{2+}$ and NpO_2^+.

One may thus speculate that these elements are reduced to their tetravalent states which are expected to have a much stronger sorption compared with the species discussed above. The effect of reduction is dominated for the experiments performed with the fine grain size fraction, A (0,065–0,125 mm), of the matrix rock materials, i.e. KA3065A02:1, KA3065A02:6 and KA3065A03_Batch_1. As can be observed in Figure 4-33, the most predominant sorption is observed for ^{99}Tc and ^{237}Np. The same strong adsorption for U and Np in the small size fraction was observed in the site investigation program SKB-PLU /Byegård et al. 2008, Selnert et al. 2009b/ and speculations were made of the enrichment of iron containing minerals in the smallest size fraction. The observed R_d-values are close to 1 m^3/kg. The sorption of ^{236}U does not reach the same R_d-values. Instead a sorption coefficient of 0.1 m^3/kg is reached. The sorption of ^{236}U is anyway high for the A (0.065–0.125 mm) size fraction compared to the two larger particle sizes as can be observed in Figure 4-34.

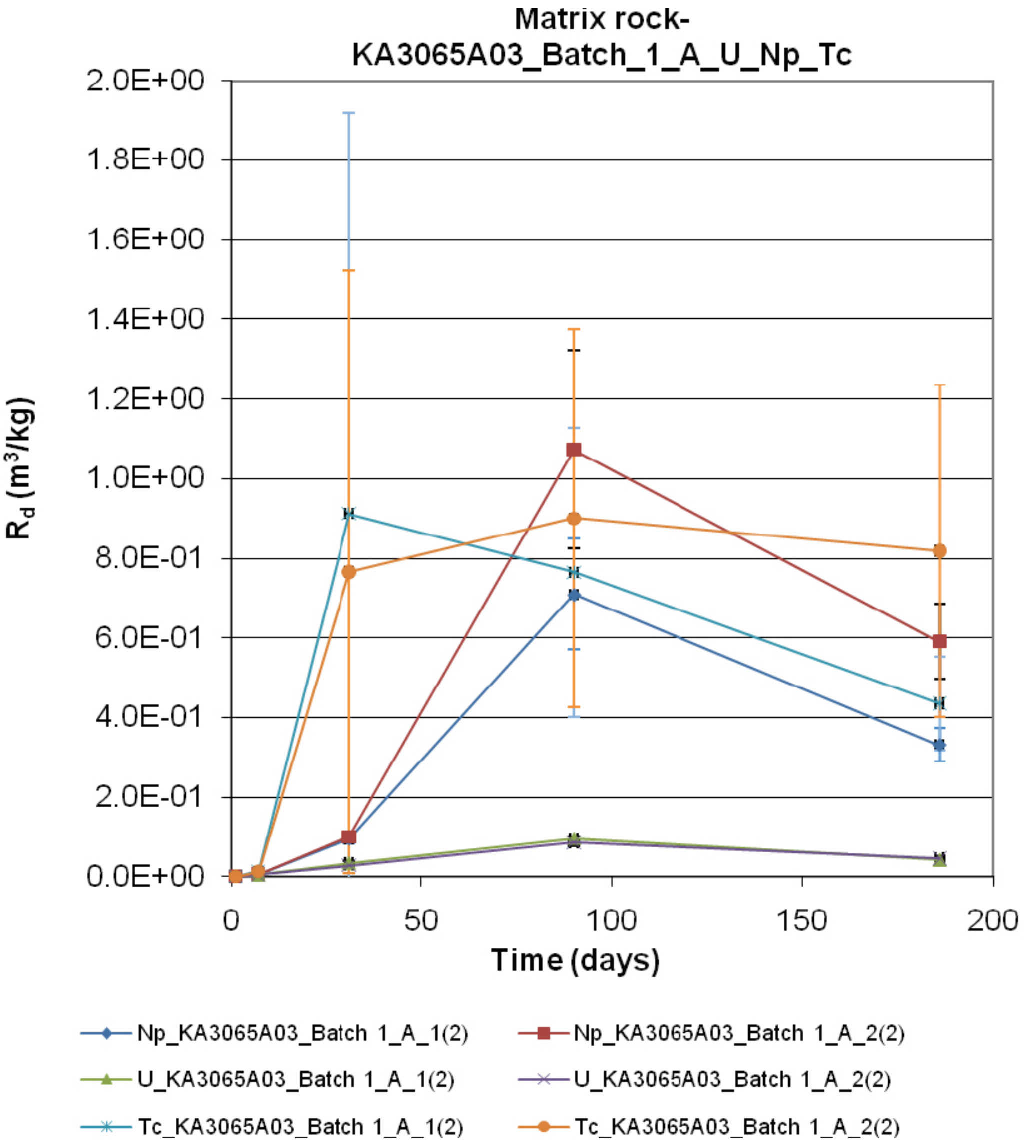

Figure 4-33. *Sorption behaviour of ^{99}Tc, ^{236}U and ^{237}Np on the size fraction A (0,065–0,125 mm) of KA3065A03_Batch_1 (matrix rock), as a function of time. Size fraction A=0.063–0.125 mm, B=0.25–0.5 mm and C=1–2 mm.*

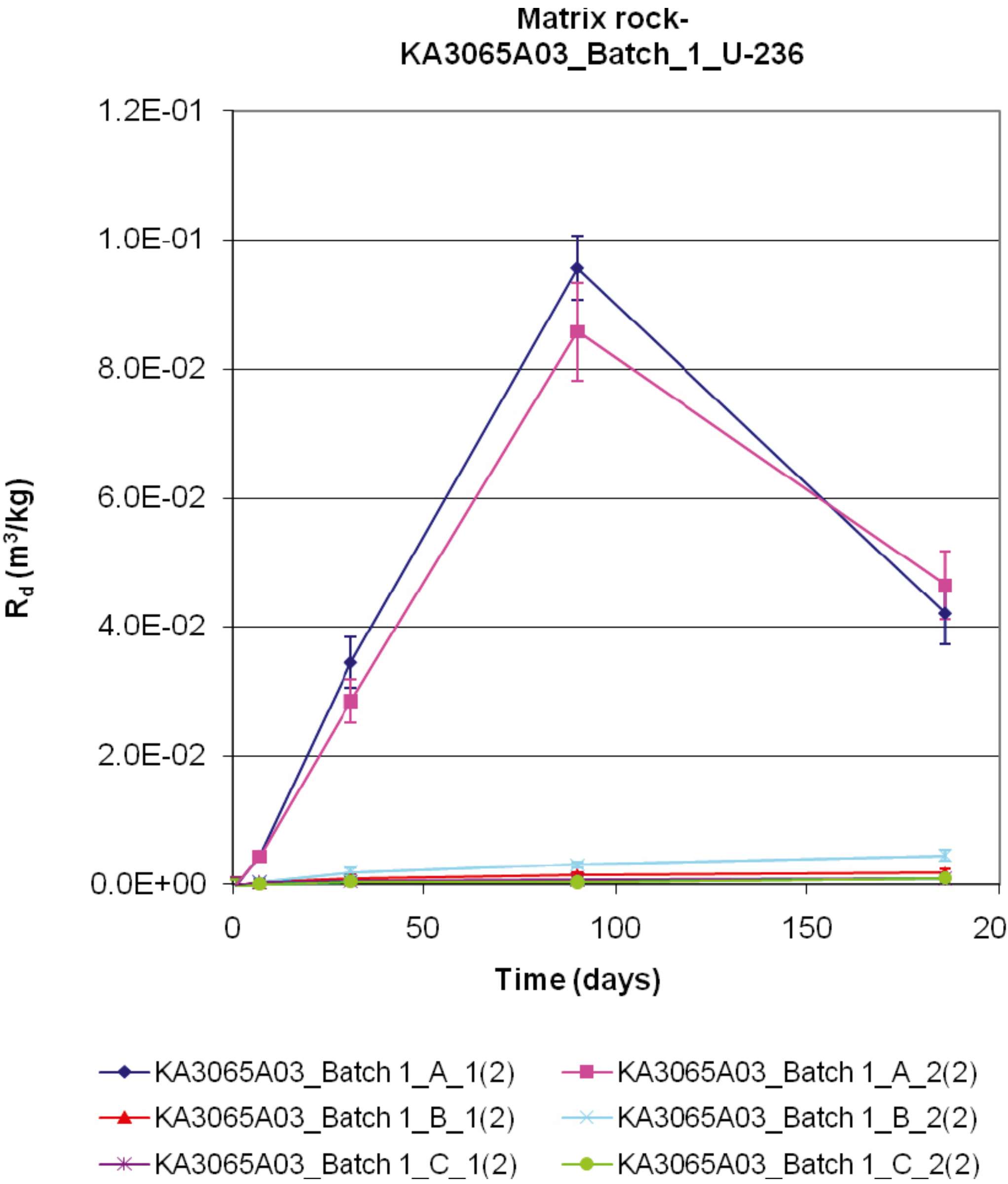

Figure 4-34. *Sorption of ^{236}U on different size fractions of KA3065A03:Batch_1 (matrix rock), as a function of time. Size fraction A=0.063–0.125 mm, B=0.25–0.5 mm and C=1–2 mm.*

4.4.6 Effects of very low and very high sorption

For the anions and ^{22}Na the observed sorption is so low that it is difficult to evaluate any results, e.g. see Figure 4-35. This is due to the methodology used in this and previous work for the batch sorption experiments; i.e. it is not possible to statistically verify any decrease of tracer concentration in the aqueous phase for the most weakly sorbing tracers. In order to optimize the method for low sorption one has to consider e.g. the solid to liquid ratio, the total amount of radionuclide added, the method used for measurement of radioactivity (counting statistics) and errors included in the method itself. Weighing is believed to be the major source of uncertainty in the present work. In order to determine the uncertainty a combined uncertainty analysis for the whole method would be preferable.

In the same manner the methodology needs optimization for high sorption in order to make it possible to measure high distribution ratios, i.e. R_d values. The used methodology makes it possible to measure R_d values up to about 1 m^3/kg. As indicated in the presented diagrams the possible dynamic range of R_d that can be studied by this methodology is in the order of 10^{-3}–1 m^3/kg. This is in agreement with the dynamic range of the R_d results in the Site Investigations /Selnert et al. 2008, 2009a/.

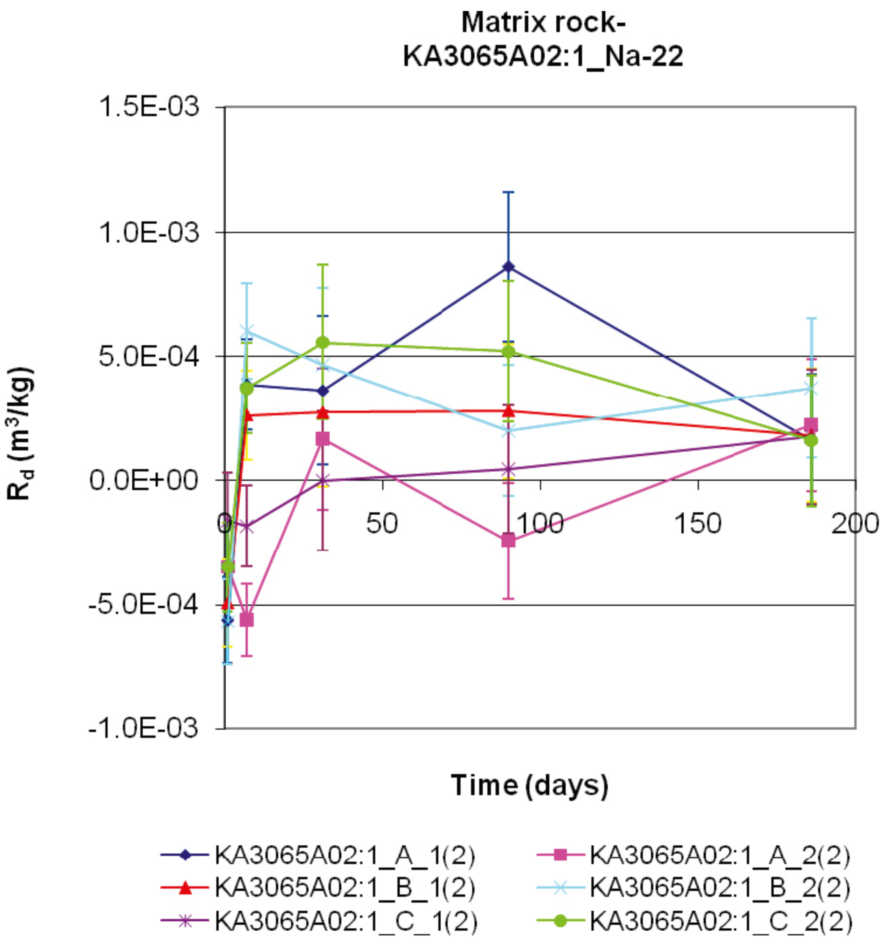

Figure 4-35. *Sorption behaviour of ^{22}Na on different size fractions of KA3065A02:1 as a function of time. Size fraction A=0,063–0,125 mm, B=0,25–0,5 mm and C=1–2 mm.*

4.4.7 Sorption mechanism

It is somewhat difficult to draw any conclusions about the sorption mechanisms involved for the various radionuclides studied. It seems, however, to be some correlation between a few groups of radionuclides. Traditionally one often speaks about elements where the sorption can be divided in ion exchange or by surface complexation. It seems like the alkaline and alkaline earth metals represent a separate group of tracers with ion exchange as the dominating sorption mechanism. As observed for ^{22}Na, ^{137}Cs, ^{133}Ba and ^{226}Ra there is a relatively fast sorption and the R_d values seems almost to reach plateaus for each radionuclide and each particle size fraction at least for the experiments performed with the matrix rock, i.e. KA3065A02:1, KA3065A02:6 and KA3065A03_Batch_1. A few elements show such a low sorption that they are not suitable for studies by the batch sorption procedure used in this work, e.g. ^{75}Se and ^{22}Na.

Elements that may be described by surface complexation are in this study represented by ^{57}Co, ^{63}Ni, ^{109}Cd and ^{236}U. These elements show a tendency not to reach sorption equilibrium after 186 days but rather a linear increase in R_d-values as a function of time.

Another mechanism involved in the sorption behaviour is probably caused by redox-reactions. As observed for ^{99}Tc, ^{237}Np and ^{236}U there is a clear tendency for strong sorption, especially regarding the experiment performed with the finest grain size fraction (A), i.e. 0,065–0,125 mm. The experiments are carried out in such way, that one may expect reducing conditions. The strong sorption could be explained by the fact that the finest size fractions (A) contains single mineral grains with fresh mineral grain surfaces exposed to the water phase , whereas the larger grains (B, C) consists of aggregates with several mineral grains /Byegård et al. 2008, Selnert et al. 2009b/. The explanation may thus be that mineral grains containing Fe(II) minerals are exposed and made available in order to reduce Tc(VII)O_4^- to Tc(IV), Np(V)O_2^+ to Np(IV) and U(VI)O_2^{2+} to U(IV) in the finest size fraction (A).

Beside the radionuclides discussed so far there is also a strong sorption observed for $^{110\,m}$Ag and ^{153}Gd.

5 Discussion and conclusions

5.1 Porosity

The results of the porosity ranges of the unaltered matrix rock samples are consistent with earlier results from /Vilks et al. 2005/ of LTDE-SD materials and with results for Ävrö granodiorite obtained during the Site Investigations. No major porosity variations are observed within the unaltered matrix rock samples. The general impression of the porosity investigations of the LTDE-SD materials is that coherence with results from Vilks and the Site Investigations is established.

A strongly increased porosity is found in fracture material samples, both with water saturation and the PMMA method.

The porosity distribution in the matrix rock is relatively homogeneous with grain boundary porosity as is visualised by the PMMA technique, while a strongly heterogeneous porosity distribution is found in fracture mineralizations and altered rock.

The expected porosity properties of different parts of the rock materials relevant for the in situ experiment are pointed out below, without respect to the actual amounts of fracture material found on the stub surface which were quite low /Nilsson et al. 2010/. The findings from the porosity studies presented in this report using water saturation measurements and PMMA studies give the following expectations for different materials in the LTDE-SD experiment:

- *Fracture mineralizations and cataclasitic rock matrix*: a strongly increased porosity (up to about 5%) compared to that of matrix rock is expected, with a heterogeneous distribution and a decreasing gradient inwards.
- *Rock with different degrees of alteration close to the fracture surface:* porosity from ~0.2 to a few % with a more heterogeneous distribution than in the matrix rock is expected near the fracture surface. A decreasing gradient inwards is expected for areas with elevated porosity near the surface.
- *Mylonitized parts close to the fracture surface:* in these areas, that are estimated to apply for a minor part of the stub area, a low porosity that may even be decreased compared to the porosity of matrix rock is expected. The quantity of mylonite seems to be confined to minor areas in the rock samples examined; it should be acknowledged though that only a few samples are studied and that this quantification is uncertain.
- *Matrix rock:* a relatively homogeneous distribution is expected and the porosity is typically ~0.3%.

5.2 Diffusivity

The diffusion study in this report was aimed to measure the H^3HO diffusivity in the most relevant rock pieces from the 36 mm borehole section and complementing samples from the exploration borehole in order to enable comparisons with the Site Investigation results using the same method as applied in the Site Investigations. The larger and broader study of diffusivity within the LTDE-SD project is presented with conclusions in the report by /Vilks et al. 2005/, from which some of the main findings are listed in Section 1.3.

The diffusivities obtained in A02 and A03 samples representing unaltered matrix rock are all in the relatively narrow range from $2.7 \cdot 10^{-14}$ to $6.5 \cdot 10^{-14}$ m^2/s, a result which is in line with the fact that the sample positions in the rock are close to each other and that homogeneous and relatively undisturbed specimens were used. The diffusivity range is within the range for H^3HO reported by Vilks ($1.3 \cdot 10^{-14}$ to $4.6 \cdot 10^{-11}$ m^2/s) for LTDE-SD samples, although roughly one decade lower than the geometric mean of H^3HO reported by Vilks to $4.9 \cdot 10^{-13}$ m^2/s. The diffusivity range is also within that observed in the Site Investigations.

The results of the ^{36}Cl diffusion in two samples are contradictory in that more than an order of magnitude lower diffusivity is estimated for one sample while the other give practically identical results as for H^3HO. For estimation purposes of a possible anion exclusion effect, the large quantity of samples studied with iodine and H^3HO on LTDE-SD materials by Vilks is recommended to be used.

5.3 Sorption

A general comparison of the rock materials used in the investigation shows the trend of higher sorption values in the two fractures samples compared to the matrix rock samples. There is a, however, also difference within the group of fracture materials with the material sampled in the experimental borehole KA3065A03 fracture (i.e. the replica) showing stronger sorption than the corresponding fracture sample from the KA3065A02 pilot borehole. This is probably explained by the fact that the latter, besides chlorite/calcite fracture material, also contains the significant amount of matrix rock. The material from the KA3065A03 fracture is a sample with more or less solely fracture minerals which is likely to increase the sorption.

The red stained and altered matrix rock material (A02:1) show very little differences in sorption pattern from the non-altered matrix. It is indicated that the sorption of Cs is in the range of 0.5 orders of magnitude lower in the altered sample compared to the non-altered rock; an observation that is interesting to compare to the mineralogical analyses results of approximately half the amount of biotite in the altered samples compared to the non-altered samples. This indicates that Cs may be sorbing in biotite and other sheet silicates. Cs is known to displace Na in the interlayers of illite, where Cs becomes fixed by collapsing the interlayer since it has a smaller hydration radius compared to Na. Ba and Sr, cannot do this, and so are weakly sorbed, which would be expected of group 1 and group 2 elements.

For the different tracers involved in the study, the finding can be summarized by:

- For the presumed non-sorbing tracer (^{36}Cl) and the very weakly sorbing tracer (^{22}Na), it is obvious that the experimental technique is not sensitive enough to measure (if any) sorption, i.e. a K_d detection limit of $1 \cdot 10^{-3}$ m^3/kg is estimated.
- For the ^{137}Cs tracer, very high K_d values can be found for the fracture material studied; values up to 1 m^3/kg is measured for the experimental section replica material, 1-2 mm size fraction. This is significantly higher than the matrix rock where corresponding K_d values in the range of $(1–5) \cdot 10^{-2}$ m^3/kg are observed. Furthermore, for the replicas material, ^{137}Cs is the strongest sorbing tracer, except for the tracer that could not be found in the aqueous phase at the termination of the experiment (186 days of contact time).
- The ^{133}Ba and ^{226}Ra (expected to sorb mainly by cation exchange and less influenced by surface complexation) show lower sorption than ^{137}Cs; typically 0.5 to 1 orders of magnitude lower for ^{226}Ra and 1–2 orders of magnitudes lower for ^{133}Ba. The larger differences are observed for the fracture material and the lower values are observed for the matrix rock samples.
- For the divalent transition metals studied, the sorption is in the order of ^{109}Cd < ^{63}Ni < ^{57}Co. For the fracture samples, K_d values in the range of 10^{-1}–1 m^3/kg can be observed for ^{57}Co; the sorption of ^{109}Cd is generally one order of magnitude lower and ^{63}Ni is found in between. For the matrix rock samples, the range of K_d values for ^{57}Co is $(4–6) \cdot 10^{-2}$ m^3/kg and the same trend is observed also here; i.e. the sorption of ^{109}Cd is generally one order of magnitude lower and ^{63}Ni is found in between. For the matrix rock samples studied, ^{57}Co is the strongest sorbing tracers of the tracers that could be measured in the aqueous phase, i.e. higher sorption than for ^{137}Cs.
- For the redox-sensitive tracers studied, it is shown that:
  - No sorption of ^{99}Tc can be found which indicate that the conditions applied during the experiment is not enough to obtain an electrochemical reduction from the non-sorbing TcO_4^- to the presumed strongly sorbing tetravalent form of this element.
  - Regarding the ^{237}Np and ^{236}U, adsorption corresponding to K_d values of $(6–11) \cdot 10^{-4}$ m^3/kg and $(9–16) \cdot 10^{-4}$ m^3/kg, respectively, is measured for the matrix rock samples. For the fracture samples, K_d values up to $1 \cdot 10^{-2}$ m^3/kg for ^{237}Np and $6 \cdot 10^{-2}$ m^3/kg for ^{236}U have been found. The comparatively low losses of tracers indicate that these tracers are present in their oxidized form (NpO_2^+ and UO_2^{2+}, respectively) and that no reduction to their presumably strongly sorbing tetravalent form occurs under the present laboratory conditions.

- The trivalent lanthanide ^{153}Gd together with the $^{110\,m}$Ag isotope are completely lost from the aqueous phase and based on detection limits it is shown that the K_d is higher than 0.4 m^3/kg for ^{153}Gd and higher than 0.01 m^3/kg for ^{153}Gd. This is not unexpected and is e.g. in line with the results for Eu(III)/Am(III) in the SKB site investigation /Byegård et al. 2008, Selnert et al. 2009b/. The loss of $^{110\,m}$Ag from the aqueous phase is more complex and will probably require an elaborate speciation calculation to obtain information of which chemical species that are present in the groundwater.
- ^{75}Se is likely to be present as SeO_4^{2-} in the groundwater but seems, despite its anionic form, to adsorb weakly to the rock material. The K_d is in the range of $(1.4–1.9)\cdot 10^{-3}$ m^3/kg for matrix rock and $(3–5)\cdot 10^{-3}$ m^3/kg for fracture material. As for $^{110\,m}$Ag, an interpretation of the ^{75}Se behaviour probably demands an elaborate speciation calculation.

5.4 Sorption-diffusion experiments on intact drill cores

Sorption-diffusion studies on intact rock samples show concentration losses that were basically in line to what could be expected from the outcome of the batch sorption experiments within the LTDE-SD and the Site Investigation program. For a majority of the predicted concentration losses (19 of 29) the calculated concentration loss was under-predicted, 6 were well-predicted and 4 were over-predicted. Consequently, the general indication is that the intact rock samples have slightly higher retardation properties than what is predicted using through-diffusion diffusivity and K_d values from batch experiments using crushed rock material (1–2 mm fraction).

Modelling of the diffusion process showed that the product of the sorption coefficient and the formation factor, $K_d\cdot F_{f,}$ determines the concentration loss in the sorption-diffusion experiment on intact drill cores. As is mentioned above, the observed concentration loss, and thus $K_d\cdot F_{f,}$, is in most cases higher than expected from batch sorption (K_d) and through-diffusion (F_f) experiments and either an increased K_d or increased F_f can be used to give a best fit to the measurements results. Consequently, the individual values of K_d and F_f could only be determined by the results of the analysis of the tracer concentration profiles in the rock.

In general, when $K_d\cdot F_{f,}$ determined from the intact core result is compared to that calculated from batch sorption and through-diffusion values, the method agreement is best for the ion-exchange sorbing tracers and the surface complexation sorbing tracers, while larger deviation is indicated for the redox sensitive elements U and Np. The much higher concentration loss of U and Np in the intact drill cores than expected is interpreted as a reduction that takes place in the water-drill core interface.

References

SKB's (Svensk Kärnbränslehantering AB) publications can be found at www.skb.se/publications.

Andersson P, Byegård J, Dershowitz B, Doe T, Hermanson J, Meier P, Tullborg E-L, Winberg A (ed), 2002. Final report of the TRUE Block Scale project. 1. Characterisation and model development. SKB TR-02-13, Svensk Kärnbränslehantering AB.

Brunauer S, Emmett P H, Teller E, 1938. Adsorption of gases in multimolecular layers. Journal of the American Chemical Society, 60, pp 309–319.

Byegård J, Johansson H, Skålberg M, Tullborg E-L, 1998. The interaction of sorbing and non-sorbing tracers with different Äspö rock types. Sorption and diffusion experiments in the laboratory scale. SKB TR-98-18, Svensk Kärnbränslehantering AB.

Byegård J, Selnert E, Tullborg E-L, 2008. Bedrock transport properties. Data evaluation and retardation model. Site descriptive modelling SDM-Site Forsmark. SKB R-08-98, Svensk Kärnbränslehantering AB.

Crank J, 1975. The mathematics of diffusion. 2nd ed. Oxford: Clarendon.

Löfgren M, Neretnieks I, 2005. Oskarshamn site investigation. Formation factor logging in situ and in the laboratory by electrical methods in KSH01A and KSH02. Measurements and evaluation of methodology. SKB P-05-27, Svensk Kärnbränslehantering AB.

Mills R, Lobo V M M, 1989. Self-diffusion in electrolyte solutions: a critical examination of data compiled from the literature. Amsterdam: Elsevier. (Physical Sciences Data 36).

Nilsson K, Byegård J, Selnert E, Widestrand H, Höglund S, Gustafsson E, 2010. Äspö Hard Rock Laboratory. Long Term Sorption Diffusion Experiment (LTDE-SD). Results from rock sample analyses and modelling. SKB R-10-68, Svensk Kärnbränslehantering AB.

Ohlsson Y, Neretnieks I, 1995. Literature survey of matrix diffusion theory and of experiments and data including natural analogues. SKB TR 95-12, Svensk Kärnbränslehantering AB.

Penttinen L, Siitari-Kauppi M, Ikonen J, 2006. Oskarshamn site investigation. Determination of porosity and micro fracturing using the ^{14}C-PMMA technique in samples taken from Oskarshamn area. SKB P-06-62, Svensk Kärnbränslehantering AB.

Rhén I (ed), Gustafson G, Stanfors R, Wikberg P, 1997. Äspö HRL – Geoscientific evaluation 1997/5. Models based on site characterization 1986–1995. SKB TR 97-06, Svensk Kärnbränslehantering AB.

Selnert E, Byegård J, Widestrand H, 2008. Forsmark site investigation. Laboratory measurements within the site investigation programme for the transport properties of the rock. Final report. SKB P-07-139, Svensk Kärnbränslehantering AB.

Selnert E, Byegård J, Widestrand H, 2009a. Oskarshamn site investigation. Laboratory measurements within the site investigation programme for the transport properties of the rock. Final report. SKB P-07-179, Svensk Kärnbränslehantering AB.

Selnert E, Byegård J, Widestrand H, Carlsten S, Döse C, Tullborg E-L, 2009b. Bedrock transport properties. Data evaluation and retardation model. Site descriptive modelling, SDM-Site Laxemar. SKB R-08-100, Svensk Kärnbränslehantering AB.

Siitari-Kauppi M, 2002. Development of ^{14}C-polymethacrylate method for the characterisation of low porosity media. Ph.D. thesis. University of Helsinki, Finland.

SS-EN 1936:1999. Natural stone test methods: determination of real density and apparent density, and of total and open porosity. Stockholm: Swedish Standards Institute.

Stephens M B, Fox A, La Pointe P R, Simeonov A, Isaksson H, Hermanson J, Öhman J, 2007. Geology Forsmark. Site descriptive modelling Forsmark stage 2.2. SKB R-07-45, Svensk Kärnbränslehantering AB.

Vilks P, Miller N H, Stanchell F W, 2005. Laboratory program supporting SKB's Long Term Diffusion Experiment. Report 06819-REP-01300-10111-R00, Atomic Energy of Canada Limited.

Wahlgren C-H, Bergman T, Persson Nilsson K, Eliasson T, Ahl M, Ekström M, 2005. Oskarshamn site investigation. Bedrock map of the Laxemar subarea and surroundings. Description of rock types, modal and geochemical analyses, including the cored boreholes KLX03, KSH03 and KAV01. SKB P-05-180, Svensk Kärnbränslehantering AB.

Wahlgren C-H, Curtis P, Hermanson J, Forsberg O, Öhman J, Fox A, La Pointe P, Drake H, Triumf C-A, Mattsson H, Thunehed H, Juhlin C, 2008. Geology Laxemar. Site descriptive modelling, SDM-Site Laxemar. SKB R-08-54, Svensk Kärnbränslehantering AB.

Wass E, 2005. LTDE Long-Term Diffusion Experiment. Hydraulic conditions of the LTDE experimental volume – results from Pre-Tests 0.1–6. SKB IPR-05-25, Svensk Kärnbränslehantering AB.

Widestrand H, Byegård J, Ohlsson Y, Tullborg E L, 2003. Strategy for the use of laboratory methods in the site investigations programme for the transport properties of the rock. SKB R-03-20, Svensk Kärnbränslehantering AB.

Widestrand H, Byegård J, Börjesson S, Bergelin A, Wass E, 2006. LTDE Long-Term Diffusion Experiment. Functionality tests with short-lived radionuclides 2005. SKB IPR-06-05, Svensk Kärnbränslehantering AB.

Widestrand H, Byegård J, Cvetkovic V, Winberg A, Andersson P, Tullborg E-L, Siitari-Kauppi, 2007. Sorbing tracer experiments in a crystalline rock fracture at Äspö (Sweden): 1. Experimental setup and microscale characterization of retention properties. Water Resources Research, 43, W10413.

Widestrand H, Byegård J, Kronberg M, Nilsson K, Höglund S, Gustafsson E, 2010. Äspö Hard Rock Laboratory. Long Term Sorption Diffusion Experiment (LTDE-SD). Performance of main in situ experiment and results from water phase measurements. SKB R-10-67, Svensk Kärnbränslehantering AB.

Winberg A, Andersson P, Hermanson J, Byegård J, Cvetkovic V, Birgersson L, 2000. Äspö hard rock laboratory. Final report of the first stage of the tracer retention understanding experiments. SKB TR-00-07, Svensk Kärnbränslehantering AB.

Winberg A, Andersson P, Byegård J, Poteri A, Cvetkovic V, Dershowitz W, Doe T, Hermanson J, Jaime Gómez-Hernández J, Hautojärvi A, Billaux D, Tullborg E-L, Holton D, Meier P, Medina A, 2003a. Final report of the TRUE Block Scale project. 4. Synthesis of flow, transport and retention in the block scale. SKB TR-02-16, Svensk Kärnbränslehantering AB.

Winberg A, Hermansson J, Tullborg E-L, Staub I, 2003b. Äspö Hard Rock Laboratory. Long-Term Diffusion Experiment. Structural model of the LTDE site and detailed description of the characteristics of the experimental volume including target structure and intact rock section. SKB IPR-03-51, Svensk Kärnbränslehantering AB.

Chemical analysis of rock samples

The results from geochemical analyses of main and trace elements for rock samples A02:6 and Batch 1 (synonymous to A03:1). The analyses were performed at the ALS Scandinavia, Luleå.

Element	Sample	A02:6	A03:1 Batch 1
SiO_2	%	68.5	69.5
Al_2O_3	%	14.4	14.1
CaO	%	2.06	1.77
Fe_2O_3	%	3.01	2.44
K_2O	%	4.73	5.10
MgO	%	1.03	0.775
MnO	%	0.0454	0.0385
Na_2O	%	3.26	3.08
P_2O_5	%	0.152	0.121
TiO_2	%	0.436	0.346
Sum	**%**	**97.6**	**97.3**
LOI	%	0.6	0.6
Ba	mg/kg	1,540	1,660
Be	mg/kg	1.84	1.69
Co	mg/kg	< 6	< 6
Cr	mg/kg	21.6	17.5
Cs	mg/kg	2.51	2.05
Cu	mg/kg	55.1	< 6
Ga	mg/kg	14.9	14
Hf	mg/kg	6.58	22
Mo	mg/kg	3.22	< 2
Nb	mg/kg	8.42	7.67
Ni	mg/kg	< 10	< 10
Rb	mg/kg	132	136
S	mg/kg	21.2	16.0
Sc	mg/kg	3.02	4.56
Sn	mg/kg	4.77	7.70
Sr	mg/kg	741	725
Ta	mg/kg	0.696	0.679
Th	mg/kg	3.63	3.38
U	mg/kg	2.47	3.13
V	mg/kg	37.8	31.0
W	mg/kg	0.621	0.678
Y	mg/kg	15.2	46.0
Zn	mg/kg	56.2	46.6
Zr	mg/kg	317	938
La	mg/kg	92.3	54.9
Ce	mg/kg	234	157
Pr	mg/kg	12.6	9.15
Nd	mg/kg	37.0	27.7
Sm	mg/kg	4.59	3.94
Eu	mg/kg	0.620	0.425
Gd	mg/kg	2.27	2.29
Tb	mg/kg	0.330	0.316
Dy	mg/kg	2.08	1.99
Ho	mg/kg	0.418	0.388
Er	mg/kg	1.13	1.11
Tm	mg/kg	0.172	0.167
Yb	mg/kg	1.19	1.08
Lu	mg/kg	0.181	0.153

Appendix 2

Rock sample positions on the cores

Borehole KA3065A02 (the exploration borehole)

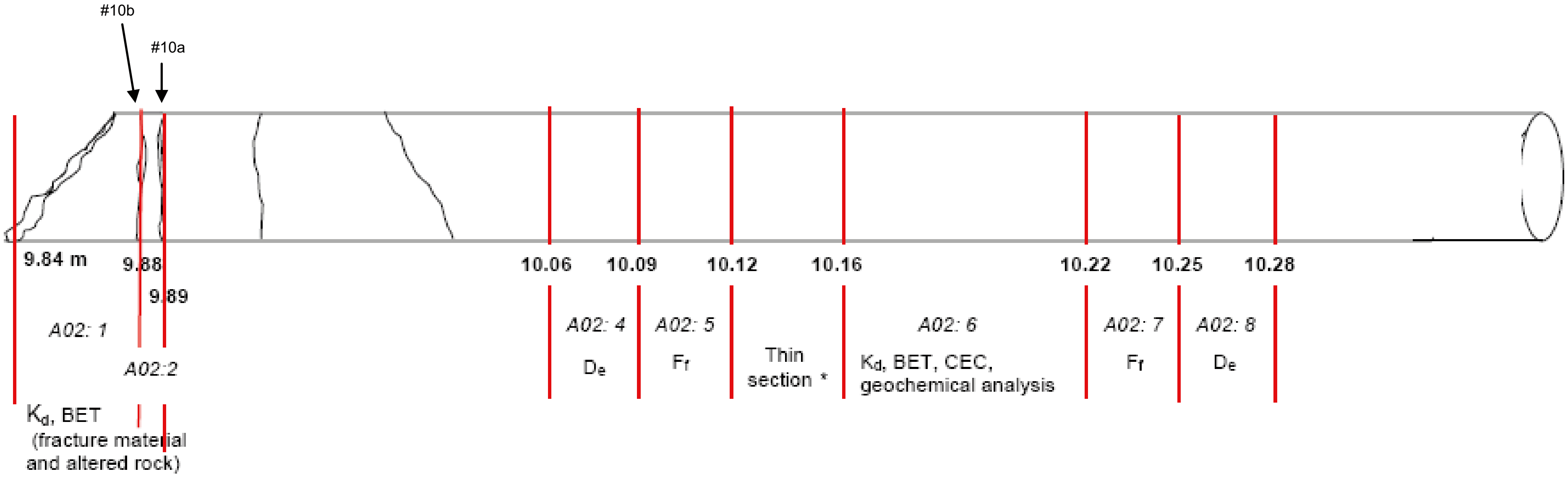

*Only a very small part of the section is used.

Figure A2-1. *Schematic illustration of the borehole KA3065A02 with the positions of each rock sample marked with section up and section low at the rock core. The measured parameter is noted in each interval. The structures #10a, which corresponds to the target stub fracture in KA3065A03, and structure #10b are indicated (from /Winberg et al. 2003b/).*

Borehole KA3065A03 (the 36 mm diameter borehole)

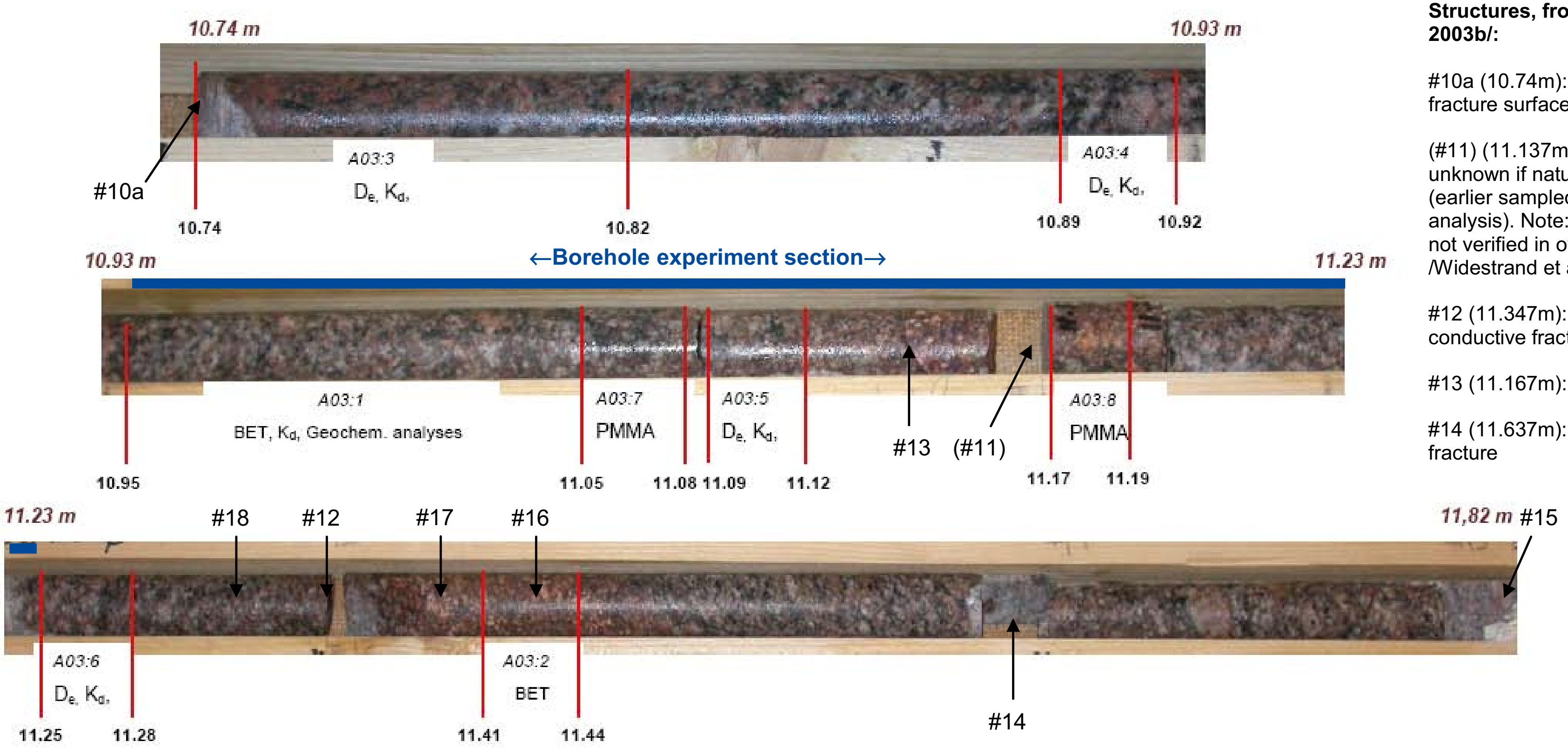

Structures, from /Winberg et al. 2003b/:

#10a (10.74m): the natural fracture surface of the stub

(#11) (11.137m): Suspected, unknown if natural or open/closed (earlier sampled for thin section analysis). Note: this fracture was not verified in overcore drilling /Widestrand et al., 2010/.

#12 (11.347m): Open potential conductive fracture

#13 (11.167m): Sealed fracture

#14 (11.637m): Open conductive fracture

Figure A2-2. *Photographs of borehole KA3065A03, divided in three sections. The positions of each rock sample marked with section up and section low at the rock core. The sample ID and the measured parameters are noted in each interval. The experiment section at 10.949 m–11.249 m is marked with a blue line. Interpreted intersecting structures by /Winberg et al. 2003b/ is marked with # at approximate positions. Note that the only fracture in the experiment section that was verified by the analysis of the overcore drilling is the sealed fracture #13 /Widestrand et al. 2010/.*

PMMA-results

In this section the result of the ^{14}C-PMMA- measurements are presented. Each rock sample is represented with photographs, autoradiographs and porosity histograms of one or several subsamples of the initial rock sample. Two porosity profiles are reported as well. The porosity is equal to the average porosity of the sample as evaluated in the PMMA-method.

Subsamples representing different areas of the original sample are indexed with A, B etc after the sample number.

A03:7 (PMMA 1)

In the two figures below, two subsamples representing two different surface areas of the rock sample A03:7 are shown. The autoradiograph reveals grain boundary pores which are visible around feldspar and quartz grains. In addition dark minerals show high porosities. The porosity of this sample is 0.51%.

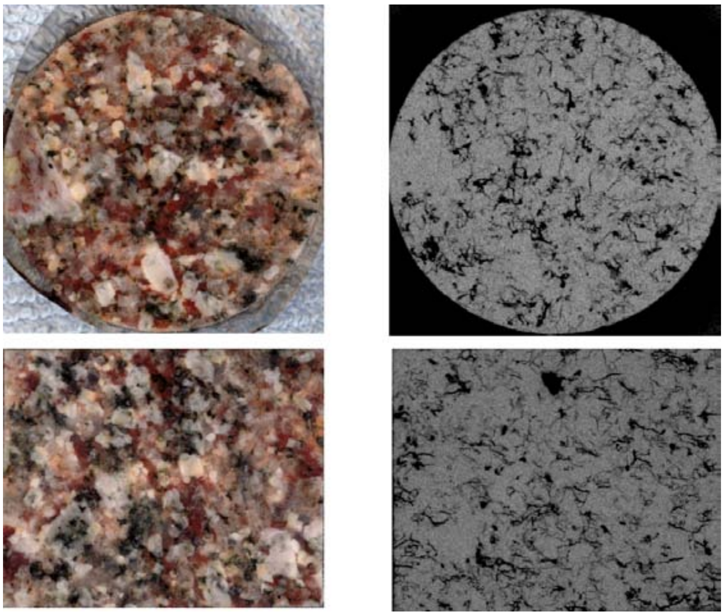

Photo image of; sample A03:7A (upper left) and the corresponding autoradiograph upper (right) with a diameter of 22 mm, sample A03:7B (lower left) and the corresponding autoradiograph (lower right). The width of the sample A03:7B is 23 mm.

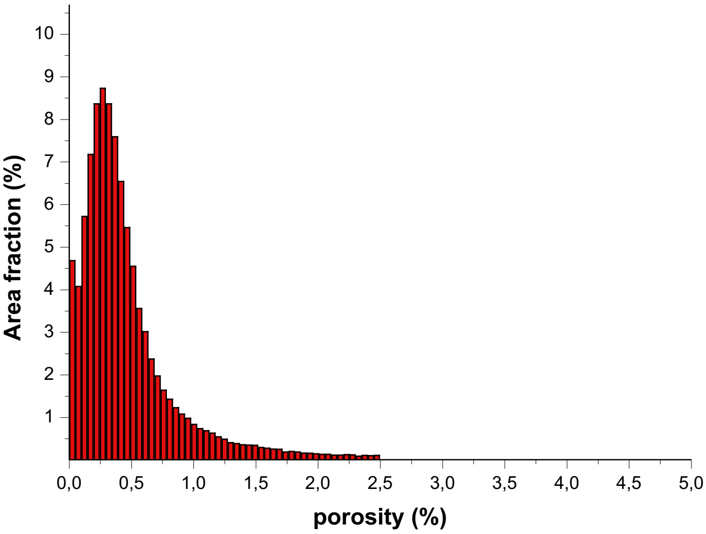

Porosity histogram of sample A03:7. The porosity is 0.51%.

A03:8 (PMMA 2)

The autoradiograph reveals grain boundary pores which exist around feldspar and quartz grains. As in sample A03:7, the dark minerals show high porosities. The porosity of this sample is 0.61%.

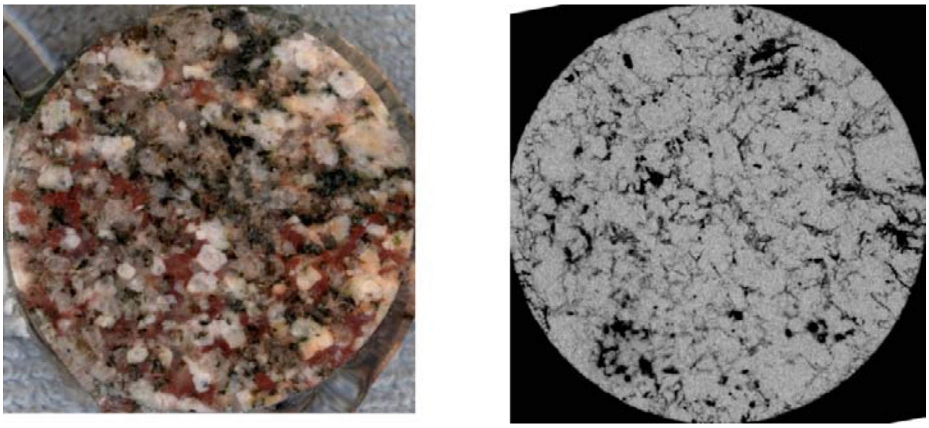

Photo image of sample A03:8A (left) and corresponding autoradiograph (right). The sample diameter is 22 mm.

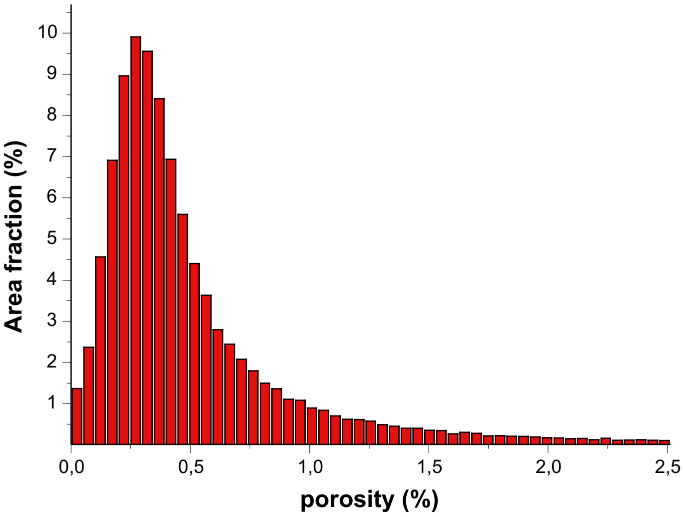

Porosity histogram of sample A03:8 with a porosity of 0.61%.

A03:10 (“10, stor sten”)

This sample has been subdivided into three pieces to get information of both the strongly altered rim close to the open fracture which consists of fracture minerals and rock fragments, sealed fractures, as well as the altered red-stained bedrock.

In the figure below it is shown that sealed fractures with chlorite/epidote and/or calcite show high porosity in the autoradiographs, up to 30%. The bedrock (i.e. altered variety of Ävrö granodiorite) in turn, has a porosity of 3%. The porosity for the whole rock sample is estimated to 3.6%.

The porosity of the subsample A03:10B is 1.5% for the altered bedrock and 11% for altered rim with minerals as chlorite and epidote, i.e. the alteration rim is clearly more porous than the adjacent rock. However the altered bedrock is still about 5 times more porous than the less disturbed matrix rock in A02 and A03.

A porosity profile is evaluated on rock sample A03:10C as well, from the fracture mineralization with mainly epidote, chlorite and rock fragments into a calcite fracture (partly open), an epidote sealed area with low porosity and finally red-stained bedrock. As can be seen in the figure below, the alteration rim is clearly more porous than the red-stained bedrock. The porosity of the red-stained bedrock is 2% and the porosity of alteration rim is 15%. The porosity profile of rock sample A03:10C is shown below, it is obvious that the porosity varies strongly within the evaluated cm-deep profile.

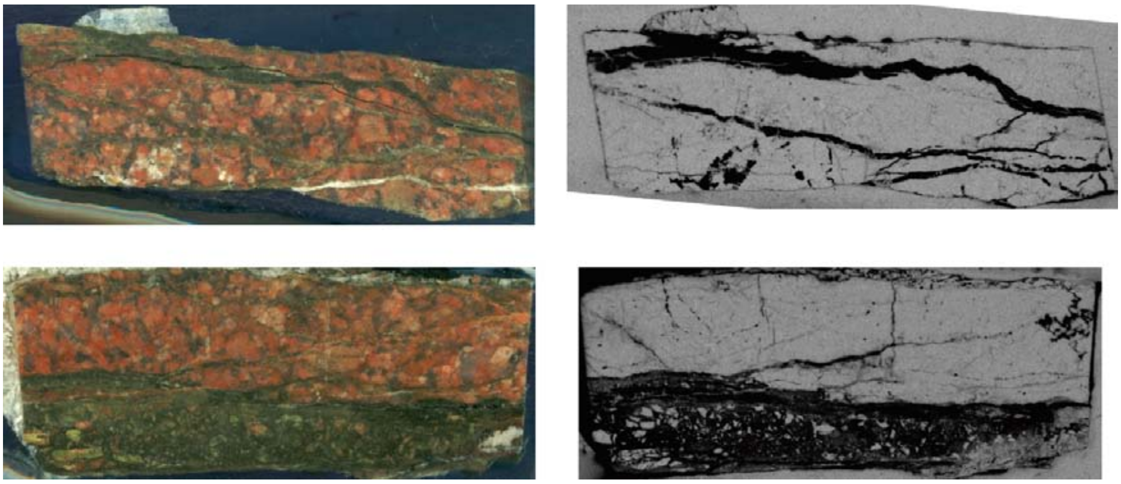

Photo image of; sample A03:10A (upper left) and corresponding autoradiograph (upper right) with a width of 45 mm; sample A03:10B (lower left) and corresponding autoradiograph (lower right) which has a width of 42 mm.

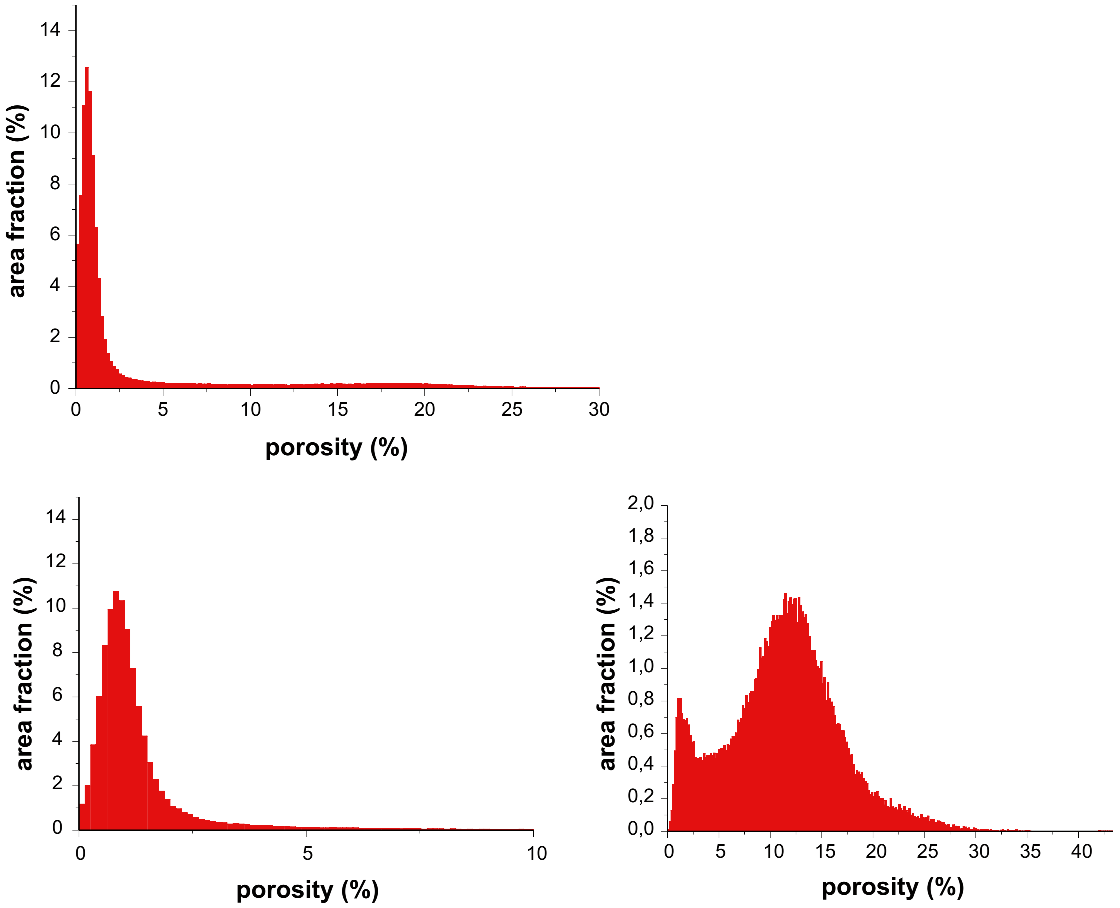

Porosity histograms, measured on the whole sample area, of; sample A03:10A (upper), with a porosity of 3.6%.; sample A03:10B (lower left) of bedrock with a porosity of 1.5% and of alteration rim 11.2%. Note the different scales on the x-axis.

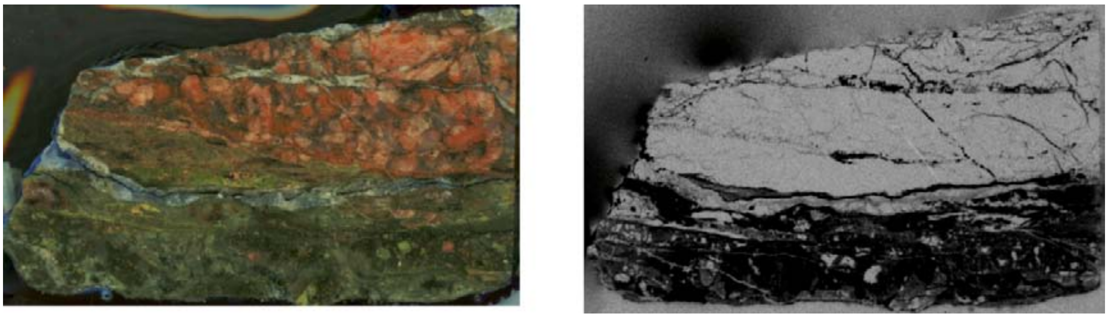

Photo image of sample A03:10C (left) and corresponding autoradiograph (right). The width of sample is 23 mm.

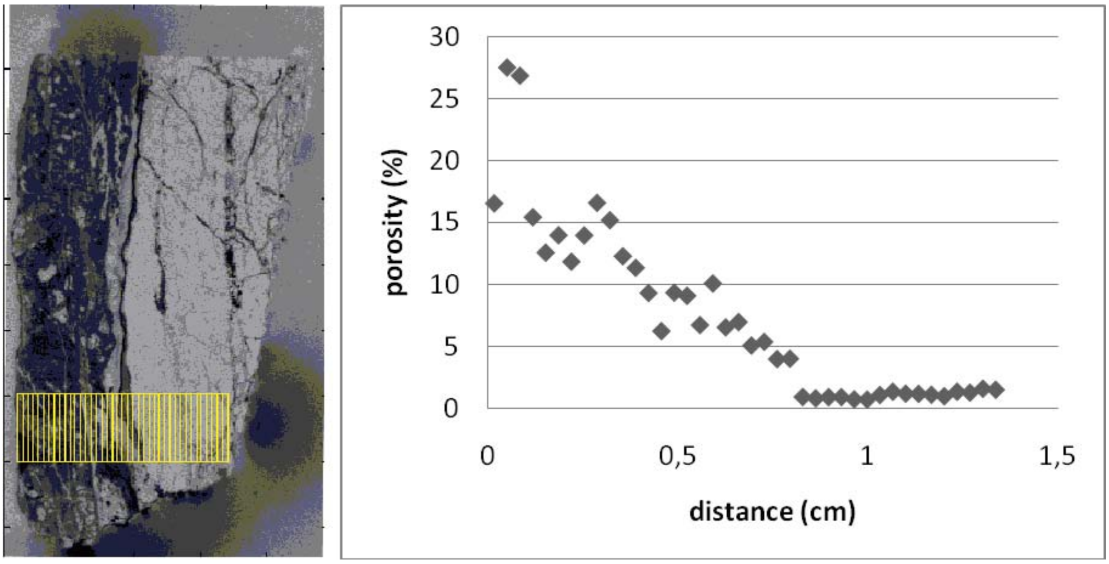

Porosity profile (to the right) and the area (yellow mark) of the measured porosity profile on the rock sample (to the left) A03:10C. The natural fracture surface is at position 0.0 cm.

A03:11 (#10)

The alteration rim is clearly more porous than the unaltered rock matrix in this sample as well. The porosity in the thin bedrock material between the interface of altered rim (fracture minerals with rock fragments) and calcite fracture coating (white colour in the photo image) is low. The porosity of the calcite coating is 1.7% and the porosity of the altered rim is 11%. The large difference in porosity is clearly shown in the profile. It is notable that the right part of the rim is low-porous.

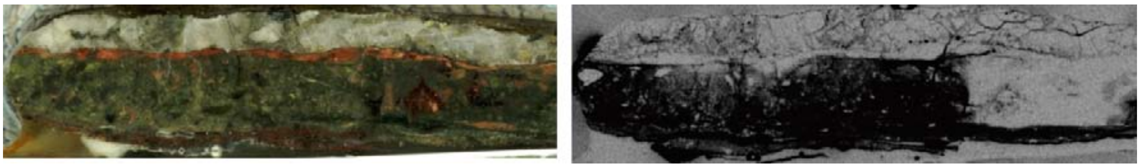

Photo image of sample A03:11 (left) and corresponding autoradiograph (right). The width of the sample is 23 mm.

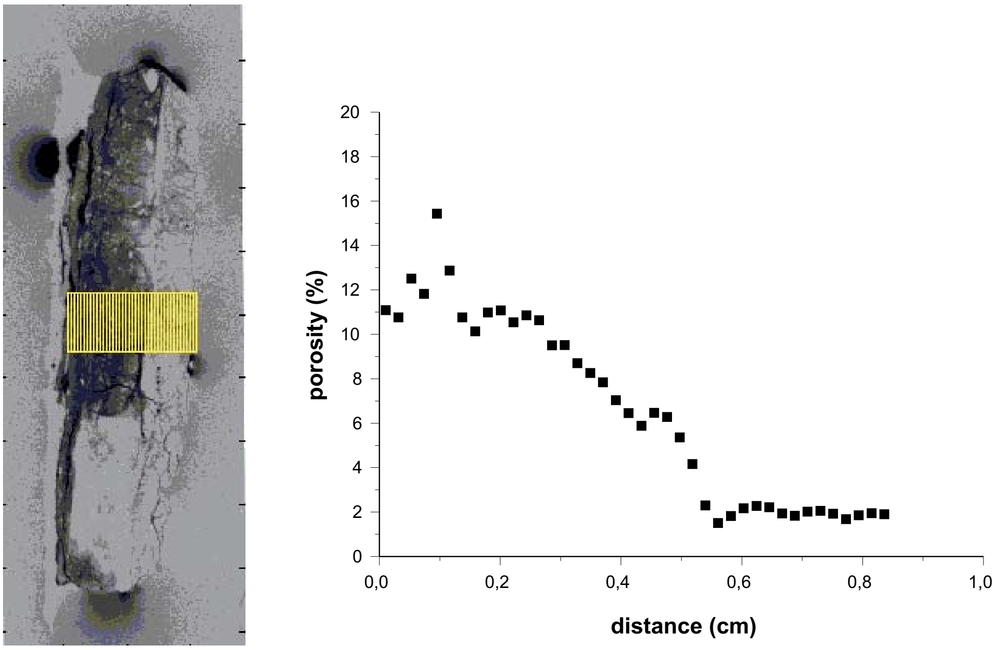

Porosity profile of the marked area on rock sample A03:11. Both sides of the sample had been in contact with open fractures. The 0.0 cm position represents the yellow surface section to the left in the figure. The sample was in contact with open fractures on both sides (left and right) at position 0.0 and ~0.85 cm respectively.

A19

This core sample is taken close to the stub surface of KA3065A03, but outside of the instrumented area. The core was split in to pieces, A19A contains the fracture surface and the first 9 cm:s of the core and A19B constitutes the 9 to 18 cm part of the core. The autoradiograph reveals grain boundary pores. The porosity close to the fracture surface (see an arrow in the figure below) seems to be even less than deeper in the matrix where a few micro fractures cutting the whole sample core are found. Likewise in sample A03:7 and A03:8 the dark minerals show higher porosities than found in other minerals. The porosity of the A19 A sample is 0.22% and 0.18% of the A19B sample.

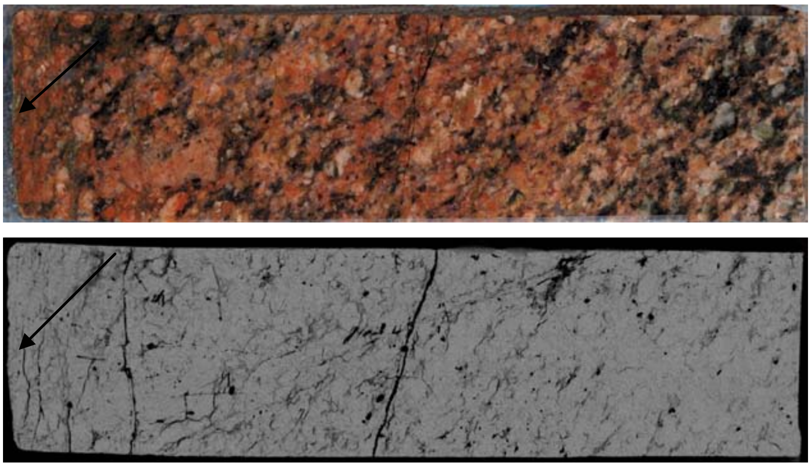

Photo image of sample SKB A19 A (upper) and corresponding autoradiograph (lower). The horizontal width of the sample, with fracture surface to the left, is 9 cm. A porosity of 0.22% is detected.

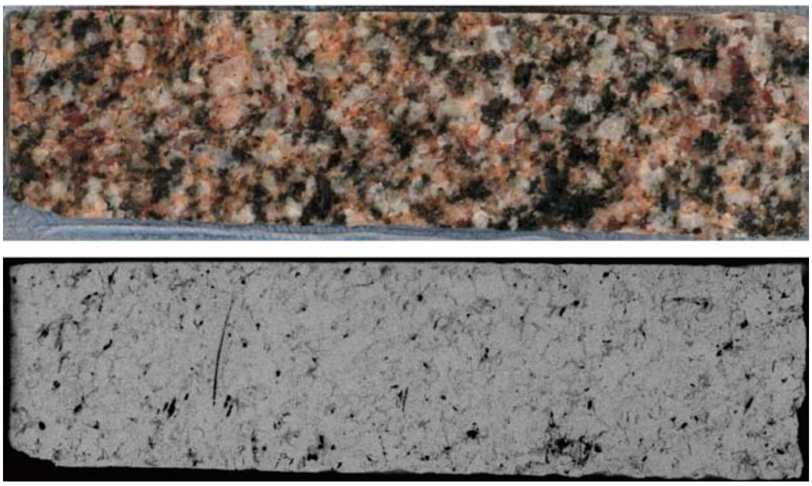

Photo image of sample SKB A19B (top) and corresponding autoradiograph (bottom). The width of the sample is 9 cm and a porosity of 0.18% is detected.

Appendix 4

Through-diffusion results

The complete version of Table 4-2, i.e. Table A4-1, is presented on this page and is followed by the concentration-time curves.

Table A4-1. Complete results from the through-diffusion and electrical resistivity experiments of the LTDE-SD samples. The errors given represent individual uncertainty (2 σ) in the estimation procedure for each through-diffusion sample. The Forsmark and Laxemar Site Investigations samples results are included for comparison.

Sample	**Thickness** (mm)	**Exp. time** H^3HO/ Cl-36 (d)	ε **(vol.%)** (water saturation)	$F_{\mathrm{f,\ electrical\ resistivity}}$ (–)	$F_{\mathrm{f,\ H^3HO}}$ **(–)** (D_e and α fitted)	$D_{\mathrm{e,H^3HO}}$ **(m^2/s)** (D_e and α fitted)	α (–) (D_e and α fitted	$D_{\mathrm{e,H^3H\,O}}$ **(m^2/s)** D_e fitted, $\alpha=\varepsilon$	$D_{\mathrm{e,Cl\text{-}36}}$ **(m^2/s)** (D_e and α fitted)	**Comments**
A02:5	30	–	0.28	$5.7\cdot10^{-5}$	–	–	–	–	–	Repeated measurements gave a variation of about ± 1%
A02:7	30	–	0.23	$3.9\cdot10^{-5}$	–	–	–	–	–	Repeated measurements gave a variation of about ± 1%
A02:4	30	388/–	0.23	–	$(3.1 \pm 0.2)\cdot10^{-5}$	$(6.5 \pm 0.4)\cdot10^{-14}$	$(2.9 \pm 0.7)\cdot10^{-3}$	$6.1\cdot10^{-14}$	Not used	
A02:8	30	388/–	0.17	–	$(1.4 \pm 0.1)\cdot10^{-5}$	$(3.0 \pm 0.2)\cdot10^{-14}$	$(2.1 \pm 0.4)\cdot10^{-3}$	$2.7\cdot10^{-14}$	Not used	
A03:3	70	334/513	0.33	–	No break-through	No break-through	No break-through	No break-through	No break-through	No verified breakthrough observed during exp.time.
A03:4	30	–	0.16	–	–	–	–	–	–	Disrupted due to mechanical failure.
A03:5	30	388/513	0.19	–	$(2.1 \pm 0.1)\cdot10^{-5}$	$(4.5 \pm 0.1)\cdot10^{-14}$	Not evaluated	$5.2\cdot10^{-14}$	$(5 \pm 2)\cdot10^{-14}$	α could not be evaluated due to disturbance of initial contamination. Cl-36 detected after 316 days, evaluated on 4 data points.
A03:6	30	388/513	0.27	–	$(2.0 \pm 0.2)\cdot10^{-5}$	$(4.3 \pm 0.4)\cdot10^{-14}$	Not evaluated	$5.8\cdot10^{-14}$	Not detected	α could not be evaluated due to disturbance of initial contamination. Cl-36 was not detected within 513 days. Note that detection limits are different between H^3HO and Cl-36.
KFM02A 276.06	30		18.4		$1.6\cdot10^{-2}$	$3.4\cdot10^{-11}$	$1.0\cdot10^{-1}$			
KFM03A 242,43	30		0.19		$8.2\cdot10^{-5}$	$1.8\cdot10^{-13}$	$4.3\cdot10^{-3}$			
KFM07A 608,75	30		0.29		$6.7\cdot10^{-4}$	$1.4\cdot10^{-12}$	$4.7\cdot10^{-3}$			
KFM09A 713,67	30		0.24		$(1.2\cdot10^{-4})$*	$(2.5\cdot10^{-13})$*	–*			
KSH01 891,91	30		0.46		$5.2\cdot10^{-4}$	$1.1\cdot10^{-12}$	$1.2\cdot10^{-2}$			
KSH01 981,43	30		0.29		$2.2\cdot10^{-4}$	$4.8\cdot10^{-13}$	$8.8\cdot10^{-3}$			
KLX02 235,08	30		0.39		$3.2\cdot10^{-4}$	$6.8\cdot10^{-13}$	$1.4\cdot10^{-2}$			
KLX04 726,07	30		0.08		$(1.1\cdot10^{-4})$*	$(2.4\cdot10^{-13})$*	–*			
KLX08 417,05	30		0.45		$(4.6\cdot10^{-4})$*	$(9.8\cdot10^{-13})$*	–*			
KLX10 995,79	30		0.06		$(2.2\cdot10^{-4})$*	$(4.8\cdot10^{-13})$*	–*			

*Rock type mean value, the specific sample was not measured.

A02:4, H^3HO:

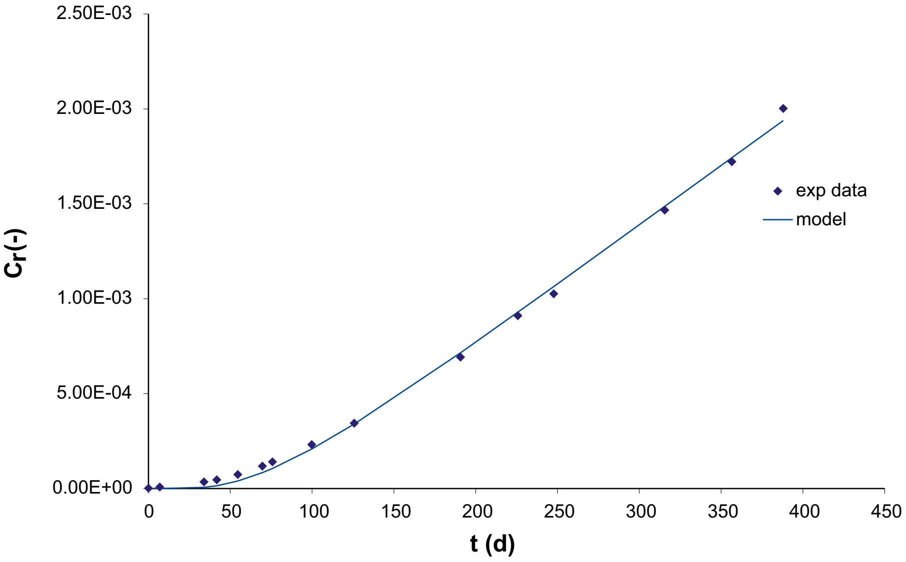

A02:8, H^3HO:

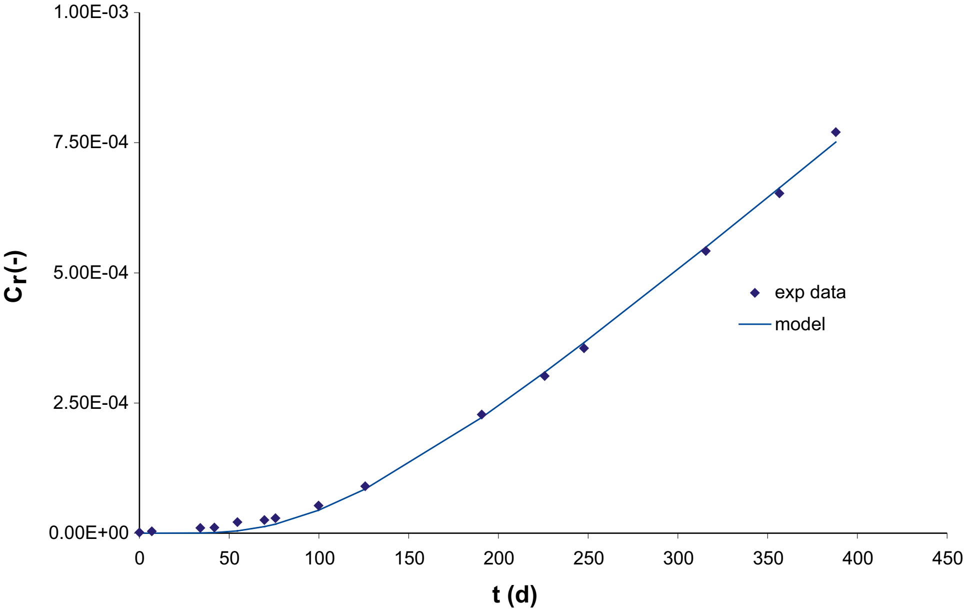

A03:5, H^3HO:

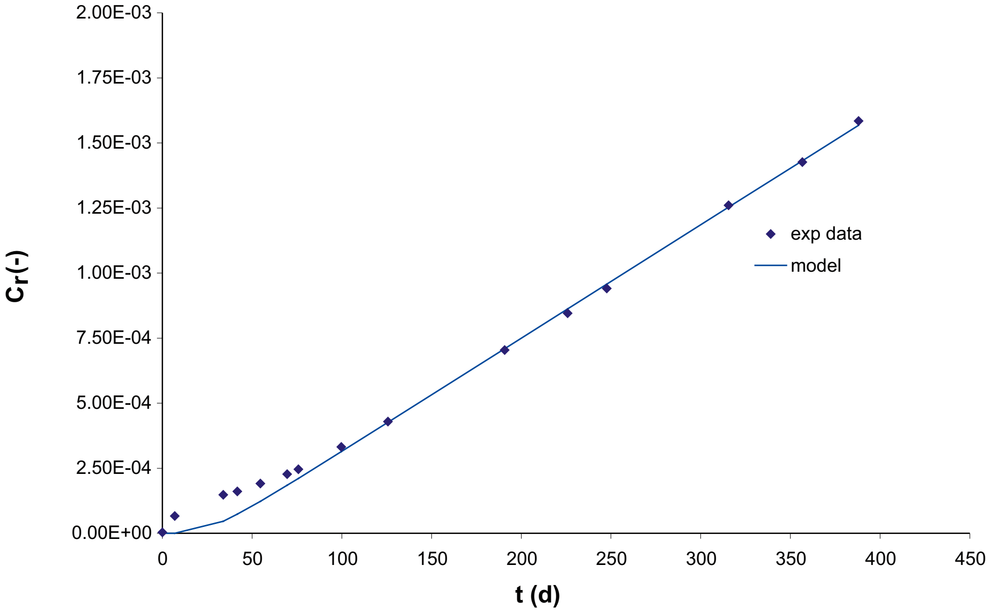

A03:5, Cl-36:

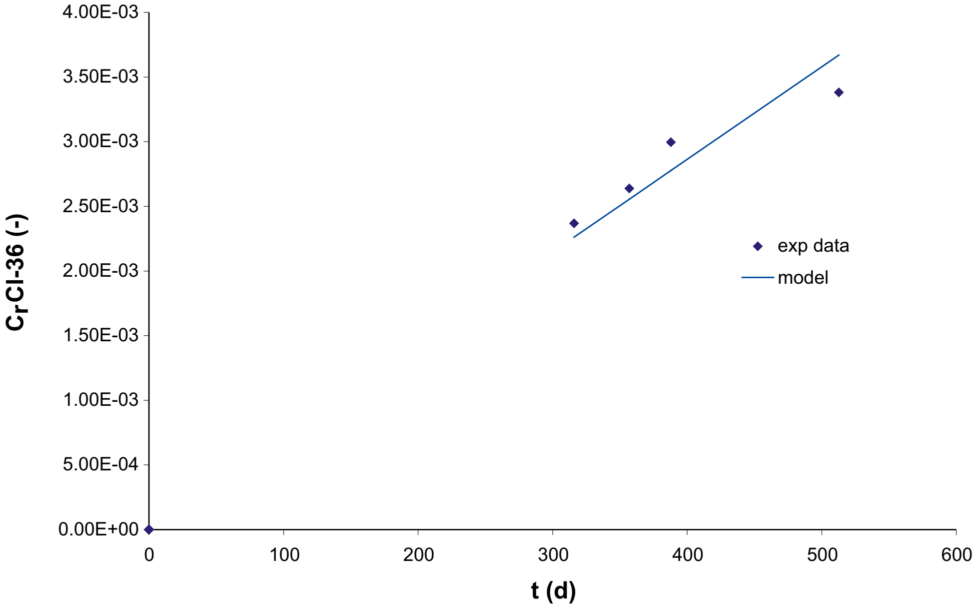

A03:6, H^3HO:

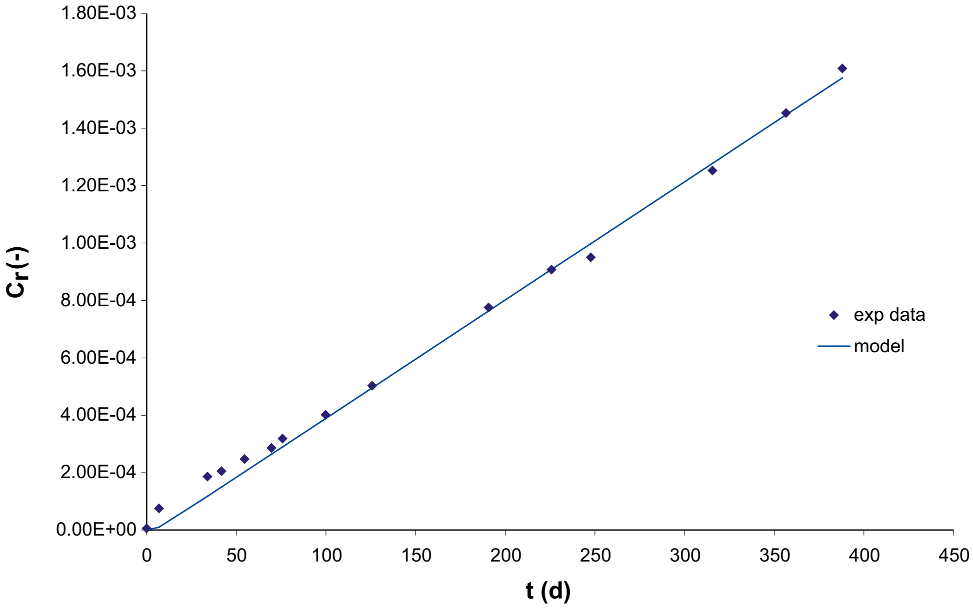
1.80E-03
1.60E-03
1.40E-03
1.20E-03
1.00E-03
8.00E-04
6.00E-04
4.00E-04
2.00E-04
0.00E+00
c_r (-)
0
50
100
150
200
250
300
350
400
450
t (d)
exp data
model

Results from sorption-diffusion on LTDE-SD samples

Note: the sampling times have been slightly adjusted in the presented concentration-time curves in order to increase the readability for individual tracers. The following sampling times were applied:

- A03:3/Diff I: 0.0 (after injection), 1.0, 15.7, 45.9, 92.9 and 183.9 days.
- Samples A03:4/DiffII, A03:5/DiffIII, A03:6/DiffIV, and epoxy resin control disc: 0.0, 0.7, 7.6, 41.8, 102.8 and 194.8 days.

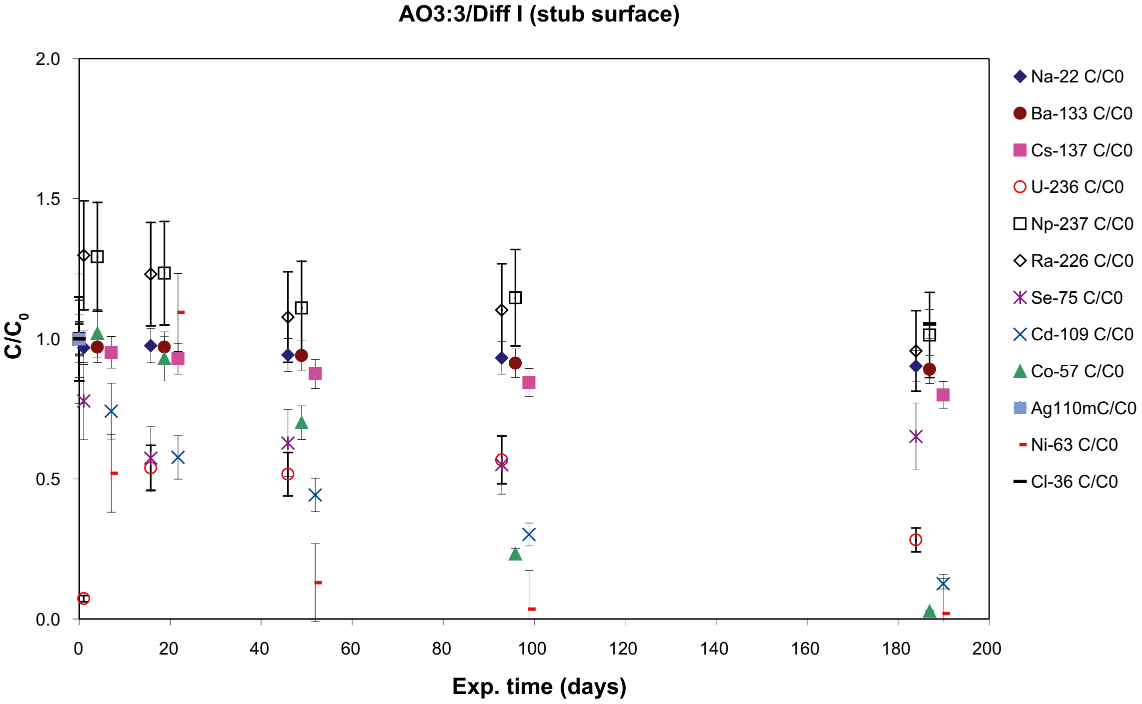

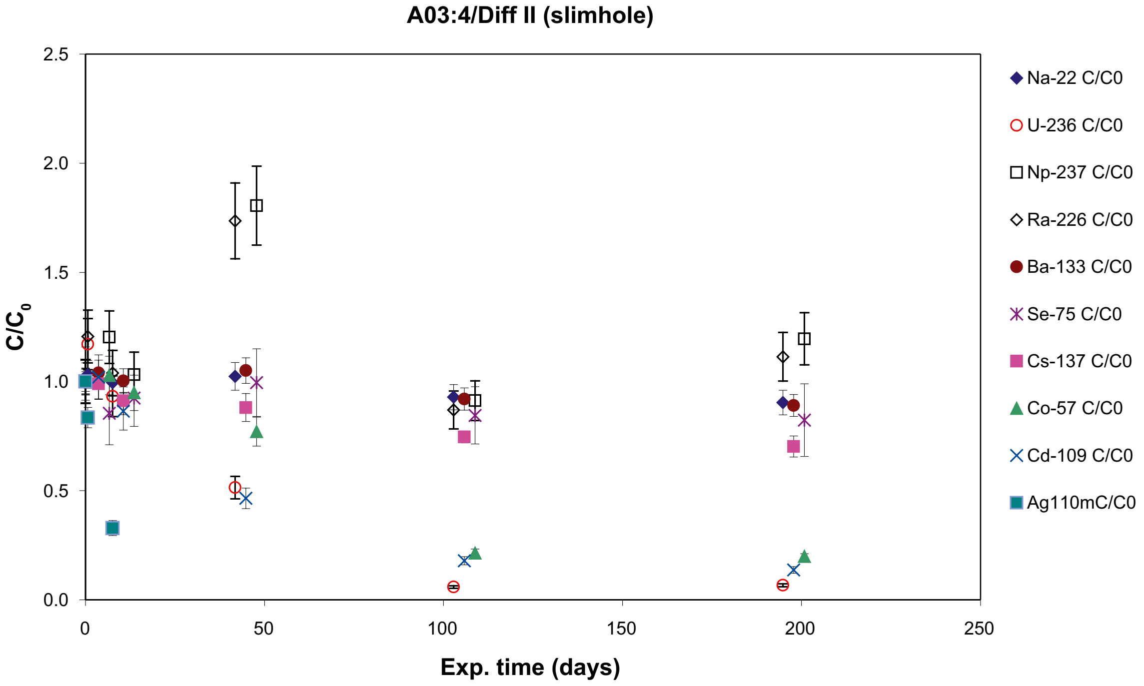
A03:4/Diff II (slimhole)
C/C0
2.5
2.0
1.5
1.0
0.5
0.0
0
50
100
150
200
250
Exp. time (days)
Na-22 C/C0
U-236 C/C0
Np-237 C/C0
Ra-226 C/C0
Ba-133 C/C0
Se-75 C/C0
Cs-137 C/C0
Co-57 C/C0
Cd-109 C/C0
Ag110mC/C0

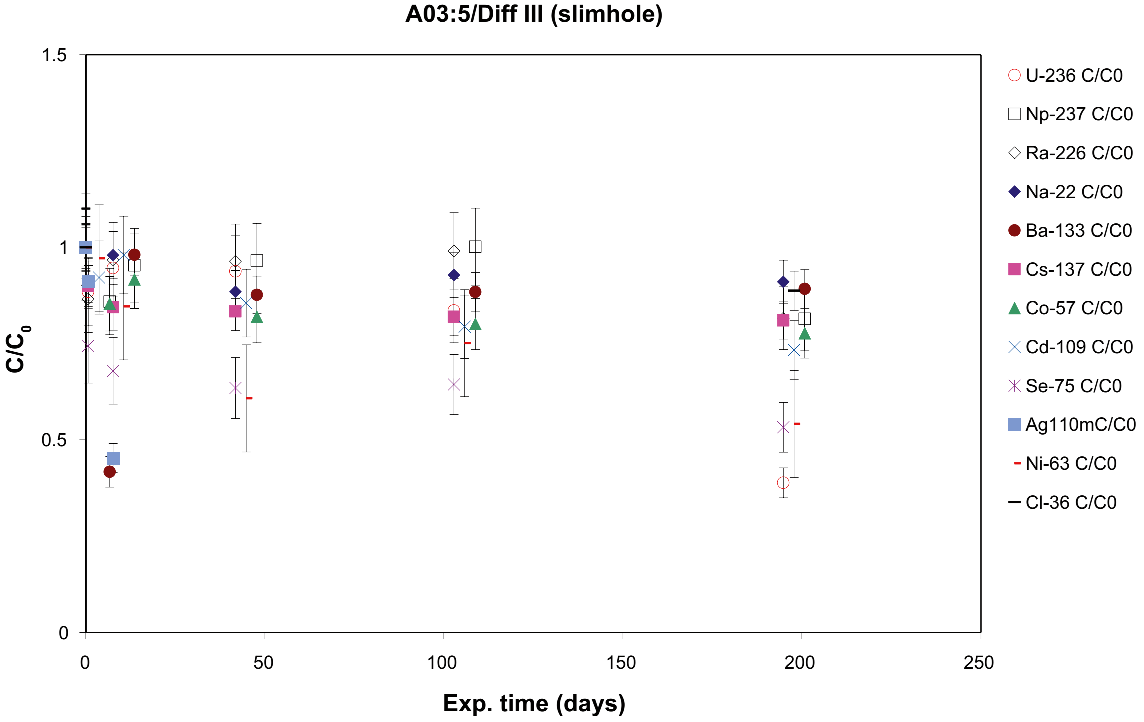
A03:5/Diff III (slimhole)
C/C0
1.5
1
0.5
0
0
50
100
150
200
250
Exp. time (days)
U-236 C/C0
Np-237 C/C0
Ra-226 C/C0
Na-22 C/C0
Ba-133 C/C0
Cs-137 C/C0
Co-57 C/C0
Cd-109 C/C0
Se-75 C/C0
Ag110mC/C0
Ni-63 C/C0
Cl-36 C/C0

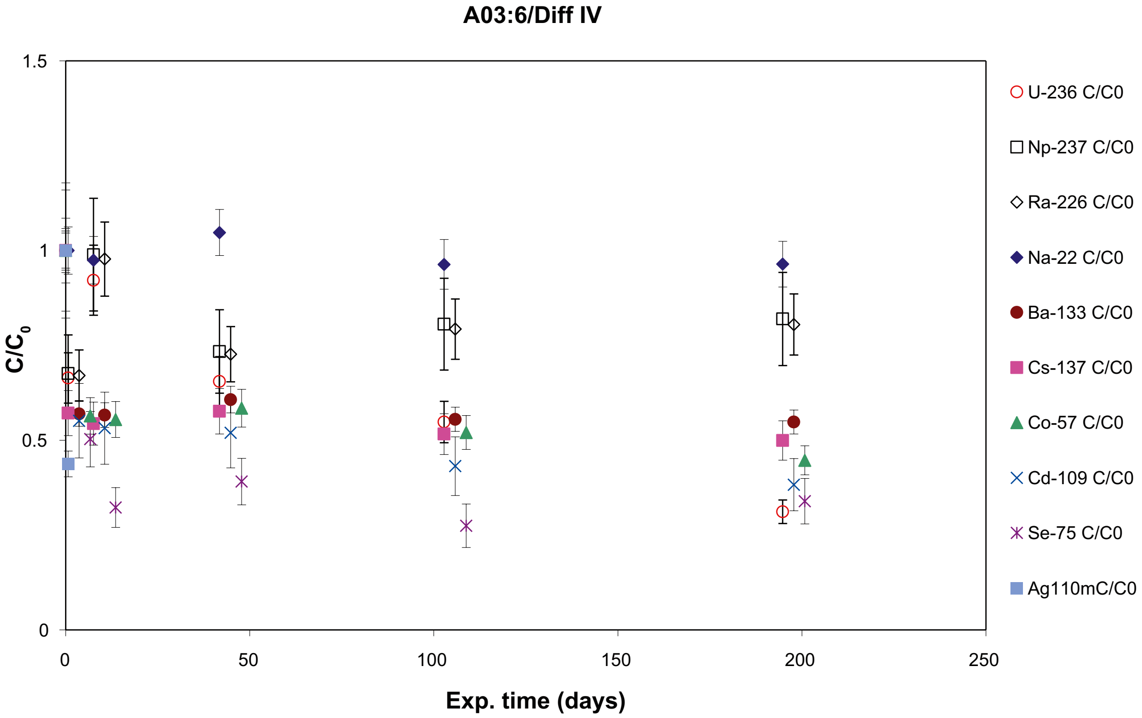
A03:6/Diff IV
1.5
1
0.5
0
C/C0
0
50
100
150
200
250
Exp. time (days)
U-236 C/C0
Np-237 C/C0
Ra-226 C/C0
Na-22 C/C0
Ba-133 C/C0
Cs-137 C/C0
Co-57 C/C0
Cd-109 C/C0
Se-75 C/C0
Ag110mC/C0

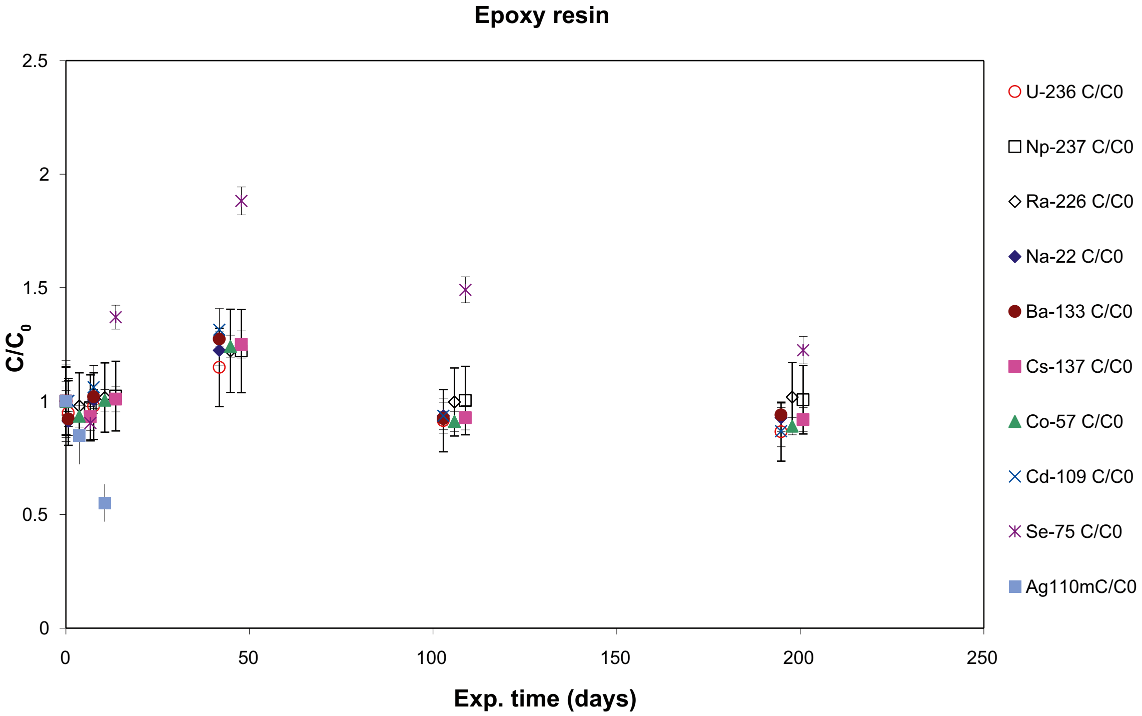
Epoxy resin
2.5
2
1.5
1
0.5
0
C/C0
0
50
100
150
200
250
Exp. time (days)
U-236 C/C0
Np-237 C/C0
Ra-226 C/C0
Na-22 C/C0
Ba-133 C/C0
Cs-137 C/C0
Co-57 C/C0
Cd-109 C/C0
Se-75 C/C0
Ag110mC/C0

Appendix 6

Results from sorption-diffusion on Laxemar and Forsmark samples

Note 1: the sampling times have been slightly adjusted in the presented concentration-time curves in order to increase the readability for individual tracers. The following sampling times were applied for all samples:

- 0 (after injection), 0.9, 12.2, 32.9, 100.9 and 186.9 days.

Note 2: ^{153}Gd was completely sorbed in all samples. ^{175}Hf was completely sorbed in samples for which Hf is not included in the figure.

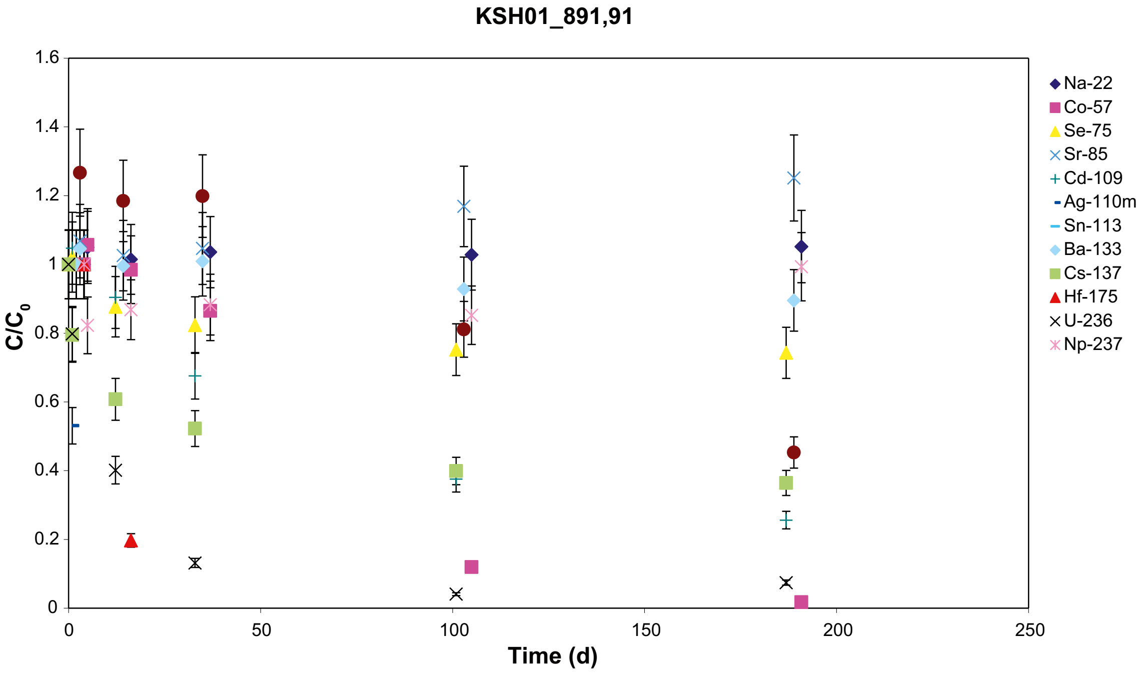

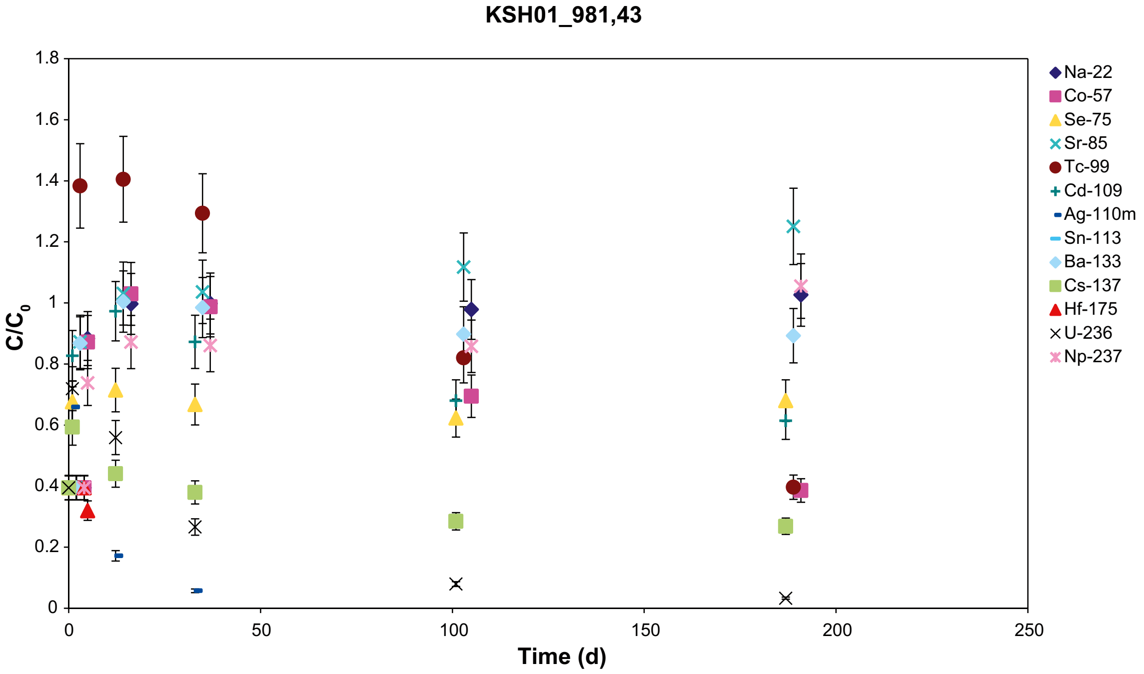
KSH01_981,43
C/C0
1.8
1.6
1.4
1.2
1
0.8
0.6
0.4
0.2
0
0
50
100
150
200
250
Time (d)
Na-22
Co-57
Se-75
Sr-85
Tc-99
Cd-109
Ag-110m
Sn-113
Ba-133
Cs-137
Hf-175
U-236
Np-237

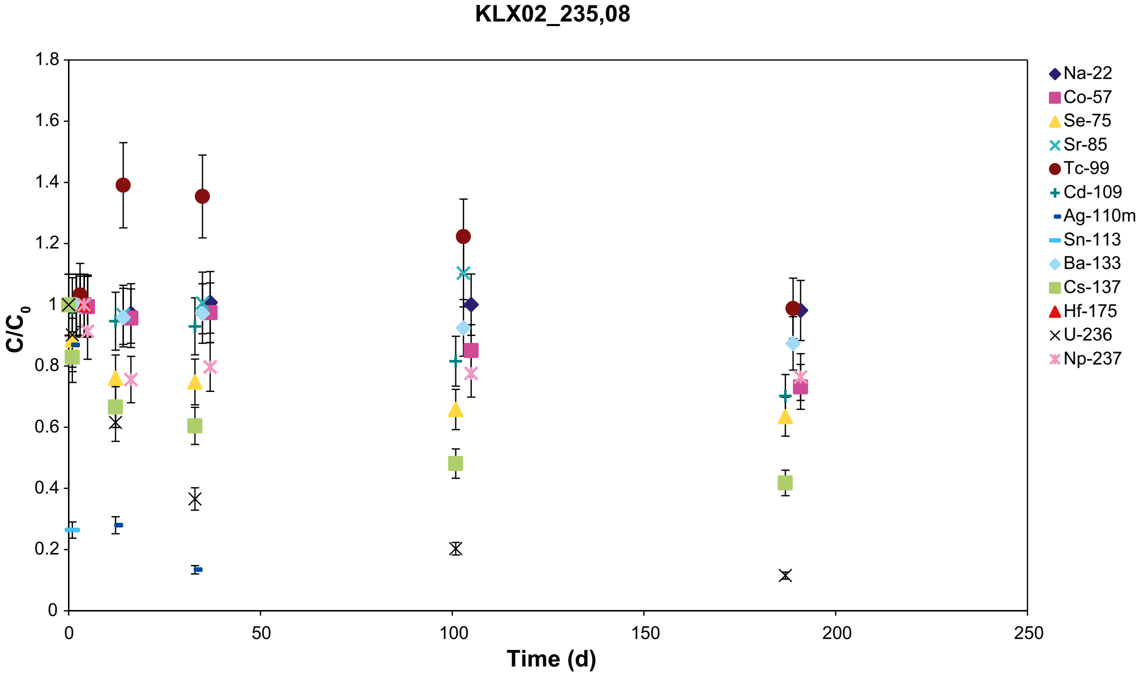
KLX02_235,08
C/C0
1.8
1.6
1.4
1.2
1
0.8
0.6
0.4
0.2
0
0
50
100
150
200
250
Time (d)
Na-22
Co-57
Se-75
Sr-85
Tc-99
Cd-109
Ag-110m
Sn-113
Ba-133
Cs-137
Hf-175
U-236
Np-237

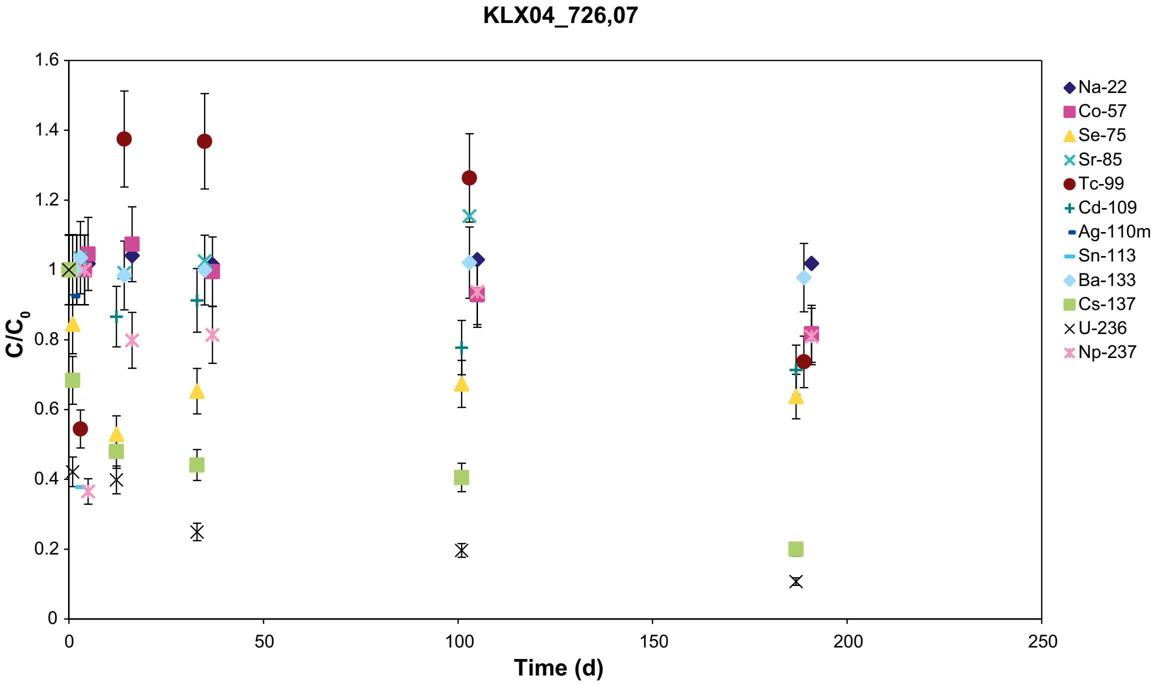
KLX04_726,07
C/C$_0$
1.6
1.4
1.2
1
0.8
0.6
0.4
0.2
0
0
50
100
150
200
250
Time (d)
Na-22
Co-57
Se-75
Sr-85
Tc-99
Cd-109
Ag-110m
Sn-113
Ba-133
Cs-137
U-236
Np-237

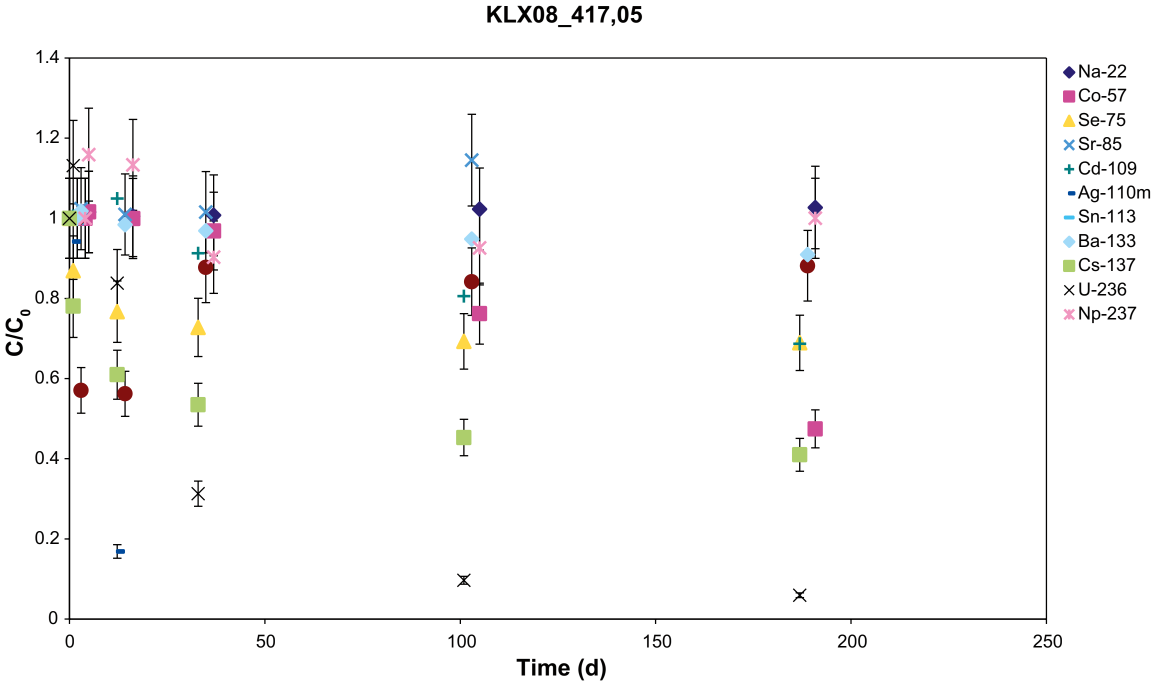
KLX08_417,05
C/C$_0$
1.4
1.2
1
0.8
0.6
0.4
0.2
0
0
50
100
150
200
250
Time (d)
Na-22
Co-57
Se-75
Sr-85
Cd-109
Ag-110m
Sn-113
Ba-133
Cs-137
U-236
Np-237

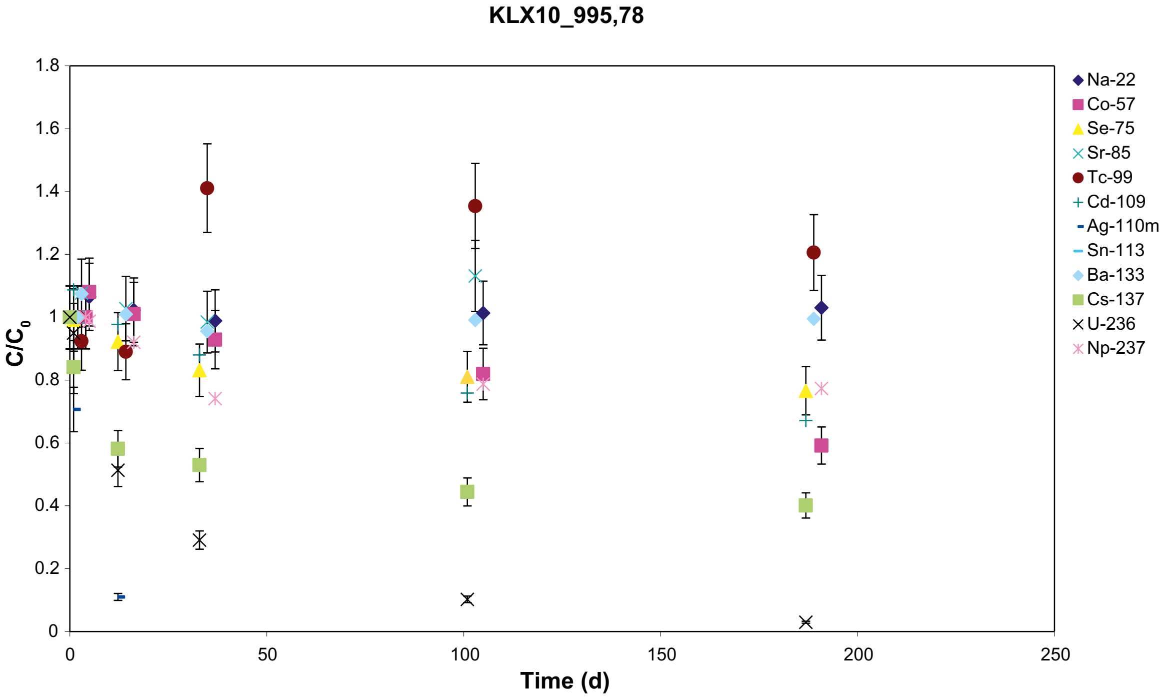
KLX10_995,78
C/C0
Time (d)
0
0.2
0.4
0.6
0.8
1
1.2
1.4
1.6
1.8
0
50
100
150
200
250
Na-22
Co-57
Se-75
Sr-85
Tc-99
Cd-109
Ag-110m
Sn-113
Ba-133
Cs-137
U-236
Np-237

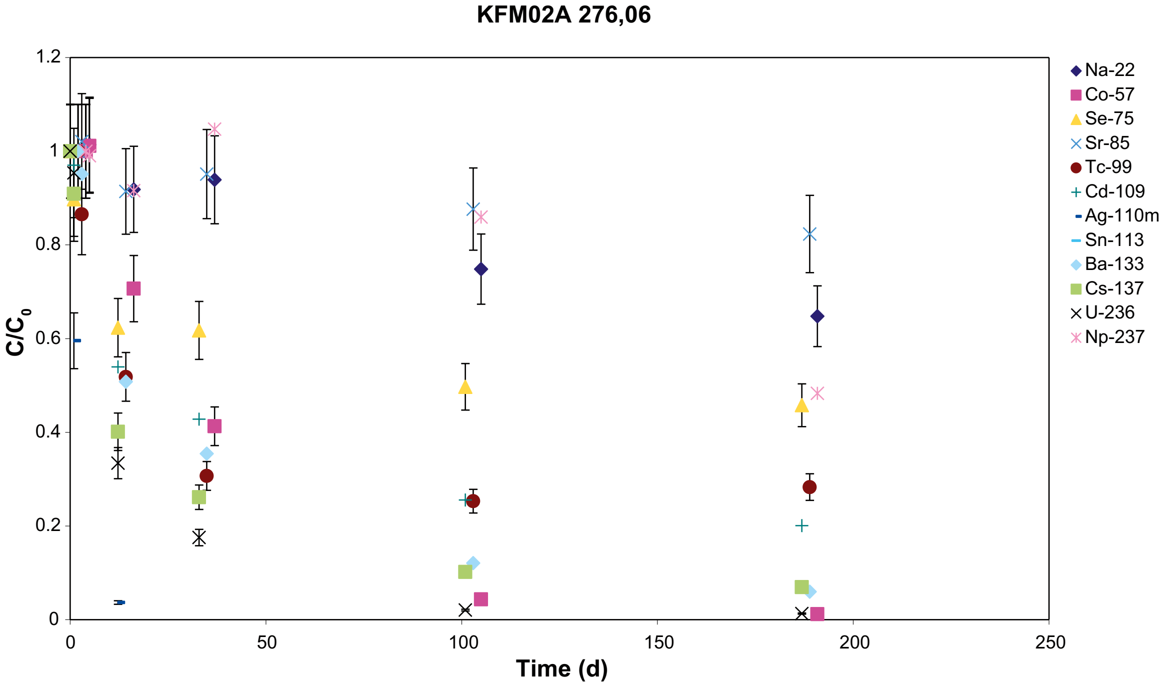
KFM02A 276,06
C/C0
Time (d)
0
0.2
0.4
0.6
0.8
1
1.2
0
50
100
150
200
250
Na-22
Co-57
Se-75
Sr-85
Tc-99
Cd-109
Ag-110m
Sn-113
Ba-133
Cs-137
U-236
Np-237

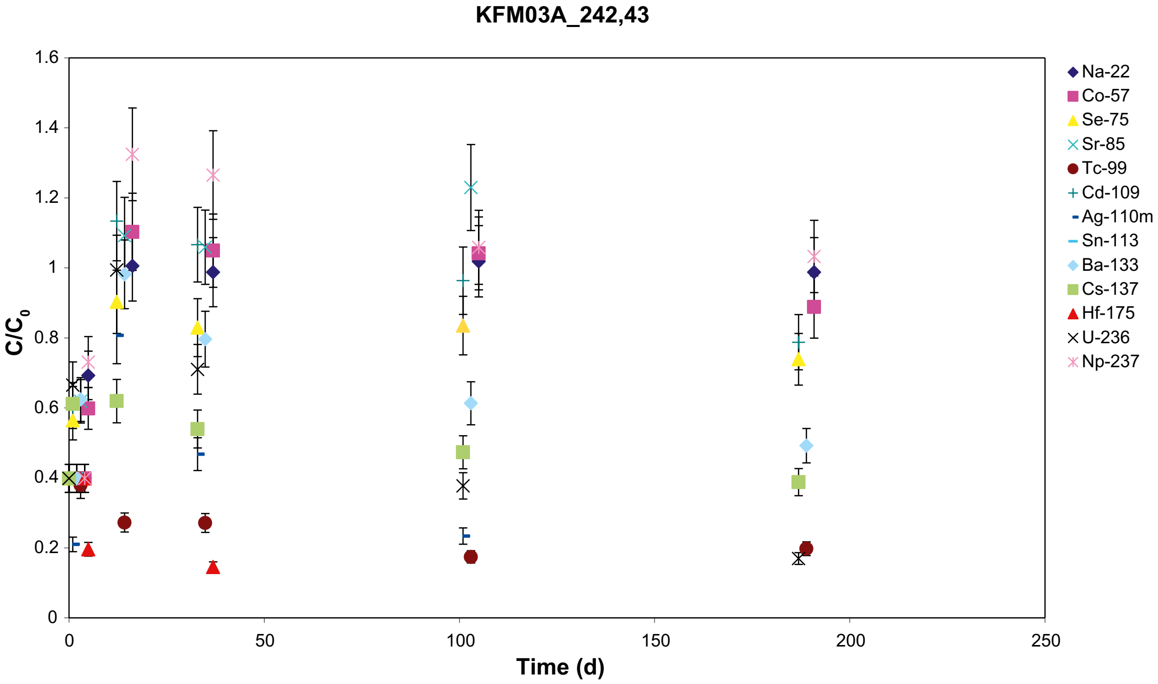
KFM03A_242,43
C/C0
Time (d)
0
0.2
0.4
0.6
0.8
1
1.2
1.4
1.6
0
50
100
150
200
250
Na-22
Co-57
Se-75
Sr-85
Tc-99
Cd-109
Ag-110m
Sn-113
Ba-133
Cs-137
Hf-175
U-236
Np-237

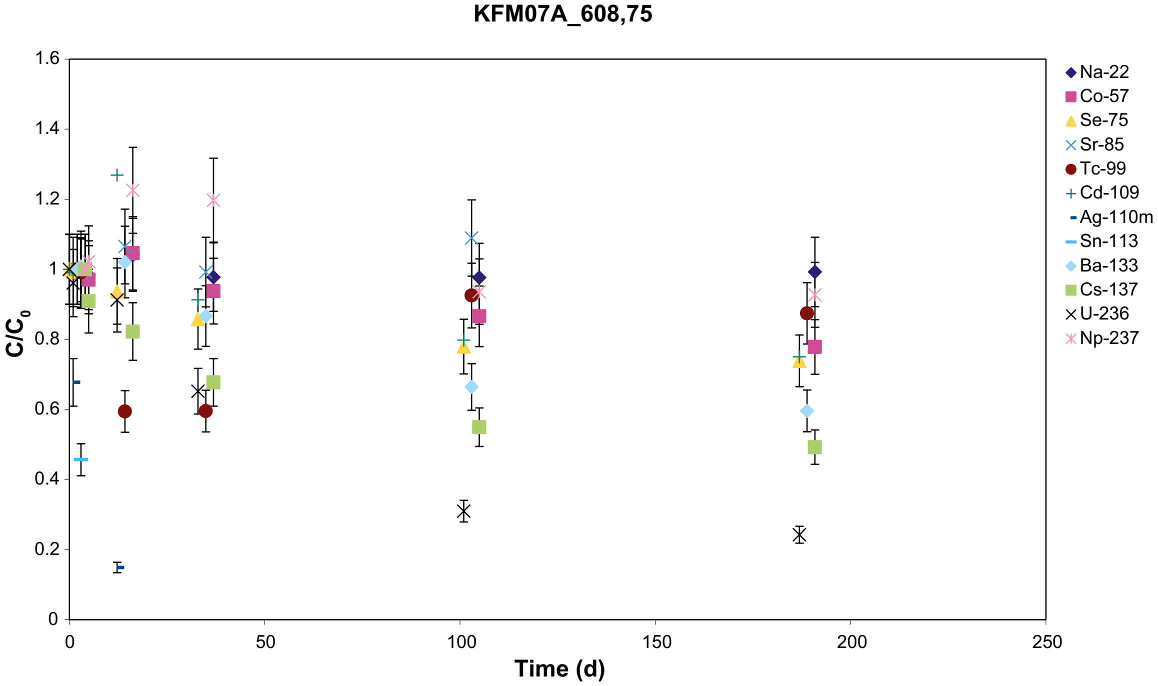
KFM07A_608,75
C/C0
Time (d)
0
0.2
0.4
0.6
0.8
1
1.2
1.4
1.6
0
50
100
150
200
250
Na-22
Co-57
Se-75
Sr-85
Tc-99
Cd-109
Ag-110m
Sn-113
Ba-133
Cs-137
U-236
Np-237

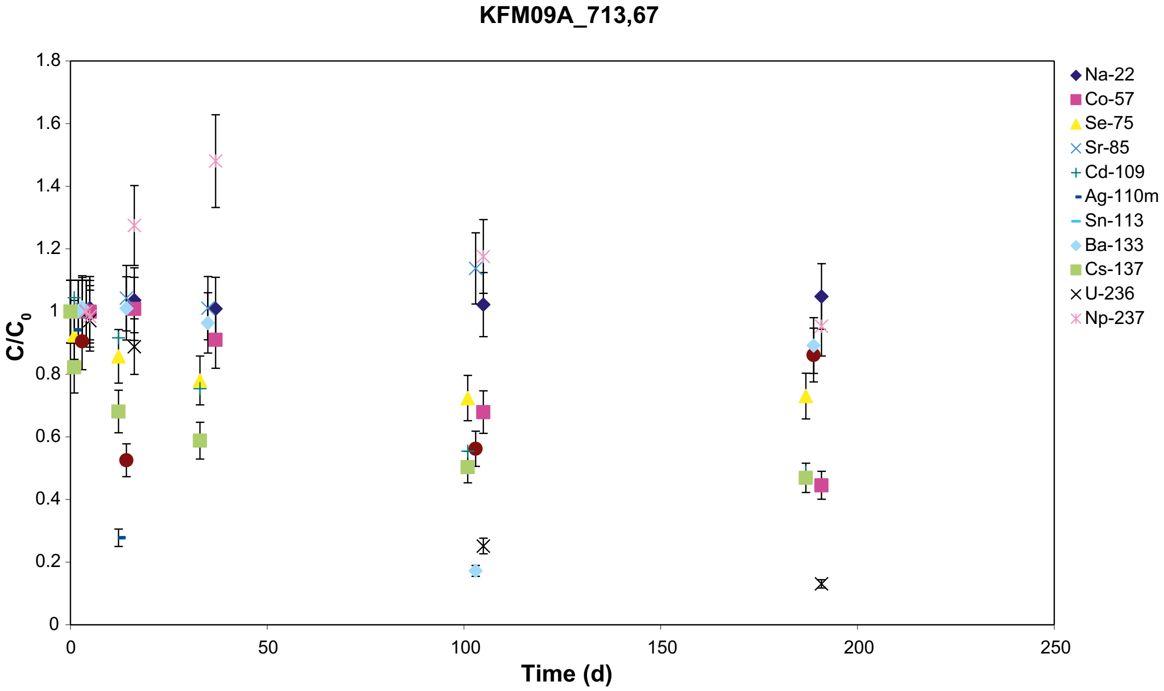
KFM09A_713,67
C/C$_0$
1.8
1.6
1.4
1.2
1
0.8
0.6
0.4
0.2
0
0
50
100
150
200
250
Time (d)
Na-22
Co-57
Se-75
Sr-85
Cd-109
Ag-110m
Sn-113
Ba-133
Cs-137
U-236
Np-237

Appendix 7

Predictions of loss of tracer in the aqueous phase for LTDE-SD sorption-diffusion intact rock samples

The calculation methodology is defined in Section 3.4.1. The fixed ε and D_e values are from water saturation and through-diffusion measurements of the respective sample and the fixed K_d applied are from batch sorption data of the most representative 1–2 mm fraction at 186 days. The data selection is presented in Table 4-3. The penetration profiles are the calculated for each aqueous phase concentration calculation.

Predictions of Cs-137 in A03:3/Diff I:

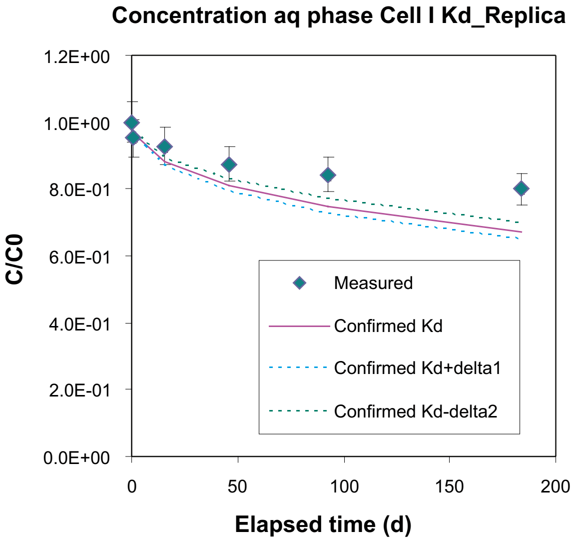

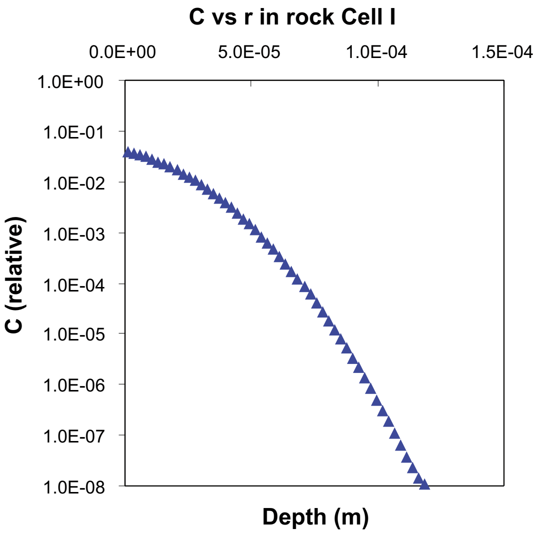

Predictions of Cs-137 in A03:4/Diff II:

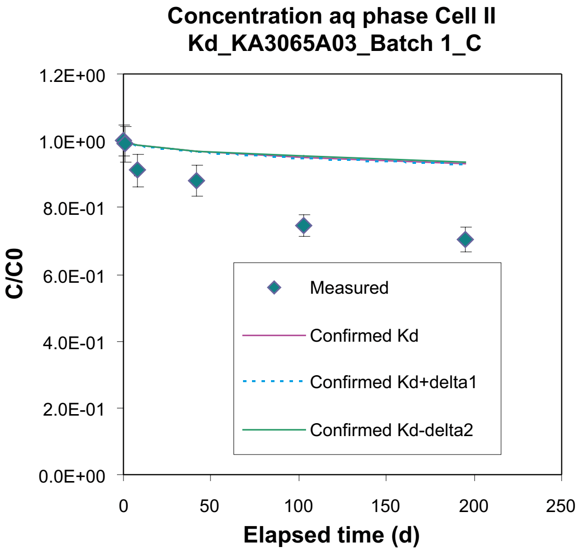

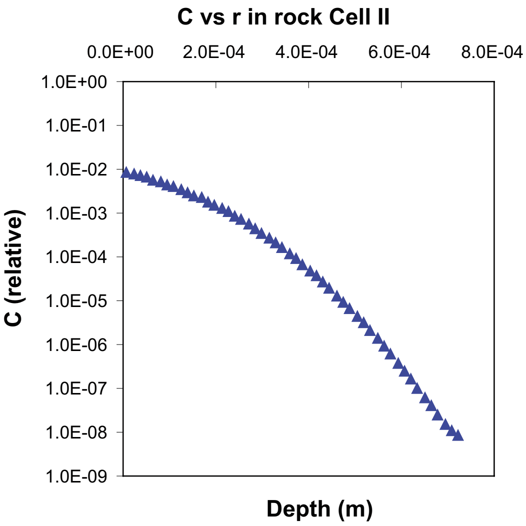

Predictions of Cs-137 in A03:5/Diff III:

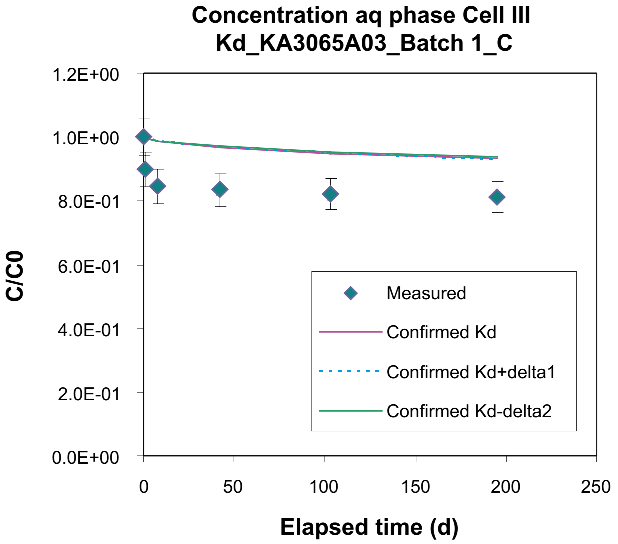

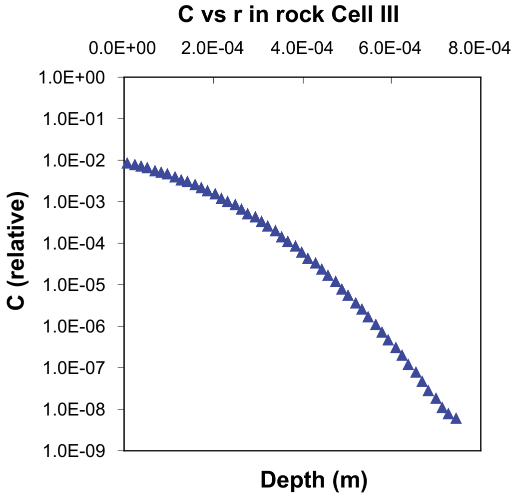

Predictions of Cs-137 in A03:6/Diff IV:

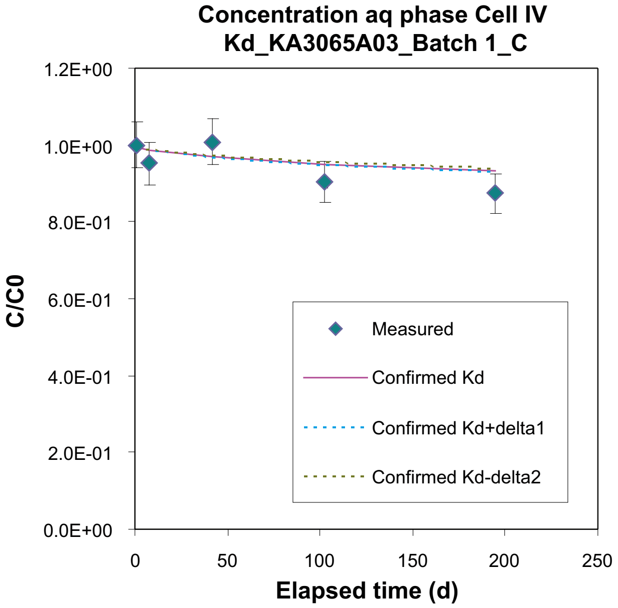

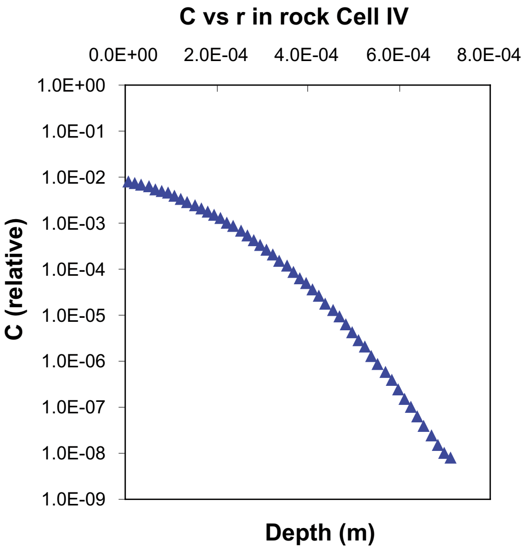

Predictions of Ni-63 in A03:3/Diff I:

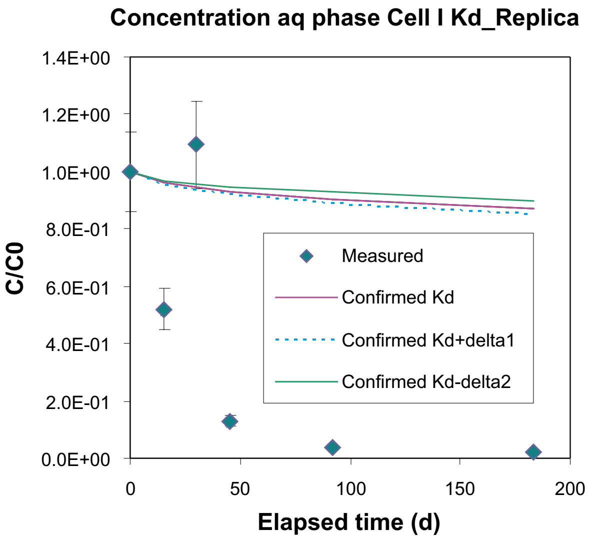

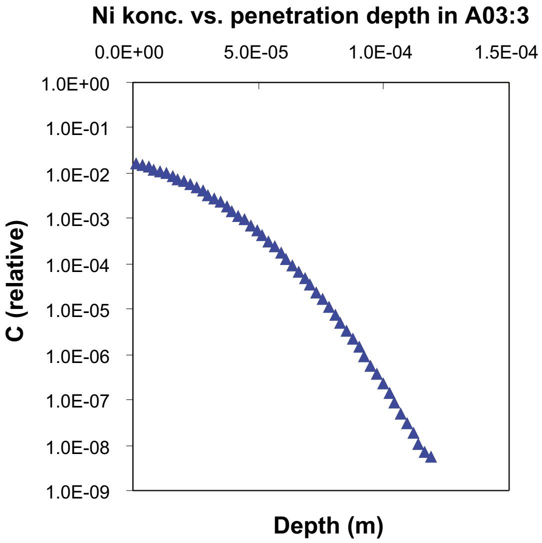

Predictions of Ni-63 in A03:5/Diff III:

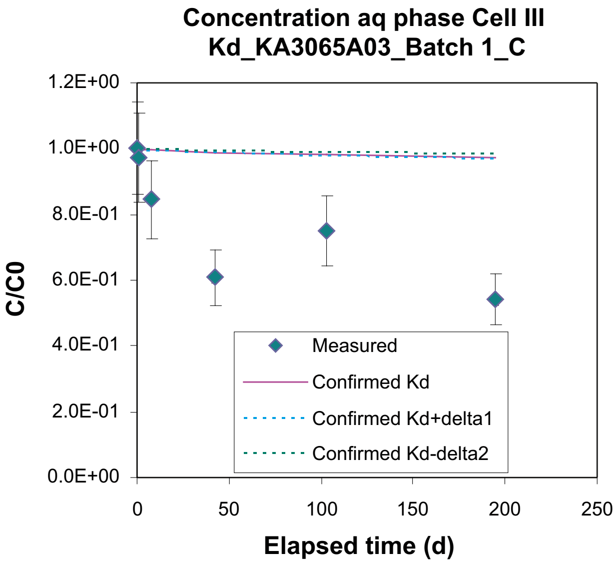

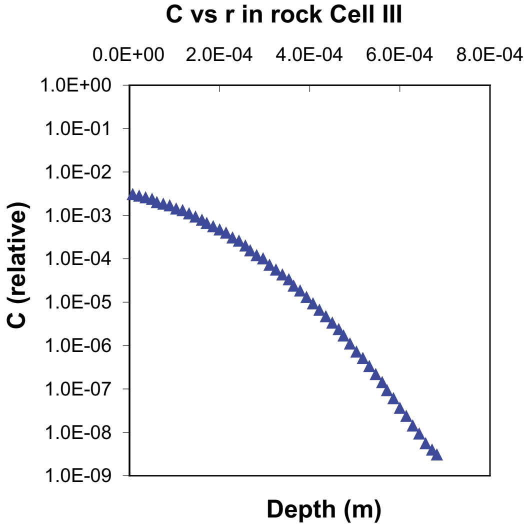

Predictions of Ni-63 in A03:6/Diff IV:

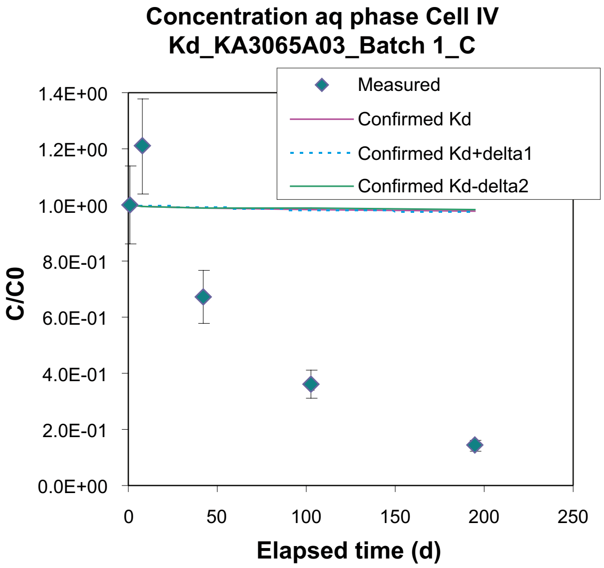

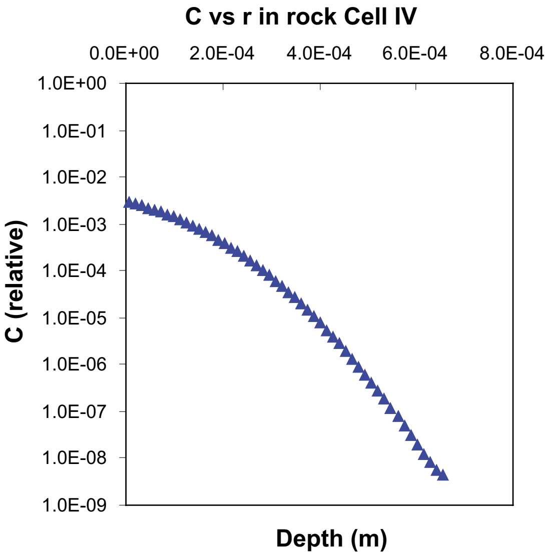

Appendix 8

Predictions of loss of tracer in the aqueous phase for Forsmark and Laxemar sorption-diffusion intact rock samples

The calculation methodology is defined in Section 3.4.1. K_d, ε and F_f were fixed in all predictions. The different cases numbered with #1–#6 that were calculated are presented in Table 4-6 and the additional sample specific and rock type specific data in Table 4-8. Either sample specific data or rock type specific data were used:

- **Sample specific**, means that the values of the diffusion parameters (i.e. the formation factor and the porosity) had been determined for the particular drill core sample used in the experiment, i.e. by applying through diffusion experiment and water saturation porosity measurement data as presented in Table 4-2. F_f was calculated from $D_{e(H3HO)}$ using Equation 3-1. With respect to sorption parameters, the term sample specific refers to batch sorption experiments (1–2 mm fraction at 186 days) done using rock material in the absolute vicinity of the sample position of the particular drill core used in the experiment.
- **Rock type mean value**, means that the values used for K_d, F_f and/or ε had been determined in the site investigations as values representative for the entire rock type, i.e. average values for a large number of determinations done on the rock type present in the particular drill core sample.

The data selection used is presented in a Table for each rock sample below.

#1. Predictions for KLX02 235.08 Ävrö granodiorite. Sample specific F_f and ε. K_d from LTDE-SD results (Table 4-11):

Sample specific data

Tracer	K_d (m³/kg)	F_f	ε
Na-22	2.90E-04	3.19E-04	3.90E-03
Co-57	4.96E-02	3.19E-04	3.90E-03
Se-75	1.62E-03	3.19E-04	3.90E-03
Sr-85			
Zr-95			
Tc-99	2.30E-04	3.19E-04	3.90E-03
Cd-109	5.07E-03	3.19E-04	3.90E-03
Ag-110 m			
Sn-113			
Ba-133	2.13E-03	3.19E-04	3.90E-03
Cs-137	2.19E-02	3.19E-04	3.90E-03
Hf-175			
U-236	1.22E-03	3.19E-04	3.90E-03
Np-237	8.27E-04	3.19E-04	3.90E-03

#1. Predictions for KLX02 235.08 Ävrö granodiorite. Sample specific K_d, F_f and ε:

Na-22:

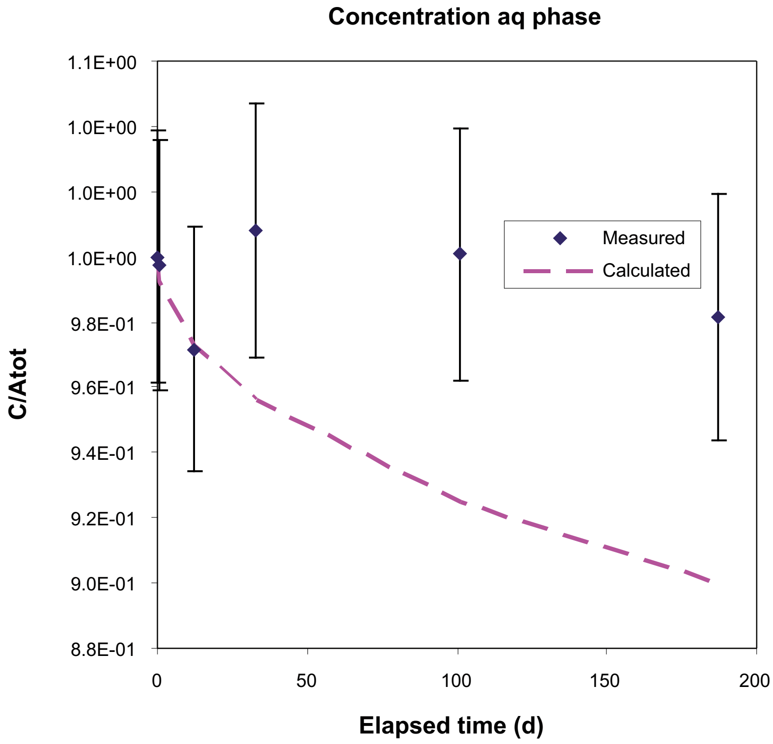

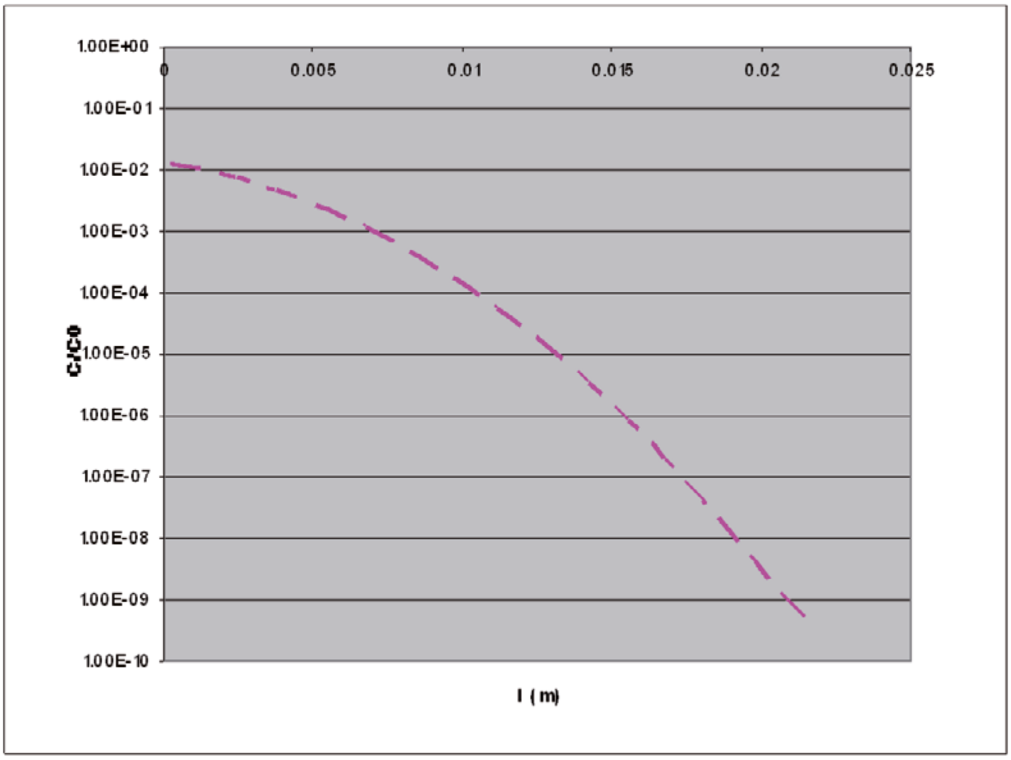

#1. Predictions for KLX02 235.08 Ävrö granodiorite. Sample specific K_d, F_f and ε:

Co-57:

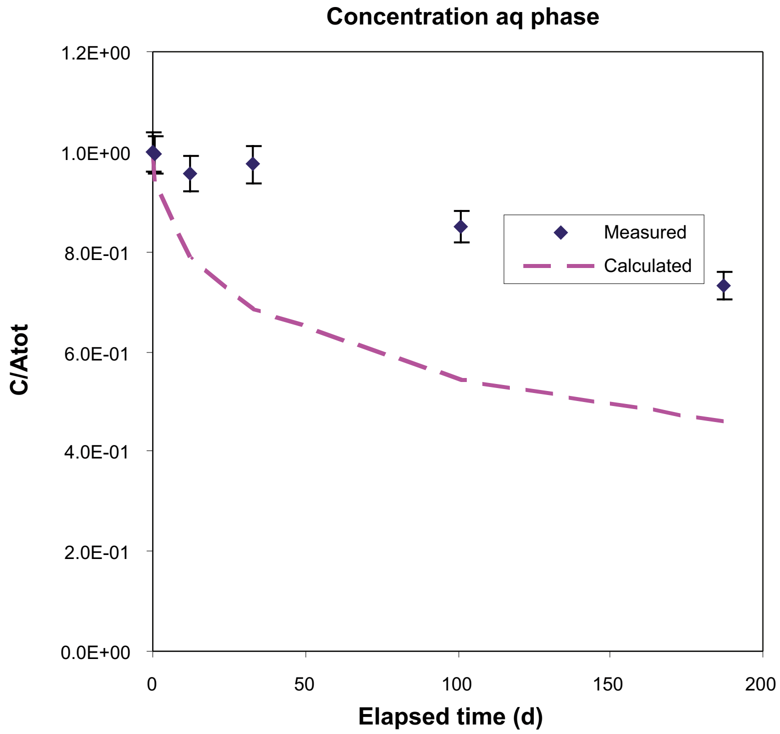

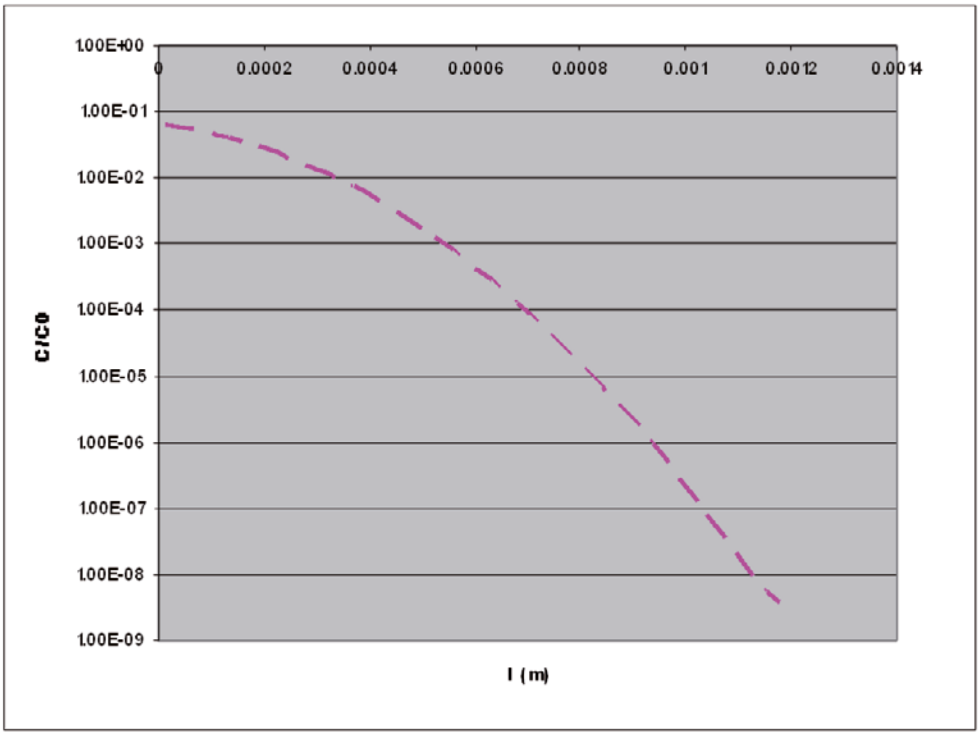

#1. Predictions for KLX02 235.08 Ävrö granodiorite. Sample specific K_d, F_f and ε:

Se-75:

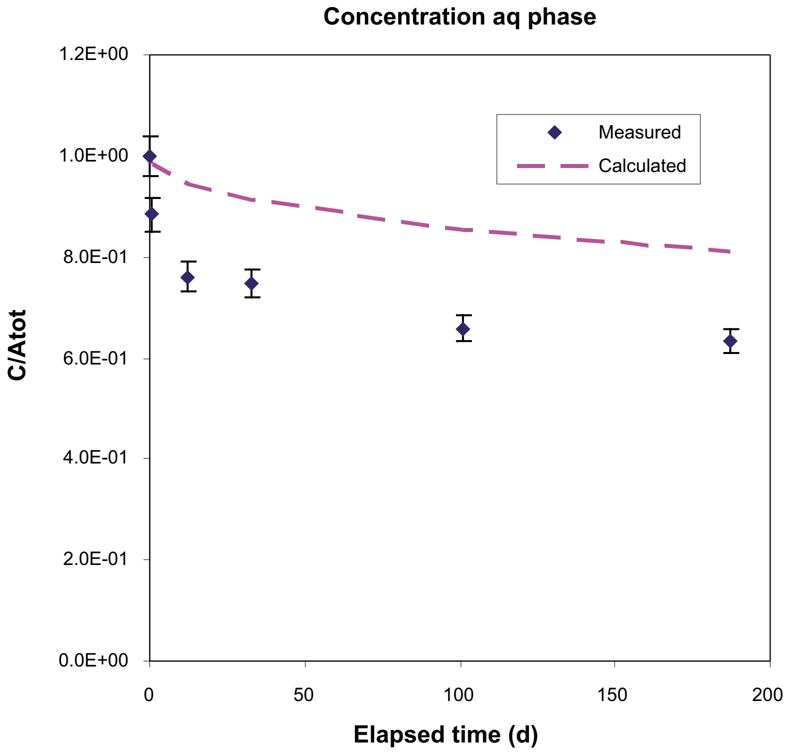

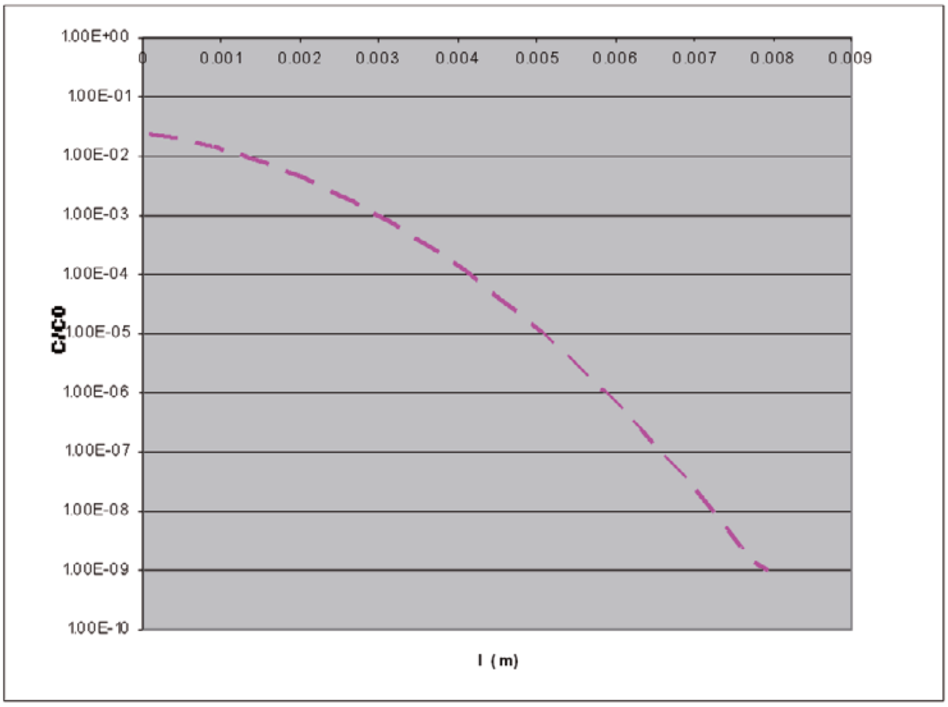

#1. Predictions for KLX02 235.08 Ävrö granodiorite. Sample specific K_d, F_f and ε:

Tc-99:

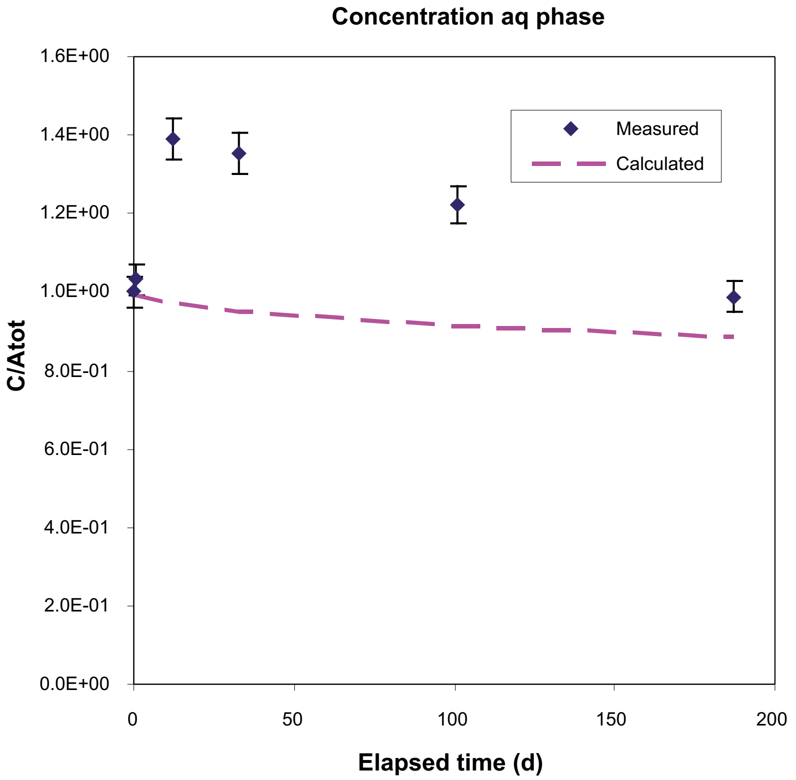

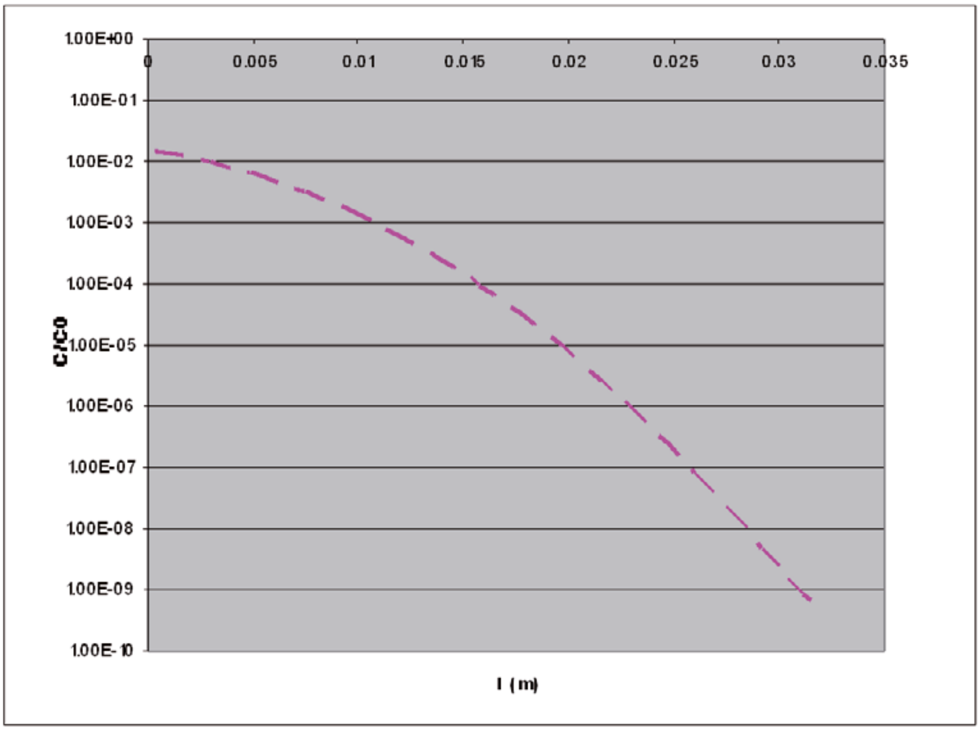

#1. Predictions for KLX02 235.08 Ävrö granodiorite. Sample specific K_d, F_f and ε:

Cd-109:

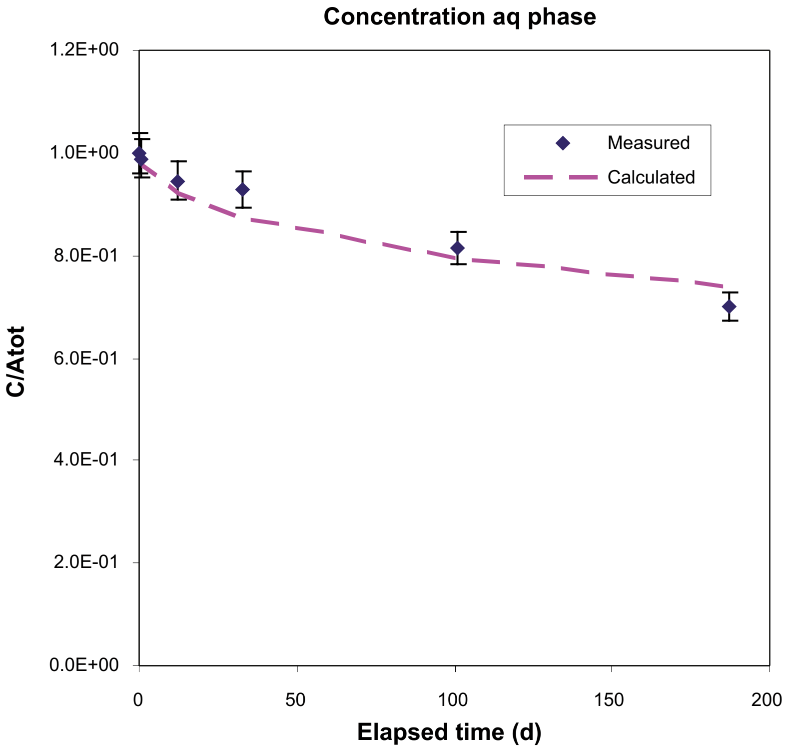

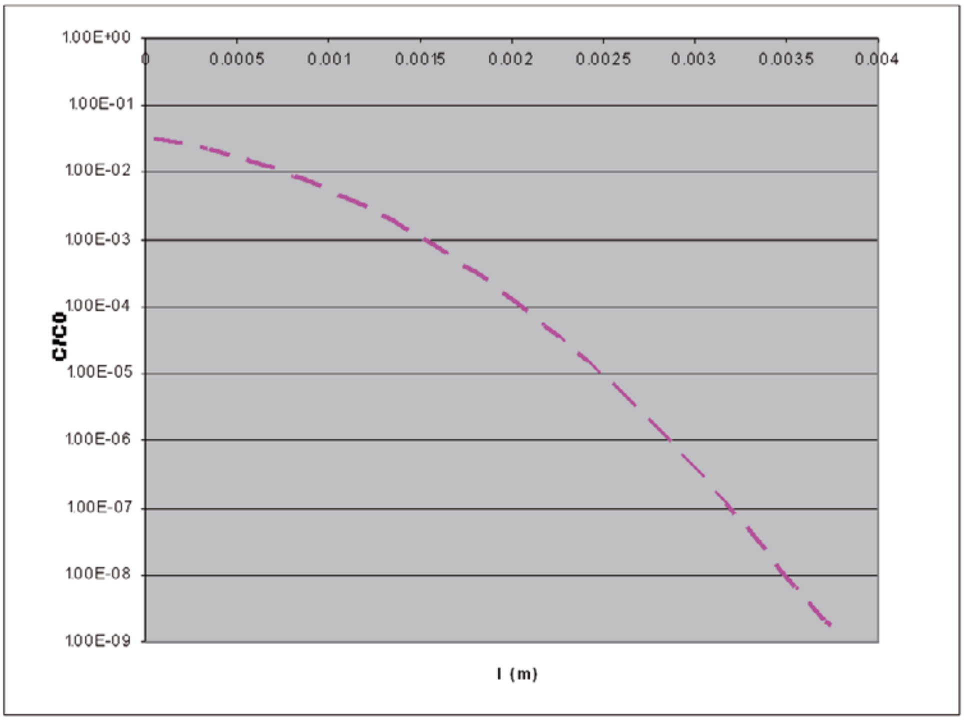

#1. Predictions for KLX02 235.08 Ävrö granodiorite. Sample specific K_d, F_f and ε:

Ba-133:

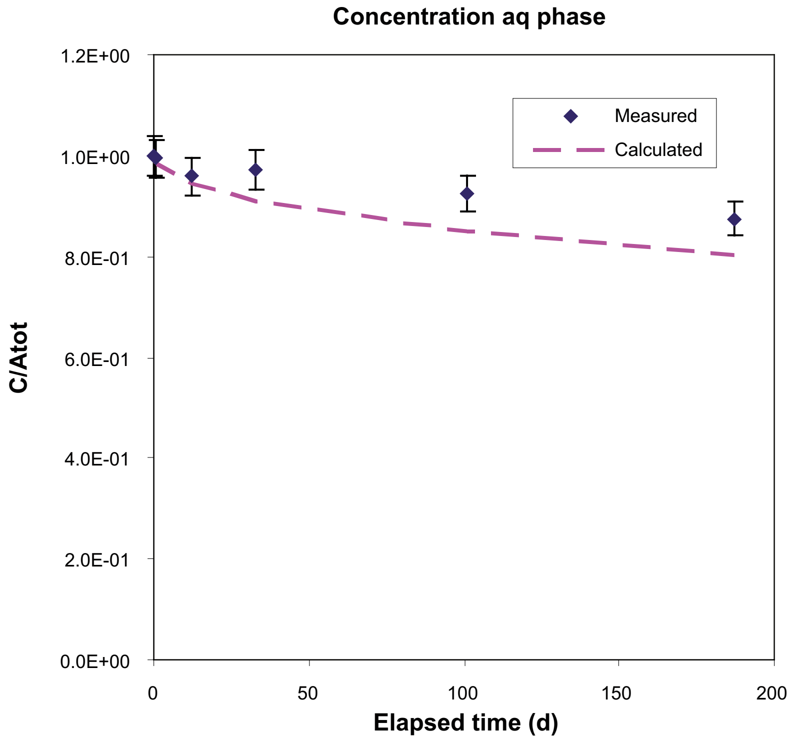

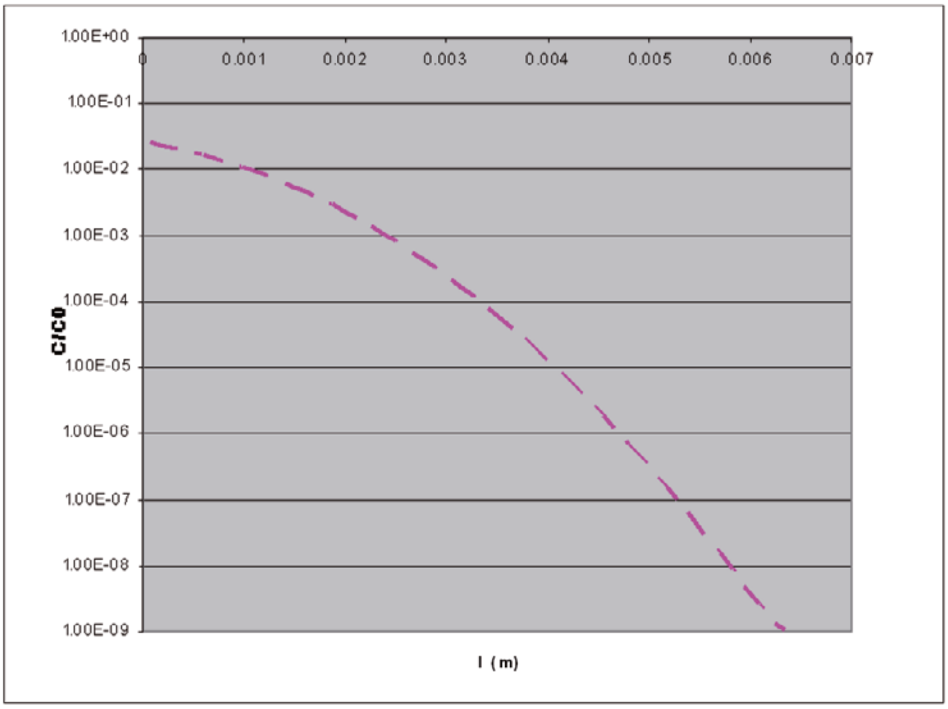

#1. Predictions for KLX02 235.08 Ävrö granodiorite. Sample specific K_d, F_f and ε:

Cs-137:

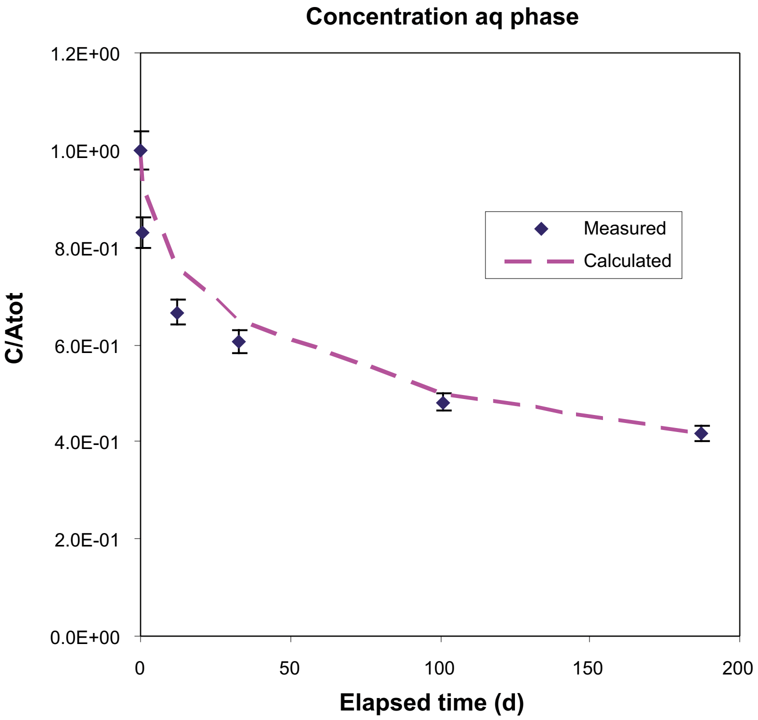

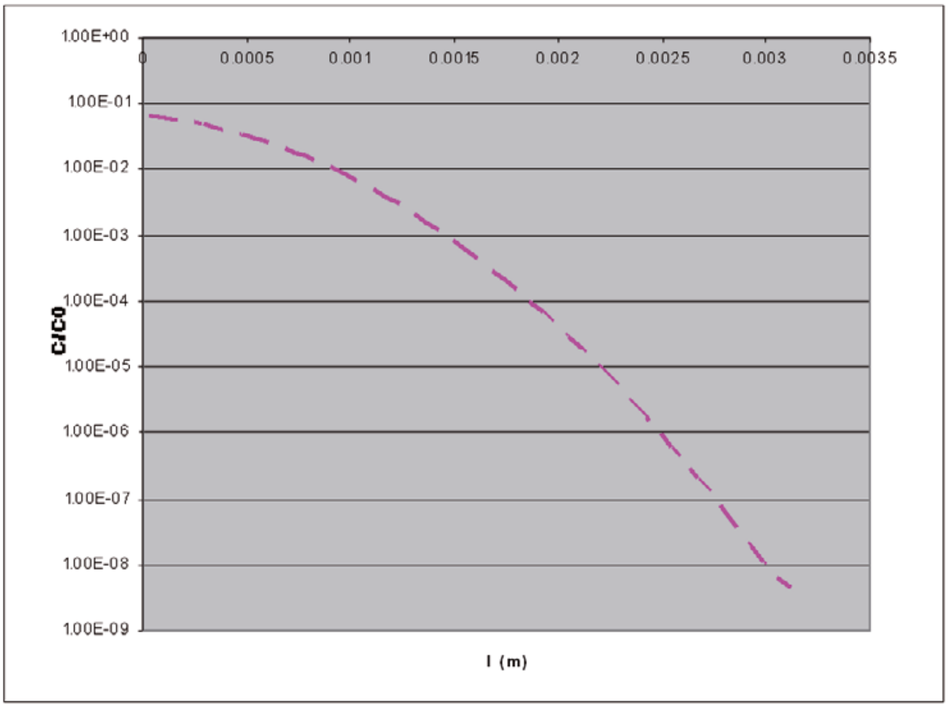

#1. Predictions for KLX02 235.08 Ävrö granodiorite. Sample specific K_d, F_f and ε:

U-236:

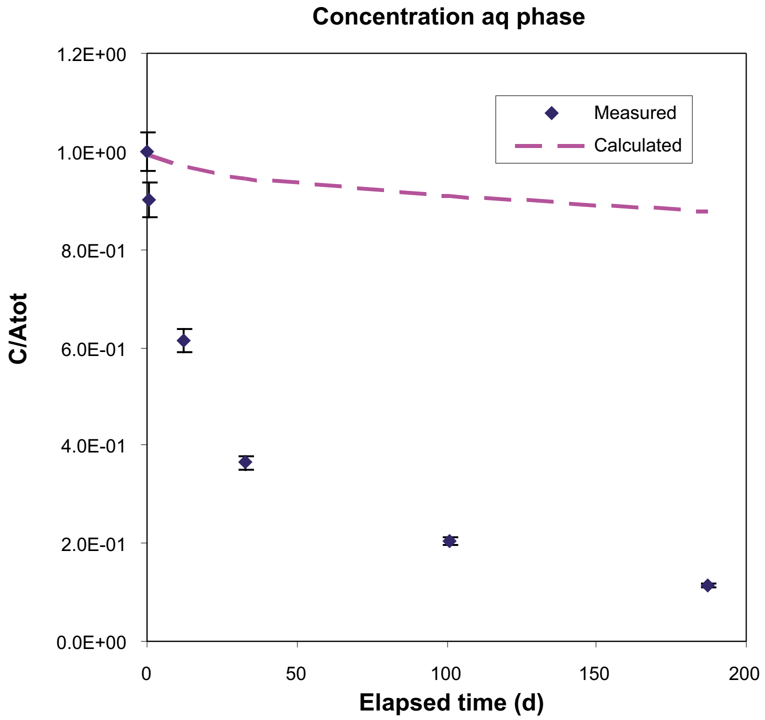

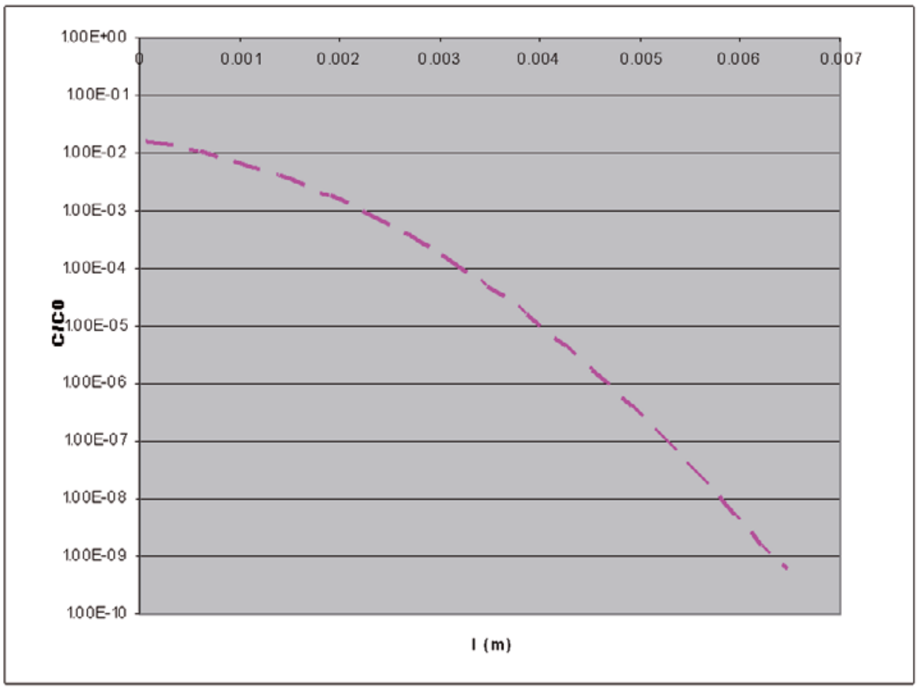

#1. Predictions for KLX02 235.08 Ävrö granodiorite. Sample specific K_d, F_f and ε:

Np-237:

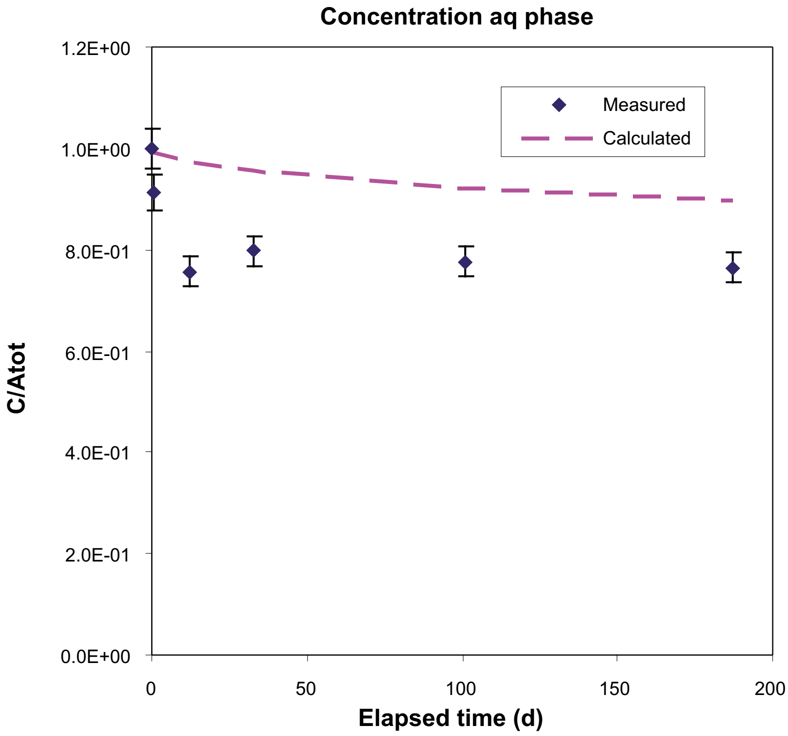

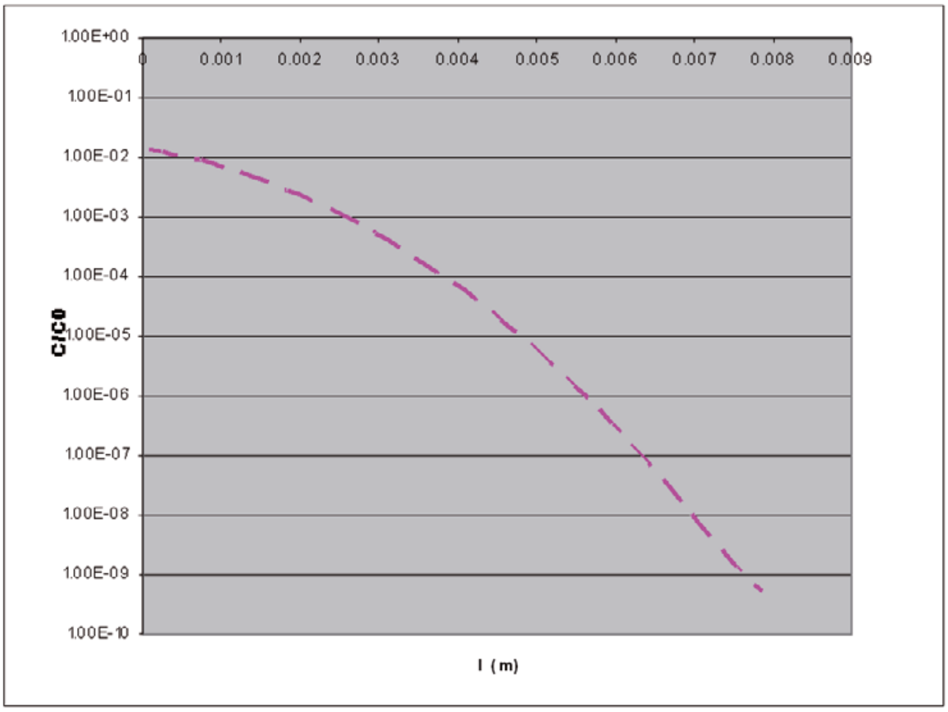

#2. Predictions for KLX02 235.08 Ävrö granodiorite. Rock type mean values for K_d(m^3/kg), F_f and ε:

Rock type mean value

Tracer	K_d (m^3/kg)	F_f	ε
Na-22	N.a.		
Co-57	N.a.		
Se-75	N.a.		
Sr-85	3.91E-04	1.53E-04	3.18E-03
Zr-95	N.a.		
Tc-99	N.a.		
Cd-109	N.a.		
Ag-110 m	N.a.		
Sn-113	N.a.		
Ba-133	N.a.		
Cs-137	5.46E-03	1.53E-04	3.18E-03
Hf-175	N.a.		
U-236	N.a.		
Np-237	N.a.		

#2. Predictions for KLX02 235.08 Ävrö granodiorite. Rock type mean values for K_d(m^3/kg), F_f and ε:

Tracer: Sr-85

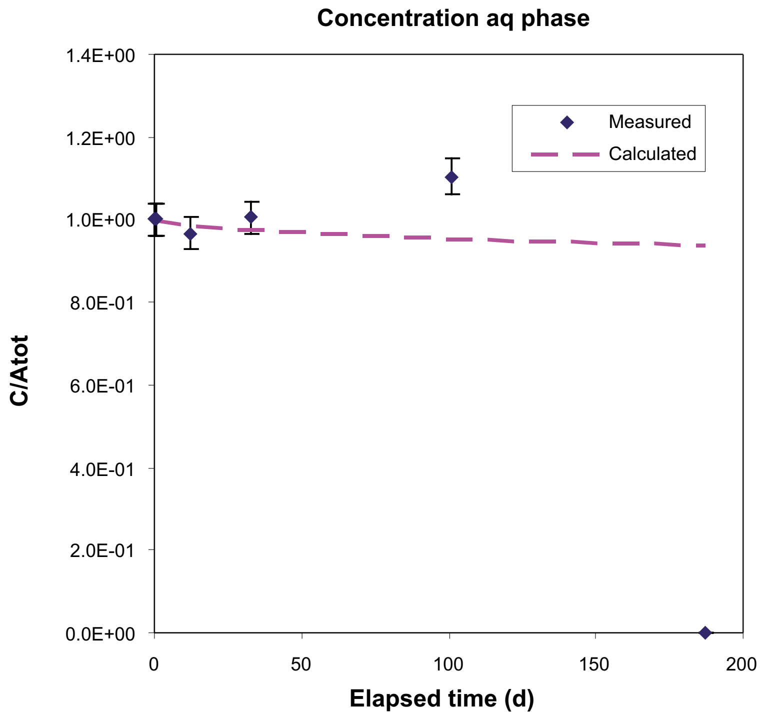

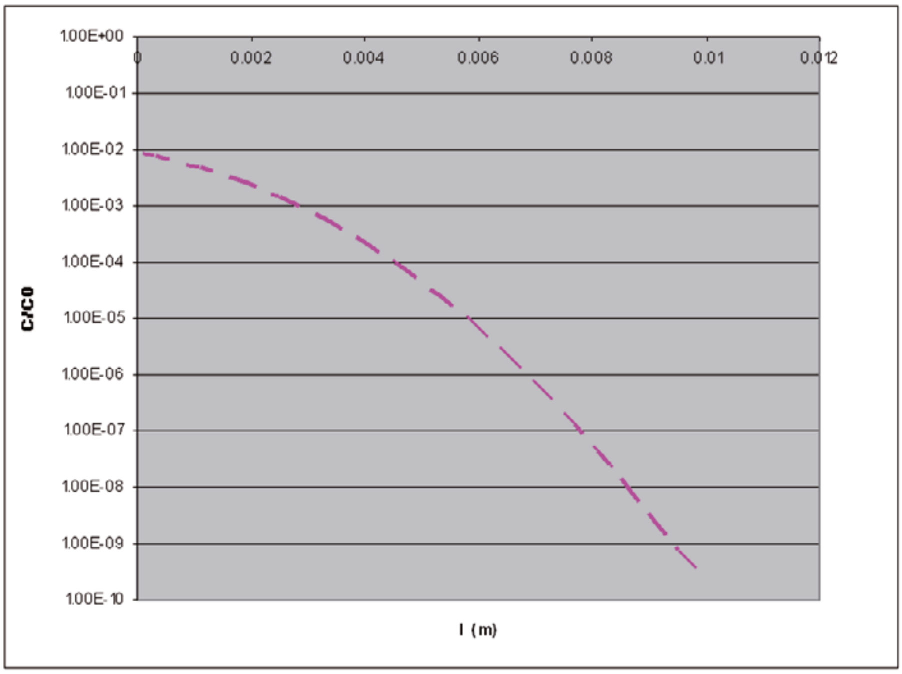

#2. Predictions for KLX02 235.08 Ävrö granodiorite. Rock type average values for K_d, F_f and ε:

Tracer: Cs-137

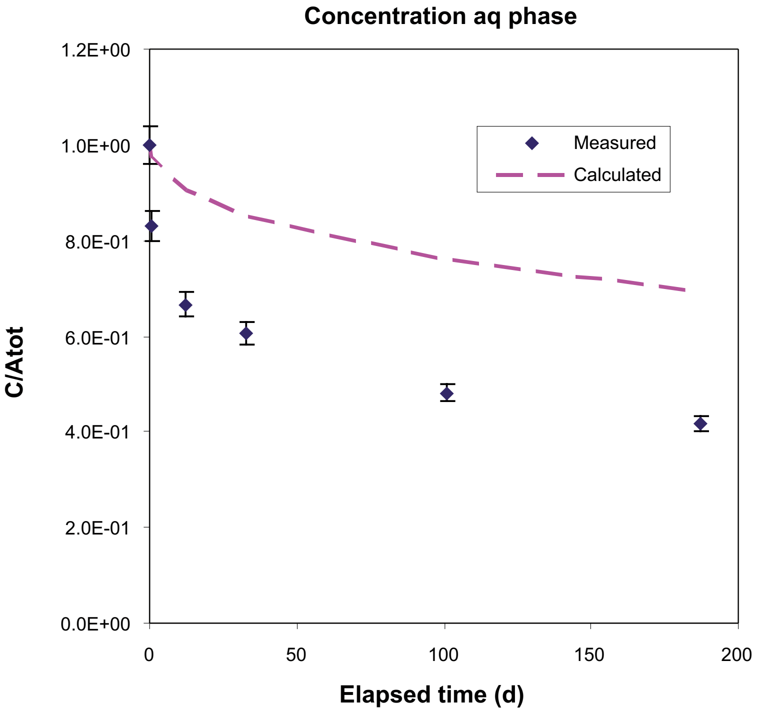

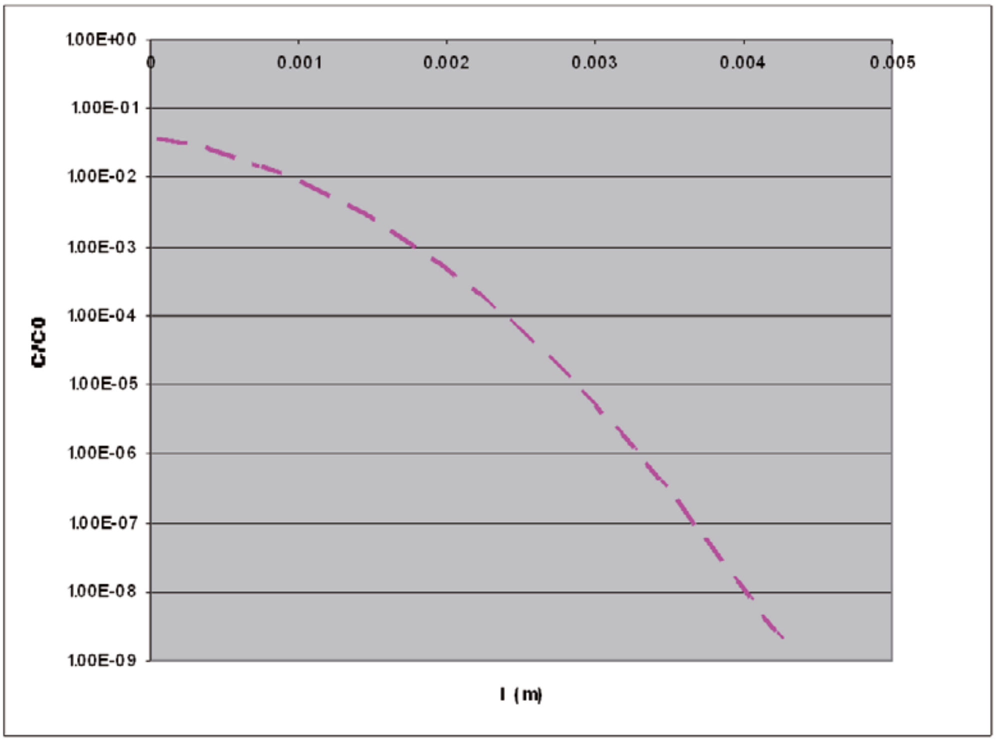

#3. Predictions for Cs-137. Sample specific K_d(m^3/kg), F_f and ε:

Tracer: Cs-137

Sample specific data

Core name	K_d (m^3/kg)	F_f	ε
KSH01_891.91			
KSH01_981.43	1.61E-02	2.25E-04	2.90E-03
KLX02_235.08			
KLX04_726.07			
KLX08_417.05			
KLX10_995.78			
KFM02_276.06	2.00E-03	1.60E-02	1.84E-01
KFM03A_242.43	8.38E-03	8.22E-05	1.89E-03
KFM07A_608.75			
KFM09A_713.67			

#3. Predictions for Cs-137. Sample specific K_d(m^3/kg), F_f and ε:

KSH01_981.43:

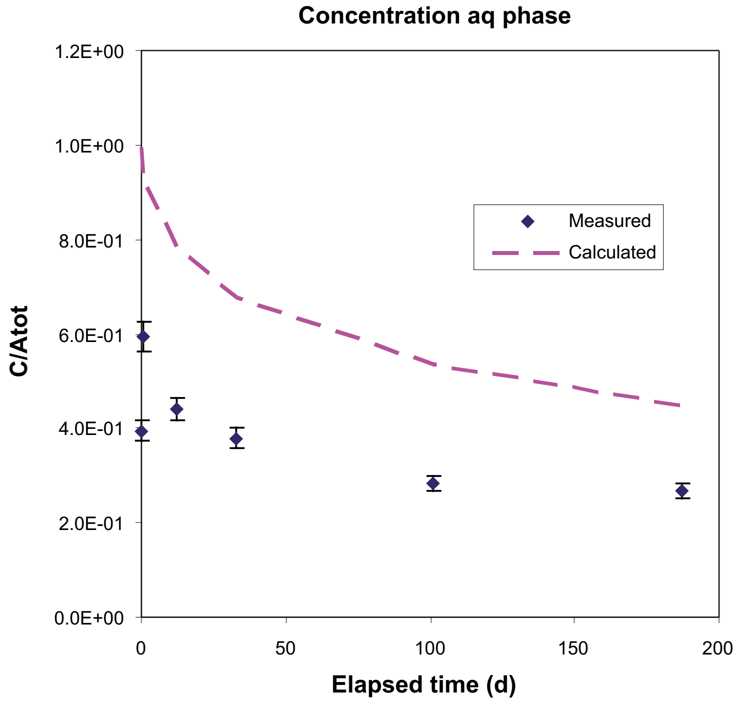

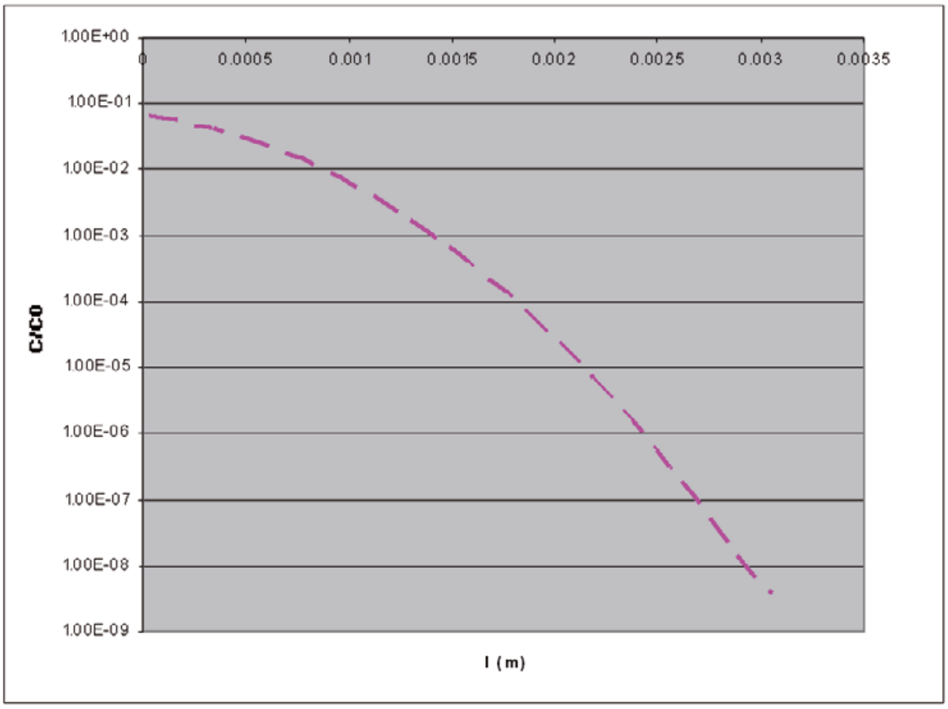

#3. Predictions for Cs-137. Sample specific K_d(m^3/kg), F_f and ε:

KFM02A 276.06:

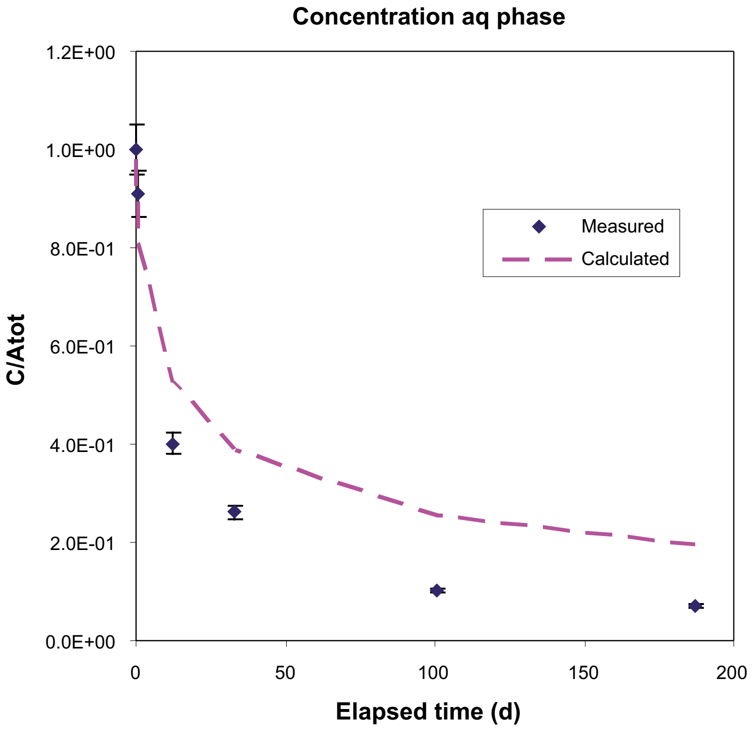

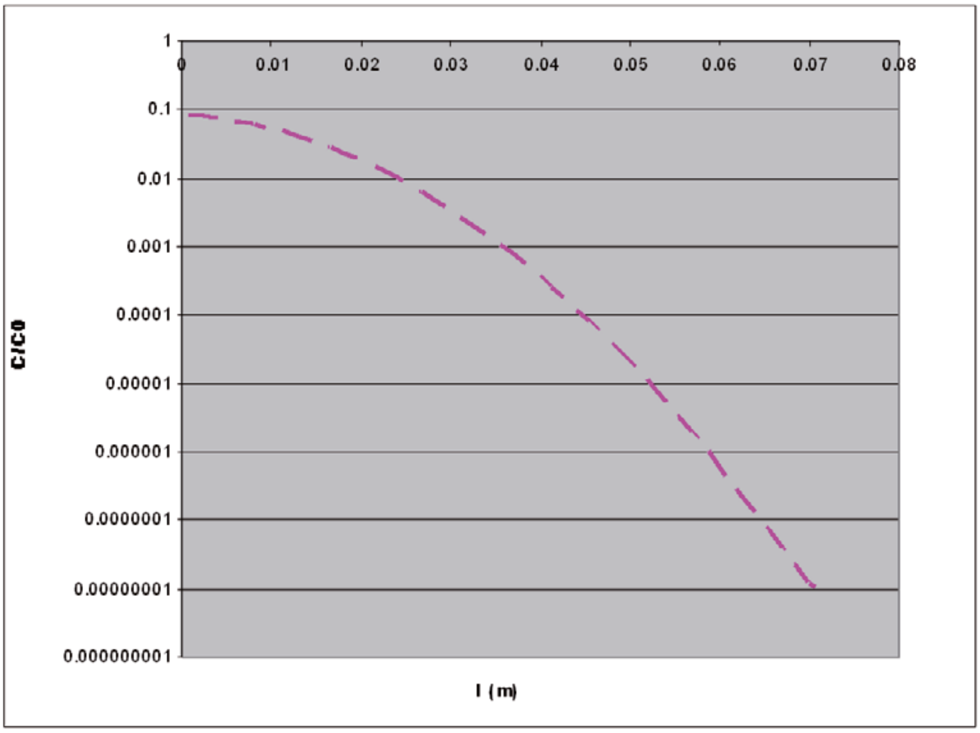

#3. Predictions for Cs-137. Sample specific K_d(m^3/kg), F_f and ε:

KFM03A_242.43:

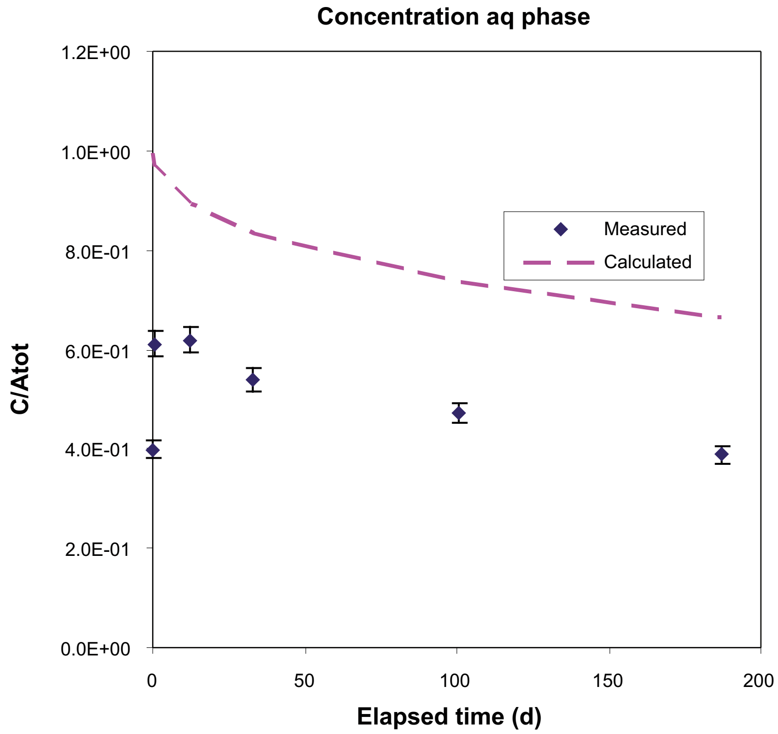

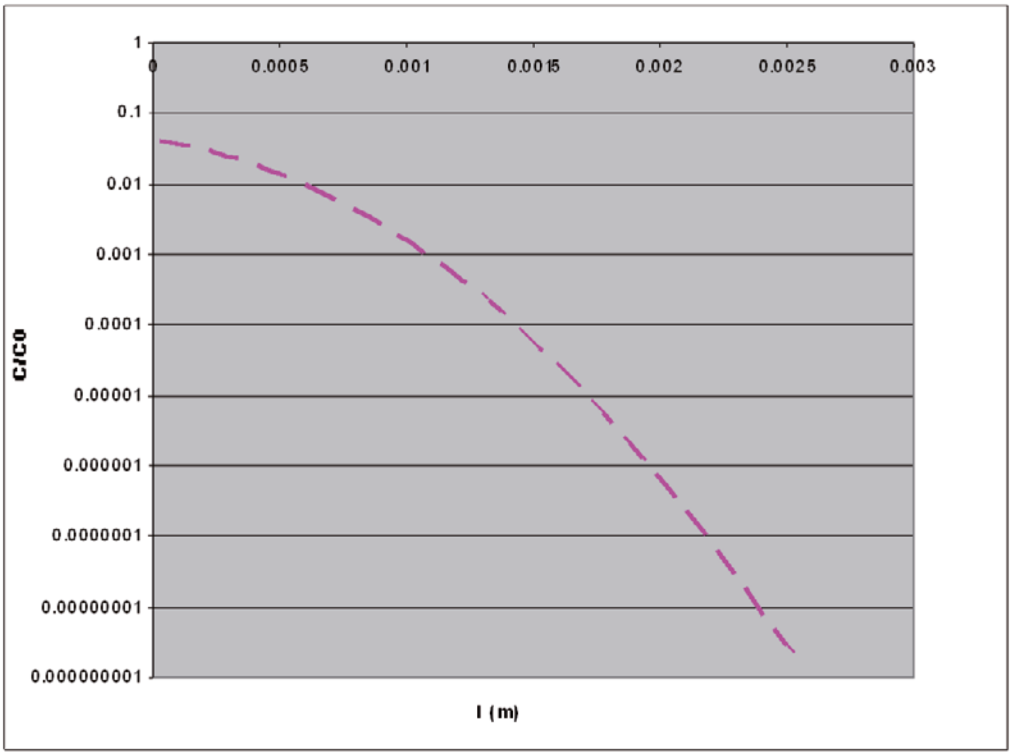

#4. Predictions for Cs-137. Rock type mean values for K_d(m^3/kg), F_f and ε:

Tracer: Cs-137

Rock type mean values

Core id	K_d (m^3/kg)	F_f	ε
KSH01_891.91	2.89E-02	4.12E-04	3.49E-03
KSH01_981.43	2.41E-02	1.14E-04	1.90E-03
KLX02_235.08	5.46E-03	1.53E-04	3.18E-03
KLX04_726.07	2.41E-02	1.14E-04	1.90E-03
KLX08_417.05	2.89E-02	4.12E-04	3.49E-03
KLX10_995.78	2.41E-02	1.14E-04	1.90E-03
KFM02A 276.06	2.00E-03	1.21E-02	1.31E-01
KFM03A_242.43	8.38E-03	7.79E-05	1.57E-03
KFM07A_608.75	3.99E-03	1.63E-04	9.98E-03
KFM09A_713.67	3.99E-03	1.63E-04	9.98E-03

KSH01_891.91

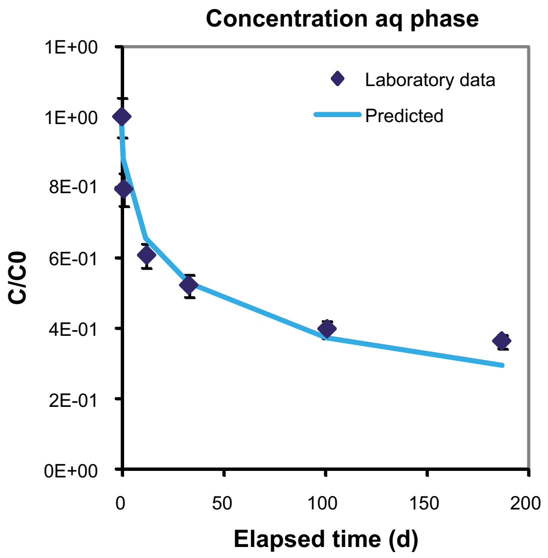

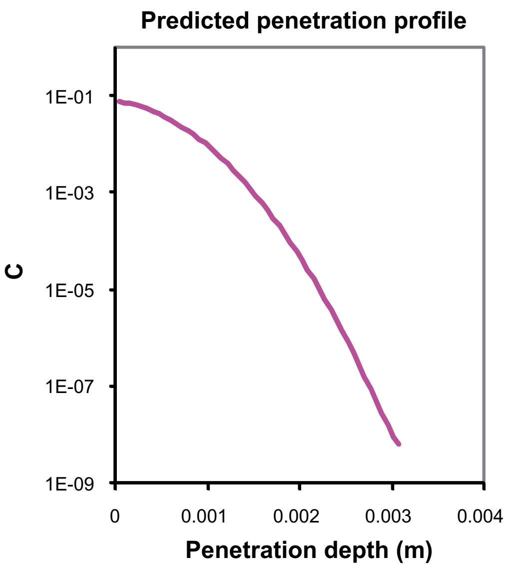

KSH01_981.43

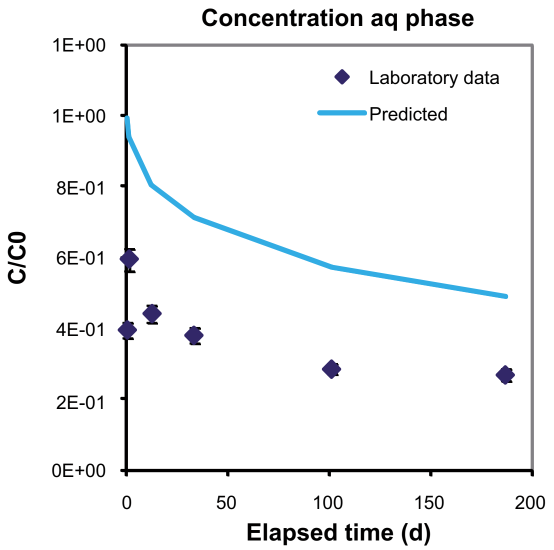

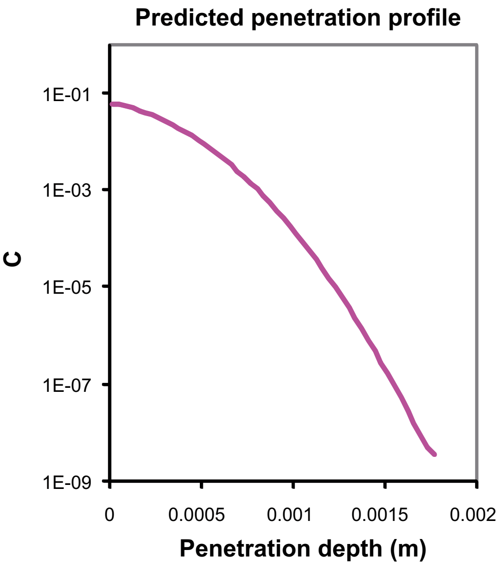

KLX02_235.08

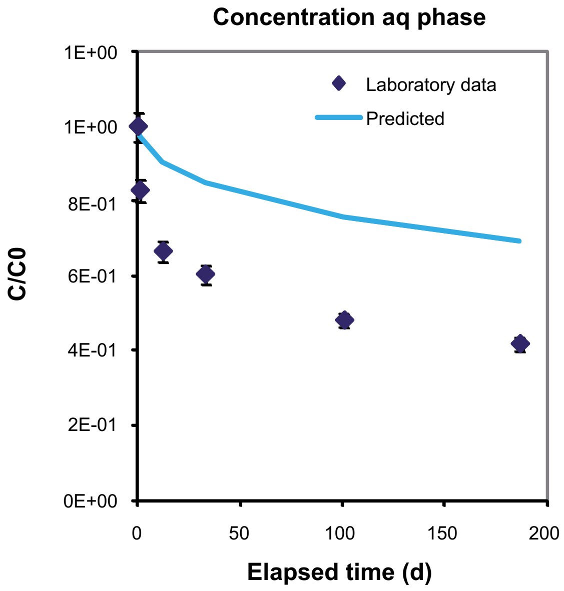

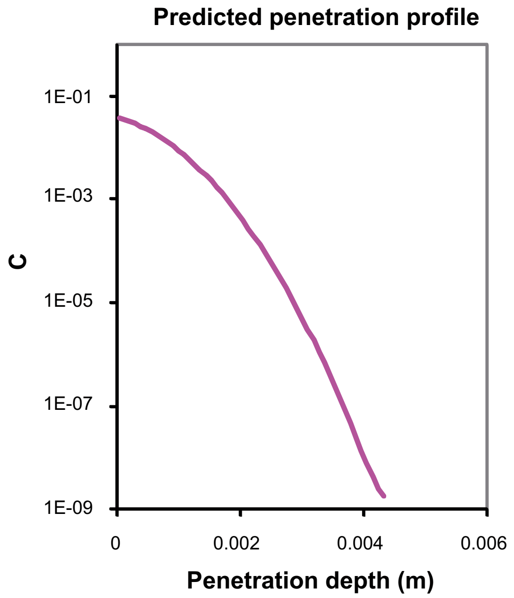

KLX04_726.07

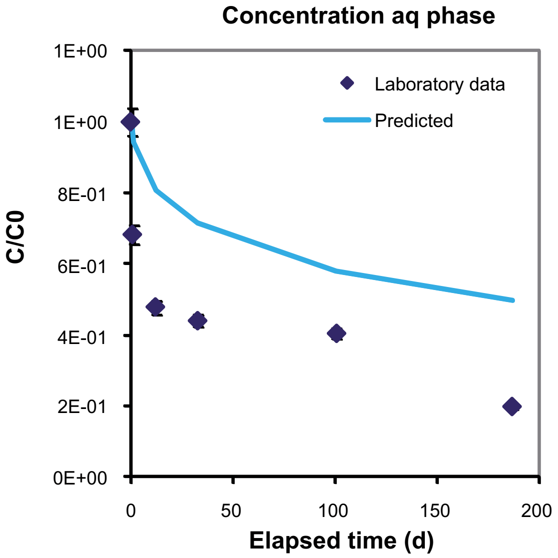

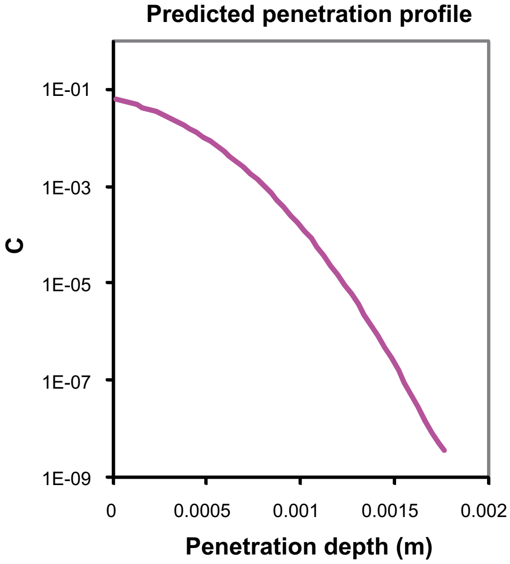

KLX08_417.05

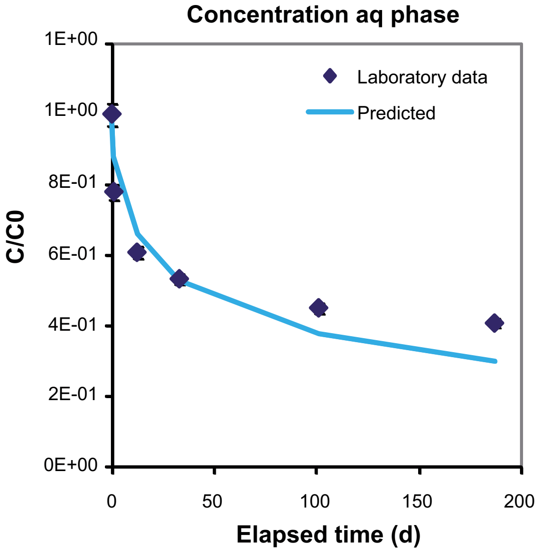

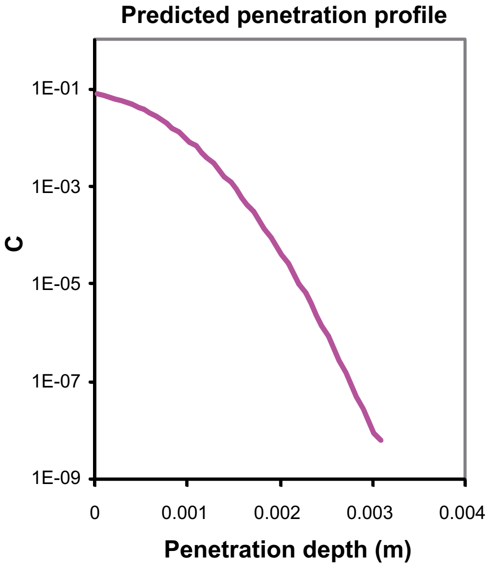

KLX10_995.78

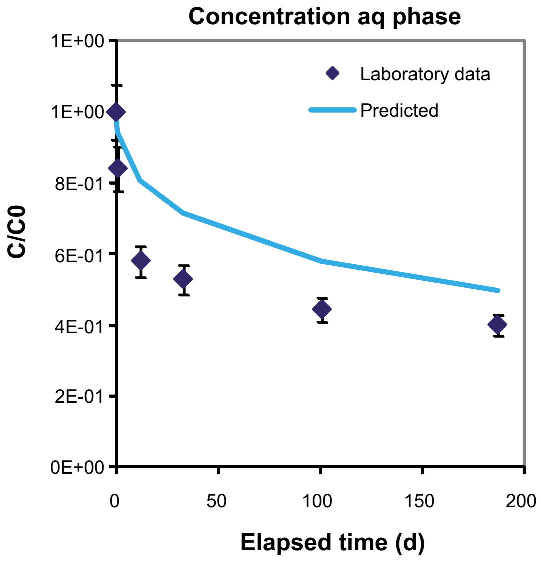

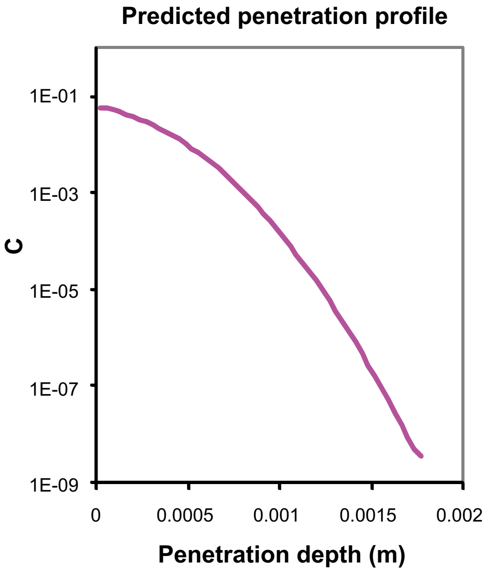

KFM02A 276.06

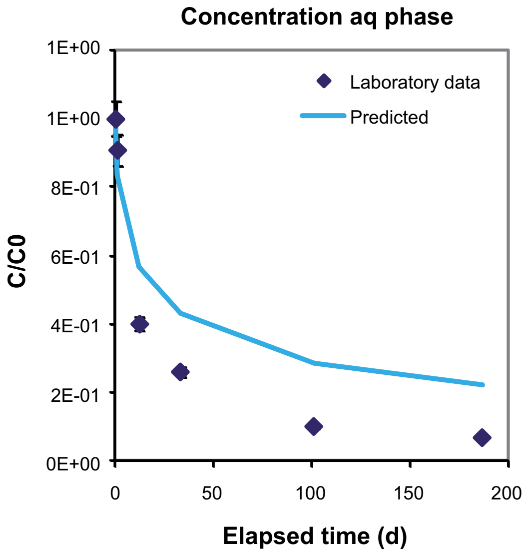

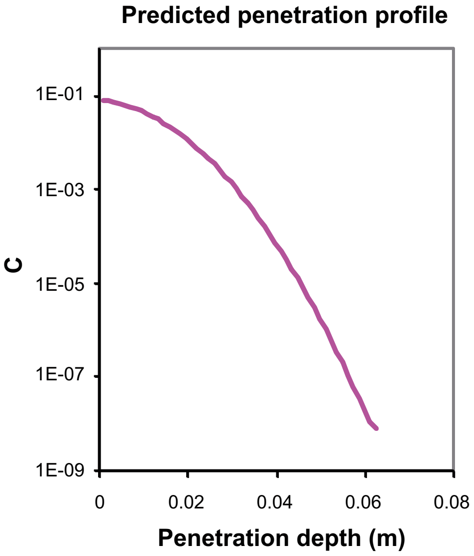

KFM03A_242.43

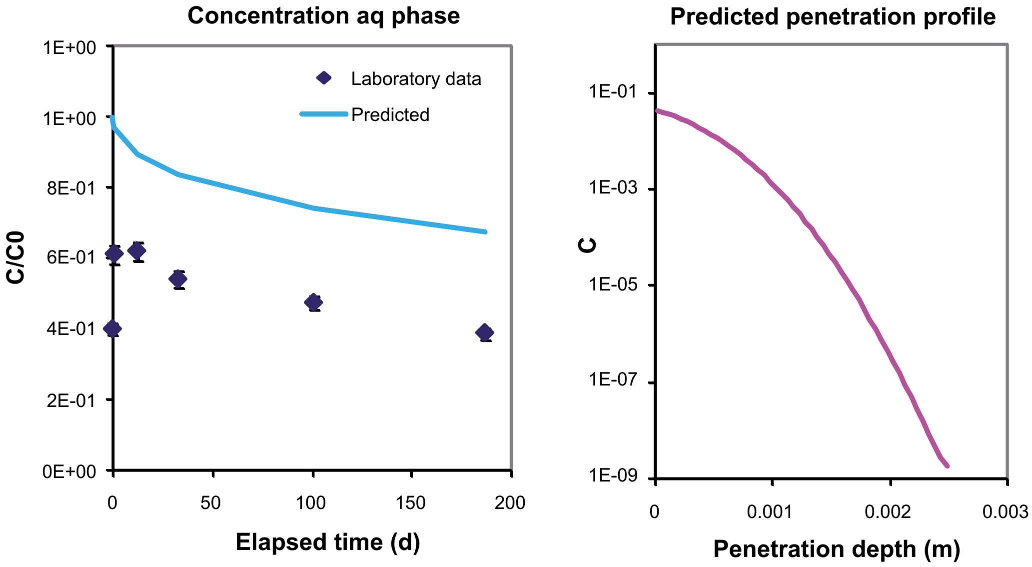

KFM07A_608.75

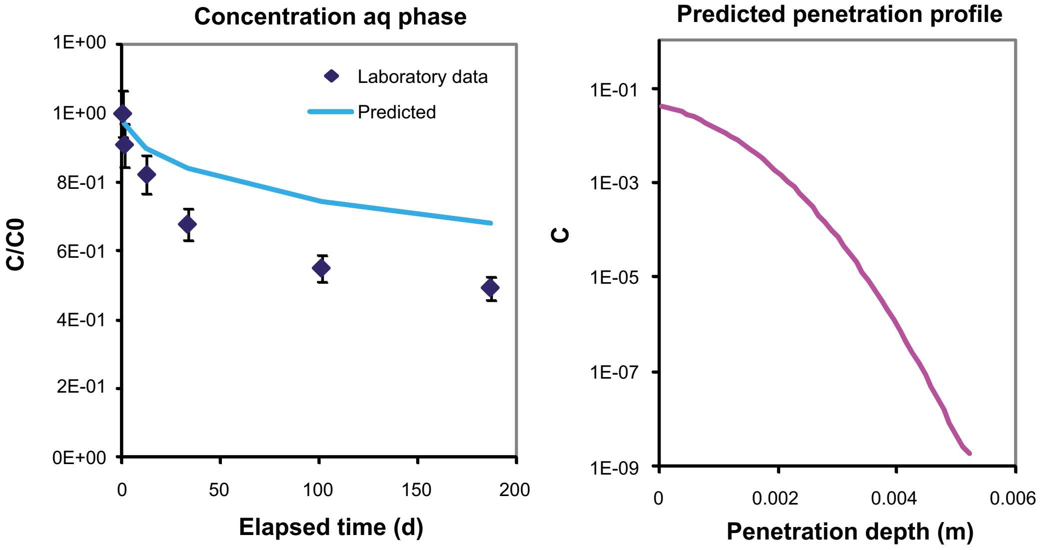

KFM09A_713.67

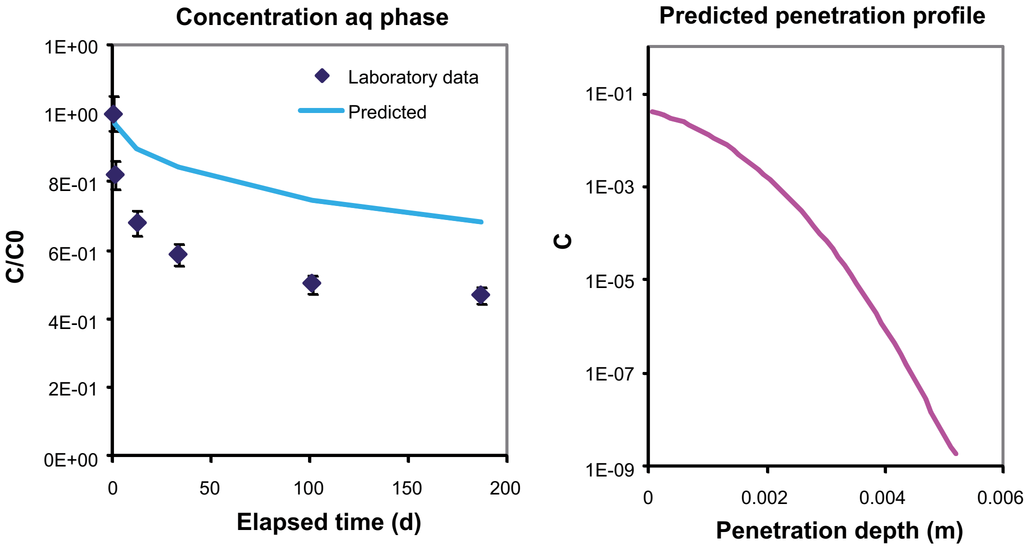

#5. Predictions for Cs-137. Rock type mean values for K_d (m^3/kg), sample specific F_f and ε:

Tracer: Cs-137

	Sample specific data		Rock type mean value
Core id	**F_f**	**ε**	**K_d (m^3/kg)**
KSH01_891.91	5.16E-04	4.60E-03	2.89E-02
KSH01_981.43	2.25E-04	2.90E-03	2.41E-02
KLX02_235.08	3.19E-04	3.90E-03	5.46E-03
KLX04_726.07			
KLX08_417.05	4.60E-04	4.50E-03	2.89E-02
KLX10_995.78	2.25E-04	6.00E-04	2.41E-02
KFM02A 276.06	1.60E-02	1.84E-01	2.00E-03
KFM03A_242.43	8.22E-05	1.89E-03	8.38E-03
KFM07A_608.75	6.67E-04	6.20E-03	3.99E-03
KFM09A_713.67			

KSH01_891.91

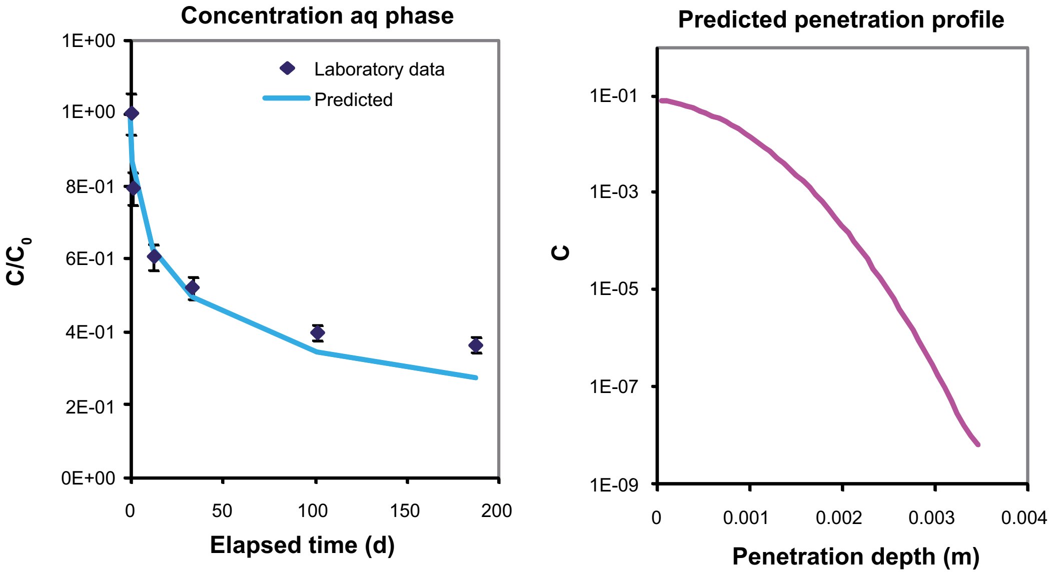

KSH01_981.43

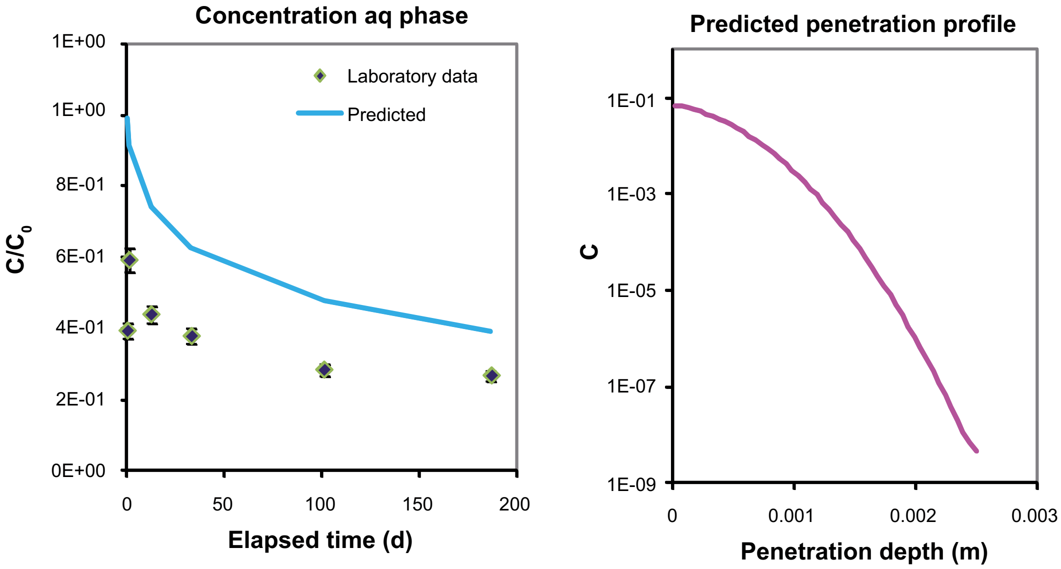

KLX02_235.08

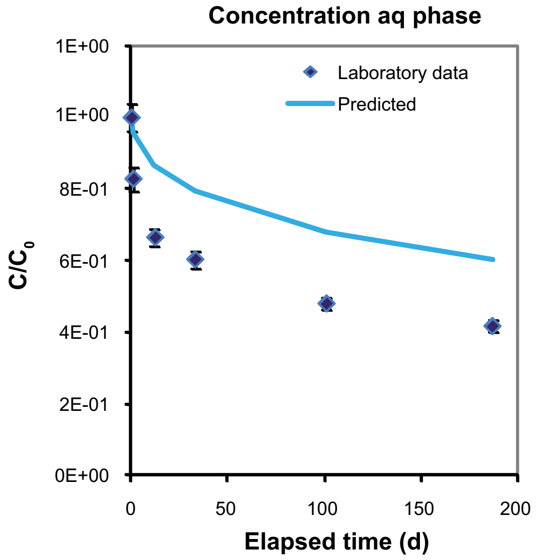

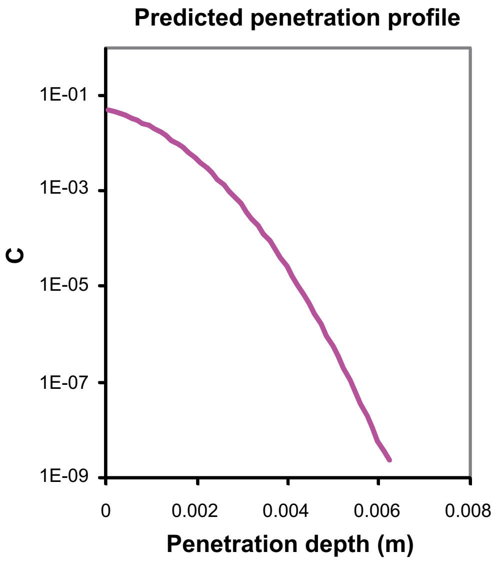

KLX08_417.05

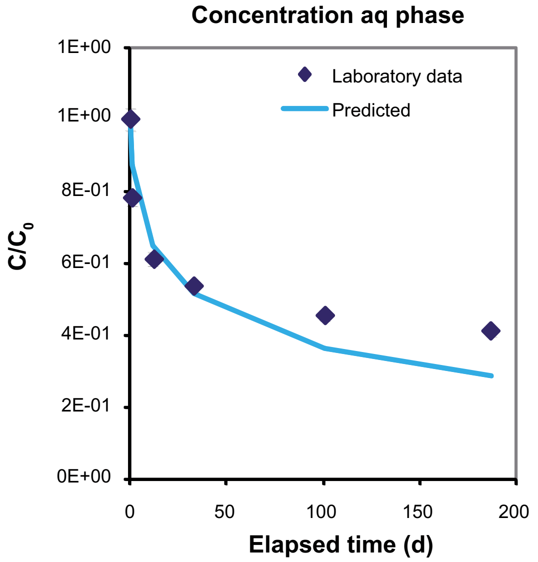

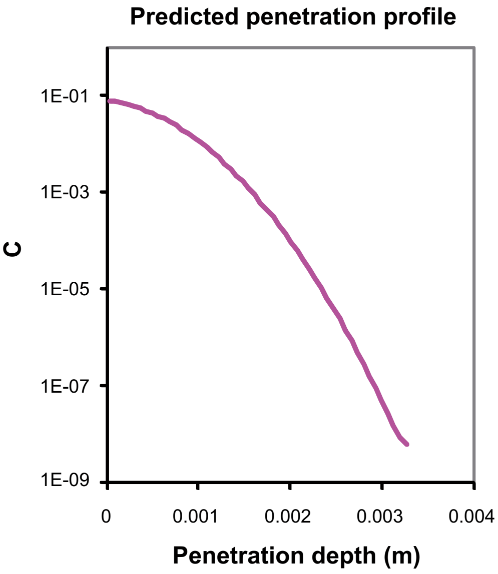

KLX10_995.78

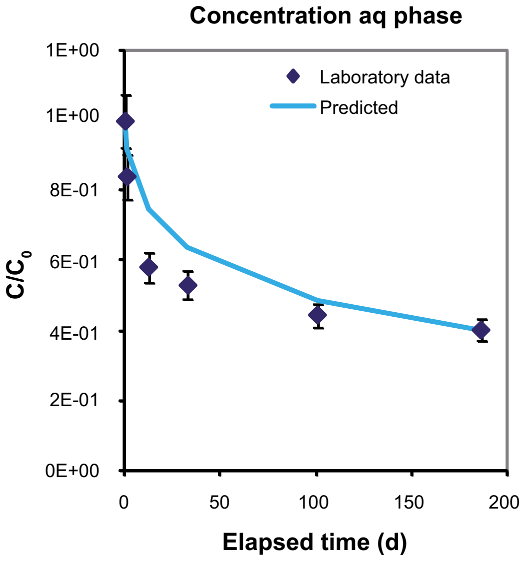

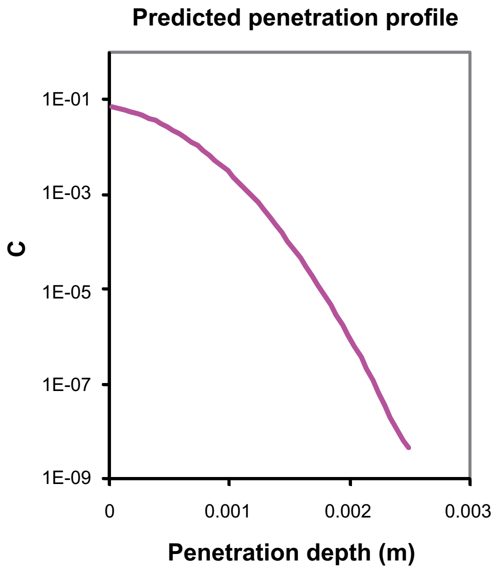

KFM02A 276.06

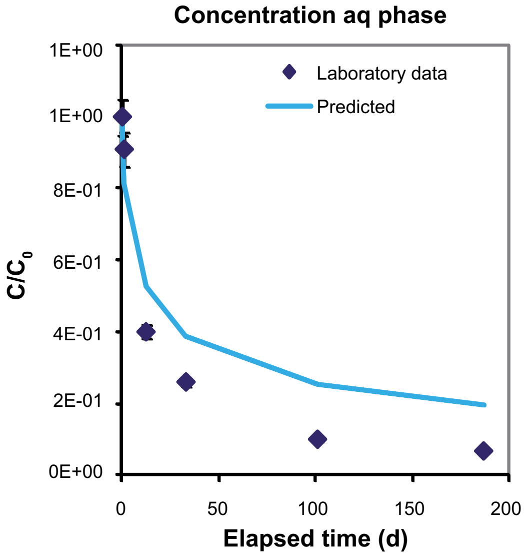

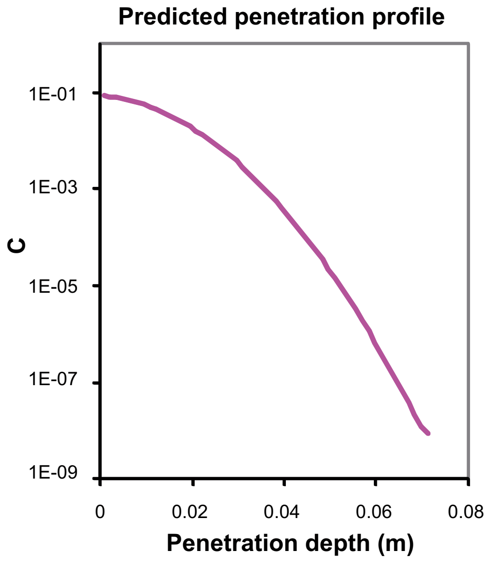

KFM03A_242.43

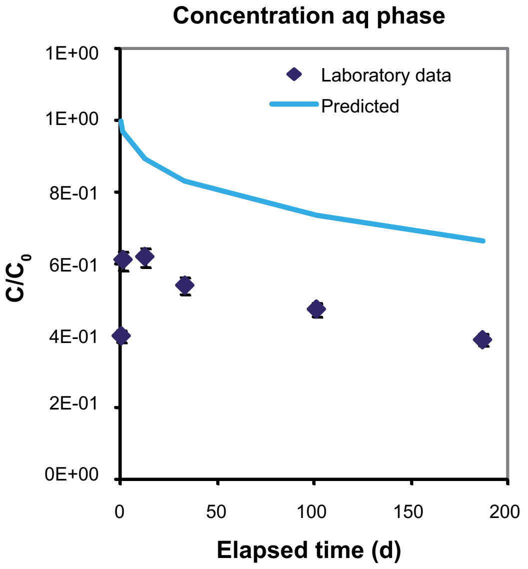

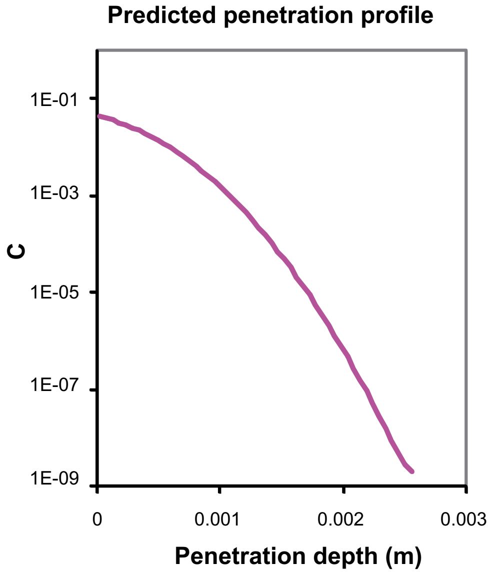

KFM07A_608.75

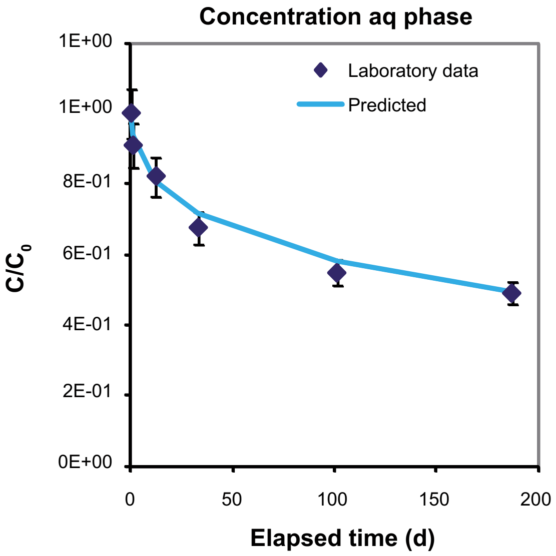

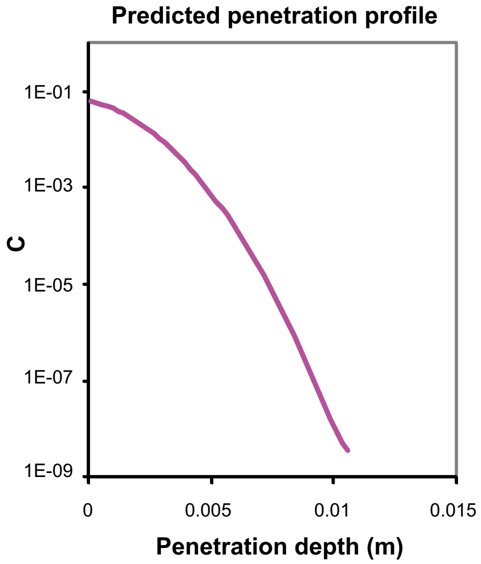

#6. Predictions for Cs-137. Sample specific data for K_d(m³/kg), rock type mean values for F_f and ε:

Tracer: Cs-137

	Sample specific data	Rock type mean values	
Core id	K_d (m³/kg)	F_f	ε
KSH01_891.91	1.61E-02	1.14E-04	1.90E-03
KSH01_981.43			
KLX02_235.08			
KLX04_726.07			
KLX08_417.05			
KLX10_995.78			
KFM02A 276.06	2.00E-03	1.21E-02	1.31E-01
KFM03A_242.43	8.38E-03	7.79E-05	1.57E-03
KFM07A_608.75			
KFM09A_713.67			

KSH01_891.91

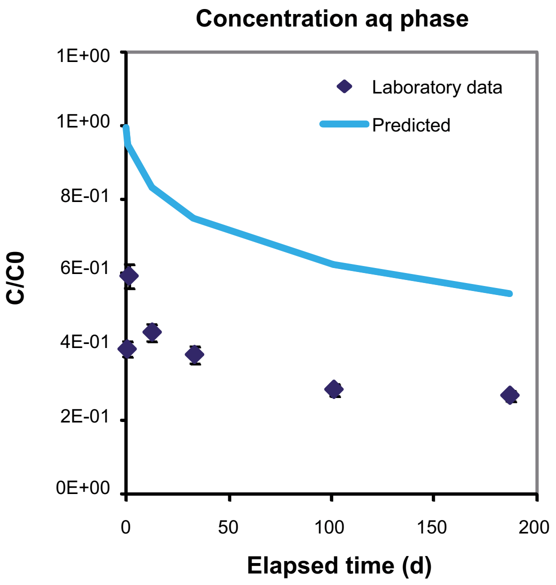

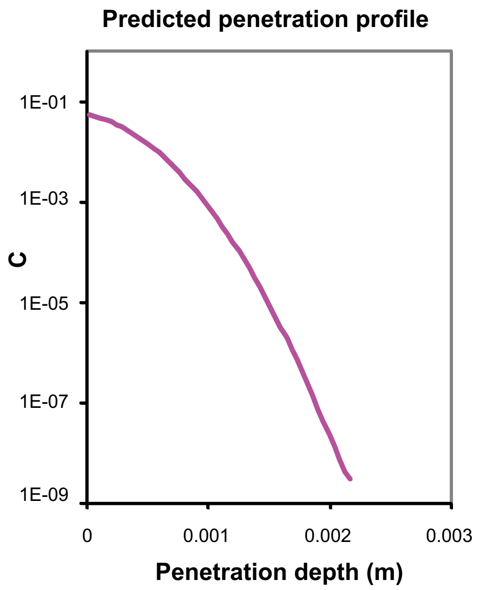

KFM02A 276.06

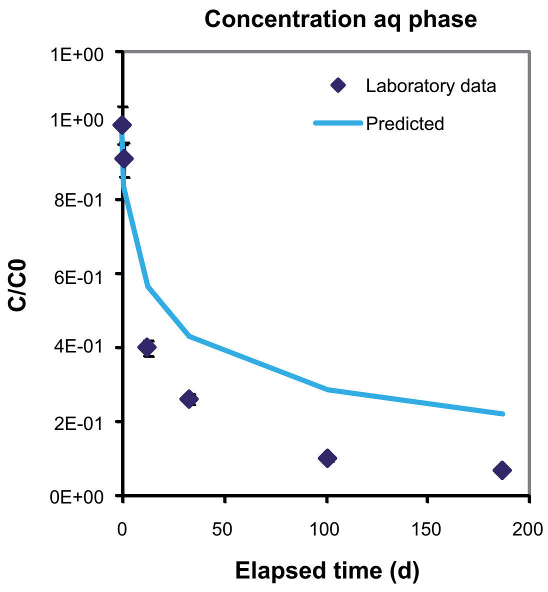

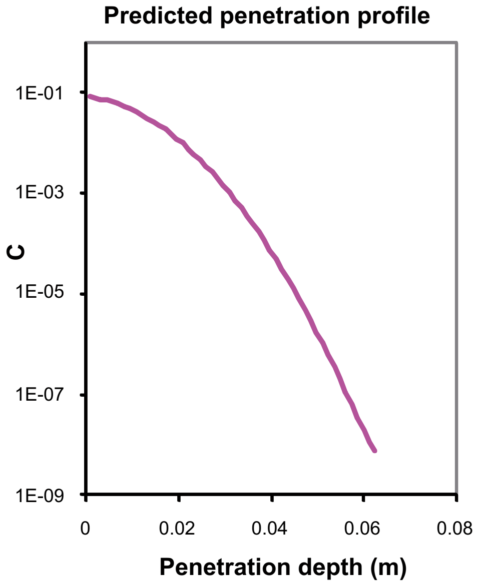

KFM03A_242.43

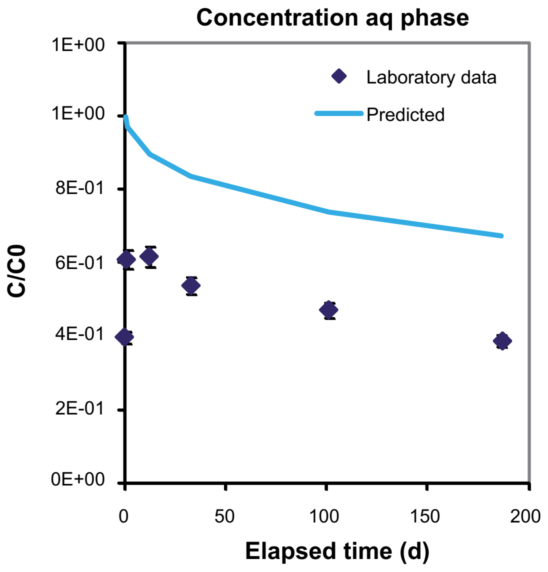

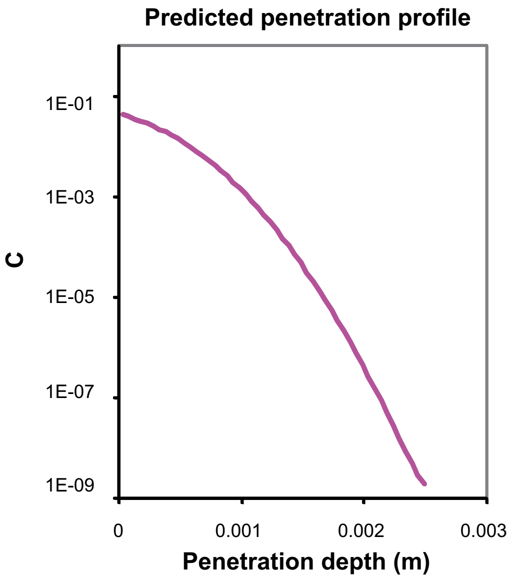

Appendix 9

Estimations for LTDE-SD samples

This appendix presents figures from estimations described in Section 4.3.3 for aqueous phase concentrations and the penetration profiles that are the calculated for each aqueous phase concentration calculation.

Na-22 (K_d (m^3/kg) estimated)

A03:3/Diff I:

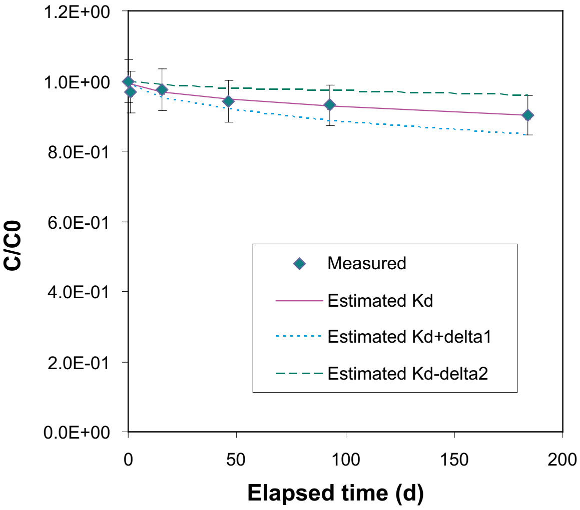

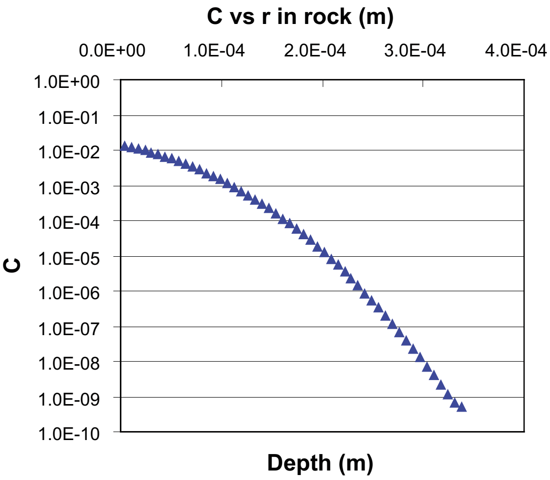

Comment: The short and unrealistic penetration depth is a result of the very large concentration decrease of sodium in combination with low diffusivity of the sample. The uncertainty in the estimation is not shown in the penetration depth figure.

A03:5/Diff III:

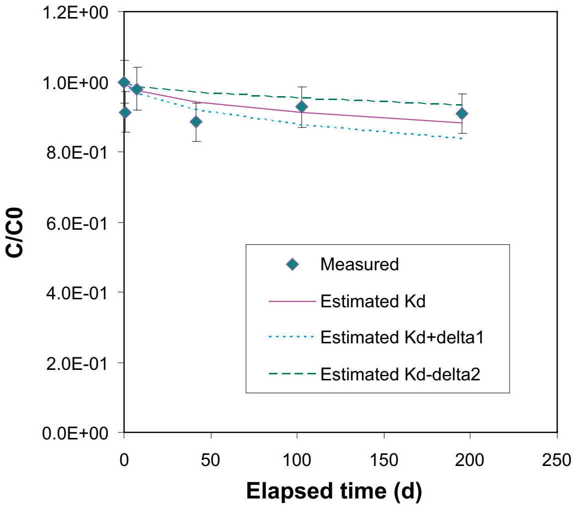

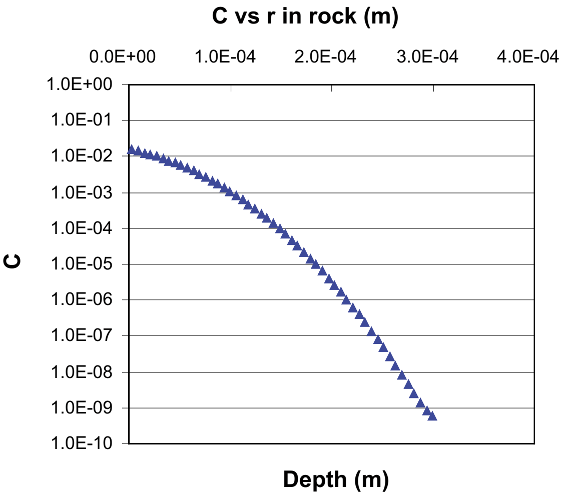

Comment: The short and unrealistic penetration depth is a result of the very large concentration decrease of sodium in combination with low diffusivity of the sample. The uncertainty in the estimation is not shown in the penetration depth figure.

Co-57 (K_d (m^3/kg) estimated)

A03:3/Diff I:

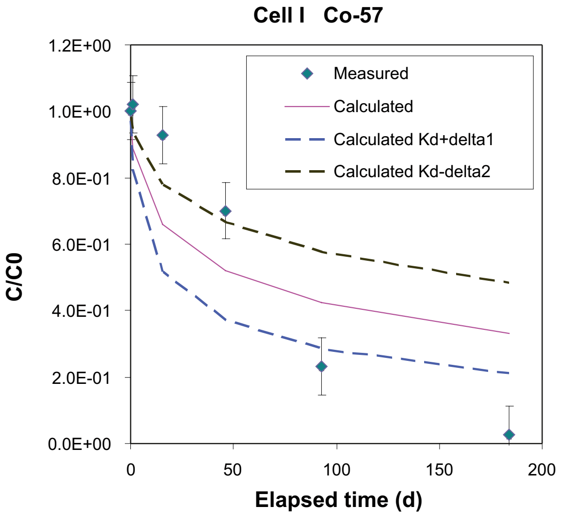

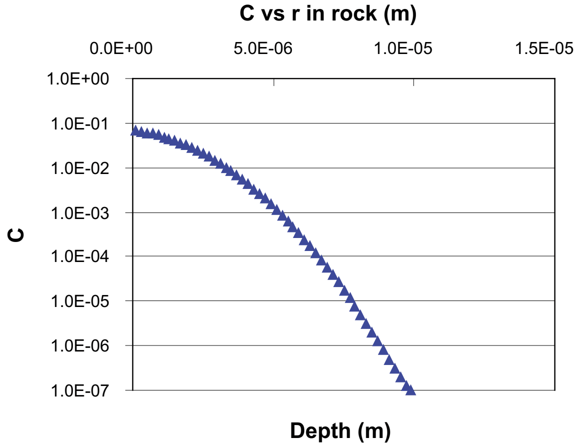

A03:5/Diff III:

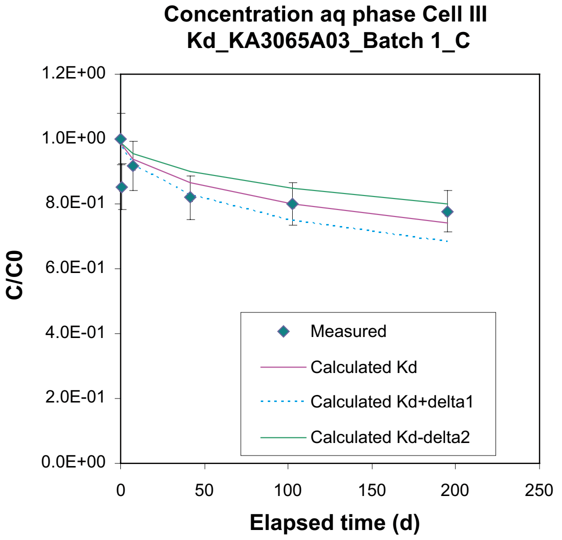

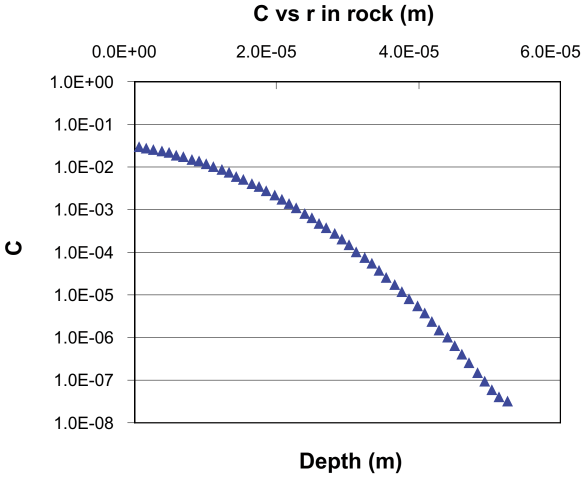

Ni-63 (K_d (m^3/kg) estimated)

A03:5/Diff I:

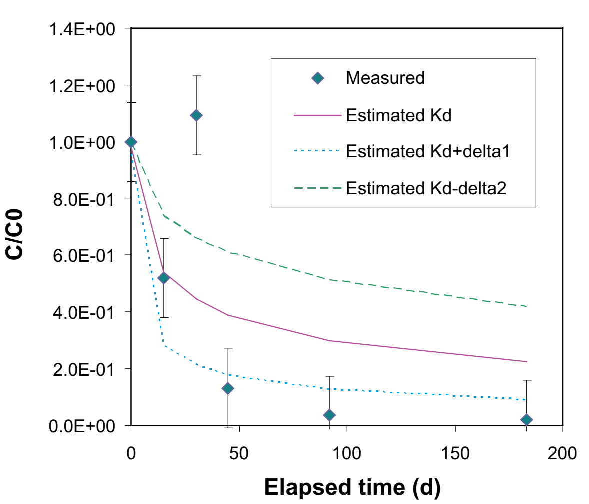

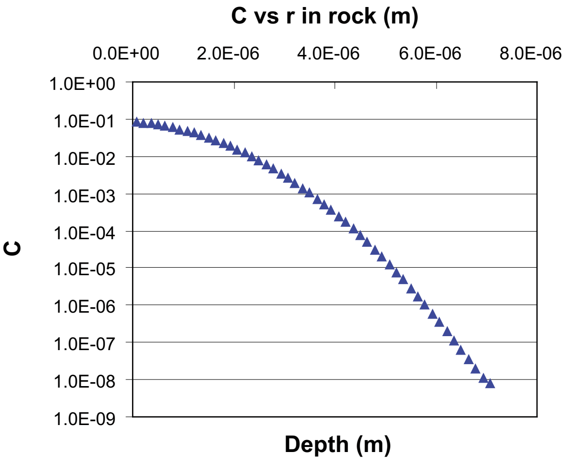

A03:5/Diff III:

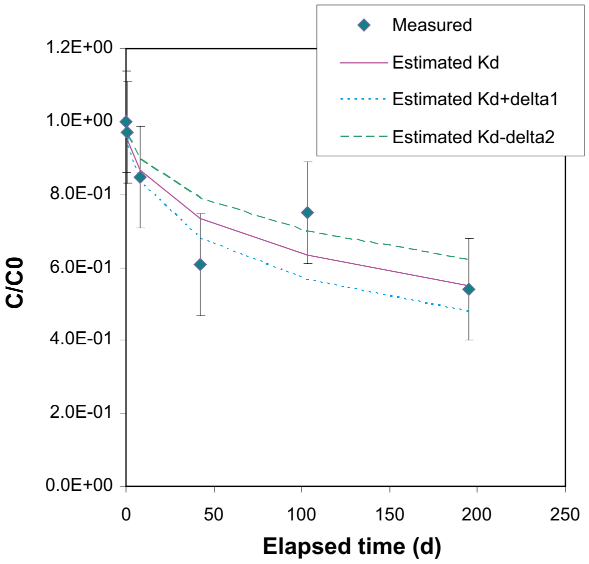

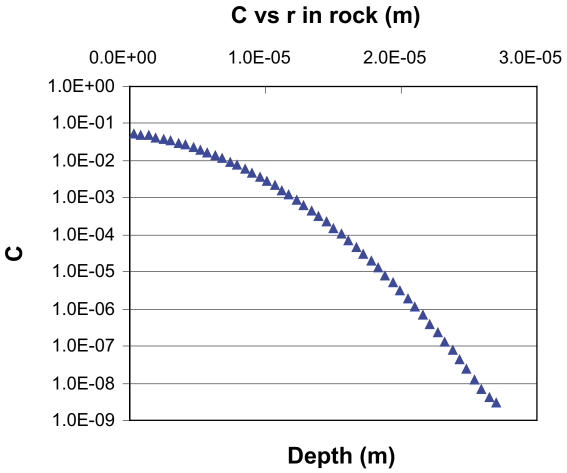

Ni-63 (F_f estimated)

A03:5/Diff I:

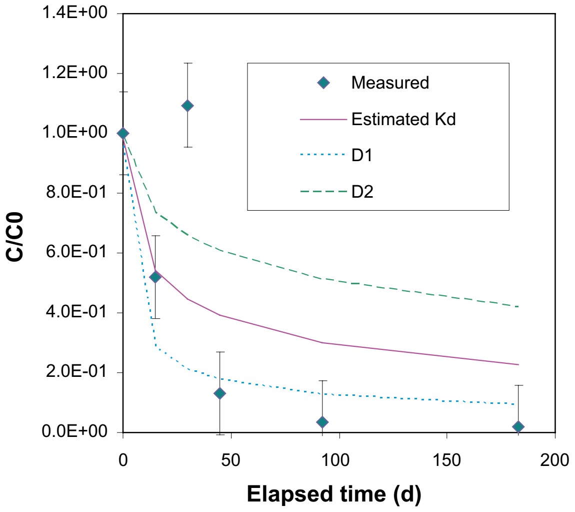

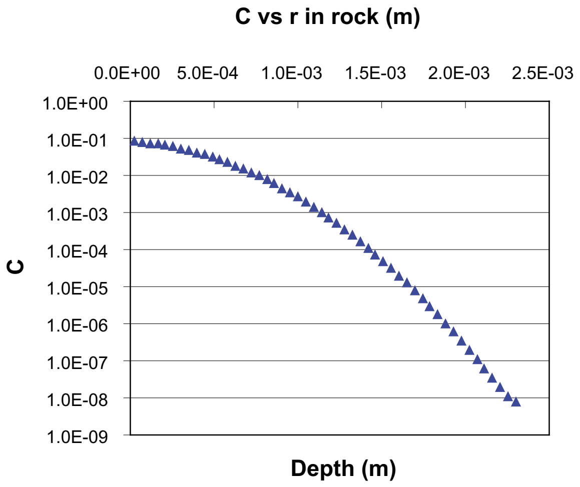

A03:5/Diff III:

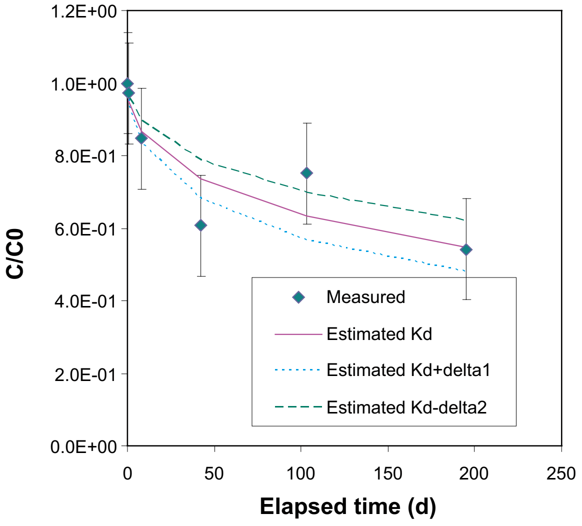

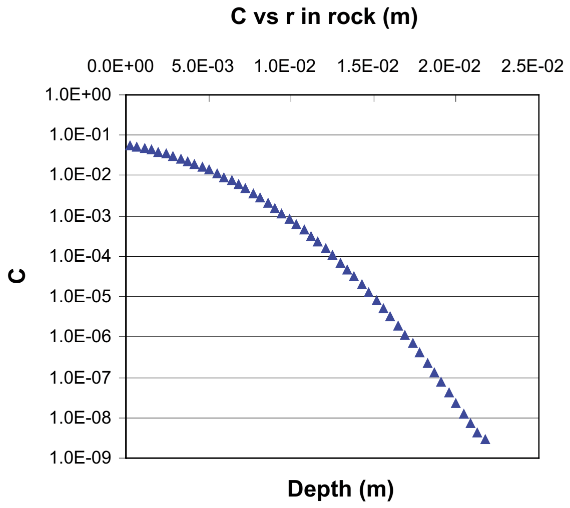

Ni-63 (K_d (m^3/kg) and F_f estimated)

A03:5/Diff I:

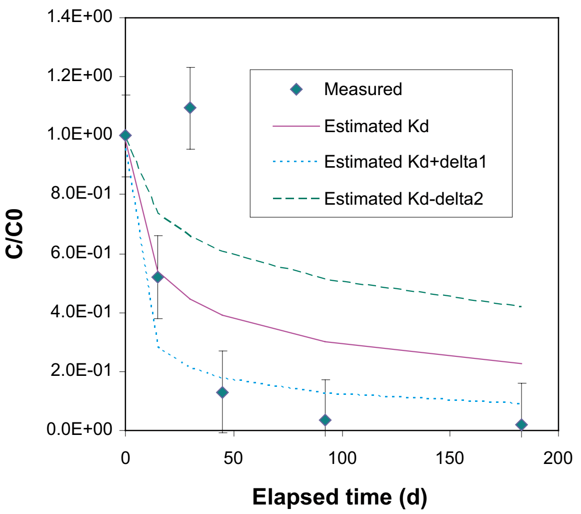

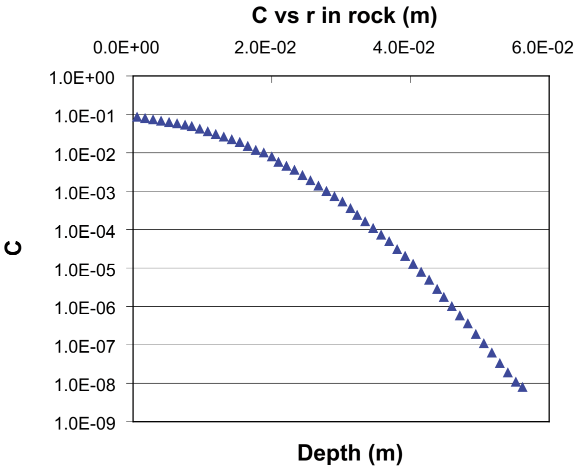

A03:5/Diff III:

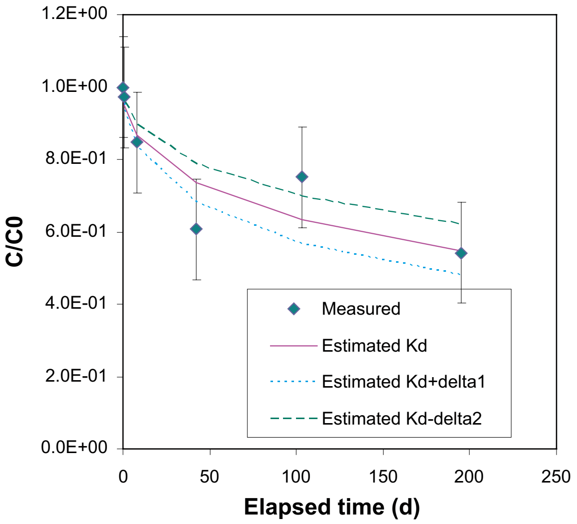

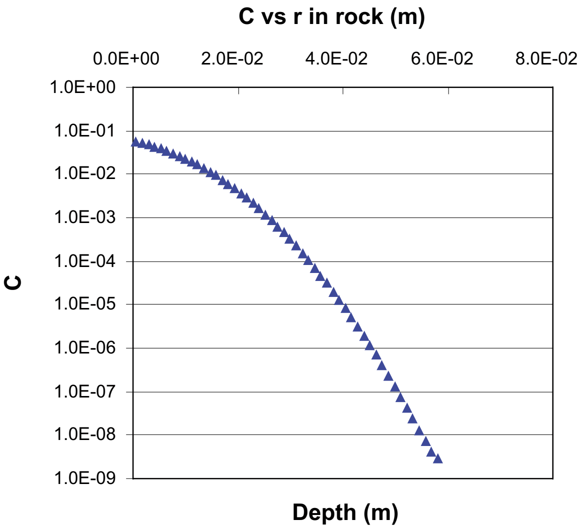

Cd-109 (K_d (m^3/kg) estimated)

A03:5/Diff I:

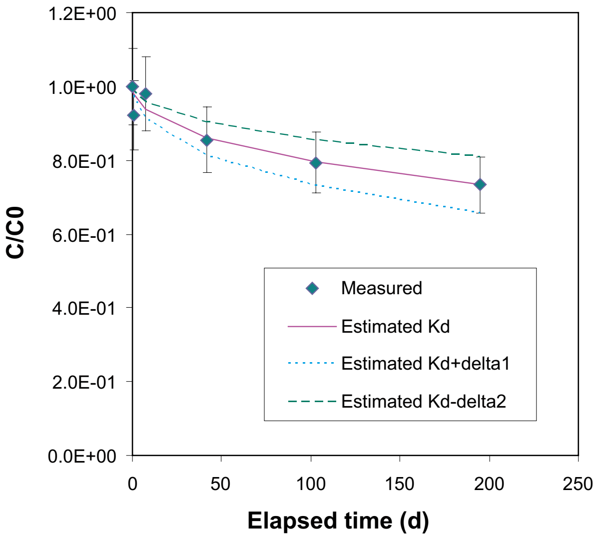

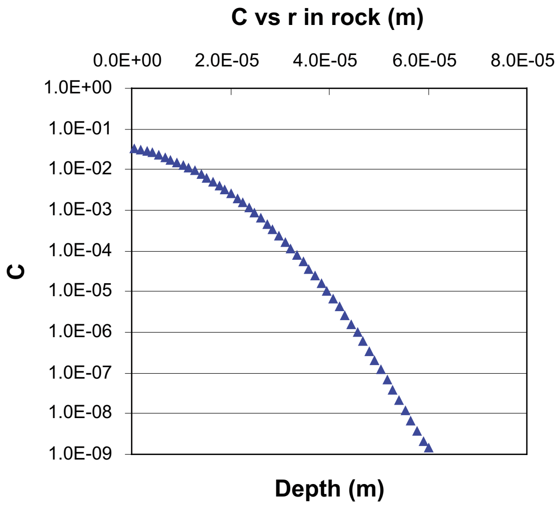

A03:5/Diff III:

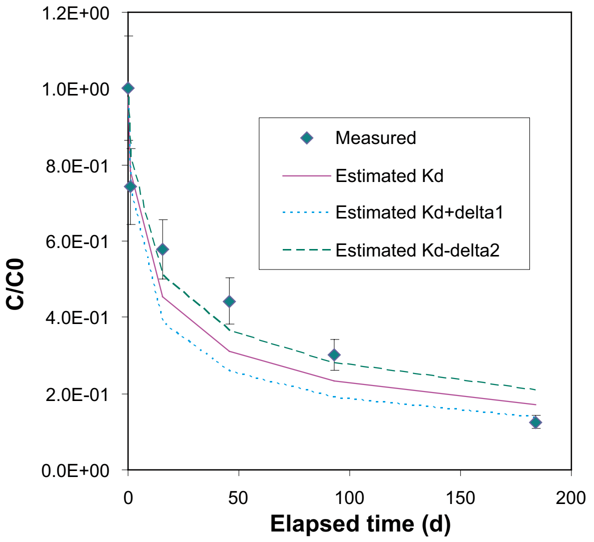

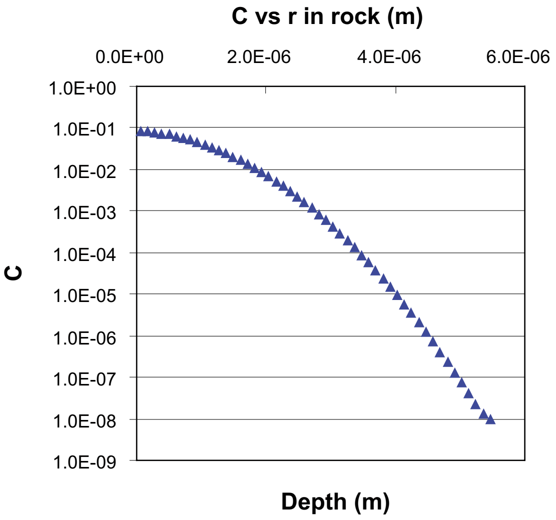

Ba-133 (K_d (m^3/kg) estimated)

A03:5/Diff I:

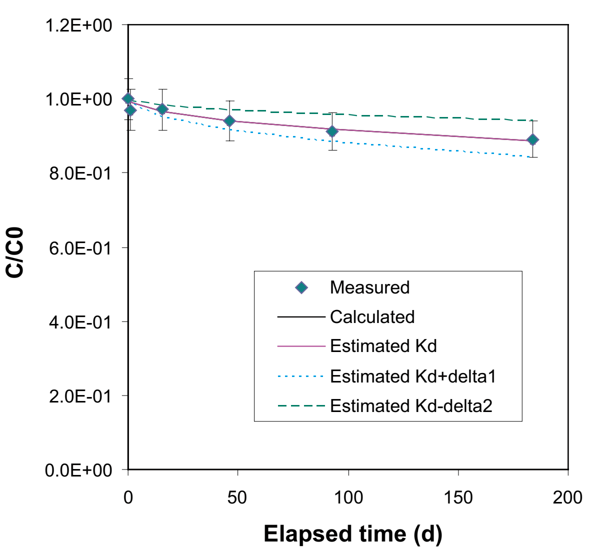

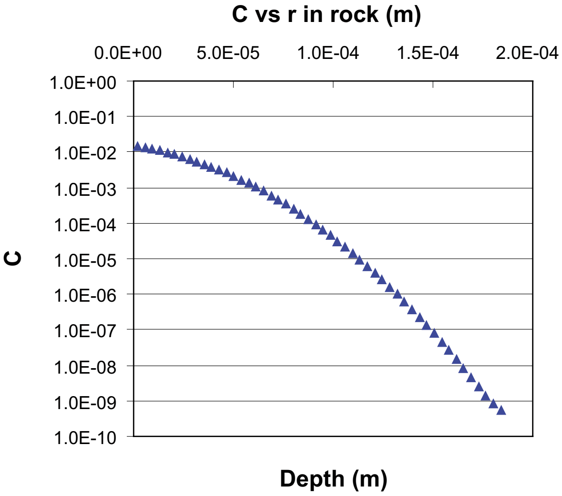

A03:5/Diff III:

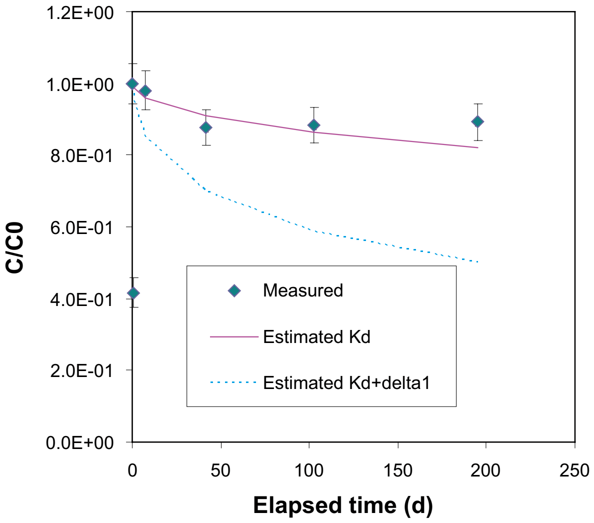

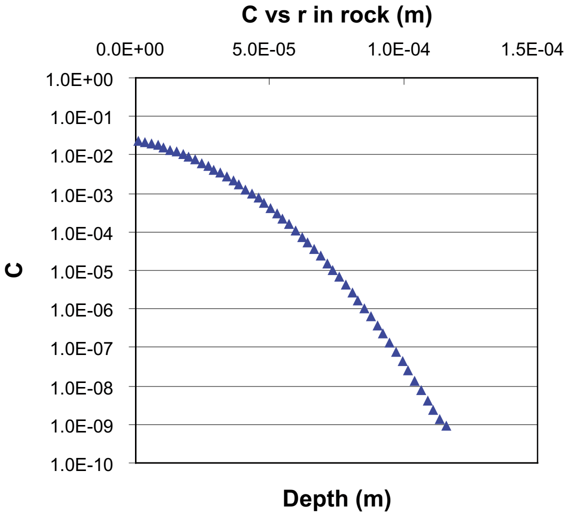

Cs-137 (K_d (m^3/kg) estimated)

A03:5/Diff I:

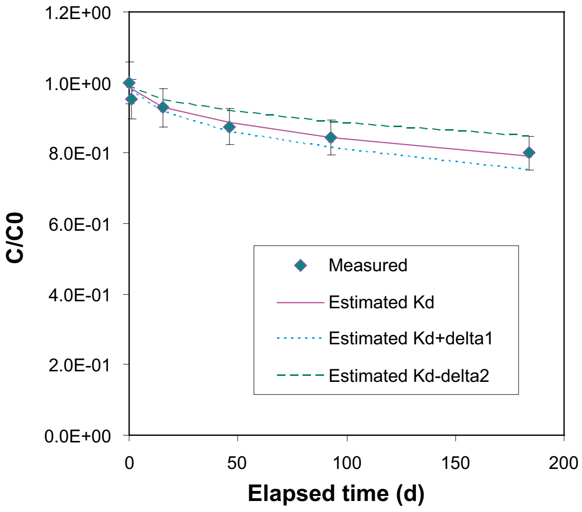

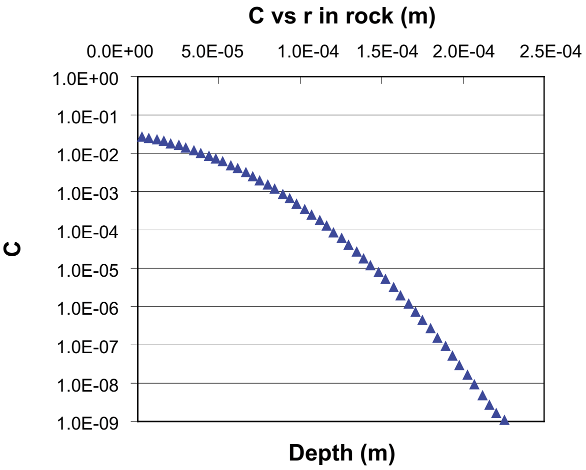

A03:5/Diff III:

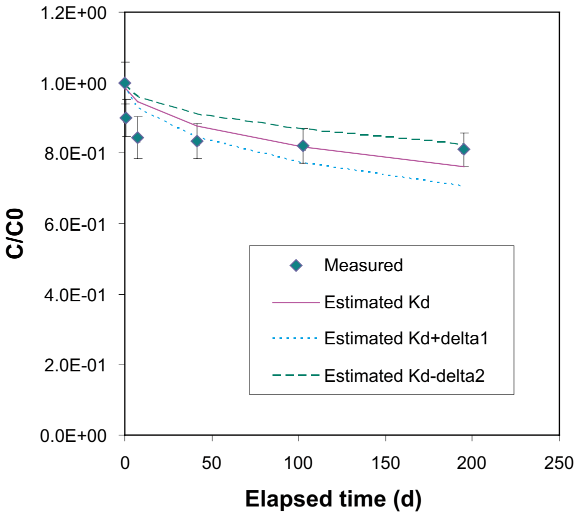

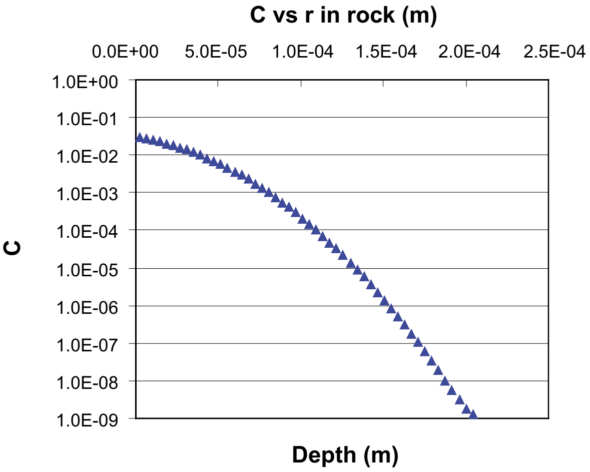

Cs-137 (F_f estimated)

A03:5/Diff I:

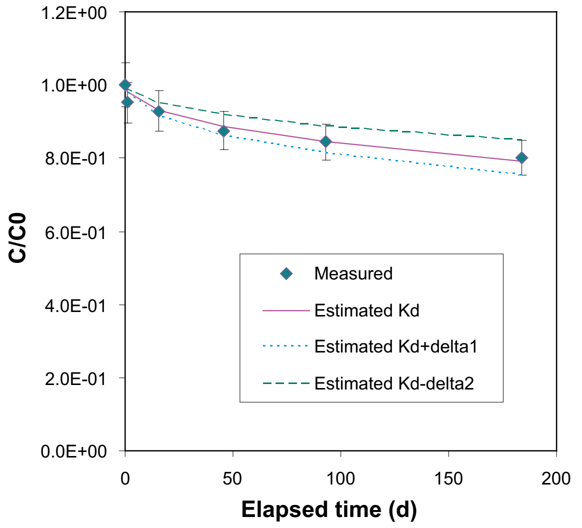

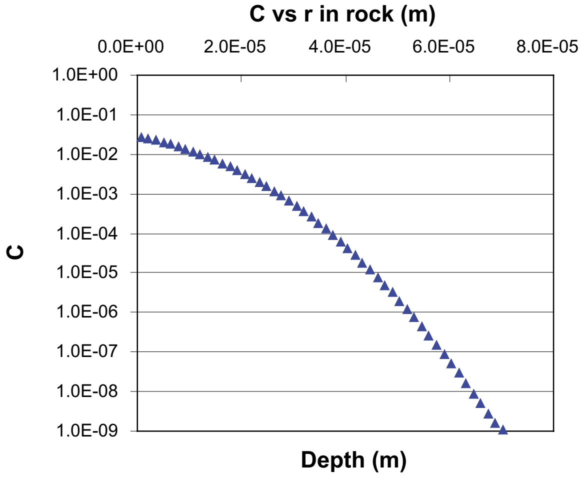

A03:5/Diff III:

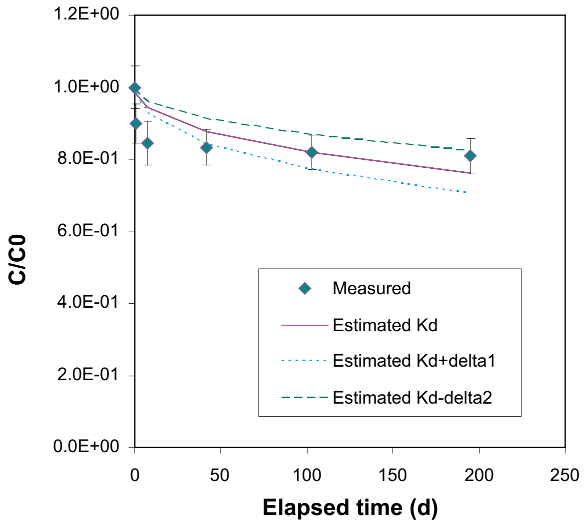

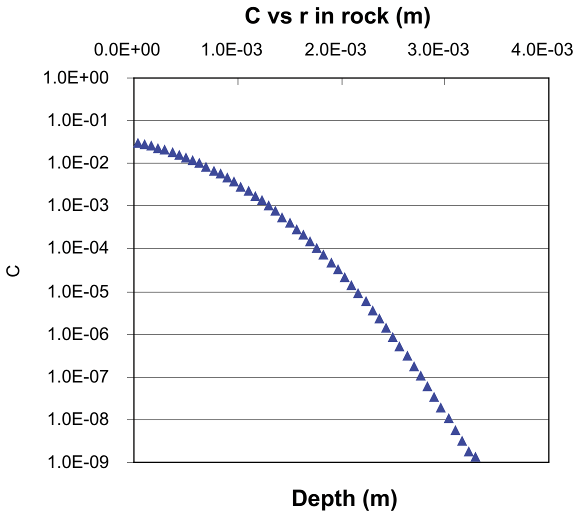

Cs-137 (K_d (m^3/kg) and F_f estimated)

A03:5/Diff I:

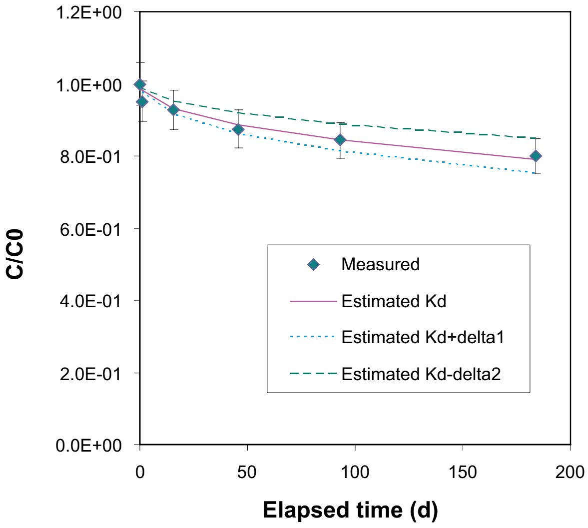

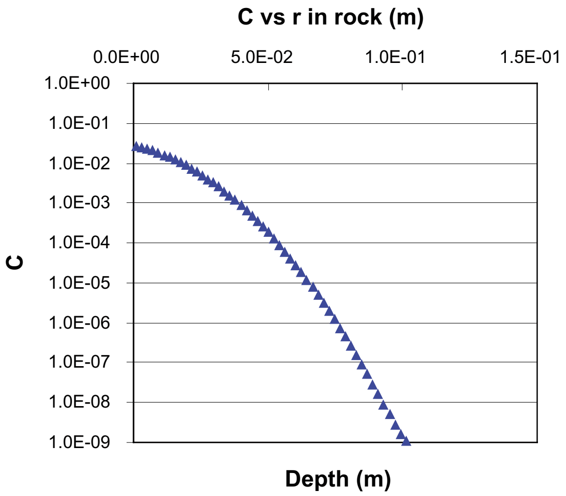

A03:5/Diff III:

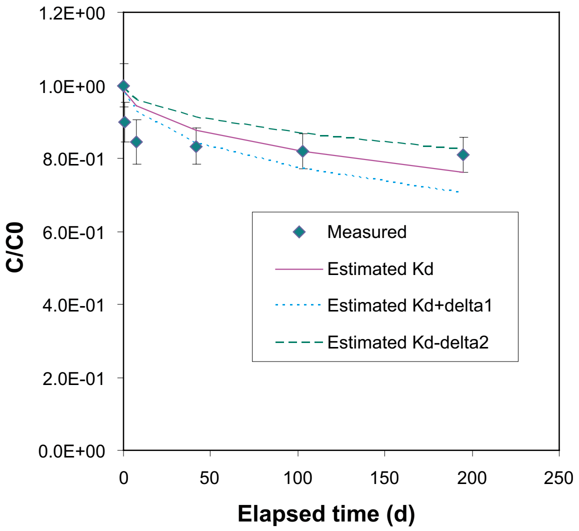

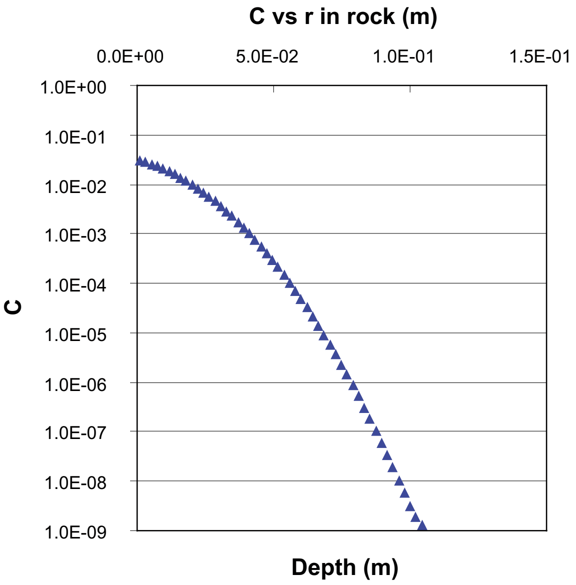

Appendix 10

Estimations for Laxemar and Forsmark samples

Table A10-1. Results from estimation of K_d (m³/kg) with fixed F_f. Sample specific values and rock type mean values have been used for F_f. The shortening "not calc." given in the table should be read "not calculated" and "no conv." should be read "no convergence".

		Sample specific value					Rock type mean value				
Nuclide	Core	F_f	ε	K_d (m³/kg)	delta +	delta –	F_f	ε	K_d (m³/kg)	delta +	delta –
Co-57	KSH01_891.91	5.2E-04	4.6E-03	1.5E+1	2.2E+2	9.9E+0	4.1E-04	3.5E-03	1.8E+1	2.8E+2	1.2E+1
	KSH01_981.43	2.3E-04	2.9E-03	4.1E-02	4.0E-02	2.1E-02	1.1E-04	1.9E-03	8.1E-02	7.9E-02	4.1E-02
	KLX02_235.08	3.2E-04	3.9E-03	3.7E-03	1.8E-03	1.3E-03	1.5E-04	3.2E-03	7.7E-03	3.7E-03	2.8E-03
	KLX04_726.07	no data	8.0E-04	not calc.			1.1E-04	1.9E-03	2.0E-03	2.6E-03	1.4E-03
	KLX08_417.05	4.6E-04	4.5E-03	1.1E-02	9.4E-03	5.4E-03	4.1E-04	3.5E-03	1.2E-02	1.0E-02	6.0E-03
	KLX10_995.78	2.3E-04	6.0E-04	9.8E-03	7.7E-03	4.8E-03	1.1E-04	1.9E-03	2.0E-02	1.5E-02	9.6E-03
	KFM02A 276.06	1.6E-02	1.8E-01	1.0E+0	9.7E+0	6.8E-01	1.2E-02	1.3E-01	1.4E+0	1.3E+1	8.9E-01
	KFM03A_242.43	8.2E-05	1.9E-03	8.3E-04	3.5E-02	no conv.	7.8E-05	1.6E-03	8.7E-04	3.7E-02	no conv.
	KFM07A_608.75	6.7E-04	6.2E-03	7.9E-04	4.8E-04	3.5E-04	1.6E-04	1.0E-02	3.2E-03	2.0E-03	1.4E-03
	KFM09A_713.67	no data	2.4E-03	not calc.			1.6E-04	1.0E-02	4.2E-02	2.9E-02	1.8E-02
Cs-137	KSH01_891.91	5.2E-04	4.6E-03	2.0E-02	5.5E-03	4.2E-03	4.1E-04	3.5E-03	2.5E-02	6.9E-03	5.3E-03
	KSH01_981.43	2.3E-04	2.9E-03	1.4E-01	3.5E-02	2.7E-02	1.1E-04	1.9E-03	2.7E-01	1.9E-01	1.1E-01
	KLX02_235.08	3.2E-04	3.9E-03	2.7E-02	6.6E-03	5.3E-03	1.5E-04	3.2E-03	5.6E-02	1.4E-02	1.1E-02
	KLX04_726.07	no data	8.0E-04	not calc.			1.1E-04	1.9E-03	2.4E-01	1.2E-01	7.6E-02
	KLX08_417.05	4.6E-04	4.5E-03	1.8E-02	7.6E-03	5.3E-03	4.1E-04	3.5E-03	2.0E-02	8.5E-03	5.9E-03
	KLX10_995.78	2.3E-04	6.0E-04	3.9E-02	1.6E-02	1.1E-02	1.1E-04	1.9E-03	7.6E-02	3.1E-02	2.2E-02
	KFM02A 276.06	1.6E-02	1.8E-01	1.2E-02	5.8E-03	3.4E-03	1.2E-02	1.3E-01	1.6E-02	7.6E-03	4.6E-03
	KFM03A_242.43	8.2E-05	1.9E-03	9.9E-02	9.4E-02	4.7E-02	7.8E-05	1.6E-03	1.0E-01	9.9E-02	5.0E-02
	KFM07A_608.75	6.7E-04	6.2E-03	4.6E-03	6.5E-04	8.1E-04	1.6E-04	1.0E-02	1.9E-02	2.6E-03	3.3E-03
	KFM09A_713.67	no data	2.4E-03	not calc.			1.6E-04	1.0E-02	3.1E-02	1.1E-02	8.5E-03
U-236	KSH01_891.91	5.2E-04	4.6E-03	5.4E+0	6.5E+0	2.4E+0	4.1E-04	3.5E-03	6.8E+0	8.1E+0	3.0E+0
	KSH01_981.43	2.3E-04	2.9E-03	1.0E+1	1.5E+1	5.0E+0	1.1E-04	1.9E-03	2.1E+1	3.1E+1	9.8E+0
	KLX02_235.08	3.2E-04	3.9E-03	1.2E+0	5.0E-01	3.2E-01	1.5E-04	3.2E-03	2.5E+0	1.0E+0	6.7E-01
	KLX04_726.07	no data	8.0E-04	not calc.			1.1E-04	1.9E-03	4.6E+0	4.3E+0	1.9E+0

		Sample specific value					Rock type mean value				
Nuclide	**Core**	F_f	ε	K_d (m³/kg)	delta +	delta –	F_f	ε	K_d (m³/kg)	delta +	delta –
	KLX08_417.05	4.6E-04	4.5E-03	2.1E+0	2.6E+0	9.3E-01	4.1E-04	3.5E-03	2.3E+0	2.9E+0	1.0E+0
	KLX10_995.78	2.3E-04	6.0E-04	1.3E+1	2.8E+1	6.7E+0	1.1E-04	1.9E-03	2.5E+1	5.5E+1	1.3E+1
	KFM02A 276.06	1.6E-02	1.8E-01	1.3E+0	4.3E+0	7.6E-01	1.2E-02	1.3E-01	1.8E+0	5.7E+0	1.0E+0
	KFM03A_242.43	8.2E-05	1.9E-03	1.1E+0	1.3E+0	5.3E-01	7.8E-05	1.6E-03	1.2E+0	1.3E+0	5.6E-01
	KFM07A_608.75	6.7E-04	6.2E-03	9.5E-02	5.0E-02	3.1E-02	1.6E-04	1.0E-02	3.9E-01	2.0E-01	1.3E-01
	KFM09A_713.67	no data	2.4E-03	not calc.			1.6E-04	1.0E-02	1.2E+0	2.7E+0	6.9E-01
Ba-133	KSH01_891.91	5.2E-04	4.6E-03	1.4E-04	1.4E-04	8.8E-05	4.1E-04	3.5E-03	1.7E-04	1.7E-04	1.1E-04
	KSH01_981.43	2.3E-04	2.9E-03	5.5E-04	9.8E-04	4.7E-04	1.1E-04	1.9E-03	1.1E-03	1.9E-03	9.2E-04
	KLX02_235.08	3.2E-04	3.9E-03	6.1E-04	4.6E-04	2.2E-04	1.5E-04	3.2E-03	1.3E-03	9.6E-04	4.6E-04
	KLX04_726.07	no data	8.0E-04	not calc.			1.1E-04	1.9E-03	1.8E-06	4.9E-05	no conv.
	KLX08_417.05	4.6E-04	4.5E-03	1.4E-04	1.2E-04	5.6E-05	4.1E-04	3.5E-03	1.5E-04	1.3E-04	6.2E-05
	KLX10_995.78	2.3E-04	6.0E-04	7.1E-06	2.8E-04	no conv.	1.1E-04	1.9E-03	1.4E-05	5.5E-04	no conv.
	KFM02A 276.06	1.6E-02	1.8E-01	3.0E-02	2.8E-02	1.2E-02	1.2E-02	1.3E-01	4.0E-02	3.7E-02	1.6E-02
	KFM03A_242.43	8.2E-05	1.9E-03	6.9E-02	9.9E-02	4.3E-02	7.8E-05	1.6E-03	7.2E-02	1.0E-01	4.5E-02
	KFM07A_608.75	6.7E-04	6.2E-03	4.0E-03	1.8E-03	1.3E-03	1.6E-04	1.0E-02	1.6E-02	7.3E-03	5.4E-03
	KFM09A_713.67	no data	2.4E-03	not calc.			1.6E-04	1.0E-02	5.7E-01	1.8E+0	3.7E-01
Cd-109	KSH01_891.91	5.2E-04	4.6E-03	6.6E-02	3.4E-02	2.2E-02	4.1E-04	3.5E-03	8.2E-02	4.3E-02	2.7E-02
	KSH01_981.43	2.3E-04	2.9E-03	1.3E-02	7.2E-03	5.0E-03	1.1E-04	1.9E-03	2.5E-02	1.4E-02	9.9E-03
	KLX02_235.08	3.2E-04	3.9E-03	5.1E-03	1.6E-03	1.3E-03	1.5E-04	3.2E-03	1.1E-02	3.4E-03	2.8E-03
	KLX04_726.07	no data	8.0E-04	not calc.			1.1E-04	1.9E-03	1.2E-02	3.3E-03	2.8E-03
	KLX08_417.05	4.6E-04	4.5E-03	2.6E-03	1.5E-03	1.1E-03	4.1E-04	3.5E-03	3.0E-03	1.7E-03	1.2E-03
	KLX10_995.78	2.3E-04	6.0E-04	7.4E-03	3.3E-03	2.5E-03	1.1E-04	1.9E-03	1.5E-02	6.6E-03	5.0E-03
	KFM02A 276.06	1.6E-02	1.8E-01	5.4E-03	8.5E-04	7.2E-04	1.2E-02	1.3E-01	7.2E-03	1.1E-03	9.5E-04
	KFM03A_242.43	8.2E-05	1.9E-03	4.0E-03	4.6E-02	4.0E-03	7.8E-05	1.6E-03	4.3E-03	4.9E-02	no conv.
	KFM07A_608.75	6.7E-04	6.2E-03	1.1E-03	1.6E-03	8.2E-04	1.6E-04	1.0E-02	4.6E-03	6.7E-03	3.4E-03
	KFM09A_713.67	no data	2.4E-03	not calc.			1.6E-04	1.0E-02	4.8E-02	1.4E-02	1.1E-02
Na-22	KLX02_235.08	3.2E-04	3.9E-03	2.6E-06	6.6E-05	no conv.	1.5E-04	3.2E-03	7.2E-06	1.4E-04	no conv.
Se-75	KLX02_235.08	3.2E-04	3.9E-03	1.4E-02	5.8E-03	4.3E-03	1.5E-04	3.2E-03	2.8E-02	1.2E-02	9.0E-03
Sr-85	KLX02_235.08	3.2E-04	3.9E-03	2.7E-05	2.4E-04	2.7E-05	1.5E-04	3.2E-03	5.9E-05	5.0E-04	5.9E-05
Tc-99	KLX02_235.08	3.2E-04	3.9E-03	1.0E-10	2.6E-04	no conv.	1.5E-04	3.2E-03	1.0E-10	5.1E-04	no conv.
Ag-110 m	KLX02_235.08	3.2E-04	3.9E-03	1.7E+0	8.2E-01	5.0E-01	1.5E-04	3.2E-03	3.6E+0	1.7E+0	1.0E+0
Sn-113	KLX02_235.08	3.2E-04	3.9E-03	4.3E+1	4.2E+0	3.8E+0	1.5E-04	3.2E-03	9.0E+1	8.9E+0	7.9E+0
Np-237	KLX02_235.08	3.2E-04	3.9E-03	1.1E-02	1.0E-02	6.2E-03	1.5E-04	3.2E-03	2.4E-02	2.2E-02	1.3E-02

Table A10-2. Results from estimation of F_f with fixed rock type mean value of K_d (m^3/kg) and ε*) (see Table 4-7). The shortening "not calc." given in the table should be read "not calculated".

Nuclide	Core	Rock type mean value K_d (m^3/kg)	F_f	Δ +	Δ –
Cs-137	KSH01_891.91	2,9E-02	3.5E-04	9.8E-05	7.6E-05
	KSH01_981.43	2,4E-02	1.3E-03	9.1E-04	5.0E-04
	KLX02_235.08	5,5E-03	1.6E-03	3.8E-04	3.1E-04
	KLX04_726.07	2,4E-02	1.1E-03	5.8E-04	3.6E-04
	KLX08_417.05	2,9E-02	2.8E-04	1.2E-04	8.4E-05
	KLX10_995.78	2,4E-02	3.6E-04	1.5E-04	1.0E-04
	KFM02A 276.06	2,0E-03	9.2E-02	4.5E-02	2.7E-02
	KFM03A_242.43	8,4E-03	9.7E-04	9.2E-04	4.6E-04
	KFM07A_608.75	4,0E-03	7.7E-04	1.1E-04	1.4E-04
	KFM09A_713.67	4,0E-03	1.3E-03	4.7E-04	3.5E-04
U-236	KSH01_891.91	4,0E-03	7.0E-01	8.3E-01	3.1E-01
	KSH01_981.43	1,2E-02	1.9E-01	2.8E-01	9.0E-02
	KLX02_235.08	no data	not calc.		
	KLX04_726.07	1,2E-02	4.2E-02	3.9E-02	1.7E-02
	KLX08_417.05	4,0E-03	2.4E-01	2.9E-01	1.1E-01
	KLX10_995.78	1,2E-02	2.3E-01	5.0E-01	1.2E-01
	KFM02A 276.06	no data	not calc.		
	KFM03A_242.43	no data	not calc.		
	KFM07A_608.75	7,8E-04	8.0E-02	4.2E-02	2.6E-02
	KFM09A_713.67	7,8E-04	2.5E-01	5.6E-01	1.4E-01

*) For U-236 ε was allowed to vary in the modelling. As this tracer is insensitive to the porosity it did not have any effect on the results.

Table A10-3. Results from calculation of $K_d \cdot F_f$ (m^3/kg) for Ävrö granodiorite, both from experimental data and estimated (fitted) data, for various tracers.

Nuclide	K_d (1–2 mm fraction) (m^3/kg)	F_f (H^3HO)	K_d (1–2 mm fraction) · F_f (H^3HO) (m^3/kg)	K_d (estimated) · F_f (estimated) (m^3/kg)
Na-22	2,9E-04	3,2E-04	9.3E-08	1.9E-09
Co-57	5,0E-02	3,2E-04	1.6E-05	1.2E-06
Se-75	1,6E-03	3,2E-04	5.2E-07	4.3E-06
Sr-85				8.4E-10
Tc-99	2,3E-04	3,2E-04	7.3E-08	3.8E-04
Cd-109	5,1E-03	3,2E-04	1.6E-06	1.6E-06
Ag-110 m				5.4E-04
Sn-113				1.4E-02
Ba-133	2,1E-03	3,2E-04	6.8E-07	1.9E-07
Cs-137	2,2E-02	3,2E-04	7.0E-06	8.6E-06
U-236	1,2E-03	3,2E-04	3.9E-07	3.8E-04
Np-237	8,3E-04	3,2E-04	2.6E-07	3.6E-06

Table A10-4. Results from calculation of $K_d \cdot F_f$ for Cs-137, both from experimental data and estimated (fitted) data, for various cores.

Core	K_d (m^3/kg)	F_f (H^3HO)	K_d (1–2 mm fraction)· F_f (H^3H O) (m^3/kg)	K_d (estimated)·F_f (estimated) (m^3/kg)
KSH01_891.91	2.9E-02	4.1E-04	1.2E-05	1.0E-05
KSH01_981.43	2.4E-02	1.1E-04	2.7E-06	3.1E-05
KLX02_235.08	5.5E-03	1.5E-04	8.3E-07	8.6E-06
KLX04_726.07	2.4E-02	1.1E-04	2.7E-06	2.7E-05
KLX08_417.05	2.9E-02	4.1E-04	1.2E-05	8.1E-06
KLX10_995.78	2.4E-02	1.1E-04	2.7E-06	8.7E-06
KFM02A 276.06	2.0E-03	1.2E-02	2.4E-05	1.9E-04
KFM03A_242.43	8.4E-03	7.8E-05	6.5E-07	8.1E-06
KFM07A_608.75	4.0E-03	1.6E-04	6.5E-07	3.1E-06
KFM09A_713.67	4.0E-03	1.6E-04	6.5E-07	5.1E-06

Table A10-5. Results from calculation of $K_d \cdot F_f$ for U-236, both from experimental data and estimated (fitted) data, for various cores.

Core	K_d (1–2 mm fraction) (m^3/kg)	F_f (meas)	K_d (1–2 mm fraction) · F_f (H^3H O) (m^3/kg)	K_d (estimated) · F_f (estimated) (m^3/kg)
KSH01_891.91	4,01E-03	4,01E-03	1,6E-05	2,8E-03
KSH01_981.43	1,25E-02	1,25E-02	1,6E-04	2,4E-03
KLX02_235.08	1,22E-03			3,8E-04
KLX04_726.07	1,25E-02	1,25E-02	1,6E-04	5,2E-04
KLX08_417.05	4,01E-03	4,01E-03	1,6E-05	9,5E-04
KLX10_995.78	1,25E-02	1,25E-02	1,6E-04	2,8E-03
KFM02A 276.06				2,1E-02
KFM03A_242.43				9,4E-05
KFM07A_608.75	7,84E-04	7,84E-04	6,1E-07	6,3E-05
KFM09A_713.67	7,84E-04	7,84E-04	6,1E-07	2,0E-04

Appendix 11

Results from the batch sorption experiments

Table A11-1. R_d (m^3/kg), results from the batch sorption experiments.
Na-22

Contact time (d)	1.0		7.0		31.0		90.0		186.0	
Core	**R_d (m^3/kg)**	**+/–**	**R_d (m^3/kg)**	**+/–**	**R_d (m^3/kg)**	**+/–**	**R_d (m^3/kg)**	**+/–**	**R_d (m^3/kg)**	**+/–**
KA3065A02:1_A_1(2)	–5.6E-04	1.7E-04	3.9E-04	1.8E-04	3.6E-04	3.0E-04	8.6E-04	3.0E-04	1.6E-04	2.6E-04
KA3065A02:1_A_2(2)	–3.5E-04	1.8E-04	–5.6E-04	1.5E-04	1.7E-04	2.8E-04	–2.4E-04	2.3E-04	2.2E-04	2.7E-04
KA3065A02:1_B_1(2)	–4.9E-04	1.8E-04	2.6E-04	1.8E-04	2.7E-04	3.0E-04	2.8E-04	2.7E-04	1.8E-04	2.7E-04
KA3065A02:1_B_2(2)	–5.7E-04	1.7E-04	6.0E-04	1.9E-04	4.7E-04	3.1E-04	2.0E-04	2.6E-04	3.7E-04	2.8E-04
KA3065A02:1_C_1(2)	–1.6E-04	1.9E-04	-1.8E-04	1.6E-04	1.0E-06	2.8E-04	4.6E-05	2.6E-04	1.8E-04	2.7E-04
KA3065A02:1_C_2(2)	–3.5E-04	1.8E-04	3.7E-04	1.8E-04	5.6E-04	3.1E-04	5.2E-04	2.8E-04	1.6E-04	2.6E-04
KA3065A02:2_A_1(2)	–1.8E-04	5.9E-04	-2.8E-04	9.3E-04	–1.3E-04	6.5E-04	–5.6E-04	2.5E-04	1.2E-04	8.3E-04
KA3065A02:2_A_2(2)	4.7E-04	6.5E-04	9.5E-05	9.7E-04	–1.3E-05	6.4E-04	–1.4E-05	2.7E-04	5.0E-04	8.7E-04
KA3065A02:2_B_1(2)	1.2E-04	5.9E-04	2.4E-04	9.8E-04	1.2E-04	6.4E-04	–3.1E-04	2.5E-04	5.1E-04	8.5E-04
KA3065A02:2_B_2(2)	–3.5E-04	5.6E-04	1.7E-04	1.0E-03	3.4E-04	7.1E-04	–1.7E-04	2.7E-04	–1.0E-04	7.8E-04
KA3065A02:2_C_1(2)	–5.2E-05	1.9E-04	-1.3E-05	1.6E-04	5.6E-04	3.0E-04	4.9E-04	2.7E-04	6.3E-04	2.8E-04
KA3065A02:2_C_2(2)	–4.7E-04	1.7E-04	2.9E-04	1.7E-04	3.0E-05	2.7E-04	6.5E-04	2.8E-04	3.8E-05	2.5E-04
KA3065A02:6_A_1(2)	–8.4E-05	1.9E-04	–1.4E-04	1.6E-04	1.3E-06	2.7E-04	–8.1E-05	2.4E-04	–1.0E-05	2.4E-04
KA3065A02:6_A_2(2)	8.8E-05	2.0E-04	6.1E-04	1.9E-04	5.7E-04	3.1E-04	3.1E-04	2.7E-04	–5.4E-05	2.5E-04
KA3065A02:6_B_1(2)	–1.6E-05	1.9E-04	8.8E-04	2.0E-04	5.7E-04	3.1E-04	8.7E-04	3.0E-04	3.2E-04	2.7E-04
KA3065A02:6_B_2(2)	–3.6E-04	1.7E-04	2.5E-04	1.7E-04	2.0E-04	2.8E-04	1.4E-04	2.5E-04	–5.5E-05	2.4E-04
KA3065A02:6_C_1(2)	–3.6E-05	1.8E-04	8.5E-04	1.9E-04	9.4E-05	2.7E-04	–6.3E-05	2.3E-04	8.4E-05	2.5E-04
KA3065A02:6_C_2(2)	–4.5E-04	1.7E-04	–6.0E-05	1.6E-04	3.4E-05	2.6E-04	–5.4E-05	2.3E-04	7.5E-04	2.9E-04
KA3065A03_Batch 1_A_1(2)	–6.0E-04	1.7E-04	–2.2E-04	1.6E-04	2.2E-04	2.9E-04	–3.0E-04	2.3E-04	–1.0E-04	2.5E-04
KA3065A03_Batch 1_A_2(2)	–6.4E-04	1.7E-04	3.6E-05	1.7E-04	7.4E-05	2.8E-04	–1.9E-04	2.4E-04	–1.1E-05	2.5E-04
KA3065A03_Batch 1_B_1(2)	–2.8E-04	1.8E-04	–8.8E-05	1.6E-04	3.5E-04	2.9E-04	3.1E-04	2.6E-04	1.9E-04	2.6E-04
KA3065A03_Batch 1_B_2(2)	–5.8E-04	1.7E-04	–1.8E-04	1.6E-04	–2.2E-04	2.6E-04	–3.5E-04	2.3E-04	–1.3E-04	2.5E-04
KA3065A03_Batch 1_C_1(2)	–4.2E-04	1.8E-04	1.1E-04	1.7E-04	4.3E-04	3.0E-04	2.4E-04	2.6E-04	4.2E-05	2.6E-04
KA3065A03_Batch 1_C_2(2)	–2.4E-04	1.8E-04	3.4E-04	1.8E-04	4.6E-04	3.0E-04	–8.1E-05	2.4E-04	5.3E-04	2.8E-04
KA3065A03_Replica_A_1(2)	–1.5E-04	5.8E-04	–2.6E-05	9.7E-04	6.3E-06	6.6E-04	–1.7E-04	2.7E-04	–2.0E-04	7.5E-04
KA3065A03_Replica_A_2(2)	–7.8E-04	4.7E-04	–4.7E-04	8.3E-04	–3.9E-04	5.7E-04	–1.1E-03	1.9E-04	–7.1E-04	6.2E-04
KA3065A03_Replica_B_1(2)	1.1E-03	7.5E-04	1.2E-03	1.2E-03	5.7E-04	7.4E-04	6.8E-04	3.3E-04	9.0E-04	9.7E-04
KA3065A03_Replica_B_2(2)	6.2E-04	6.7E-04	3.0E-04	1.0E-03	2.3E-05	6.4E-04	3.5E-06	2.7E-04	3.4E-04	8.4E-04
KA3065A03_Replica_C_1(2)	–2.6E-04	1.8E-04	2.0E-04	1.7E-04	5.4E-04	3.1E-04	1.5E-04	2.6E-04	7.1E-05	2.6E-04
KA3065A03_Replica_C_2(2)	–4.4E-04	1.7E-04	–9.4E-05	1.6E-04	1.4E-04	2.8E-04	–3.6E-04	2.2E-04	–2.6E-04	2.3E-04

Table A11-1. R_d (m^3/kg) results from the batch sorption experiments (Continued).
Cl-36

Contact time (d)	1.0		7.0		31.0		90.0		186.0	
Core	**R_d (m^3/kg)**	**+/–**	**R_d (m^3/kg)**	**+/–**	**R_d (m^3/kg)**	**+/–**	**R_d (m^3/kg)**	**+/–**	**R_d (m^3/kg)**	**+/–**
KA3065A02:1_A_1(2)										
KA3065A02:1_A_2(2)										
KA3065A02:1_B_1(2)										
KA3065A02:1_B_2(2)										
KA3065A02:1_C_1(2)										
KA3065A02:1_C_2(2)										
KA3065A02:2_A_1(2)										
KA3065A02:2_A_2(2)										
KA3065A02:2_B_1(2)										
KA3065A02:2_B_2(2)										
KA3065A02:2_C_1(2)										
KA3065A02:2_C_2(2)										
KA3065A02:6_A_1(2)										
KA3065A02:6_A_2(2)										
KA3065A02:6_B_1(2)										
KA3065A02:6_B_2(2)										
KA3065A02:6_C_1(2)										
KA3065A02:6_C_2(2)										
KA3065A03_Batch 1_A_1(2)	–1.8E-04	6.5E-04							–1.8E-04	6.1E-04
KA3065A03_Batch 1_A_2(2)										
KA3065A03_Batch 1_B_1(2)										
KA3065A03_Batch 1_B_2(2)										
KA3065A03_Batch 1_C_1(2)	3.9E-04	7.6E-04							–8.2E-05	6.3E-04
KA3065A03_Batch 1_C_2(2)										
KA3065A03_Replica_A_1(2)										
KA3065A03_Replica_A_2(2)										
KA3065A03_Replica_B_1(2)										
KA3065A03_Replica_B_2(2)										
KA3065A03_Replica_C_1(2)	1.6E-04	7.3E-04							–1.9E-04	6.2E-04
KA3065A03_Replica_C_2(2)										

Table A11-1. R_d (m^3/kg) results from the batch sorption experiments (Continued).
Co-57

Contact time (d)	1.0		7.0		31.0		90.0		186.0	
Core	**R_d (m^3/kg)**	**+/–**	**R_d (m^3/kg)**	**+/–**	**R_d (m^3/kg)**	**+/–**	**R_d (m^3/kg)**	**+/–**	**R_d (m^3/kg)**	**+/–**
KA3065A02:1_A_1(2)	–5.5E-04	5.9E-04	5.8E-03	1.2E-03	2.9E-02	6.8E-03	1.2E-01	1.6E-02	1.6E-01	1.5E-02
KA3065A02:1_A_2(2)	–5.4E-05	6.6E-04	4.6E-03	1.1E-03	3.0E-02	6.9E-03	8.9E-02	1.2E-02	1.5E-01	1.4E-02
KA3065A02:1_B_1(2)	–8.6E-04	5.5E-04	4.5E-03	1.0E-03	1.8E-02	4.6E-03	5.6E-02	7.5E-03	9.7E-02	8.5E-03
KA3065A02:1_B_2(2)	–7.2E-04	5.7E-04	5.5E-03	1.2E-03	1.9E-02	4.7E-03	5.1E-02	6.8E-03	9.1E-02	8.0E-03
KA3065A02:1_C_1(2)	–7.6E-04	5.7E-04	1.6E-03	7.1E-04	7.8E-03	2.5E-03	2.3E-02	3.3E-03	4.7E-02	4.1E-03
KA3065A02:1_C_2(2)	–2.9E-04	6.3E-04	4.1E-03	1.0E-03	1.3E-02	3.5E-03	3.4E-02	4.7E-03	5.7E-02	5.0E-03
KA3065A02:2_A_1(2)	9.7E-03	2.2E-03	1.0E-01	2.3E-02	2.4E-01	4.5E-02	3.0E-01	5.8E-02	5.8E-02	1.5E-02
KA3065A02:2_A_2(2)	2.1E-02	3.9E-03	1.3E-01	2.9E-02	3.1E-01	6.0E-02	5.5E-01	1.2E-01	5.6E-01	1.4E-01
KA3065A02:2_B_1(2)	1.1E-02	2.4E-03	9.2E-02	2.0E-02	2.3E-01	4.3E-02	3.2E-01	6.2E-02	5.9E-01	1.6E-01
KA3065A02:2_B_2(2)	1.4E-02	2.8E-03	1.1E-01	2.4E-02	2.5E-01	4.7E-02	3.1E-01	5.8E-02	4.9E-01	1.4E-01
KA3065A02:2_C_1(2)	1.4E-03	8.7E-04	1.3E-02	2.0E-03	7.2E-02	1.5E-02	1.6E-01	2.1E-02	2.7E-01	2.9E-02
KA3065A02:2_C_2(2)	6.4E-04	7.5E-04	1.7E-02	2.5E-03	6.9E-02	1.5E-02	2.3E-01	3.2E-02	2.7E-01	2.9E-02
KA3065A02:6_A_1(2)	3.6E-04	7.1E-04	8.3E-03	1.5E-03	6.4E-02	1.4E-02	2.9E-01	4.4E-02	5.8E-01	1.1E-01
KA3065A02:6_A_2(2)	5.3E-04	7.5E-04	9.1E-03	1.6E-03	6.3E-02	1.4E-02	3.0E-01	4.3E-02	3.3E-01	4.0E-02
KA3065A02:6_B_1(2)	–1.9E-04	6.4E-04	6.3E-03	1.3E-03	2.5E-02	5.9E-03	8.5E-02	1.1E-02	1.2E-01	1.1E-02
KA3065A02:6_B_2(2)	–6.0E-04	5.6E-04	6.1E-03	1.2E-03	3.1E-02	7.0E-03	9.2E-02	1.2E-02	1.2E-01	1.1E-02
KA3065A02:6_C_1(2)	–4.4E-04	5.8E-04	3.5E-03	9.0E-04	8.2E-03	2.5E-03	2.3E-02	3.3E-03	5.1E-02	4.5E-03
KA3065A02:6_C_2(2)	–8.9E-04	5.1E-04	2.0E-03	7.3E-04	8.5E-03	2.5E-03	2.6E-02	3.7E-03	7.1E-02	6.0E-03
KA3065A03_Batch 1_A_1(2)	–3.6E-04	6.2E-04	6.9E-03	1.3E-03	1.0E-01	2.2E-02	5.9E-01	1.1E-01	5.1E-01	8.7E-02
KA3065A03_Batch 1_A_2(2)	–5.3E-04	5.9E-04	7.2E-03	1.4E-03	1.0E-01	2.1E-02	5.9E-01	1.2E-01	1.3E+0	4.2E-01
KA3065A03_Batch 1_B_1(2)	–5.0E-04	5.8E-04	3.2E-03	8.8E-04	1.4E-02	3.7E-03	4.4E-01	8.7E-02	7.8E-02	6.9E-03
KA3065A03_Batch 1_B_2(2)	–6.8E-04	5.7E-04	3.5E-03	9.4E-04	1.5E-02	3.9E-03	4.5E-01	9.7E-02	7.6E-02	6.7E-03
KA3065A03_Batch 1_C_1(2)	–8.8E-04	5.4E-04	2.0E-03	7.5E-04	7.8E-03	2.4E-03	1.9E-02	2.8E-03	3.5E-02	3.1E-03
KA3065A03_Batch 1_C_2(2)	–8.2E-04	5.4E-04	2.2E-03	7.7E-04	7.2E-03	2.3E-03	1.5E-02	2.4E-03	3.7E-02	3.3E-03
KA3065A03_Replica_A_1(2)	3.2E-02	5.6E-03	2.1E-01	4.5E-02	5.4E-01	1.2E-01	7.5E-01	1.8E-01	6.4E-01	1.9E-01
KA3065A03_Replica_A_2(2)	3.2E-02	5.5E-03	2.7E-01	6.0E-02	3.4E-01	6.7E-02	4.3E-01	1.0E-01	1.2E+0	4.2E-01
KA3065A03_Replica_B_1(2)	2.8E-02	5.0E-03	2.6E-01	5.8E-02	6.0E-01	1.4E-01	6.8E-01	1.6E-01	6.8E-01	1.9E-01
KA3065A03_Replica_B_2(2)	2.7E-02	4.7E-03	2.9E-01	6.5E-02	6.4E-01	1.4E-01	5.5E-01	1.3E-01	> 1E+0	
KA3065A03_Replica_C_1(2)	3.3E-03	1.2E-03	5.4E-02	7.0E-03	3.3E-01	7.2E-02	4.7E-01	7.9E-02	5.9E-01	1.0E-01
KA3065A03_Replica_C_2(2)	1.9E-03	9.5E-04	4.5E-02	5.9E-03	2.5E-01	5.4E-02	3.6E-01	5.9E-02	4.7E-01	7.5E-02

Table A11-1. R_d (m^3/kg) results from the batch sorption experiments (Continued).
Ni-63

Contact time (d)	1.0		7.0		31.0		90.0		186.0	
Core	R_d (m^3/kg)	+/–	R_d (m^3/kg)	+/–	R_d (m^3/kg)	+/–	R_d (m^3/kg)	+/–	R_d (m^3/kg)	+/–
KA3065A02:1_A_1(2)									5.1E-02	1.77E-02
KA3065A02:1_A_2(2)										
KA3065A02:1_B_1(2)										
KA3065A02:1_B_2(2)										
KA3065A02:1_C_1(2)									2.5E-02	9.1E-03
KA3065A02:1_C_2(2)										
KA3065A02:2_A_1(2)										
KA3065A02:2_A_2(2)										
KA3065A02:2_B_1(2)										
KA3065A02:2_B_2(2)										
KA3065A02:2_C_1(2)									4.6E-02	1.6E-02
KA3065A02:2_C_2(2)										
KA3065A02:6_A_1(2)									1.0E-01	3.8E-02
KA3065A02:6_A_2(2)										
KA3065A02:6_B_1(2)										
KA3065A02:6_B_2(2)										
KA3065A02:6_C_1(2)									1.3E-02	5.1E-03
KA3065A02:6_C_2(2)										
KA3065A03_Batch 1_A_1(2)	–7.6E-05	1.3E-03							6.5E-02	2.3E-02
KA3065A03_Batch 1_A_2(2)										
KA3065A03_Batch 1_B_1(2)										
KA3065A03_Batch 1_B_2(2)										
KA3065A03_Batch 1_C_1(2)	–4.4E-04	1.2E-03	8.1E-05	1.3E-03	4.5E-03	2.6E-03	5.9E-03	3.0E-03	8.2E-03	3.7E-03
KA3065A03_Batch 1_C_2(2)										
KA3065A03_Replica_A_1(2)	1.8E-02	6.8E-03							4.1E-01	2.0E-01
KA3065A03_Replica_A_2(2)										
KA3065A03_Replica_B_1(2)										
KA3065A03_Replica_B_2(2)										
KA3065A03_Replica_C_1(2)	2.0E-03	1.9E-03	2.1E-02	7.7E-03	1.1E-01	3.9E-02	2.1E-01	8.4E-02	2.7E-01	1.2E-01
KA3065A03_Replica_C_2(2)										

Table A11-1. R_d (m^3/kg) results from the batch sorption experiments (Continued).
Se-75

Contact time (d)	1.0		7.0		31.0		90.0		186.0	
Core	R_d (m^3/kg)	+/–	R_d (m^3/kg)	+/–	R_d (m^3/kg)	+/–	R_d (m^3/kg)	+/–	R_d (m^3/kg)	+/–
KA3065A02:1_A_1(2)	3.7E-04	3.1E-03	1.9E-03	2.1E-03	2.1E-03	3.1E-03	4.3E-03	1.0E-03	4.0E-03	1.7E-03
KA3065A02:1_A_2(2)	3.1E-04	3.1E-03	–3.0E-04	1.3E-03	1.8E-03	3.0E-03	2.8E-03	8.6E-04	3.9E-03	1.7E-03
KA3065A02:1_B_1(2)	–9.0E-04	2.3E-03	7.1E-04	1.7E-03	1.5E-03	2.8E-03	7.8E-04	6.1E-04	1.8E-03	1.3E-03
KA3065A02:1_B_2(2)	3.2E-03	5.0E-03	2.4E-04	1.5E-03	4.0E-03	4.1E-03	1.6E-03	6.7E-04	7.6E-03	2.6E-03
KA3065A02:1_C_1(2)	8.5E-04	3.5E-03	–7.2E-04	1.2E-03	4.8E-04	2.4E-03	1.6E-05	4.9E-04	2.7E-03	1.5E-03
KA3065A02:1_C_2(2)	–2.1E-04	2.8E-03	–7.3E-04	1.2E-03	4.4E-03	4.3E-03	8.1E-04	5.9E-04	5.6E-04	9.9E-04
KA3065A02:2_A_1(2)	3.5E-03	6.2E-03	1.1E-03	1.2E-03	2.7E-03	4.2E-03	2.8E-03	2.2E-03	1.6E-02	1.3E-02
KA3065A02:2_A_2(2)	4.4E-03	6.9E-03	1.2E-03	1.2E-03	2.4E-03	3.9E-03	–1.5E-04	1.2E-03	2.2E-03	3.7E-03
KA3065A02:2_B_1(2)	8.7E-04	3.9E-03	1.3E-03	1.1E-03	3.8E-03	4.7E-03	–6.7E-05	1.2E-03	4.3E-03	5.0E-03
KA3065A02:2_B_2(2)	–1.1E-03	2.6E-03	4.7E-03	2.0E-03	1.3E-03	3.3E-03	1.9E-03	1.9E-03	> 1E-02	
KA3065A02:2_C_1(2)	–8.2E-04	2.3E-03	–7.8E-04	1.1E-03	1.7E-03	2.9E-03	2.1E-03	7.1E-04	7.0E-03	2.3E-03
KA3065A02:2_C_2(2)	–2.3E-04	2.6E-03	8.8E-04	1.7E-03	2.3E-03	3.1E-03	2.0E-03	7.0E-04	3.5E-03	1.6E-03
KA3065A02:6_A_1(2)	–6.0E-04	2.4E-03	–6.0E-05	1.4E-03	1.1E-03	2.5E-03	1.0E-03	6.1E-04	3.6E-03	1.6E-03
KA3065A02:6_A_2(2)	3.3E-03	5.1E-03	1.6E-03	1.9E-03	1.5E-03	2.8E-03	4.0E-03	1.0E-03	6.1E-03	2.1E-03
KA3065A02:6_B_1(2)	–1.3E-03	2.1E-03	–9.8E-04	1.1E-03	1.0E-03	2.6E-03	3.0E-04	5.3E-04	2.6E-03	1.4E-03
KA3065A02:6_B_2(2)	–1.3E-03	2.0E-03	-8.4E-04	1.1E-03	2.0E-03	3.0E-03	1.8E-03	6.8E-04	2.2E-03	1.3E-03
KA3065A02:6_C_1(2)	3.2E-04	3.0E-03	–2.3E-04	1.3E-03	5.3E-04	2.3E-03	–1.2E-04	4.7E-04	1.2E-03	1.1E-03
KA3065A02:6_C_2(2)	6.4E-04	3.2E-03	–4.6E-04	1.2E-03	2.3E-04	2.1E-03	–7.1E-04	4.0E-04	1.5E-03	1.1E-03
KA3065A03_Batch 1_A_1(2)	–1.3E-03	2.0E-03	1.2E-03	1.8E-03	4.8E-03	4.5E-03	1.1E-03	6.2E-04	7.8E-03	2.6E-03
KA3065A03_Batch 1_A_2(2)	–1.2E-03	2.1E-03	–5.2E-04	1.3E-03	5.1E-03	4.6E-03	9.9E-03	4.2E-03	4.3E-03	1.8E-03
KA3065A03_Batch 1_B_1(2)	–1.1E-03	2.1E-03	–5.1E-04	1.2E-03	–3.1E-05	2.0E-03	–2.1E-04	4.5E-04	1.9E-03	1.2E-03
KA3065A03_Batch 1_B_2(2)	–4.9E-04	2.6E-03	–5.9E-04	1.2E-03	–1.4E-04	2.0E-03	–1.0E-04	4.8E-04	2.2E-03	1.3E-03
KA3065A03_Batch 1_C_1(2)	2.7E-04	3.1E-03	–2.8E-04	1.3E-03	1.6E-03	2.9E-03	2.4E-04	5.1E-04	1.4E-03	1.1E-03
KA3065A03_Batch 1_C_2(2)	2.3E-04	3.0E-03	1.5E-04	1.5E-03	2.6E-03	3.3E-03	–4.4E-04	4.6E-04	2.4E-03	1.4E-03
KA3065A03_Replica_A_1(2)	2.3E-03	5.2E-03	1.4E-03	1.2E-03	2.6E-04	2.7E-03	6.5E-04	1.5E-03	2.7E-03	4.1E-03
KA3065A03_Replica_A_2(2)	7.7E-04	3.9E-03	–7.7E-04	7.3E-04	3.2E-03	4.4E-03	–4.2E-04	1.1E-03	3.1E-04	2.5E-03
KA3065A03_Replica_B_1(2)	4.2E-05	3.4E-03	1.3E-04	9.2E-04	2.1E-03	3.8E-03	2.7E-03	2.1E-03	1.6E-02	1.4E-02
KA3065A03_Replica_B_2(2)	–4.8E-04	3.0E-03	1.0E-03	1.1E-03	1.5E-03	3.4E-03	3.7E-03	2.4E-03	6.3E-03	6.3E-03
KA3065A03_Replica_C_1(2)	1.1E-04	2.9E-03	6.2E-05	1.5E-03	2.4E-03	3.2E-03	1.6E-03	6.6E-04	1.3E-03	1.1E-03
KA3065A03_Replica_C_2(2)	2.9E-04	3.0E-03	5.4E-05	1.4E-03	2.2E-03	3.1E-03	8.5E-04	6.1E-04	4.8E-03	1.9E-03

Table A11-1. R_d (m^3/kg) results from the batch sorption experiments (Continued).
Tc-99

Contact time (d)	1.0		7.0		31.0		90.0		186.0	
Core	**R_d (m^3/kg)**	**+/–**	**R_d (m^3/kg)**	**+/–**	**R_d (m^3/kg)**	**+/–**	**R_d (m^3/kg)**	**+/–**	**R_d (m^3/kg)**	**+/–**
KA3065A02:1_A_1(2)	6.8E-04	4.1E-04	7.1E-03	9.0E-04	1.4E-01	2.5E-02	8.8E-01	4.0E-01	7.0E-02	6.6E-03
KA3065A02:1_A_2(2)	3.9E-04	3.9E-04	3.0E-03	5.4E-04	8.3E-02	1.1E-02	1.1E+0	6.5E-01	9.5E-02	9.4E-03
KA3065A02:1_B_1(2)	2.6E-04	4.1E-04	4.2E-05	3.2E-04	7.6E-05	3.5E-04	4.4E-04	2.5E-04	3.3E-04	3.7E-04
KA3065A02:1_B_2(2)	–2.2E-05	3.6E-04	2.8E-05	3.2E-04	5.1E-05	3.6E-04	3.3E-04	2.4E-04	1.2E-04	3.3E-04
KA3065A02:1_C_1(2)	1.5E-04	3.8E-04	–8.3E-05	3.4E-04	2.2E-04	3.8E-04	2.7E-04	2.3E-04	2.1E-04	3.4E-04
KA3065A02:1_C_2(2)	2.9E-05	3.6E-04	5.5E-05	3.3E-04	2.0E-04	3.6E-04	3.3E-04	2.5E-04	2.8E-04	3.5E-04
KA3065A02:2_A_1(2)	8.5E-05	5.3E-04	1.2E-04	1.1E-03	5.5E-04	8.1E-04	8.6E-04	1.1E-03	1.1E-03	1.1E-03
KA3065A02:2_A_2(2)	8.0E-04	6.0E-04	1.4E-03	1.4E-03	6.1E-03	1.7E-03	1.5E-02	4.0E-03	9.2E-03	2.7E-03
KA3065A02:2_B_1(2)	1.7E-04	5.5E-04	–1.7E-05	1.0E-03	1.3E-04	6.9E-04	–6.6E-05	8.0E-04	1.4E-04	8.1E-04
KA3065A02:2_B_2(2)	–3.7E-05	5.3E-04	1.4E-04	1.1E-03	2.3E-04	7.6E-04	7.1E-05	8.9E-04	4.6E-05	8.4E-04
KA3065A02:2_C_1(2)	1.4E-04	4.0E-04	1.3E-04	3.6E-04	1.4E-04	3.6E-04	2.3E-04	2.1E-04	2.3E-04	3.4E-04
KA3065A02:2_C_2(2)	1.0E-04	4.1E-04	2.4E-05	3.1E-04	1.3E-04	3.5E-04	6.1E-04	2.4E-04	1.7E-05	3.1E-04
KA3065A02:6_A_1(2)	4.0E-04	4.2E-04	5.6E-03	7.0E-04	1.5E-01	3.3E-02	1.0E+0	6.6E-01	2.1E-01	3.6E-02
KA3065A02:6_A_2(2)	7.3E-04	4.1E-04	5.5E-03	7.5E-04	8.8E-02	1.2E-02	1.1E+0	6.7E-01	4.3E-01	1.1E-01
KA3065A02:6_B_1(2)	4.6E-04	4.1E-04	7.1E-04	3.6E-04	7.5E-04	4.0E-04	8.9E-04	2.5E-04	6.2E-04	3.9E-04
KA3065A02:6_B_2(2)	–1.1E-05	3.3E-04	1.3E-05	3.2E-04	3.5E-05	3.3E-04	2.2E-04	2.1E-04	1.9E-04	3.3E-04
KA3065A02:6_C_1(2)	4.0E-04	3.8E-04	1.0E-04	3.4E-04	2.3E-04	3.5E-04	1.6E-04	2.1E-04	1.7E-04	3.3E-04
KA3065A02:6_C_2(2)	4.2E-05	3.8E-04	2.0E-04	3.4E-04	1.5E-04	3.4E-04	3.1E-04	2.1E-04	3.0E-04	3.2E-04
KA3065A03_Batch 1_A_1(2)	7.9E-04	4.2E-04	1.4E-02	1.4E-03	9.1E-01	1.0E+0	7.7E-01	3.6E-01	4.4E-01	1.2E-01
KA3065A03_Batch 1_A_2(2)	8.3E-04	4.2E-04	1.3E-02	1.3E-03	7.7E-01	7.6E-01	9.0E-01	4.7E-01	8.2E-01	4.2E-01
KA3065A03_Batch 1_B_1(2)	3.3E-04	3.7E-04	3.2E-04	3.4E-04	9.4E-04	4.1E-04	1.4E-03	2.7E-04	1.2E-03	4.2E-04
KA3065A03_Batch 1_B_2(2)	1.2E-04	3.6E-04	9.3E-04	4.0E-04	5.1E-03	7.5E-04	8.6E-03	6.5E-04	1.2E-02	1.3E-03
KA3065A03_Batch 1_C_1(2)	3.4E-04	3.9E-04	2.9E-04	3.4E-04	3.1E-04	3.7E-04	3.5E-04	2.3E-04	2.0E-04	3.6E-04
KA3065A03_Batch 1_C_2(2)	2.6E-04	3.7E-04	6.0E-05	3.1E-04	3.0E-04	3.8E-04	1.7E-05	2.5E-04	2.3E-04	3.5E-04
KA3065A03_Replica_A_1(2)	2.4E-05	5.1E-04	3.4E-04	1.2E-03	2.3E-03	1.1E-03	2.7E-03	1.4E-03	2.7E-03	1.4E-03
KA3065A03_Replica_A_2(2)	–5.1E-04	4.5E-04	-3.9E-04	9.3E-04	7.9E-04	8.1E-04	7.1E-04	9.6E-04	1.3E-03	1.1E-03
KA3065A03_Replica_B_1(2)	1.1E-03	6.6E-04	1.3E-03	1.4E-03	5.4E-04	7.9E-04	1.3E-03	1.1E-03	9.8E-04	1.0E-03
KA3065A03_Replica_B_2(2)	2.0E-04	5.3E-04	2.4E-05	1.1E-03	4.5E-05	6.9E-04	1.9E-04	8.8E-04	–6.6E-06	8.0E-04
KA3065A03_Replica_C_1(2)	3.0E-04	4.0E-04	2.1E-05	3.2E-04	2.4E-05	3.5E-04	6.6E-05	2.2E-04	1.9E-04	3.5E-04
KA3065A03_Replica_C_2(2)	–1.5E-04	3.4E-04	–3.3E-04	3.0E-04	–1.2E-04	3.3E-04	–2.3E-04	1.9E-04	–1.8E-04	3.0E-04

Table A11-1. R_d (m^3/kg) results from the batch sorption experiments (Continued).
Cd-109

Contact time (d)	1.0		7.0		31.0		90.0		186.0	
Core	**R_d (m^3/kg)**	**+/–**	**R_d (m^3/kg)**	**+/–**	**R_d (m^3/kg)**	**+/–**	**R_d (m^3/kg)**	**+/–**	**R_d (m^3/kg)**	**+/–**
KA3065A02:1_A_1(2)	–4.9E-04	2.1E-04	5.0E-03	1.1E-03	1.1E-02	1.3E-03	2.2E-02	2.2E-03	1.6E-02	1.1E-03
KA3065A02:1_A_2(2)	–2.6E-04	2.1E-04	2.9E-03	8.3E-04	1.2E-02	1.4E-03	1.3E-02	1.4E-03	2.0E-02	1.5E-03
KA3065A02:1_B_1(2)	–9.8E-04	1.9E-04	2.1E-03	7.6E-04	5.7E-03	8.4E-04	1.0E-02	1.1E-03	1.5E-02	1.1E-03
KA3065A02:1_B_2(2)	–9.0E-04	2.0E-04	3.0E-03	8.6E-04	5.0E-03	7.7E-04	8.9E-03	1.0E-03	1.4E-02	9.6E-04
KA3065A02:1_C_1(2)	–9.7E-04	1.9E-04	5.0E-04	5.7E-04	2.0E-03	5.2E-04	4.6E-03	6.6E-04	6.3E-03	4.8E-04
KA3065A02:1_C_2(2)	–8.7E-04	2.0E-04	1.6E-03	6.9E-04	3.2E-03	6.1E-04	5.6E-03	7.4E-04	5.6E-03	4.4E-04
KA3065A02:2_A_1(2)	4.1E-03	4.9E-04	1.7E-02	3.1E-03	4.1E-02	5.6E-03	3.5E-02	8.7E-03	4.2E-02	1.6E-02
KA3065A02:2_A_2(2)	9.5E-03	8.5E-04	3.1E-02	5.6E-03	4.5E-02	8.2E-03	5.8E-02	1.6E-02	7.8E-02	2.7E-02
KA3065A02:2_B_1(2)	4.1E-03	4.7E-04	1.5E-02	2.9E-03	2.3E-02	3.5E-03	2.3E-02	6.1E-03	4.8E-02	1.7E-02
KA3065A02:2_B_2(2)	6.0E-03	6.3E-04	2.4E-02	4.3E-03	2.6E-02	4.1E-03	2.8E-02	7.8E-03	2.9E-02	1.1E-02
KA3065A02:2_C_1(2)	3.9E-04	2.3E-04	4.7E-03	1.0E-03	1.2E-02	1.3E-03	2.0E-02	2.0E-03	2.6E-02	2.0E-03
KA3065A02:2_C_2(2)	–2.0E-04	2.2E-04	5.2E-03	1.1E-03	8.9E-03	1.1E-03	2.4E-02	2.5E-03	2.6E-02	2.0E-03
KA3065A02:6_A_1(2)	4.4E-05	2.3E-04	4.9E-03	1.1E-03	1.8E-02	2.0E-03	2.4E-02	2.6E-03	2.6E-02	2.2E-03
KA3065A02:6_A_2(2)	3.1E-04	2.5E-04	5.6E-03	1.2E-03	1.4E-02	1.6E-03	2.1E-02	2.2E-03	2.3E-02	1.8E-03
KA3065A02:6_B_1(2)	–4.2E-04	2.1E-04	3.7E-03	9.3E-04	7.8E-03	1.0E-03	1.5E-02	1.6E-03	1.5E-02	1.1E-03
KA3065A02:6_B_2(2)	–8.2E-04	1.9E-04	3.7E-03	9.1E-04	8.2E-03	1.0E-03	1.8E-02	1.9E-03	2.5E-02	1.4E-03
KA3065A02:6_C_1(2)	–6.9E-04	1.9E-04	1.7E-03	6.7E-04	1.0E-03	4.2E-04	2.4E-03	4.7E-04	3.6E-03	3.0E-04
KA3065A02:6_C_2(2)	–1.0E-03	1.8E-04	6.5E-04	5.5E-04	1.4E-03	4.5E-04	3.5E-03	5.6E-04	6.9E-03	4.9E-04
KA3065A03_Batch 1_A_1(2)	–4.5E-04	2.2E-04	6.4E-03	1.3E-03	2.4E-02	2.7E-03	2.5E-02	2.7E-03	2.4E-02	1.8E-03
KA3065A03_Batch 1_A_2(2)	–6.6E-05	2.3E-04	5.7E-03	1.2E-03	2.4E-02	2.9E-03	2.2E-02	2.4E-03	2.7E-02	2.3E-03
KA3065A03_Batch 1_B_1(2)	–7.8E-04	1.9E-04	1.6E-03	6.8E-04	4.1E-03	6.9E-04	6.2E-03	7.8E-04	8.0E-03	5.7E-04
KA3065A03_Batch 1_B_2(2)	–9.4E-04	1.9E-04	2.1E-03	7.5E-04	4.2E-03	7.0E-04	6.5E-03	8.1E-04	1.1E-02	7.7E-04
KA3065A03_Batch 1_C_1(2)	–1.1E-03	1.8E-04	6.7E-04	5.8E-04	1.7E-03	4.8E-04	2.8E-03	5.2E-04	3.6E-03	3.4E-04
KA3065A03_Batch 1_C_2(2)	–9.7E-04	1.9E-04	7.4E-04	5.9E-04	1.7E-03	4.9E-04	2.3E-03	4.8E-04	4.4E-03	3.7E-04
KA3065A03_Replica_A_1(2)	1.1E-02	9.9E-04	4.9E-02	9.6E-03	1.0E-01	2.5E-02	1.5E-01	6.1E-02	2.2E-01	1.4E-01
KA3065A03_Replica_A_2(2)	9.3E-03	8.6E-04	3.5E-02	6.9E-03	8.8E-02	2.8E-02	8.9E-02	3.3E-02	> 2E-01	
KA3065A03_Replica_B_1(2)	1.1E-02	9.5E-04	3.7E-02	5.8E-03	2.1E-01	1.5E-01	1.6E-01	7.0E-02	6.8E-02	2.3E-02
KA3065A03_Replica_B_2(2)	9.3E-03	7.4E-04	3.6E-02	5.8E-03	5.1E-02	6.9E-03	7.9E-02	2.0E-02	1.6E-01	7.1E-02
KA3065A03_Replica_C_1(2)	8.2E-04	2.7E-04	1.2E-02	2.0E-03	4.6E-02	6.0E-03	1.0E-01	2.5E-02	1.2E-01	1.4E-02
KA3065A03_Replica_C_2(2)	4.6E-04	2.5E-04	1.3E-02	2.0E-03	3.8E-02	5.1E-03	7.9E-02	1.4E-02	6.3E-02	1.1E-02

Table A11-1. R_d (m³/kg) results from the batch sorption experiments (Continued).
Ag-110 m

Contact time (d)	1.0		7.0		31.0		90.0		186.0	
Core	R_d (m³/kg)	+/–	R_d (m³/kg)	+/–	R_d (m³/kg)	+/–	R_d (m³/kg)	+/–	R_d (m³/kg)	+/–
KA3065A02:1_A_1(2)	> 1E-02		> 1E-02		> 1E-02		> 1E-02		> 1E-02	
KA3065A02:1_A_2(2)	8.2E-03	5.2E-03	> 1E-02		> 1E-02		> 1E-02		> 1E-02	
KA3065A02:1_B_1(2)	–6.3E-04	1.5E-03	1.1E-03	1.4E-03	> 1E-02		> 1E-02		> 1E-02	
KA3065A02:1_B_2(2)	2.7E-04	2.1E-03	9.5E-03	4.0E-03	> 1E-02		> 1E-02		> 1E-02	
KA3065A02:1_C_1(2)	–9.8E-04	1.4E-03	1.7E-03	1.6E-03	1.5E-02	7.7E-03	> 1E-02		> 1E-02	
KA3065A02:1_C_2(2)	–3.2E-04	1.6E-03	7.5E-03	3.5E-03	1.1E-02	5.6E-03	> 1E-02		> 1E-02	
KA3065A02:2_A_1(2)	> 8E-03		> 8E-03		> 8E-03		> 8E-03		> 8E-03	
KA3065A02:2_A_2(2)	> 8E-03		> 8E-03		> 8E-03		> 8E-03		> 8E-03	
KA3065A02:2_B_1(2)	8.1E-03	5.1E-03	> 8E-03		> 8E-03		> 8E-03		> 8E-03	
KA3065A02:2_B_2(2)	> 8E-03		> 8E-03		> 8E-03		> 8E-03		> 8E-03	
KA3065A02:2_C_1(2)	9.7E-04	2.1E-03	1.7E-02	8.3E-03	> 1E-02		> 1E-02		> 1E-02	
KA3065A02:2_C_2(2)	6.2E-04	1.9E-03	3.9E-03	2.1E-03	> 1E-02		> 1E-02		> 1E-02	
KA3065A02:6_A_1(2)	> 1E-02		> 1E-02		> 1E-02		> 1E-02		> 1E-02	
KA3065A02:6_A_2(2)	1.3E-02	7.2E-03	> 1E-02		> 1E-02		> 1E-02		> 1E-02	
KA3065A02:6_B_1(2)	9.2E-04	2.1E-03	> 1E-02		> 1E-02		> 1E-02		> 1E-02	
KA3065A02:6_B_2(2)	8.7E-04	2.0E-03	> 1E-02		> 1E-02		> 1E-02		> 1E-02	
KA3065A02:6_C_1(2)	1.1E-03	2.1E-03	> 1E-02		> 1E-02		> 1E-02		> 1E-02	
KA3065A02:6_C_2(2)	1.1E-03	2.1E-03	> 1E-02		> 1E-02		> 1E-02		> 1E-02	
KA3065A03_Batch 1_A_1(2)	1.8E-02	1.0E-02	> 1E-02		> 1E-02		> 1E-02		> 1E-02	
KA3065A03_Batch 1_A_2(2)	> 1E-02		> 1E-02		> 1E-02		> 1E-02		> 1E-02	
KA3065A03_Batch 1_B_1(2)	1.1E-03	2.1E-03	5.1E-03	2.4E-03	> 1E-02		> 1E-02		> 1E-02	
KA3065A03_Batch 1_B_2(2)	9.4E-05	1.8E-03	> 1E-02		> 1E-02		> 1E-02		> 1E-02	
KA3065A03_Batch 1_C_1(2)	2.9E-04	1.9E-03	5.9E-03	2.8E-03	> 1E-02		> 1E-02		> 1E-02	
KA3065A03_Batch 1_C_2(2)	–2.4E-04	1.6E-03	4.3E-03	2.3E-03	> 1E-02		> 1E-02		> 1E-02	
KA3065A03_Replica_A_1(2)	> 8E-3		> 8E-03		> 8E-03		> 8E-03		> 8E-03	
KA3065A03_Replica_A_2(2)	> 8E-3		> 8E-03		> 8E-03		> 8E-03		> 8E-03	
KA3065A03_Replica_B_1(2)	> 8E-3		> 8E-03		> 8E-03		> 8E-03		> 8E-03	
KA3065A03_Replica_B_2(2)	> 8E-3		> 8E-03		> 8E-03		> 8E-03		> 8E-03	
KA3065A03_Replica_C_1(2)	> 1E-02		> 1E-02		> 1E-02		> 1E-02		> 1E-02	
KA3065A03_Replica_C_2(2)	2.4E-03	2.7E-03	> 1E-02		> 1E-02		> 1E-02		> 1E-02	

Table A11-1. R_d (m^3/kg) results from the batch sorption experiments (Continued).
Ba-133

Contact time (d)	1.0		7.0		31.0		90.0		186.0	
Core	R_d (m^3/kg)	+/–	R_d (m^3/kg)	+/–	R_d (m^3/kg)	+/–	R_d (m^3/kg)	+/–	R_d (m^3/kg)	+/–
KA3065A02:1_A_1(2)	3.1E-04	1.5E-04	3.6E-03	4.2E-04	4.6E-03	7.4E-04	6.5E-03	6.6E-04	5.9E-03	2.5E-04
KA3065A02:1_A_2(2)	9.0E-04	1.7E-04	2.2E-03	3.4E-04	4.6E-03	7.3E-04	4.2E-03	5.1E-04	5.9E-03	2.5E-04
KA3065A02:1_B_1(2)	–5.0E-05	1.4E-04	2.4E-03	3.6E-04	3.3E-03	6.2E-04	3.8E-03	4.9E-04	4.2E-03	2.1E-04
KA3065A02:1_B_2(2)	4.4E-05	1.5E-04	2.8E-03	3.7E-04	3.4E-03	6.4E-04	3.4E-03	4.7E-04	3.7E-03	1.9E-04
KA3065A02:1_C_1(2)	3.6E-05	1.5E-04	6.0E-04	2.6E-04	1.5E-03	4.8E-04	1.9E-03	3.7E-04	2.1E-03	1.5E-04
KA3065A02:1_C_2(2)	–1.9E-04	1.4E-04	1.6E-03	3.1E-04	2.1E-03	5.2E-04	2.4E-03	4.0E-04	1.9E-03	1.5E-04
KA3065A02:2_A_1(2)	3.9E-03	1.2E-03	9.2E-03	2.2E-03	1.2E-02	2.0E-03	1.1E-02	2.0E-03	1.5E-02	3.4E-03
KA3065A02:2_A_2(2)	7.2E-03	1.6E-03	1.2E-02	2.5E-03	1.2E-02	2.0E-03	1.4E-02	2.4E-03	1.6E-02	3.6E-03
KA3065A02:2_B_1(2)	3.8E-03	1.1E-03	7.5E-03	1.8E-03	8.6E-03	1.6E-03	7.9E-03	1.6E-03	1.2E-02	2.8E-03
KA3065A02:2_B_2(2)	2.9E-03	1.0E-03	7.4E-03	1.9E-03	9.9E-03	1.8E-03	9.6E-03	1.8E-03	9.1E-03	2.4E-03
KA3065A02:2_C_1(2)	9.2E-04	1.7E-04	3.5E-03	4.0E-04	7.3E-03	9.5E-04	8.6E-03	7.9E-04	1.0E-02	3.8E-04
KA3065A02:2_C_2(2)	5.8E-04	1.6E-04	5.0E-03	4.8E-04	6.8E-03	9.0E-04	1.0E-02	9.1E-04	9.6E-03	3.7E-04
KA3065A02:6_A_1(2)	1.2E-03	1.8E-04	3.4E-03	4.0E-04	5.0E-03	7.6E-04	5.7E-03	6.1E-04	6.5E-03	2.7E-04
KA3065A02:6_A_2(2)	1.8E-03	2.0E-04	5.1E-03	5.0E-04	6.4E-03	8.8E-04	6.6E-03	6.7E-04	6.1E-03	2.4E-04
KA3065A02:6_B_1(2)	4.9E-04	1.6E-04	3.2E-03	3.9E-04	3.7E-03	6.5E-04	4.7E-03	5.5E-04	4.1E-03	2.0E-04
KA3065A02:6_B_2(2)	6.2E-05	1.4E-04	2.4E-03	3.4E-04	3.2E-03	6.0E-04	3.5E-03	4.6E-04	3.3E-03	1.7E-04
KA3065A02:6_C_1(2)	8.9E-05	1.4E-04	1.8E-03	3.1E-04	1.1E-03	4.3E-04	1.2E-03	3.2E-04	1.6E-03	1.3E-04
KA3065A02:6_C_2(2)	–3.1E-04	1.3E-04	7.3E-04	2.5E-04	1.1E-03	4.2E-04	1.4E-03	3.3E-04	3.1E-03	1.7E-04
KA3065A03_Batch 1_A_1(2)	3.3E-04	1.5E-04	2.5E-03	3.6E-04	5.0E-03	7.7E-04	4.0E-03	5.0E-04	4.8E-03	2.2E-04
KA3065A03_Batch 1_A_2(2)	3.9E-04	1.6E-04	3.3E-03	4.0E-04	4.5E-03	7.2E-04	4.4E-03	5.3E-04	5.3E-03	2.3E-04
KA3065A03_Batch 1_B_1(2)	3.3E-04	1.5E-04	1.5E-03	3.0E-04	2.7E-03	5.7E-04	3.2E-03	4.5E-04	3.2E-03	1.8E-04
KA3065A03_Batch 1_B_2(2)	4.8E-05	1.5E-04	1.4E-03	3.0E-04	2.2E-03	5.4E-04	2.3E-03	4.0E-04	3.1E-03	1.8E-04
KA3065A03_Batch 1_C_1(2)	–2.7E-04	1.3E-04	9.0E-04	2.7E-04	1.8E-03	5.0E-04	1.5E-03	3.5E-04	1.7E-03	1.3E-04
KA3065A03_Batch 1_C_2(2)	–1.5E-04	1.4E-04	1.1E-03	2.8E-04	1.5E-03	4.7E-04	1.2E-03	3.2E-04	2.3E-03	1.5E-04
KA3065A03_Replica_A_1(2)	7.7E-03	1.7E-03	1.4E-02	3.0E-03	1.7E-02	2.7E-03	1.7E-02	3.2E-03	2.1E-02	4.5E-03
KA3065A03_Replica_A_2(2)	6.8E-03	1.5E-03	1.3E-02	2.8E-03	1.5E-02	2.5E-03	1.2E-02	2.1E-03	1.5E-02	3.5E-03
KA3065A03_Replica_B_1(2)	7.9E-03	1.7E-03	1.8E-02	3.6E-03	1.5E-02	2.4E-03	1.7E-02	2.8E-03	1.8E-02	4.0E-03
KA3065A03_Replica_B_2(2)	7.7E-03	1.6E-03	1.5E-02	3.2E-03	1.4E-02	2.3E-03	1.6E-02	2.7E-03	1.9E-02	4.2E-03
KA3065A03_Replica_C_1(2)	2.2E-03	2.1E-04	1.1E-02	8.1E-04	1.5E-02	1.6E-03	1.5E-02	1.2E-03	1.6E-02	6.2E-04
KA3065A03_Replica_C_2(2)	1.3E-03	1.8E-04	9.7E-03	7.5E-04	1.6E-02	1.7E-03	1.4E-02	1.2E-03	1.4E-02	5.9E-04

Table A11-1. R_d (m^3/kg) results from the batch sorption experiments (Continued).
Cs-137

Contact time – days	1.0		7.0		31.0		90.0		186.0	
Core	**R_d (m^3/kg)**	**+/–**	**R_d (m^3/kg)**	**+/–**	**R_d (m^3/kg)**	**+/–**	**R_d (m^3/kg)**	**+/–**	**R_d (m^3/kg)**	**+/–**
KA3065A02:1_A_1(2)	2.8E-03	5.6E-04	1.7E-02	1.7E-03	2.6E-02	2.5E-03	3.2E-02	2.0E-03	3.0E-02	1.2E-03
KA3065A02:1_A_2(2)	4.1E-03	6.5E-04	1.4E-02	1.5E-03	2.6E-02	2.6E-03	2.5E-02	1.6E-03	3.2E-02	1.3E-03
KA3065A02:1_B_1(2)	1.5E-03	4.6E-04	1.2E-02	1.3E-03	1.9E-02	2.0E-03	2.1E-02	1.4E-03	2.5E-02	1.1E-03
KA3065A02:1_B_2(2)	1.9E-03	4.9E-04	1.3E-02	1.4E-03	1.9E-02	2.0E-03	1.8E-02	1.3E-03	2.2E-02	9.3E-04
KA3065A02:1_C_1(2)	8.7E-04	4.1E-04	4.1E-03	6.8E-04	8.6E-03	1.1E-03	1.1E-02	8.7E-04	1.3E-02	6.2E-04
KA3065A02:1_C_2(2)	6.2E-04	3.9E-04	5.1E-03	7.6E-04	8.2E-03	1.0E-03	9.9E-03	7.8E-04	1.0E-02	5.0E-04
KA3065A02:2_A_1(2)	3.4E-02	4.4E-03	9.9E-02	2.0E-02	1.3E-01	1.7E-02	1.0E-01	1.7E-02	1.0E-02	3.2E-03
KA3065A02:2_A_2(2)	7.2E-02	8.9E-03	1.1E-01	2.3E-02	1.2E-01	1.6E-02	1.2E-01	2.0E-02	1.1E-02	3.3E-03
KA3065A02:2_B_1(2)	2.4E-02	3.2E-03	7.2E-02	1.5E-02	9.2E-02	1.2E-02	8.4E-02	1.4E-02	7.5E-03	2.6E-03
KA3065A02:2_B_2(2)	2.1E-02	3.0E-03	7.1E-02	1.5E-02	9.1E-02	1.2E-02	8.9E-02	1.5E-02	5.5E-03	2.2E-03
KA3065A02:2_C_1(2)	2.8E-03	5.4E-04	2.6E-02	2.4E-03	7.1E-02	6.4E-03	8.6E-02	5.4E-03	9.4E-02	4.0E-03
KA3065A02:2_C_2(2)	6.2E-03	8.1E-04	4.3E-02	3.8E-03	7.7E-02	6.9E-03	1.1E-01	6.7E-03	1.1E-01	4.8E-03
KA3065A02:6_A_1(2)	1.1E-02	1.2E-03	8.2E-02	7.2E-03	1.3E-01	1.2E-02	1.5E-01	9.7E-03	1.6E-01	8.1E-03
KA3065A02:6_A_2(2)	1.7E-02	1.6E-03	9.7E-02	8.4E-03	1.5E-01	1.4E-02	1.6E-01	1.0E-02	1.7E-01	8.2E-03
KA3065A02:6_B_1(2)	4.4E-03	6.8E-04	3.0E-02	2.8E-03	7.1E-02	6.4E-03	9.5E-02	5.9E-03	9.6E-02	4.1E-03
KA3065A02:6_B_2(2)	2.4E-03	5.1E-04	2.5E-02	2.4E-03	6.8E-02	6.1E-03	8.0E-02	4.9E-03	9.0E-02	3.9E-03
KA3065A02:6_C_1(2)	2.7E-03	5.4E-04	1.3E-02	1.4E-03	1.9E-02	1.9E-03	2.2E-02	1.5E-03	2.8E-02	1.2E-03
KA3065A02:6_C_2(2)	1.6E-03	4.5E-04	9.1E-03	1.1E-03	1.7E-02	1.8E-03	2.2E-02	1.5E-03	3.6E-02	1.5E-03
KA3065A03_Batch 1_A_1(2)	5.9E-03	8.0E-04	3.5E-02	3.2E-03	6.7E-02	6.0E-03	5.7E-02	3.5E-03	6.5E-02	2.7E-03
KA3065A03_Batch 1_A_2(2)	5.8E-03	7.8E-04	3.9E-02	3.5E-03	6.1E-02	5.5E-03	5.5E-02	3.4E-03	6.1E-02	2.5E-03
KA3065A03_Batch 1_B_1(2)	3.3E-03	5.8E-04	1.7E-02	1.7E-03	3.7E-02	3.5E-03	4.5E-02	2.8E-03	5.0E-02	2.1E-03
KA3065A03_Batch 1_B_2(2)	2.8E-03	5.5E-04	1.7E-02	1.7E-03	3.3E-02	3.1E-03	3.8E-02	2.4E-03	4.7E-02	1.9E-03
KA3065A03_Batch 1_C_1(2)	1.5E-03	4.5E-04	7.0E-03	9.1E-04	1.4E-02	1.6E-03	1.8E-02	1.2E-03	2.1E-02	8.9E-04
KA3065A03_Batch 1_C_2(2)	1.7E-03	4.7E-04	7.8E-03	9.7E-04	1.4E-02	1.5E-03	1.6E-02	1.1E-03	2.3E-02	9.8E-04
KA3065A03_Replica_A_1(2)	2.6E-01	3.5E-02	4.9E-01	1.1E-01	6.4E-01	1.1E-01	9.5E-01	2.2E-01	1.0E+0	2.9E-01
KA3065A03_Replica_A_2(2)	2.3E-01	3.2E-02	4.8E-01	1.1E-01	9.0E-01	2.0E-01	8.0E-01	2.0E-01	9.3E-01	2.7E-01
KA3065A03_Replica_B_1(2)	1.1E-01	1.4E-02	6.7E-01	1.5E-01	8.4E-01	1.6E-01	8.0E-01	1.7E-01	9.8E-01	2.7E-01
KA3065A03_Replica_B_2(2)	1.3E-01	1.6E-02	5.7E-01	1.3E-01	1.0E+0	2.3E-01	8.8E-01	2.0E-01	1.1E+0	3.3E-01
KA3065A03_Replica_C_1(2)	2.8E-02	2.5E-03	4.1E-01	4.2E-02	8.1E-01	1.1E-01	8.1E-01	9.7E-02	7.9E-01	8.6E-02
KA3065A03_Replica_C_2(2)	9.5E-03	1.1E-03	3.7E-01	3.8E-02	7.4E-01	9.4E-02	7.9E-01	1.0E-01	9.2E-01	1.3E-01

Table A11-1. R_d (m^3/kg) results from the batch sorption experiments (Continued).
Gd-153

Contact time – days	1.0		7.0		31.0		90.0		186.0	
Core	R_d (m^3/kg)	+/–	R_d (m^3/kg)	+/–	R_d (m^3/kg)	+/–	R_d (m^3/kg)	+/–	R_d (m^3/kg)	+/–
KA3065A02:1_A_1(2)	> 4E-01		> 4E-01		> 4E-01		> 4E-01		> 4E-01	
KA3065A02:1_A_2(2)	> 4E-01		> 4E-01		> 4E-01		> 4E-01		> 4E-01	
KA3065A02:1_B_1(2)	2.8E-02	6.8E-03	> 4E-01		> 4E-01		> 4E-01		> 4E-01	
KA3065A02:1_B_2(2)	2.3E-02	1.6E-02	7.7E-02	3.8E-02	> 4E-01		> 4E-01		> 4E-01	
KA3065A02:1_C_1(2)	3.7E-02	6.5E-03	> 4E-01		> 4E-01		> 4E-01		> 4E-01	
KA3065A02:1_C_2(2)	4.6E-02	1.5E-02	> 4E-01		> 4E-01		> 4E-01		> 4E-01	
KA3065A02:2_A_1(2)	> 4E-01		> 4E-01		> 4E-01		> 1E-01		> 1E-01	
KA3065A02:2_A_2(2)	1.4E-01	6.3E-02	> 4E-01		> 4E-01		> 1E-01		> 1E-01	
KA3065A02:2_B_1(2)	> 4E-01		> 4E-01		> 4E-01		> 1E-01		> 1E-01	
KA3065A02:2_B_2(2)	4.0E-01	6.3E-01	> 4E-01		> 4E-01		> 1E-01		> 1E-01	
KA3065A02:2_C_1(2)	> 4E-01		> 4E-01		> 4E-01		> 4E-01		> 4E-01	
KA3065A02:2_C_2(2)	> 4E-01		> 4E-01		> 4E-01		> 4E-01		> 4E-01	
KA3065A02:6_A_1(2)	4.61E-02	8.21E-03	> 4E-01		> 4E-01		> 4E-01		> 4E-01	
KA3065A02:6_A_2(2)	> 4E-01		> 4E-01		> 4E-01		> 4E-01		> 4E-01	
KA3065A02:6_B_1(2)	7.5E-02	1.4E-02	> 4E-01		> 4E-01		> 4E-01		> 4E-01	
KA3065A02:6_B_2(2)	3.1E-02	2.0E-02	6.8E-02	3.1E-02	> 4E-01		> 4E-01		> 4E-01	
KA3065A02:6_C_1(2)	9.2E-02	7.0E-02	> 4E-01		> 4E-01		> 4E-01		> 4E-01	
KA3065A02:6_C_2(2)	3.2E-02	7.7E-03	> 4E-01		> 4E-01		> 4E-01		> 4E-01	
KA3065A03_Batch 1_A_1(2)	> 4E-01		> 4E-01		> 4E-01		> 4E-01		> 4E-01	
KA3065A03_Batch 1_A_2(2)	2.1E-01	2.3E-01	> 4E-01		> 4E-01		> 4E-01		> 4E-01	
KA3065A03_Batch 1_B_1(2)	1.9E-02	4.2E-03	8.9E-02	2.9E-02	> 4E-01		> 4E-01		> 4E-01	
KA3065A03_Batch 1_B_2(2)	> 4E-01		> 4E-01		> 4E-01		> 4E-01		> 4E-01	
KA3065A03_Batch 1_C_1(2)	> 4E-01		> 4E-01		> 4E-01		> 4E-01		> 4E-01	
KA3065A03_Batch 1_C_2(2)	1.2E-01	9.0E-02	8.6E-02		> 4E-01		> 4E-01		> 4E-01	
KA3065A03_Replica_A_1(2)	> 4E-01		> 4E-01		> 4E-01		> 4E-01		> 4E-01	
KA3065A03_Replica_A_2(2)	> 4E-01		> 4E-01		> 4E-01		> 4E-01		> 4E-01	
KA3065A03_Replica_B_1(2)	> 4E-01		> 4E-01		> 4E-01		> 4E-01		> 4E-01	
KA3065A03_Replica_B_2(2)	> 4E-01		> 4E-01		> 4E-01		> 4E-01		> 4E-01	
KA3065A03_Replica_C_1(2)	> 4E-01		> 4E-01		> 4E-01		> 4E-01		> 4E-01	
KA3065A03_Replica_C_2(2)	> 4E-01		> 4E-01		> 4E-01		> 4E-01		> 4E-01	

Table A11-1. R_d (m^3/kg) results from the batch sorption experiments (Continued).
Ra-226

Contact time – days	**1.0**		**7.0**		**31.0**		**90.0**		**186.0**	
Core	**R_d (m^3/kg)**	**+/–**	**R_d (m^3/kg)**	**+/–**	**R_d (m^3/kg)**	**+/–**	**R_d (m^3/kg)**	**+/–**	**R_d (m^3/kg)**	**+/–**
KA3065A02:1_A_1(2)	3.3E-03	6.8E-04	1.1E-02	1.0E-03	1.8E-02	2.9E-03	2.3E-02	2.1E-03	2.7E-02	2.2E-03
KA3065A02:1_A_2(2)	3.6E-03	6.9E-04	1.0E-02	1.1E-03	1.7E-02	2.3E-03	2.3E-02	1.9E-03	2.8E-02	3.9E-03
KA3065A02:1_B_1(2)	1.9E-03	5.3E-04	5.7E-03	8.4E-04	1.0E-02	1.3E-03	1.4E-02	8.5E-04	1.7E-02	1.4E-03
KA3065A02:1_B_2(2)	1.5E-03	5.2E-04	6.2E-03	9.1E-04	9.7E-03	1.4E-03	1.4E-02	7.7E-04	1.6E-02	1.8E-03
KA3065A02:1_C_1(2)	8.4E-04	5.3E-04	2.4E-03	4.1E-04	4.9E-03	8.2E-04	7.2E-03	7.0E-04	8.9E-03	9.7E-04
KA3065A02:1_C_2(2)	6.1E-04	4.9E-04	2.6E-03	5.0E-04	4.8E-03	7.6E-04	6.4E-03	7.5E-04	7.7E-03	1.0E-03
KA3065A02:2_A_1(2)	1.5E-02	2.4E-03	5.3E-02	1.9E-02	5.6E-02	1.5E-02	7.0E-02	1.7E-02	7.5E-02	2.0E-02
KA3065A02:2_A_2(2)	3.2E-02	6.3E-03	5.9E-02	2.0E-02	6.9E-02	1.9E-02	7.6E-02	2.1E-02	8.2E-02	2.5E-02
KA3065A02:2_B_1(2)	1.1E-02	2.0E-03	2.7E-02	8.0E-03	3.9E-02	6.8E-03	4.0E-02	1.0E-02	4.7E-02	1.2E-02
KA3065A02:2_B_2(2)	9.4E-03	1.8E-03	3.1E-02	1.0E-02	3.6E-02	7.6E-03	4.3E-02	1.0E-02	4.7E-02	1.3E-02
KA3065A02:2_C_1(2)	1.8E-03	4.9E-04	9.9E-03	1.3E-03	2.3E-02	2.9E-03	3.2E-02	2.6E-03	3.7E-02	3.6E-03
KA3065A02:2_C_2(2)	3.1E-03	6.7E-04	1.3E-02	1.4E-03	2.5E-02	3.1E-03	3.8E-02	3.9E-03	3.8E-02	3.6E-03
KA3065A02:6_A_1(2)	3.6E-03	7.7E-04	1.3E-02	1.2E-03	2.0E-02	2.6E-03	2.6E-02	2.1E-03	3.1E-02	3.0E-03
KA3065A02:6_A_2(2)	5.5E-03	8.3E-04	1.4E-02	1.4E-03	2.2E-02	2.7E-03	2.8E-02	2.3E-03	3.3E-02	3.9E-03
KA3065A02:6_B_1(2)	2.3E-03	5.5E-04	7.0E-03	9.4E-04	1.2E-02	1.9E-03	1.6E-02	9.9E-04	1.8E-02	2.3E-03
KA3065A02:6_B_2(2)	1.5E-03	5.1E-04	5.6E-03	7.9E-04	1.0E-02	1.3E-03	1.4E-02	1.0E-03	1.7E-02	1.5E-03
KA3065A02:6_C_1(2)	1.2E-03	5.7E-04	2.4E-03	3.7E-04	4.1E-03	6.7E-04	5.5E-03	7.3E-04	7.0E-03	8.9E-04
KA3065A02:6_C_2(2)	1.0E-03	4.6E-04	2.5E-03	4.1E-04	4.3E-03	7.4E-04	6.3E-03	5.0E-04	8.0E-03	9.8E-04
KA3065A03_Batch 1_A_1(2)	3.0E-03	7.5E-04	1.1E-02	1.2E-03	1.7E-02	2.0E-03	2.1E-02	1.7E-03	2.4E-02	2.5E-03
KA3065A03_Batch 1_A_2(2)	3.2E-03	6.6E-04	1.1E-02	1.0E-03	1.5E-02	2.1E-03	2.2E-02	2.5E-03	2.5E-02	2.6E-03
KA3065A03_Batch 1_B_1(2)	2.3E-03	5.7E-04	5.8E-03	5.5E-04	9.5E-03	1.3E-03	1.3E-02	9.8E-04	1.5E-02	2.0E-03
KA3065A03_Batch 1_B_2(2)	2.1E-03	6.3E-04	5.2E-03	7.9E-04	9.1E-03	1.3E-03	1.2E-02	9.1E-04	1.5E-02	1.5E-03
KA3065A03_Batch 1_C_1(2)	1.5E-03	5.4E-04	2.9E-03	5.2E-04	4.4E-03	7.2E-04	5.8E-03	4.5E-04	6.9E-03	7.9E-04
KA3065A03_Batch 1_C_2(2)	1.3E-03	5.2E-04	2.5E-03	6.0E-04	4.1E-03	6.8E-04	5.0E-03	4.3E-04	6.6E-03	8.9E-04
KA3065A03_Replica_A_1(2)	3.6E-02	6.5E-03	8.3E-02	3.4E-02	1.1E-01	4.6E-02	1.2E-01	3.8E-02	1.5E-01	5.3E-02
KA3065A03_Replica_A_2(2)	3.9E-02	8.5E-03	6.9E-02	2.8E-02	8.1E-02	3.2E-02	9.5E-02	3.2E-02	9.9E-02	3.0E-02
KA3065A03_Replica_B_1(2)	1.9E-02	3.5E-03	8.6E-02	3.4E-02	8.6E-02	4.2E-02	9.1E-02	2.2E-02	8.4E-02	2.5E-02
KA3065A03_Replica_B_2(2)	2.0E-02	3.5E-03	7.5E-02	2.8E-02	8.0E-02	3.0E-02	9.1E-02	2.5E-02	7.9E-02	2.3E-02
KA3065A03_Replica_C_1(2)	7.8E-03	1.1E-03	4.6E-02	7.3E-03	7.5E-02	1.5E-02	7.6E-02	8.0E-03	7.6E-02	9.0E-03
KA3065A03_Replica_C_2(2)	3.7E-03	7.5E-04	3.6E-02	7.0E-03	6.9E-02	1.1E-02	6.8E-02	5.1E-03	7.4E-02	6.9E-03

Table A11-1. R_d (m^3/kg) results from the batch sorption experiments (Continued).
U-236

Contact time – days	1.0		7.0		31.0		90.0		186.0	
Core	**R_d (m^3/kg)**	**+/–**	**R_d (m^3/kg)**	**+/–**	**R_d (m^3/kg)**	**+/–**	**R_d (m^3/kg)**	**+/–**	**R_d (m^3/kg)**	**+/–**
KA3065A02:1_A_1(2)	1.6E-04	1.3E-03	3.2E-03	5.2E-04	1.8E-02	2.4E-03	4.3E-02	4.3E-03	1.9E-02	2.5E-03
KA3065A02:1_A_2(2)	6.3E-06	1.3E-03	1.3E-03	4.9E-04	1.2E-02	1.8E-03	2.9E-02	2.0E-03	1.9E-02	2.6E-03
KA3065A02:1_B_1(2)	–2.8E-05	1.3E-03	5.1E-04	4.6E-04	1.3E-03	5.8E-04	2.9E-03	3.5E-04	4.5E-03	9.2E-04
KA3065A02:1_B_2(2)	–4.5E-04	1.1E-03	4.7E-04	4.7E-04	1.4E-03	6.0E-04	3.0E-03	3.5E-04	4.4E-03	8.8E-04
KA3065A02:1_C_1(2)	–2.5E-04	1.2E-03	2.3E-05	4.4E-04	4.7E-04	5.0E-04	1.1E-03	2.7E-04	1.9E-03	6.1E-04
KA3065A02:1_C_2(2)	–2.6E-04	1.2E-03	1.4E-04	4.6E-04	6.1E-04	5.0E-04	9.9E-04	3.0E-04	1.3E-03	6.1E-04
KA3065A02:2_A_1(2)	1.2E-03	7.3E-04	6.8E-03	2.4E-03	1.3E-02	2.1E-03	2.3E-02	4.6E-03	2.6E-02	5.0E-03
KA3065A02:2_A_2(2)	2.6E-03	9.1E-04	6.8E-03	2.3E-03	1.4E-02	2.2E-03	3.3E-02	6.4E-03	4.4E-02	8.3E-03
KA3065A02:2_B_1(2)	1.7E-03	7.8E-04	4.4E-03	1.8E-03	1.1E-02	1.6E-03	2.2E-02	4.3E-03	4.3E-02	7.8E-03
KA3065A02:2_B_2(2)	1.2E-03	7.7E-04	4.2E-03	1.8E-03	8.0E-03	1.3E-03	1.4E-02	3.0E-03	2.7E-02	5.1E-03
KA3065A02:2_C_1(2)	–2.0E-04	1.1E-03	1.1E-03	5.1E-04	2.6E-03	7.0E-04	6.0E-03	5.5E-04	1.2E-02	1.6E-03
KA3065A02:2_C_2(2)	–1.4E-04	1.2E-03	1.2E-03	4.8E-04	3.0E-03	7.3E-04	7.4E-03	7.7E-04	9.6E-03	1.4E-03
KA3065A02:6_A_1(2)	–3.5E-04	1.2E-03	2.3E-03	5.1E-04	1.7E-02	2.6E-03	4.4E-02	3.4E-03	3.1E-02	3.4E-03
KA3065A02:6_A_2(2)	–1.2E-04	1.2E-03	2.5E-03	5.2E-04	1.5E-02	2.2E-03	4.0E-02	3.5E-03	3.9E-02	5.0E-03
KA3065A02:6_B_1(2)	–7.0E-05	1.2E-03	9.9E-04	4.1E-04	1.6E-03	6.0E-04	2.4E-03	4.0E-04	3.3E-03	8.1E-04
KA3065A02:6_B_2(2)	–4.2E-04	1.1E-03	4.0E-04	4.0E-04	9.5E-04	5.3E-04	2.2E-03	3.2E-04	3.7E-03	7.5E-04
KA3065A02:6_C_1(2)	–2.7E-04	1.1E-03	3.8E-05	2.8E-04	3.5E-04	4.4E-04	4.8E-04	3.6E-04	8.8E-04	5.1E-04
KA3065A02:6_C_2(2)	–4.4E-04	1.0E-03	1.2E-04	2.9E-04	4.3E-04	5.3E-04	7.9E-04	2.4E-04	1.3E-03	5.8E-04
KA3065A03_Batch 1_A_1(2)	–1.4E-04	1.2E-03	4.4E-03	6.0E-04	3.4E-02	4.0E-03	9.6E-02	5.0E-03	4.2E-02	4.8E-03
KA3065A03_Batch 1_A_2(2)	–9.8E-05	1.2E-03	4.4E-03	6.7E-04	2.8E-02	3.4E-03	8.6E-02	7.7E-03	4.6E-02	5.3E-03
KA3065A03_Batch 1_B_1(2)	–1.4E-04	1.2E-03	3.0E-04	3.3E-04	9.3E-04	5.7E-04	1.5E-03	3.6E-04	1.8E-03	6.4E-04
KA3065A03_Batch 1_B_2(2)	–4.3E-04	1.2E-03	3.3E-04	4.9E-04	1.9E-03	6.9E-04	3.1E-03	4.3E-04	4.6E-03	9.3E-04
KA3065A03_Batch 1_C_1(2)	–1.7E-04	1.2E-03	3.4E-04	4.7E-04	5.0E-04	5.0E-04	7.5E-04	2.9E-04	9.0E-04	5.1E-04
KA3065A03_Batch 1_C_2(2)	–3.4E-04	1.1E-03	3.1E-05	4.6E-04	4.2E-04	4.4E-04	3.7E-04	2.5E-04	9.7E-04	5.6E-04
KA3065A03_Replica_A_1(2)	2.2E-03	9.5E-04	1.0E-02	3.1E-03	2.1E-02	2.5E-03	2.7E-02	5.1E-03	5.2E-02	9.8E-03
KA3065A03_Replica_A_2(2)	2.4E-03	8.9E-04	9.5E-03	2.9E-03	1.0E-02	1.6E-03	2.3E-02	4.4E-03	4.9E-02	8.8E-03
KA3065A03_Replica_B_1(2)	4.0E-03	1.2E-03	1.5E-02	4.1E-03	3.3E-02	3.9E-03	4.5E-02	8.2E-03	7.7E-02	1.5E-02
KA3065A03_Replica_B_2(2)	2.2E-03	8.5E-04	9.3E-03	2.8E-03	2.3E-02	2.6E-03	3.4E-02	6.4E-03	5.4E-02	1.0E-02
KA3065A03_Replica_C_1(2)	2.2E-04	1.3E-03	2.9E-03	5.6E-04	1.0E-02	1.4E-03	3.2E-02	2.6E-03	6.8E-02	7.5E-03
KA3065A03_Replica_C_2(2)	–1.9E-04	1.1E-03	2.0E-03	5.0E-04	8.3E-03	1.4E-03	2.4E-02	2.1E-03	5.0E-02	6.2E-03

Table A11-1. R_d (m^3/kg) results from the batch sorption experiments (Continued).
Np-237

Contact time – days	1.0		7.0		31.0		90.0		186.0	
Core	R_d (m^3/kg)	+/–	R_d (m^3/kg)	+/–	R_d (m^3/kg)	+/–	R_d (m^3/kg)	+/–	R_d (m^3/kg)	+/–
KA3065A02:1_A_1(2)	3.9E-04	1.1E-03	3.9E-03	7.2E-04	3.3E-02	4.0E-03	2.1E-01	1.9E-02	8.1E-02	7.8E-03
KA3065A02:1_A_2(2)	2.1E-04	1.0E-03	1.8E-03	5.3E-04	2.1E-02	2.7E-03	1.2E-01	9.1E-03	7.2E-02	7.2E-03
KA3065A02:1_B_1(2)	9.4E-05	1.0E-03	3.8E-04	4.4E-04	8.5E-04	5.2E-04	1.8E-03	4.4E-04	2.4E-03	6.3E-04
KA3065A02:1_B_2(2)	–2.9E-04	9.5E-04	3.1E-04	4.4E-04	8.9E-04	5.1E-04	1.6E-03	4.2E-04	2.3E-03	5.9E-04
KA3065A02:1_C_1(2)	–1.5E-04	9.4E-04	-2.5E-05	4.3E-04	4.2E-04	5.3E-04	7.5E-04	3.5E-04	1.2E-03	4.7E-04
KA3065A02:1_C_2(2)	–3.2E-04	9.0E-04	4.1E-05	4.4E-04	4.8E-04	4.6E-04	6.7E-04	3.6E-04	1.0E-03	5.2E-04
KA3065A02:2_A_1(2)	4.8E-03	1.3E-03	2.0E-02	5.7E-03	3.6E-02	5.8E-03	4.6E-02	9.7E-03	6.6E-02	1.5E-02
KA3065A02:2_A_2(2)	9.9E-03	2.1E-03	2.1E-02	6.1E-03	3.6E-02	5.9E-03	5.6E-02	1.1E-02	5.7E-02	1.3E-02
KA3065A02:2_B_1(2)	3.5E-03	1.1E-03	8.2E-03	2.9E-03	1.8E-02	3.3E-03	3.7E-02	7.8E-03	6.1E-02	1.3E-02
KA3065A02:2_B_2(2)	4.5E-03	1.3E-03	1.6E-02	4.8E-03	2.7E-02	4.5E-03	4.3E-02	9.0E-03	5.5E-02	1.2E-02
KA3065A02:2_C_1(2)	1.6E-04	9.8E-04	1.4E-03	5.6E-04	1.7E-03	6.1E-04	2.2E-03	4.4E-04	2.8E-03	6.2E-04
KA3065A02:2_C_2(2)	1.8E-04	1.0E-03	8.7E-04	4.5E-04	1.5E-03	5.4E-04	2.4E-03	4.7E-04	2.2E-03	5.4E-04
KA3065A02:6_A_1(2)	2.0E-04	1.0E-03	4.0E-03	6.8E-04	3.5E-02	4.5E-03	3.0E-01	3.2E-02	2.1E-01	2.2E-02
KA3065A02:6_A_2(2)	3.9E-04	1.0E-03	3.9E-03	7.6E-04	3.1E-02	4.0E-03	2.5E-01	2.5E-02	2.7E-01	3.1E-02
KA3065A02:6_B_1(2)	4.3E-04	1.1E-03	2.1E-03	5.4E-04	4.6E-03	8.7E-04	7.3E-03	8.6E-04	9.9E-03	1.4E-03
KA3065A02:6_B_2(2)	–4.3E-05	9.1E-04	1.4E-03	5.1E-04	3.8E-03	7.6E-04	7.3E-03	7.7E-04	1.1E-02	1.4E-03
KA3065A02:6_C_1(2)	–5.0E-05	9.3E-04	3.4E-05	3.8E-04	3.0E-04	4.5E-04	3.1E-04	3.7E-04	5.4E-04	4.3E-04
KA3065A02:6_C_2(2)	–2.9E-04	8.6E-04	1.5E-04	3.7E-04	3.7E-04	5.1E-04	5.5E-04	3.3E-04	9.0E-04	4.5E-04
KA3065A03_Batch 1_A_1(2)	3.3E-04	1.1E-03	6.6E-03	9.1E-04	9.4E-02	1.0E-02	7.1E-01	1.4E-01	3.3E-01	4.1E-02
KA3065A03_Batch 1_A_2(2)	3.5E-04	1.0E-03	6.6E-03	9.9E-04	1.0E-01	1.1E-02	1.1E+0	2.5E-01	5.9E-01	9.3E-02
KA3065A03_Batch 1_B_1(2)	1.5E-04	9.9E-04	7.6E-04	4.3E-04	2.1E-03	6.5E-04	3.3E-03	5.4E-04	3.8E-03	7.4E-04
KA3065A03_Batch 1_B_2(2)	–6.7E-05	9.6E-04	1.1E-03	4.9E-04	5.6E-03	1.1E-03	1.3E-02	1.3E-03	2.4E-02	2.8E-03
KA3065A03_Batch 1_C_1(2)	–1.9E-05	1.0E-03	3.5E-04	4.5E-04	4.8E-04	4.8E-04	5.9E-04	3.6E-04	6.1E-04	4.5E-04
KA3065A03_Batch 1_C_2(2)	–2.1E-04	9.1E-04	2.5E-05	4.2E-04	3.5E-04	4.6E-04	1.8E-04	3.4E-04	6.7E-04	4.8E-04
KA3065A03_Replica_A_1(2)	6.0E-03	1.5E-03	1.2E-02	3.7E-03	1.6E-02	2.8E-03	1.8E-02	4.1E-03	2.1E-02	5.0E-03
KA3065A03_Replica_A_2(2)	5.2E-03	1.4E-03	9.0E-03	3.1E-03	1.2E-02	2.3E-03	1.3E-02	3.2E-03	1.7E-02	4.2E-03
KA3065A03_Replica_B_1(2)	6.6E-03	1.7E-03	9.7E-03	3.3E-03	9.0E-03	1.8E-03	1.2E-02	2.9E-03	1.3E-02	3.4E-03
KA3065A03_Replica_B_2(2)	3.3E-03	1.1E-03	5.3E-03	2.3E-03	6.5E-03	1.5E-03	7.7E-03	2.2E-03	8.6E-03	2.5E-03
KA3065A03_Replica_C_1(2)	1.1E-03	1.2E-03	3.3E-03	6.6E-04	5.7E-03	1.0E-03	7.6E-03	9.0E-04	1.0E-02	1.3E-03
KA3065A03_Replica_C_2(2)	8.1E-04	1.1E-03	3.0E-03	6.3E-04	5.7E-03	1.0E-03	7.1E-03	8.8E-04	9.6E-03	1.2E-03

Appendix 12

One-dimensional diffusion model

The general one dimensional diffusion equation is expressed by;

$$\frac{\partial C}{\partial t} = D\frac{\partial^2 C}{\partial x^2} \qquad \text{(A12-1)}$$

In the present situation the interaction can be regarded as diffusion from a stirred solution of limited volume into a plane sheet. In order to benefit from the analytical solution of this case given by Crank (1975) a case where diffusion from both sides of the sheet occurs will be considered. The sheet occupies the space $-l \le x \le l$ while the solution is of limited extent and occupies the spaces $-l\text{-}a \le x \le -l$ and $l \le x \le l+a$. The occupation length of the water phase (a) is set to:

$$a = V / A + K_\text{a} \qquad \text{(A12-2)}$$

where V corresponds to the volume in the experiment cell and A is the surface area exposed to the volume.

The length of the sheet (l) has no influence of the rate of the loss of tracer in the water phase as long as the contribution of tracer diffusing from one side to the other can therefore be neglected. The length can therefore be set arbitrarily and in this particular case l has been set in order to obtain a tracer concentration in the middle of the sheet (x=0) that is at least 10^{10} times lower than the tracer concentration in surface layer of the sheet (i.e. $x=l$ or $x=-l$).

The concentration of the solute in the solution is always uniform and is initially C_0. while the sheet initially is free from solute. The following boundary conditions therefore apply:

$$C=0 \qquad \alpha_r \frac{\partial C}{\partial t} = \pm D\frac{\partial C}{\partial x} \qquad -1 \le x \le 1 \qquad t=0 \qquad \text{(A12-3)}$$

and

$$\alpha_r \frac{\partial C}{\partial t} = \pm D\frac{\partial C}{\partial x} \qquad x = \pm 1 \qquad t>0 \qquad \text{(A12-4)}$$

The analytical solution to this problem has been given by Crank (1975). The total concentration within the sheet, C_x, (including both the pore water concentration and the mass sorbed on the rock) at the distance x at a given diffusion time of t is given by the expression:

$$C_x = C_\infty \left\{ 1 + \sum_{j=1}^{\infty} \frac{2(1+\alpha_r)\exp\left(-\frac{D_a q_j^2 t}{l^2}\right)}{1+\alpha_r+\alpha_r{}^2 q_j^2} \frac{\cos\left(\frac{q_j x}{l}\right)}{\cos q_j} \right\} \qquad \text{(A12-5)}$$

where C_∞ is the concentration in the sheet after infinite time and the q_j values are the non-zero positive roots of:

$$\tan q_j = -\alpha_r q_j \qquad \text{A12-6)}$$

and α_r is the ratio of the capacities of the rock and water phase, defined as;

$$\alpha_r = \frac{a}{l(\varepsilon + K_d \rho)} \qquad \text{(A12-7)}$$

Furthermore, the decrease of the concentration of tracer in the start cell, C_1, can be calculated according to:

$$C_1 = C_{1(0)} - \frac{C_\infty m}{V_1 \rho}\left\{1 - \sum_{j=1}^{\infty} \frac{2\alpha_r(1+\alpha_r)\exp\left(\frac{-D_a q_j^2 t}{l^2}\right)}{1+\alpha_r+\alpha_r{}^2 q_j^2}\right\} \tag{A12-8}$$

where $C_{1(0)}$ corresponds to the initial concentration in the start cell.

By applying mass balance, C_∞ can be calculated according to:

$$C_\infty = \frac{C_0 a}{l + a/(\varepsilon + K_d \rho)} \tag{A12-9}$$

However, for the present measurements of sorption on intact rock pieces, the concentration profile within the rock will not be possible to measure. Instead, the decrease of the concentration in the water phase (caused by diffusion and/or sorption in the rock) will be the only available experimental parameter that can be measured. The analytical solution for calculating the total amount of tracer in the sheet (M_t) after a given experimental time (t) is expressed as:

$$\frac{M_t}{M_\infty} = 1 - \left\{\sum_{j=1}^{\infty} \frac{2\alpha_r(1+\alpha_r)}{1+\alpha_r+\alpha_r{}^2 q_j^2}\exp\left(\frac{-D_a q_j^2 t}{l^2}\right)\right\} \tag{A12-10}$$

where M_∞ correspond to the total amount of tracer in the sheet after infinite experimental time. Applying mass balance, M_∞ can be expressed as:

$$M_\infty = \frac{2aC_0}{1+\alpha_r} \tag{A12-11}$$

where C_0 is the initial concentration of tracer in the water phase. Furthermore, M_t can be expressed as:

$$M_t = (M_0 - M_{aq(t)}) = a(C_0 - C_{aq(t)}) \tag{A12-12}$$

where M_0 is the initial amount of tracer added to the system. $M_{aq(t)}$ is the amount of tracer in the water phase after an experimental time of t and $C_{aq(t)}$ is the corresponding concentration of tracer in the water phase.

By inserting Equation A12-11 and A12-12 into A12-10 and by rearranging. the following expression is obtained:

$$\frac{C_{aq(t)}}{C_0} = 1 - \left\{\frac{1}{1+\alpha_r} - \sum_{j=1}^{\infty} \frac{2\alpha_r}{1+\alpha_r+\alpha_r{}^2 q_j^2}\exp\left(\frac{-D_a q_j^2 t}{l^2}\right)\right\} \tag{A12-13}$$

Appendix 13

Rock sample descriptions

Each rock sample included in the laboratory investigations has been characterized and documented in stereomicroscope with respect to the mineralogy, fractures/microfractures and alteration. Table A13-1 and Table A13-2 present an overview of the rock samples from rock cores KA3065A02 and KA3065A03, respectively. Table A13-3 present the samples from the Site Investigations and SKB rock codes are explained in Table A13-4. The tables include sample-ID, size of the sample as well as information of the methods purposed for each sample, geological notes and photographs. Not all geological information of the rock samples can be presented in the tables and consequently, only the most important characteristics, and/or deviations from the overall mineralogical description (cf. Section 2.1), for the rock samples are included in the tables. The single rock samples location at the KA3065A02 and KA3065A03 rock cores are presented in Appendix 2.

Table A13-1. Rock samples from KA3065A02. All rock samples have a diameter of 44 mm.

Rock sample ID/Alias	Sample length	Method/Parameter achieved	Comments	Photograph
A02:1	~25 mm	BET + Batch sorption /specific surface area and K_d	Altered rock sample (medium oxidation) close to Feature 10. Small amounts of fracture minerals at the end surfaces.	
A02:2	10 mm	BET + Batch sorption /specific surface area and K_d	Altered mylonitic rock with two fracture surfaces; #10a and #10b (the target structure). Fracture minerals are: calcite, chlorite, epidote and hematite, +/– clay minerals.	
A02:4	30 mm	Through-diffusion, porosity /D_e, ε	Red-staining restricted to a supposed old fracture. Some large k-feldspar crystals. Relatively large amount of opaques and titanite	
A02:5	30 mm	Electrical resistivity, porosity/F_f, ε	Minor amount of re-crystallization. Red-staining around an old sealed fracture.	
A02:6	~60 mm	BET + Batch sorption /specific surface area and K_d, Geochemical analysis		

A02:7	30 mm	Electrical resistivity, porosity /F_f , ε	Several sealed and partly open microfractures.	
A02:8	30 mm	Through-diffusion, porosity /D_e, ε		

Table A13-2. Rock samples from KA3065A03. The rock samples have a diameter of 22 mm, except for two irregular samples and A19, which has a diameter of 24 mm.

Rock sample ID /Alias	Sample thickness	Method/ Parameter	Comments	Photograph
A03:1/ Batch 1	~90 mm	BET + Batch sorption /specific surface area and K_{d},. Geochemical analysis.	Slightly red-stained in grain boundaries	
A03:2/ Batch 2	40 mm	BET /specific surface area	Medium degree of red-staining/ oxidation. 1 sealed thin fracture #16 (orientation 45°) with quartz and/or calcite.	
A03:3/ Diff 1	~70 mm (originally 150 mm but was broken during the sample preparation)	Sorption/diffusion, through-diffusion, porosity/ D_e, K_d, ε	Very thin fracture coating at one end of the sample (to the left in the upper figure) with chlorite, calcite and chalcopyrite, representing the target fracture. This fracture is the target structure 10a. Red-stained rock, ~5 to 10 mm from the fracture surface and inwards. Sealed fractures with calcite +/– chlorite and quartz, orientation parallel to the fracture surface described above.	 
A03:4/ Diff 2	30 mm	Sorption/diffusion, through-diffusion, porosity/ D_e, K_d, ε	Slightly rust colored around titanite grains.	
A03:5/ Diff 3	30 mm	Sorption/diffusion, through-diffusion, porosity/ D_e, K_d, ε	Several sealed micro fractures, ~3 mm length.	

A03:6/ Diff 4	30 mm	Sorption/diffusion, through-diffusion porosity/ D_{e}, K_{d}, ε	Several small micro fractures, ~1 mm length.	
A03:7/ PMMA 1	27 mm	Porosity with water saturation and PMMA, ε	Red-staining (weak oxidation) and albitization. Several small micro fractures, ~1 mm length.	
A03:8/ PMMA 2	18 mm	Porosity with water saturation and PMMA, ε	Weak oxidation and albitization.	
A03:9/ Feature #10 "liten sten"	Length ~45 mm, height ~6 mm, width ~40 mm	BET + Batch sorption /specific surface area and K_{d},	Fracture coatings of calcite, chlorite, epidote and chalcopyrite, +/– quartz. Small amount of remaining red-stained rock. This sample represents fracture material in the target structure #10.	
A03:10/ Feature#10, "stor sten"	Length 70 mm	Porosity with water saturation and PMMA, ε. Thin section	Mylonitic/cataclasitic rock, with a matrix mainly consisting of epidote and chlorite, together with strongly altered (red-stained and fractured) bedrock. Fracture coatings on two sides of the sample. Fracture coatings consist of chlorite, calcite, epidote, quartz and chalcopyrite. This sample represents fracture material as well as altered rock in structure #10.	
A03:11/ Feature#10	length 50 mm, height ~10 mm, width ~20 mm	Porosity with water saturation and PMMA, ε	Fracture coating with chlorite, calcite, epidote and chalcopyrite. Mylonitic/cataclasitic rock with a matrix mainly consisting of epidote and chlorite. This sample represents fracture material in the target structure #10and mylonitic/cataclasitic rock.	
A19	175 mm	PMMA, ε	Reference sample drilled from fracture #10a and into the rock although outside the experiment section area.	 

Table A13-3. Rock samples from the Site Investigations at Forsmark and Oskarshamn.

Sample-ID	Rock type (SKB rock code)	Method/parameter	Comments	Photograph
KFM02A 276.06	Altered variety of 101057, “Episyenite”	Sorption/diffusion, porosity/ D_e, K_d, ε	Quartz dissoluted granodioritic rock. Newly formed mineral grains are present in the vugs; albite, quartz and chlorite/hematite aggregates as well as small grains of Ti-oxides.	 *
KFM03A 242,43	101054	Sorption/diffusion, porosity/ D_e, K_d, ε	Foliated fresh rock sample of tonalitic composition. No documented microfractures	
KFM07A 608,75	101057	Sorption/diffusion, porosity/ D_e, K_d, ε	Foliated fresh rock sample of granite to granodiorite. No documented microfractures	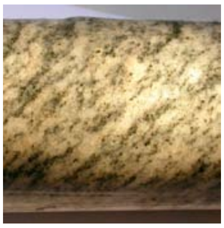
KFM09A 713,67	101057	Sorption/diffusion, porosity/ D_e, K_d, ε	Foliated fresh rock sample of granite to granodiorite. No documented microfractures	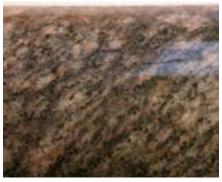
KSH01 891,91	501046	Sorption/diffusion, porosity/ D_e, K_d, ε	Fresh rock sample of Ävrö quartz monzodiorite. No documented microfractures	
KSH01 981,43	501036	Sorption/diffusion, porosity/ D_e, K_d, ε	Fresh rock sample of quartz monzodioritic composition. No documented microfractures	
KLX02 235,08	501056	Sorption/diffusion, porosity/ D_e, K_d, ε	Fresh rock sample of Ävrö granodiorite. No documented microfractures	
KLX04 726,07	501036	Sorption/diffusion, porosity/ D_e, K_d, ε	Fresh rock sample of quartz monzodioritic composition. No documented microfractures	No picture

KLX08 417,05	501046	Sorption/diffusion, porosity/ D_e, K_d, ε	Fresh rock sample of Ävrö quartz monzodiorite. One sealed thin fracture with oxidized walls.	
KLX10 995,79	501036	Sorption/diffusion, porosity/ D_e, K_d, ε	Fresh rock sample of quartz monzodioritic composition. No documented microfractures	

* The picture is from an adjacent rock sample; i.e. KFM02A 275.45.

Table A13-4. Translation table for SKB rock code and rock types.

SKB rock code	SKB rock type
Forsmark	
101054	Tonalite to granodiorite, metamorphic
101057	Granite to granodiorite, metamorphic, medium-grained
Oskarshamn	
501036	Quartz monzodiorite
501046	Ävrö quartz monzodiorite
501056	Ävrö granodiorite

Appendix 14

Selection of tracers

Below the motivation for selection of tracers is presented (from /Widestrand et al. 2010/.

Both sorbing and non-sorbing tracers were used in the experiment. The radionuclides that were used are summarised in Table A14-1. The use of the different radionuclides aims at studying different retardation processes, e.g. sorption and diffusion. The radionuclides have been categorised in two groups after their primary usage:

A. Non-sorbing tracers, i.e. tracers that are assumed to diffuse without retardation due to sorption onto mineral surfaces.

B. Sorbing tracers, i.e. tracers that are retarded by adsorption onto mineral surfaces. These tracers are aimed to estimate the impact of sorption on the penetration into the rock. The proposed tracers can be divided into three different subcategories within this group:
   1. Tracers for which the sorption is dominated by a cation exchange mechanism.
   2. Tracers for which the sorption is dominated by a surface complexation mechanism.
   3. Tracers dependent of an electrochemical reduction in order to reach the tetravalent state (oxidation state IV) which is considered to be very strongly sorbing. The corresponding higher oxidation state for the respective tracer is thus considered to be weaker sorbing.

   Consequently, the sorbing tracers are divided into the subcategories B1, B2 and B3.

A main consideration of the experiment was of course to maintain natural chemical conditions it the experiment and that one therefore should avoid to increase the natural chemical concentration of the element used as tracers. For this reason, the use of radioactive isotopes of different element aimed to be studied was very suitable technique where radioisotopes of very high specific activity were available.

However, avoiding increase of the natural concentration was not possible for every tracer element used; this mainly because of the cases when the element was not naturally present (or present in extremely low concentrations) in the groundwater. Additionally, for some cases an avoiding of an increase of the natural concentrations might have caused a low dynamic range (i.e. start concentration divided by the concentration for the detection limit). The following outline was therefore decided for the selection of chemical concentrations for the different tracers used:

- If possible, the addition of the tracer should not increase the natural concentration, i.e. the chemical concentration in the injection cocktail should be equal or below the natural elemental concentration.
- If not possible, the maximum elemental concentration of a tracer element should be $1 \cdot 10^{-6}$ M.

Regarding the selection of non-sorbing tracers, the short-lived iodine tracer (I-131) used in the functionality test was indicated to be exposed to some form of adsorptive loss and the long lived isotope I-129 was therefore rejected as an inert tracer for the main experiment. The selection of an inert tracer that could be analysed in the rock material after at least a year excluded some often used inert tracers. Tritiated water could not be used for rock analysis due to evaporation during handling; bromide tracers are too short-lived. Color dye tracers and metal-complexes are undesired due to risk of complexation of the other metal tracers with high charges (and could not meet the prerequisites of not changing the natural chemical conditions of the groundwater). Thus, ^{36}Cl proved to be the only reasonable choice, although it requires chemical separation procedures since it has no γ-emission that can be measured using γ-spectrometry.

The anionic tracers $^{35}SO_4^{2-}$ (and possibly also $^{75}SeO_4^{2-}$) could based on their negative charges be considered as potential inert tracers. However, both of them are subject for possible electrochemical reactions and/or precipitation reactions and there is no information in the literature of the use of them as groundwater tracers.

Table A14-1. Information on the radionuclide tracers used in the LTDE-SD experiment. The acronym ICP-SFMS stands for: Inductively Coupled Plasma – Sector field mass spectrometry.

Tracer	Amount	Half-life	Expected sorption mechanism	Analysis method
$^{22}Na^{+}$	3.2 MBq	2.6 y	Cation exchange	γ-spectrometry
$^{35}SO_4^{2-}$	13 MBq	87.5 d	Non-sorbing, possibly reduced to S(–II)	Liquid scintillation counting after chemical separation, BaSO4(s) precipita
$^{36}Cl^{-}$	5.9 MBq	3.0E5 y	Non-sorbing (anion exclusion?)	Liquid scintillation counting after chemical separation
$^{57}Co^{2+}$	19 MBq	272 d	Surface complexation	γ-spectrometry, after cation exchange separation
$^{63}Ni^{2+}$	30 MBq	100 y	Surface complexation	Liquid scintillation counting after chemical separation
$^{75}SeO_4^{2-}$	4.4 MBq	120 d	Non-sorbing, possibly reduced to Se(–II)	γ-spectrometry, after cation exchange separation
$^{85}Sr^{2+}$	45 MBq	65 d	Cation exchange	γ-spectrometry
^{95}Zr(IV)	0.07 MBq	64 d	Surface complexation	γ-spectrometry, after cation exchange separation
$^{95}NbO_2^{+}$	0.03 MBq	35 d	Surface complexation	γ-spectrometry, after cation exchange separation
$^{99}TcO_4^{-}$	94 µg	2.1E5 y	Non-sorbing, Tc(IV) under reuducing conditions	ICP-SFMS
$^{102}Pd^{2+}$	55 µg	Stable	Surface complexation	ICP-SFMS
$^{109}Cd^{2+}$	27 MBq	463 d	Surface complexation	γ-spectrometry, after cation exchange separation
$^{110\,m}Ag^{+}$	0.4 MBq	250 d	Surface complexation	γ-spectrometry, after cation exchange separation
^{113}Sn(IV)	0.09 MBq	115 d	Surface complexation	γ-spectrometry, after cation exchange separation
$^{133}Ba^{2+}$	1.8 MBq	10.5 y	Cation exchange	γ-spectrometry
$^{137}Cs^{+}$	8.8 MBq	30 y	Cation exchange	γ-spectrometry
^{153}Gd(III)	4.3 MBq	240 d	Surface complexation	γ-spectrometry, after cation exchange separation
^{175}Hf(IV)	1.9 MBq	70 d	Surface complexation	γ-spectrometry, after cation exchange separation
$^{226}Ra^{2+}$	0.15 MBq	1,600 y	Cation exchange	γ-spectrometry, after cation exchange separation (measured from its daughter radionuclide Bi-214)
$^{236}UO_2^{-}$	57 µg	2.3E7 y	Surface complexation, U(IV) under reducing conditions	ICP-SFMS
$^{233}PaO(OH)_3$	5.7 MBq	27 d	Surface complexation	γ-spectrometry, after cation exchange separation
$^{237}NpO_2^{+}$	310 µg	2.1E6 y	Surface complexation, Np(IV) under reducing conditions	ICP-SFMS